X-Ray Fluorescence Yields, Auger, and Coster–Kronig Transition Probabilities*

WALTER BAMBYNEK
Bureau Central de Mesures Nucléaires, EURATOM, B-2440 Geel, Belgium
BERND CRASEMANN
Department of Physics, University of Oregon, Eugene, Oregon 97403
R. W. FINK and H.-U. FREUND†
School of Chemistry, Georgia Institute of Technology, Atlanta, Georgia 30332
HANS MARK and C. D. SWIFT
Ames Research Center, NASA, Moffett Field, California 94035
R. E. PRICE
Lawrence Livermore Laboratory, Livermore, California 94550
P. VENUGOPALA RAO
Department of Physics, Emory University, Atlanta, Georgia 30322

The present status of the field of fluorescence yields, radiationless (Auger and Coster–Kronig) and radiative transition probabilities is summarized. Tables of experimental and theoretical results are included, and tables of "best values" of important quantities are presented.

CONTENTS

1. Introduction 717
1.1. History 717
1.2. Importance of Radiationless Transitions and Fluorescence Yields 717
1.2.1. Significance of Radiationless Transitions in Fundamental Research 717
1.2.2. Importance of Fluorescence Yields in Applied Physics 718
1.3. Purpose and Scope of This Review 718
1.4. Definition of Physical Quantities 718
1.4.1. Average Fluorescence Yields in the Absence of Coster–Kronig Transitions 719
1.4.2. Average Fluorescence Yields in the Presence of Coster–Kronig Transitions 719
Description in Terms of the Altered Vacancy Distributions V_i^X 719
Description in Terms of the Primary Vacancy Distribution N_i^X 719
Transformation Equations Relating the Two Descriptions 719
1.4.3. Auger Yields 721
1.4.4. Remarks on Notation 722
2. Theory 722
2.1. Matrix Elements 722
2.1.1. Radiationless Transitions—Nonrelativistic Probability 722
2.1.2. Radiationless Transitions—Relativistic Probability 723
2.1.3. Radiative Transition Probabilities 724
2.2. Wave Functions 725
2.2.1. Nonrelativistic Hydrogenic Bound-State Wave Functions; Screening 725
2.2.2. Analytic Relativistic Wave Functions 726
2.2.3. Numerical Wave Functions 726
2.2.4. Continuum Wave Functions 727
2.3. Calculation of Radiationless Transition Probabilities 728
2.3.1. Evaluation of Radial Matrix Elements 728
2.3.2. Representations: Coupling Schemes 729
2.3.3. Survey of Results 732
2.4. Radiative Transition Probabilities 739
2.4.1. Calculations 739
2.4.2. Summary of Results and Comparison with Experiment 743
2.5. Atomic Level Widths 744
2.5.1. Principles 744
2.5.2. K-Level Widths 745
2.5.3. L-Level Widths 746
3. K-Shell Fluorescence Yields 746
3.1. Experimental Methods 746
3.1.1. Fluorescent-Excitation Methods 747
Gaseous Targets 747
Solid Targets 748
3.1.2. Excitation Due to Radioactive Decay 749
Auger- and Conversion-Electron Spectroscopy With High-Resolution Spectrometers 749
Auger-Electron, X-, and β-Ray Spectroscopy 750
Auger-Electron and X-Ray Spectroscopy With Gaseous Radioactive Sources 750
Auger-Electron and X-Ray Spectroscopy With Solid Radioactive Sources 751
K X-Ray and γ-Ray or Conversion-Electron Spectroscopy 752
Determination of K X-Ray Emission Rate and Disintegration Rate 752
Coincidence Methods 753
3.1.3. Inner-Shell Vacancies Produced by Charged-Particle Impact 754
Electrons 754
Protons 754
Heavier Ions 754
3.1.4. Other Methods 754
Cloud-Chamber Technique 754
Jump of Photoionization Current at the K Edge 755
Photographic Emulsion Technique 755
3.2. Criteria for Best Methods to Determine ω_K 755
3.2.1. Measurements 755
3.2.2. Estimation of Errors 755
3.2.3. Conclusion 755
3.3. Evaluation of Most Reliable ω_K Values 755
3.3.1. Measurements Employing Electron-Capture Transitions 755
3.3.2. Reevaluation of Errors 756
3.3.3. Semiempirical Fits 756
3.4. Comparison of Experimental and Theoretical K-Shell Fluorescence Yields 761
4. L-Shell Yields 761
4.1. Primary L-Subshell Fluorescent Excitation 762
4.2. Primary L-Subshell Excitation by Charged-Particle Bombardment 763

* Work supported in part by the U.S. Atomic Energy Commission, the National Aeronautics and Space Administration, the European Atomic Energy Commission, and the U.S. Army Research Office, Durham.

† Present address: Battelle Institute e. V., D—6000 Frankfurt 90, Germany.

4.3. Primary L-Subshell Excitation Due to Radioactive Decay 763
4.3.1. L-Shell Orbital Electron Capture 763
4.3.2. L-Shell Internal Conversion 764
4.4. Primary L-Subshell Excitation through Transitions to the K Shell 765
4.5. Experimental Techniques for the Determination of L-Shell Yields 769
4.5.1. ($K\alpha$ x-ray)−(L x-ray) Coincidence Methods 775
4.5.2. (Conversion-electron)−(L x-ray) Coincidence Methods 778
4.5.3. (γ-Ray)−(L x-ray) Coincidence Method 779
4.5.4. (α-Particle)−(L x-ray) Coincidence Method 780
4.5.5. Directional Correlation Effects in Coincidence Measurements 780
4.5.6. Singles Spectrum Methods 782
4.5.7. Diffraction Spectrometry 784
4.5.8. Methods Involving X-Ray and Auger-Electron Spectroscopy 785
4.6. Experimental L-Shell Yields 786
4.7. Comparison with Theory 786
5. M-Shell Fluorescence Yields 795
5.1. Special M-Shell Relationships 795
5.2. Influence of Multiple Vacancies on M-Shell Fluorescence Yields 798
5.3. Experimental Methods for M X Rays 800
5.4. Mean M-Shell Fluorescence Yields From Singles M X-Ray Spectra 800
5.4.1. Vacancies in the K, L, and M Shells 800
5.4.2. Vacancies in the L and M Shells Only 800
5.4.3. Vacancies in the M Shell Only 800
5.5. Mean M-Shell Yields by Coincidence Methods 801
5.5.1. Mean M-Shell Fluorescence Yields from Unresolved (L X-Ray)−(M X-Ray) Coincidences 801
5.5.2. Measurements of $\bar{\omega}_{2,3}{}^{M}$ from ($K\beta_{1,3}$)−(M X-Ray) Coincidences 801
5.5.3. Measurements of $\omega_i{}^{M}$ from (Resolved L X-Ray)−(M X-Ray) Coincidences 801
5.5.4. Directional Correlation Effects 802
5.6. Tables and Discussion of M-Shell Yields 802
Concluding Remarks 805
Glossary 805
Identification of Characteristic X Rays 808
References 808

1. INTRODUCTION

1.1. History

It has been known for a long time that de-excitation of atoms can occur not only by the emission of electromagnetic radiation but also by other competing processes. In x-ray absorption experiments, Beatty (1911) and Barkla and Philpot (1913) produced evidence that atoms with K-shell vacancies emit radiation that causes higher specific ionization than expected from the characteristic fluorescence x rays. In a review paper entitled "X-Rays and the Theory of Radiation," Barkla (1918) introduced the concept of *fluorescence yield*, defining it as the ratio of the energy carried by fluorescence radiation to the energy carried by the radiation absorbed in a sample.[1] In the paper he listed values of this ratio for eight elements (Fe, Co, Ni, Cu, Zn, As, Se, and Ag). Meitner (1922) and Robinson (1923) discovered independently that atoms ionized in inner shells emit monoenergetic electrons, with energies that do not depend upon the manner in which the atoms are ionized. In a classic series of experiments involving cloud-chamber techniques, Auger (1925, 1926) produced direct proof that atoms ionized in inner shells emit electrons through radiationless transitions. Two electron tracks were observed to originate from some ionized atoms: one track (of the photoelectron) of a length depending on the energy of the incident ionizing radiation, the other track (of the Auger electron) of constant length. Because of the unequivocal nature of the evidence for radiationless transitions obtained by Auger, such transitions are named after him.

Work on the identification of different types of radiationless transitions in atoms and the measurement of radiationless transition rates continued at a steady pace during the late 1920's and the 1930's. Lay (1934) and Stephenson (1937) conducted systematic measurements of K-shell and mean L-shell fluorescence yields. Through the study of satellite lines in x-ray emission spectra, Coster and Kronig (1935) discovered radiationless transitions between L subshells. Most recently, the Auger effect has been reviewed by Burhop and Asaad (1972) and by Parilis (1969).

In recent years, there has been a considerable revival of interest in atomic radiationless transitions and fluorescence yields for reasons that are detailed in the following section.

1.2. Importance of Radiationless Transitions and Fluorescence Yields

1.2.1. Significance of Radiationless Transitions in Fundamental Research

From a fundamental viewpoint, the study of radiationless transitions is important for two reasons. Nonradiative transition probabilities are more sensitive to the detailed nature of atomic wave functions than many other measurable atomic quantities (cf. Sec. 2). A systematic study of radiationless transitions between various atomic states is therefore likely to lead to information that can be used to improve current methods for generating numerical atomic wave functions.

Furthermore, detailed knowledge of radiationless transition rates and energies is necessary for the interpretation of a large variety of measurements in nuclear and atomic physics. For example, the transition energy in nuclear electron-capture decay and the multipolarity of internally converted nuclear γ transitions can often be determined by measuring relative x-ray intensities and applying pertinent subshell fluorescence yields to derive primary vacancy distributions.

A number of more subtle effects of nuclear origin require a precise knowledge of the properties of atomic transitions for their interpretation. One example is "internal ionization" or ejection of atomic electrons during nuclear β decay, usually studied by detecting characteristic x rays of the daughter atom in coincidence with β particles (Stephas and Crasemann, 1971).

[1] For the present-day definition of *fluorescence yield*, see Sec. 1.4.

Atomic collision cross sections for processes in which inner shells are excited can often be measured through detection of characteristic radiation intensities, corrected for fluorescence yields.

The Auger cascade process is another interesting phenomenon, the study of which depends upon knowledge of fluorescence yields. An Auger event resulting from an inner-shell vacancy produces a doubly ionized atom; successive radiationless transitions can lead to highly ionized atomic states. The possibility of utilizing this process in ion sources for heavy-ion accelerators has enhanced recent interest in the subject.

1.2.2. Importance of Fluorescence Yields in Applied Physics

In the solution of many practical problems, an accurate knowledge of atomic fluorescence yields is required. For example, some important methods for the standardization of radioisotopes depend on evaluation of effects that can be caused by radiationless transitions; the same is true of the design of many radiation detection devices.

Analytical methods based on x-ray fluorescence radiation have found wide practical application in a number of fields including nondestructive testing, medical research, trace-element analysis, and analysis of samples *in situ* for geological exploration. In medical research, x-ray fluorescence analysis of samples for heavy elements in biologically important molecules has been developed into a very useful method (Schippert, Moll, and Ogilvie, 1967; Russ and McNatt, 1969). Because x-ray detectors can respond to single-photon events, it has recently been possible to develop x-ray fluorescence into an exceedingly sensitive analytical tool for determining the presence of trace elements. Thus, Johansson, Akselsson, and Johansson (1970) reported the detection of as little as 10^{-10} g of trace elements in the atmosphere, collected on a carbon foil exposed for one day. The foil was bombarded with heavy ions, and trace elements were identified through their characteristic K x rays; quantitative interpretation of the results requires knowledge of fluorescence yields. In recent years, compact x-ray fluorescence spectrometers, designed for field use, have been developed for geological exploration (Fitzgerald and Gantzel, 1970). Rock samples returned from the surface of the moon by the Apollo 11 and Apollo 12 missions have also been analyzed using an electron microprobe to produce fluorescence x rays (Brown *et al.*, 1970; Rose *et al.*, 1970).

Auger-electron spectroscopy and low-energy electron diffraction (LEED) are used extensively in surface-physics studies for detecting minute quantities of contaminants (Harris, 1968; Palmberg and Rhodin, 1968). For example, monolayers of potassium and cesium have been detected on germanium and silicon surfaces by this technique (Weber and Peria, 1967). Atoms residing in the surface of a sample can be identified from characteristic Auger-electron energies.

The importance of fluorescence yields in photon-transport processes is well known. When the Boltzmann equation describing γ-ray transport is formulated, a term describing the contribution of fluorescence yields must be included to estimate properly the dose buildup factors due to secondary radiation processes. This term is particularly important in performing accurate calculations of the dose rate at a point in the medium at which the incident radiation has traversed many mean free paths; in such cases a major part of the dose may be due to secondary fluorescence radiation. The design of minimum weight graded or stacked shields for various engineering applications also depends critically on accurate fluorescence yields.

1.3. Purpose and Scope of This Review

The purpose of this work is to summarize as thoroughly as possible the present state of the field of x-ray fluorescence yields and radiationless transitions in atoms, with adequate references to the literature on radiative transitions in the x-ray region. We omit a discussion of experimental methods in the field of Auger-electron spectroscopy in order to keep this review within reasonable limits. In the description of experimental techniques and results, a critical evaluation is presented to guide the reader in judging the validity of the work. Tables of experimental results are included and, furthermore, tables of "best values" of important quantities are presented.

The following limitations apply to results included here: (a) We present values of fluorescence yields which refer to initial single-vacancy states; (b) we consider only transitions between inner shells and thus exclude effectively (but not necessarily entirely) chemical effects; and (c) we ignore complications arising in heavy-particle collisions.

1.4. Definition of Physical Quantities

The fluorescence yield of an atomic shell or subshell is defined as the probability that a vacancy in that shell or subshell is filled through a radiative transition. An atom with a vacancy is in an excited state; let Γ be the total width of that state, related to the mean life τ of the state by $\Gamma=\hbar/\tau$. The width Γ is the sum of the radiative width Γ_R, the radiationless width Γ_A, and the Coster–Kronig width Γ_{CK}. The fluorescence yield ω is therefore given by

$$\omega=\Gamma_R/\Gamma. \tag{1-1}$$

Thus, for a sample of many atoms, the fluorescence yield of a shell is equal to the number of photons emitted when vacancies in the shell are filled, divided by the number of primary vacancies in the shell.

The application of this definition to the K shell of an atom, normally containing two $s_{1/2}$ electrons, is

straightforward. The fluorescence yield of the K shell is

$$\omega_K = I_K/n_K, \tag{1-2}$$

where I_K is the total number of characteristic K x-ray photons emitted from a sample, and n_K is the number of primary K-shell vacancies.

The definition of fluorescence yields of higher atomic shells is more complicated for two reasons:

(i) Shells above the K shell consist of more than one subshell because the electrons can have different angular-momentum quantum numbers. The average fluorescence yield thus depends, in general, on how the shells are ionized, since different ionization methods give rise to different sets of primary vacancies.

(ii) Coster–Kronig transitions, which are transitions between the subshells of an atomic shell having the same principal quantum number (Coster and Kronig, 1935), make it possible for a primary vacancy created in one of the subshells to shift to a higher subshell before the vacancy is filled by another transition.

Consequently, great care must be taken in formulating proper definitions of the quantities that are measured, and in interpreting experimental results in a manner that is consistent with these definitions.

In a previous review article (Fink *et al.*, 1966), consistent definitions of fluorescence yields and Coster–Kronig transition probabilities were provided for the three L subshells. Since some detailed experimental data for M-shell yields have already appeared in the literature and fluorescence yields and Coster–Kronig transition probabilities for even higher shells may soon be measurable, it now appears important to extend the notation system to higher shells. In the following paragraphs, we develop definitions and notations that are applicable for fluorescence yields and Coster–Kronig transition probabilities in every atomic shell.

1.4.1. Average Fluorescence Yields in the Absence of Coster–Kronig Transitions

In most experiments designed to measure the fluorescence yield of an atomic shell, primary vacancies are created in several of the subshells. Let ω_i^X be the fluorescence yield of the ith subshell of a shell whose principal quantum number is indicated by X ($X=K$, L, M, $\cdots$).[2] In accordance with Eq. (1-2), we have

$$\omega_i^X = I_i^X/n_i^X. \tag{1-3}$$

An average or mean fluorescence yield for the shell X can then be defined as

$$\bar{\omega}_X = \sum_{i=1}^{k} N_i^X \omega_i^X, \tag{1-4}$$

where N_i^X is the relative number of primary vacancies in the subshell i of shell X:

$$N_i^X = n_i^X/\sum n_i^X; \qquad \sum_{i=1}^{k} N_i^X = 1. \tag{1-5}$$

The summations in Eqs. (1-4) and (1-5) extend over all k subshells of shell X.

If we denote the total number of X-shell vacancies (in all subshells) by n_X,

$$n_X = \sum_{i=1}^{k} n_i^X, \tag{1-6}$$

then the average X-shell fluorescence yield $\bar{\omega}_X$ can be written

$$\bar{\omega}_X = I_X/n_X \tag{1-7}$$

by analogy with Eq. (1-2). Here, I_X is the number of emitted characteristic X-shell x-ray photons.

For the definition (1-4) of $\bar{\omega}_X$ to be applicable, *the primary vacancy distribution must remain unaltered* before the vacancies are filled from higher shells, i.e., Coster–Kronig transitions must be absent.

Clearly, the average fluorescence yield for the shell X obtained in any given measurement depends on the vacancy distribution. Two experiments can give different values of $\bar{\omega}_X$ if the methods used to ionize the atoms result in different primary vacancy distributions. It is important to emphasize the point here that $\bar{\omega}_X$ generally is not a fundamental property of the atom but depends both on the atomic subshell yields ω_i^X and on the parameters N_i^X peculiar to the experiment. This fact has not always been recognized and has led to confusion, different quantities often being listed as "fluorescence yields" of a shell X.

In order to determine the atomic quantities ω_i^X for all of the k subshells of shell X, it is necessary to perform k experiments, each giving rise to a different known ratio of primary vacancies. These experiments yield a set of average fluorescence yields $(\bar{\omega}_X)_1, \cdots, (\bar{\omega}_X)_k$:

$$\begin{aligned}
(\bar{\omega}_X)_1 &= \sum_{i=1}^{k} (N_i^X)_1 \omega_i^X \\
(\bar{\omega}_X)_2 &= \sum_{i=1}^{k} (N_i^X)_2 \omega_i^X \\
&\vdots \\
(\bar{\omega}_X)_k &= \sum_{i=1}^{k} (N_i^X)_k \omega_i^X.
\end{aligned} \tag{1-8}$$

The set of k equations can then be solved for the k subshell fluorescence yields ω_i^X.

1.4.2. Average Fluorescence Yields in the Presence of Coster–Kronig Transitions

The equations of the preceding section cannot be applied if the primary vacancy distribution is altered by Coster–Kronig transitions before the vacancies are filled by transitions from higher shells. In accounting

[2] The superscript X, designating the major shell, may be omitted when confusion between different major shells is unlikely to arise.

for Coster–Kronig transitions, two alternative approaches can be taken:

(i) The average fluorescence yield $\bar{\omega}_X$ can be regarded as a linear combination of the subshell fluorescence yields $\omega_i{}^X$ with a vacancy distribution $V_i{}^X$ that has been altered by Coster–Kronig transitions. This method has the advantage that it leads to equations which contain the subshell fluorescence yields $\omega_i{}^X$ from the beginning, and that it corresponds closely to the actual physical situation.

(ii) The expression for the average fluorescence yield $\bar{\omega}_X$ can be regarded mathematically as a linear combination of the primary vacancy distribution $N_i{}^X$ with a set of specially defined coefficients $\nu_i{}^X$. The definition of the $\nu_i{}^X$ must be such as to account properly for the effect of Coster–Kronig transitions. This method has the advantage that it is more convenient from the experimental point of view if the primary vacancy distribution for a given experiment is known.

Both approaches have been widely used in the literature; the failure to distinguish properly between them has sometimes led to confusion. In the following paragraphs, equations according to each approach are formulated and transformation equations that relate the two alternative descriptions are developed.

Description in terms of the altered vacancy distributions $V_i{}^X$. The mean fluorescence yield of the shell X can be written as a linear combination of the subshell fluorescence yields $\omega_i{}^X$ as follows:

$$\bar{\omega}_X = \sum_{i=1}^{k} V_i{}^X \omega_i{}^X. \tag{1–9}$$

Here, in contrast to the primary vacancy distribution $N_i{}^X$ of Eq. (1–4), the coefficients $V_i{}^X$ denote the relative numbers of vacancies in the subshells X_i *including vacancies shifted to each subshell by Coster–Kronig transitions*. The quantities $V_i{}^X$ obey the relation

$$\sum_{i=1}^{k} V_i{}^X > 1. \tag{1–10}$$

This condition, in contrast to the condition (1–5) obeyed by the primary vacancy distribution $N_i{}^X$, applies because of the way in which the subshell fluorescence yields $\omega_i{}^X$ are defined. The sum of the $V_i{}^X$ exceeds unity because some of the vacancies created in subshells below X_i must be counted more than once as Coster–Kronig transitions shift them to higher subshells.

The Coster–Kronig transition probability for shifting a vacancy from a subshell X_i to a higher subshell X_j is denoted by $f_{ij}{}^X$. Accordingly, the quantities $V_i{}^X$ can be written in terms of the relative numbers $N_i{}^X$ of primary vacancies as follows:

$$\begin{aligned}
&V_1{}^X = N_1{}^X,\\
&V_2{}^X = N_2{}^X + f_{12}{}^X N_1{}^X,\\
&V_3{}^X = N_3{}^X + f_{23}{}^X N_2{}^X + (f_{13}{}^X + f_{12}{}^X f_{23}{}^X) N_1{}^X,\\
&\vdots\\
&V_k{}^X = N_k{}^X + f_{k-1,k}{}^X N_{k-1}{}^X + (f_{k-2,k-1}{}^X f_{k-1,k}{}^X) N_{k-2}{}^X\\
&\quad + \cdots + (f_{1k}{}^X + f_{12}{}^X f_{2k}{}^X + f_{12}{}^X f_{23}{}^X f_{3k}{}^X + \cdots) N_1{}^X.
\end{aligned} \tag{1–11}$$

Description in terms of the primary vacancy distribution $N_i{}^X$. Under this alternative approach, the average fluorescence yield of the shell X is expressed as

$$\bar{\omega}_X = \sum_{i=1}^{k} N_i{}^X \nu_i{}^X, \tag{1–12}$$

which is a linear combination of the relative numbers of primary vacancies $N_i{}^X$. The coefficients $\nu_i{}^X$ in this expression are especially defined to be consistent with the defining equation (1–11). A coefficient $\nu_i{}^X$ represents the total number of characteristic X-shell x rays (not necessarily from the radiative filling of a vacancy in the X_i subshell) that result per primary vacancy in the X_i subshell. This definition is quite different from the definition of the actual subshell fluorescence yield $\omega_i{}^X$, in which it is required that characteristic x rays observed must be due to transitions to the X_i subshell.[3] The products $V_i{}^X \omega_i{}^X$ and $N_i{}^X \nu_i{}^X$ are *not* equal. Only the sums of the products, shown in Eqs. (1–9) and (1–12), are both equal to the average fluorescence yield $\bar{\omega}_X$. From the physical definition of $V_i{}^X \omega_i{}^X$ it is seen that this quantity represents the number of radiative transitions from higher shells to the ith subshell per vacancy in any subshell of the entire X shell. On the other hand, the quantity $N_i{}^X \nu_i{}^X$ is the number of x rays emitted in transitions to *all* the subshells of shell X per vacancy in the ith subshell.

Transformation equations relating the two descriptions. The transformation relations between the coefficients $\nu_i{}^X$ and the subshell fluorescence yields $\omega_i{}^X$ follow from Eqs. (1–9), (1–11), and (1–12):

$$\begin{aligned}
&\nu_1{}^X = \omega_1{}^X + f_{12}{}^X \omega_2{}^X + (f_{13}{}^X + f_{12}{}^X f_{23}{}^X) \omega_3{}^X + \cdots + (f_{1k}{}^X + f_{12}{}^X f_{2k}{}^X + f_{13}{}^X f_{3k}{}^X + \cdots + f_{1,k-1}{}^X f_{k-1,k}{}^X\\
&\qquad + \text{products of 3, 4, } \cdots, (k-1)\ f_{ij}{}^X\text{'s ordered to take the vacancy from subshell 1 to subshell } k)\, \omega_k{}^X,\\
&\vdots\\
&\nu_{k-1}{}^X = \omega_{k-1}{}^X + f_{k-1,k}{}^X \omega_k{}^X,\\
&\nu_k{}^X = \omega_k{}^X.
\end{aligned} \tag{1–13}$$

[3] Listengarten (1960) has defined "fluorescence yields" $X_i \equiv V_i \omega_i$, representing the number of x-rays from the radiative filling of a vacancy in the ith subshell, per primary vacancy in any of the subshells of a given major shell. Listengarten's X_i is not used in the present paper and should not be confused with our notation in which X_i denotes the ith subshell of the major shell X.

For clarity, we specialize the general relations between the N_i^X and V_i^X and between the ν_i^X and ω_i^X for the L and M shells separately. The customary designation of the L and M subshells is illustrated in Fig. 1–1. The notation is suitable for atoms in which the j–j coupling approximation is valid.

In the L shell, initial and final vacancy distributions are related as follows:

$$\begin{aligned} V_1^L &= N_1^L, \\ V_2^L &= N_2^L + f_{12}^L N_1^L \\ V_3^L &= N_3^L + f_{23}^L N_2^L + (f_{13}^L + f_{12}^L f_{23}^L) N_1^L. \end{aligned} \tag{1–14}$$

The relations between initial and final vacancy distributions in the M shell are:

$$\begin{aligned} V_1^M &= N_1^M, \\ V_2^M &= N_2^M + f_{12}^M N_1^M, \\ V_3^M &= N_3^M + f_{23}^M N_2^M + (f_{13}^M + f_{12}^M f_{23}^M) N_1^M, \\ V_4^M &= N_4^M + f_{34}^M N_3^M + (f_{24}^M + f_{23}^M f_{34}^M) N_2^M + (f_{14}^M + f_{13}^M f_{34}^M + f_{12}^M f_{24}^M + f_{12}^M f_{23}^M f_{34}^M) N_1^M, \\ V_5^M &= N_5^M + f_{45}^M N_4^M + (f_{35}^M + f_{34}^M f_{45}^M) N_3^M + (f_{25}^M + f_{24}^M f_{45}^M + f_{23}^M f_{35}^M + f_{23}^M f_{34}^M f_{45}^M) N_2^M \\ &\quad + (f_{15}^M + f_{14}^M f_{45}^M + f_{13}^M f_{35}^M + f_{12}^M f_{25}^M + f_{13}^M f_{34}^M f_{45}^M + f_{12}^M f_{24}^M f_{45}^M + f_{12}^M f_{23}^M f_{35}^M + f_{12}^M f_{23}^M f_{34}^M f_{45}^M) N_1^M. \end{aligned} \tag{1–15}$$

The coefficients ν_i^X and the subshell fluorescence yields ω_i^X are related as follows in the L shell:

$$\begin{aligned} \nu_1^L &= \omega_1^L + f_{12}^L \omega_2^L + (f_{13}^L + f_{12}^L f_{23}^L) \omega_3^L, \\ \nu_2^L &= \omega_2^L + f_{23}^L \omega_3^L, \\ \nu_3^L &= \omega_3^L. \end{aligned} \tag{1–16}$$

In the M shell, the following relations hold between the ν_i^M and ω_i^M:

$$\begin{aligned} \nu_1^M &= \omega_1^M + f_{12}^M \omega_2^M + (f_{13}^M + f_{12}^M f_{23}^M) \omega_3^M + (f_{14}^M + f_{13}^M f_{34}^M + f_{12}^M f_{24}^M + f_{12}^M f_{23}^M f_{34}^M) \omega_4^M \\ &\quad + (f_{15}^M + f_{14}^M f_{45}^M + f_{13}^M f_{35}^M + f_{12}^M f_{25}^M + f_{13}^M f_{34}^M f_{45}^M + f_{12}^M f_{24}^M f_{45}^M + f_{12}^M f_{23}^M f_{35}^M + f_{12}^M f_{23}^M f_{34}^M f_{45}^M) \omega_5^M, \\ \nu_2^M &= \omega_2^M + f_{23}^M \omega_3^M + (f_{24}^M + f_{23}^M f_{34}^M) \omega_4^M + (f_{25}^M + f_{24}^M f_{45}^M + f_{23}^M f_{35}^M + f_{23}^M f_{34}^M f_{45}^M) \omega_5^M, \\ \nu_3^M &= \omega_3^M + f_{34}^M \omega_4^M + (f_{35}^M + f_{34}^M f_{45}^M) \omega_5^M, \\ \nu_4^M &= \omega_4^M + f_{45}^M \omega_5^M, \\ \nu_5^M &= \omega_5^M. \end{aligned} \tag{1–17}$$

The preceding equations illustrate the fact that the process of deducing individual subshell fluorescence yields ω_i^X from measurements can be very complicated. In addition to measuring the average fluorescence yields $\bar{\omega}_X$ of a shell for a sufficient number of different primary vacancy distributions, it is also necessary to know the appropriate Coster–Kronig transition probabilities. Fortunately, it is often possible to simplify conditions in an experiment so as to remove many of the complexities. For instance, it is generally possible to measure directly the fluorescence yield ω_k^X of the subshell k with the least tightly bound electrons (e.g., ω_3^L or ω_5^M), since this subshell can be ionized without creating vacancies in any of the others. Furthermore, there are certain regions of the periodic table for which some of the Coster–Kronig transition probabilities vanish, so that the pertinent equations are simplified (cf. Sec. 4).

1.4.3. Auger Yields

The fluorescence yield ω_i^X has been defined as the probability that a vacancy in the ith subshell is filled through a radiative transition. The Auger yield a_i^X is the probability that a vacancy in the ith subshell is filled through a nonradiative transition by an electron *from a higher shell*. The italicized phrase in the definition is important because Coster–Kronig transitions are *excluded* from the definition of Auger yields. It should be remembered that the Coster–Kronig yield f_{ij}^X is the probability that a vacancy in the subshell X_i is filled by an electron making a transition from a higher subshell X_j in the *same* major shell X, while the ejected electron may come from the same or a higher major shell. It can be seen from these definitions that the following relationship must hold between the Auger yield, the fluorescence yield, and the Coster–Kronig yields:

$$\omega_i^X + a_i^X + \sum_{j=i+1}^{k} f_{ij}^X = 1. \tag{1–18}$$

By analogy with the definition (1–9) of the mean fluorescence yield, the mean Auger yield $\bar{a}_X$ is defined as

$$\bar{a}_X = \sum_{i=1}^{k} V_i^X a_i^X, \tag{1–19}$$

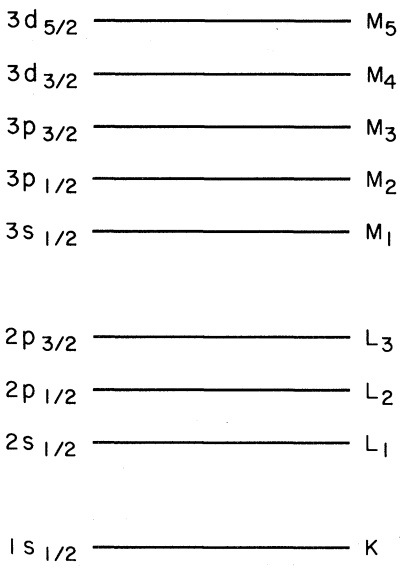

FIG. 1-1. Qualitative x-ray level diagram illustrating notation.

where the V_i^X are the altered relative vacancy numbers [Eqs. (1–11)].

The sum of the mean fluorescence yield and the mean Auger yield of a shell for the *same* initial vacancy distribution is equal to unity:

$$\bar{a}_X+\bar{\omega}_X=1. \tag{1–20}$$

1.4.4. Remarks on Notation

The notation proposed here for fluorescence yields, Auger yields, and Coster–Kronig transition probabilities is unambiguous. The notation has the following characteristics:

(i) The symbols for all average fluorescence yields carry the designation of the major shell as a subscript, consistent with past practice. Thus, ω_K is the K-shell fluorescence yield, $\bar{\omega}_L$ is the mean L-shell fluorescence yield for a given subshell vacancy distribution, and similarly for higher shells. The subscript notation for certain commonly used average fluorescence yields is retained: for example, ω_{KL} denotes the average L-shell fluorescence yield following K x-ray emission, and ω_{LM} signifies the average M-shell fluorescence yield following L x-ray emission. An analogous system is proposed for Auger yields.

(ii) The symbols for individual subshell fluorescence yields carry a subscript denoting the subshell and a superscript denoting the major shell. The subscripts are ordered such that $i=1$ denotes the most tightly bound subshell and $i=k$, the least tightly bound subshell. Thus, ω_3^M denotes the fluorescence yield of the $2p_{3/2}$ level, and a_3^M denotes the corresponding Auger yield.

(iii) The symbols for Coster–Kronig transition probabilities carry two subscripts, indicating the subshells between which the transitions occur, and a superscript denoting the major shell. Thus, f_{14}^N is the Coster–Kronig probability for an electron transition from the $4d_{3/2}$ to the $4s_{1/2}$ subshell. In order to allow for the possibility that the Coster–Kronig transition between the subshells i and j of the X shell has a small radiative component (for known cases, $f_{ij}^X(R)\ll f_{ij}^X(A)$), we introduce the symbols $f_{ij}^X(R)$ and $f_{ij}^X(A)$. Here, $f_{ij}^X(R)$ is the radiative portion of f_{ij}^X and $f_{ij}^X(A)$ is the nonradiative portion of f_{ij}^X. Consequently, we have

$$f_{ij}^X=f_{ij}^X(R)+f_{ij}^X(A). \tag{1–21}$$

(iv) The following symbols and definitions are employed for experimental quantities that frequently arise in connection with measurements of fluorescence yields:

$\Delta\Omega$	Solid angle divided by 4π
ϵ_0	Intrinsic detector efficiency (not including solid angle), i.e., detected number of photons (or particles) divided by incident number of photons (or particles)
C	Counting rate (detected number of photons or particles)
f	Attenuation factor
I	Intensity $C/(\epsilon_0 f\Delta\Omega)$
C_x	Singles x counting rate
$C_{x(y)}$	x coincidence counting rate gated by y
D	Disintegration rate.

2. THEORY

2.1. Matrix Elements

2.1.1. Radiationless Transitions—Nonrelativistic Probability

Radiationless (Auger) transitions are autoionization processes that arise from the electrostatic interaction between two electrons in an atom that initially is singly ionized in an inner shell. The basis of the quantum mechanical theory of radiationless transitions was formulated by Wentzel (1927).

The transition probability per unit time is given by the familiar formula of perturbation theory (Fermi's "Golden Rule No. 2," see, e.g., Powell and Crasemann, 1961, Sec. 11–9):

$$w_{fi}=(2\pi/\hbar)\,|\int\psi_f^*V\psi_i\,d\tau\,|^2\,\rho(E_f), \tag{2–1}$$

where ψ_f and ψ_i are the wave functions of the final and initial states, respectively, while $V=\sum_{i\neq j}(e^2/r_{ij})$, $r_{ij}=|\,\mathbf{r}_i-\mathbf{r}_j\,|$, and $\rho(E_f)$ is the density of final states for the energy E_f that satisfies conservation of energy. The expression must be summed over all possible final states.

In the simplest calculations of radiationless transition probabilities, the electrons in the unfilled shells are considered to be moving in an effective central field of

the nucleus screened by the remaining electrons in the atom (Burhop, 1952; Asaad and Burhop, 1958; Listengarten, 1960; Callan, 1961; Kostroun, Chen, and Crasemann, 1971). The central-field degeneracy is removed by the perturbations caused by the electrostatic interaction between pairs of electrons and by the coupling between spin and orbital angular momentum of each electron within an unfilled shell.

After a radiationless transition fills a single inner vacancy, an atom is left doubly ionized in other shells. The states of such nearly closed-shell configurations with two holes can be expressed in terms of completely closed-shell configurations together with the correlated two-electron configurations (Asaad and Burhop, 1958). In fact, in *LS* coupling, the electrostatic energies are the same for the two systems (Condon and Shortley, 1953, Chap. XII). The initial and final states can therefore conveniently be represented by the two-electron configurations correlated to two-hole states that consist (initially) of one inner-shell vacancy and one hole in the continuum and (finally) of two inner-shell vacancies.

The direct matrix element occurring in Eq. (2–1) then is of the form

$$D=\int\int\psi_a^*(1)\psi_b^*(2)[e^2/(|\,\mathbf{r}_1-\mathbf{r}_2\,|)]\psi_c(1)\psi_d(2)\,d\tau_1\,d\tau_2. \tag{2–2}$$

Here, ψ_b is a continuum wave function (Sec. 2.2.4), while ψ_a, ψ_c, and ψ_d are bound-state wave functions (Secs. 2.2.1–3). The one-electron wave functions of the initial and final states are assumed to be orthogonal. This assumption is justified by the small difference between the self-consistent fields of the initial and final configurations (Sachenko and Demekhin, 1967; Sachenko and Burtsev, 1967).

The exchange matrix element, proportional to the probability amplitude for the indistinguishable exchange transition ($\psi_a\rightarrow\psi_a$; $\psi_c\rightarrow\psi_b$), is

$$E=\int\int\psi_a^*(2)\psi_b^*(1)[e^2/(|\,\mathbf{r}_1-\mathbf{r}_2\,|)]\psi_c(1)\psi_d(2)\,d\tau_1\,d\tau_2. \tag{2–3}$$

The transition probability per unit time is

$$w_{fi}=(2\pi/\hbar)\,|\,D-E\,|^2\,\rho(E_f), \tag{2–4}$$

where $|\,D-E\,|$ is used because the total electron wave functions in the initial and final states must be antisymmetric.

The wave functions are conveniently normalized in a sphere of radius R_0 so large that all Auger electrons emerge virtually normal to the surface of the sphere. Except for a phase factor, the wave function then substantially approaches the form e^{ikr}/r. Therefore, the total outward flux is v/R_0 electrons per unit time, where $v=\hbar k/m$ is the electron speed. The density of final states is $\rho(E_f)=R_0(2\pi\hbar v)^{-1}$ (s wave only). Now the normalization of the continuum wave function ψ_b can be adjusted to yield one electron ejected per unit time (Oppenheimer, 1929; Gaunt, 1930); then $v/R_0=1$ and $\rho(E_f)=h^{-1}$, so that the transition probability (2–4) becomes

$$w_{fi}=(1/\hbar^2)\,|\,D-E\,|^2. \tag{2–5}$$

This formula was used by Burhop (1935) and has been used in subsequent calculations.

The total transition rate for the radiationless decay of a given excited atomic state is the properly weighted sum of the probabilities w_{fi} for all possible radiationless transitions in which angular momentum, energy, and parity are conserved (Sec. 2.3.2).

2.1.2. Radiationless Transitions—Relativistic Probability

If radiationless transitions are treated as a two-electron problem within the framework of relativistic single-particle theory, their probability amplitude is given by the Møller formula (Møller, 1931; Rose, 1961, Sec. 36), a relativistically invariant expression that includes the effects of retardation and spin–spin interaction. In this formulation, the transition probability amplitude to first order in $\alpha=e^2/\hbar c$ (Born approximation) is

$$H_{fi}=e^2\int\int\psi_f^*(2)\psi_f^*(1)(1-\boldsymbol{\alpha}_1\cdot\boldsymbol{\alpha}_2)\times(e^{ikR}/R)\psi_i(2)\psi_i(1)\,d\tau_1\,d\tau_2. \tag{2–6}$$

Here, $\psi(1)$ and $\psi(2)$ are the time-independent parts of the four-component wave functions that describe the two electrons in their respective states in a central Coulomb field. The vector Dirac matrix operators $\boldsymbol{\alpha}_1$ and $\boldsymbol{\alpha}_2$ operate on the wave functions of electrons 1 and 2, respectively. The distance between the two electrons is denoted by R, and the units are such that $m_e=c=\hbar=1$. The first term expresses the Coulomb repulsion between the two electrons, while the second is the relativistic current–current interaction. The retardation is expressed through the scalar Green's function $(\exp ikR)/R$, where $k=\omega/c=(W_i-W_f)/\hbar c$ is the wave number of the photon that would be emitted in the corresponding radiative transition. The retardation term has a negligible effect on the interaction matrix element when the radii of the affected atomic shells are small compared with the wavelength $\lambda=2\pi/k$, as is ordinarily the case (Heitler, 1954, Sec. 17; Chattarji and Talukdar, 1968).

If the time-independent parts of the charge density and current vector are denoted by ρ and $\mathbf{j}$, respectively, the probability for the direct transition is

$$(1/\hbar^2)\,|\,D\,|^2=|\,(e/\hbar)\int\int(e^{ikR}/R)(\rho_1\rho_2-\mathbf{j}_1\cdot\mathbf{j}_2)\,d\tau_1\,d\tau_2\,|^2. \tag{2–7}$$

The exchange transition probability $\hbar^{-2}\,|\,E\,|^2$ is given by an analogous expression with the final electron states interchanged. The total transition probability

per unit time is

$$w_{fi}=\hbar^{-2}\,|\,D-E\,|^2. \tag{2-8}$$

Once again, as in Eq. (2-4), using $|\,D-E\,|$ in the matrix element is equivalent to antisymmetrizing all the wave functions.

All published relativistic Auger transition-probability calculations of which we are aware have been carried out on the basis of this *ansatz* (Massey and Burhop, 1936; Asaad, 1959; Listengarten, 1961, 1962; Chattarji and Talukdar, 1968; and Bhalla, Rosner, and Ramsdale, 1970d).

2.1.3. Radiative Transition Probabilities

Clear discussions of radiative transitions in terms of multipole fields have been provided by Shore and Menzel (1968) and Moszkowski (1965), among others. Approaches to relativistic calculations of radiative transition rates have recently been reviewed by Scofield (1969). Comprehensive discussions of the subject are found in the classical treatises by Condon and Shortley (1953) and Heitler (1954). A treatment of the problem of spontaneous radiative transitions between stationary states of an electron in terms of the general S-matrix theory in quantum electrodynamics is given by Jauch and Rohrlich (1955, Sec. 15-5). Electric dipole radiation from atoms and diatomic molecules has been reviewed by Nicholls and Stewart (1962), while forbidden transitions of interest in atomic and molecular spectroscopy are discussed in a companion article by Garstang (1962).

When the multipole expansion is used, the relativistic expression for the spontaneous radiative transition probability is

$$w_{fi}=4\pi^2\alpha\omega\sum_{L=1}^{\infty}\sum_{M=-L}^{L}\{|\int\psi_f^*[\boldsymbol{\alpha}\cdot\mathbf{A}_L{}^M(m)]\psi_i\,d\tau\,|^2 + |\int\psi_f^*[\boldsymbol{\alpha}\cdot\mathbf{A}_L{}^M(e)]\psi_i\,d\tau\,|^2\}. \tag{2-9}$$

Here, w_{fi} is in quanta per second, α is the fine structure constant, ω is the circular frequency of the emitted radiation, and $\boldsymbol{\alpha}$ is the Dirac matrix for the electron undergoing the transition from state ψ_i to state ψ_f. The units are such that $\hbar=c=m_e=1$.

The terms in the multipole expansion of the vector potential of the emitted wave are (Rose, 1955; Scofield, 1969)

$$\mathbf{A}_L{}^M(m)=i(2/\pi)^{1/2}j_L(kr)[L(L+1)]^{-1/2}\mathbf{L}Y_L{}^M(\hat{\mathbf{r}}) \tag{2-10}$$

and

$$\mathbf{A}_L{}^M(e)=(2/\pi)^{1/2}k^{-1}[L(L+1)]^{-1/2}\boldsymbol{\nabla}\times\mathbf{L}j_L(kr)Y_L{}^M(\hat{\mathbf{r}}), \tag{2-11}$$

where $\mathbf{L}=-i\mathbf{r}\times\boldsymbol{\nabla}$ and $Y_L{}^M$ is a spherical harmonic.

In a spherically symmetric potential, the transition rate between single-particle electron states can be expressed in terms of the radial wave functions (Rose, 1955). The result of averaging over magnetic quantum numbers of the final state (Babushkin, 1964, 1965, 1967; Scofield, 1969) is

$$w_{fi}=2\alpha\omega^2\sum_L[f_L(m)+f_L(e)], \tag{2-12}$$

where

$$f_L(m)=\omega^{-1}B(-\kappa_i,\kappa_f,L)R_L{}^2(m), \tag{2-13a}$$

$$f_L(e)=\omega^{-1}B(\kappa_i,\kappa_f,L)R_L{}^2(e), \tag{2-13b}$$

and

$$B(\kappa_i,\kappa_f,L)=\{(2l_i+1)(2l_f+1)/[L(L+1)]\}\times C^2(l_i,l_f,L;O,O)W^2[j_il_ij_fl_f;(1/2)L]. \tag{2-14}$$

The quantum numbers κ_i and κ_f characterize the initial and final angular-momentum states, according to the definition (Bethe and Salpeter, 1957, Sec. 14),

$$\kappa=-[j+(1/2)]=-(l+1)\quad\text{if}\quad j=l+(1/2)$$
$$\kappa=+[j+(1/2)]=+l\quad\text{if}\quad j=l-(1/2) \tag{2-15}$$

so that

$$j=|\,\kappa\,|-(1/2),\qquad l=\kappa\quad\text{if}\quad\kappa>0$$
$$l=-\kappa-1\quad\text{if}\quad\kappa<0. \tag{2-16}$$

The function $B(\kappa_i,\kappa_f,L)$ vanishes unless $J=L+l_i+l_f$ is even and L,j_i,j_f form a triangle, in which case the C coefficient (Rose, 1955, Appendix B) has the value

$$C^2(l_i,l_f,L;0,0)=[(2L+1)(J-2L)!(J-2l_i)!(J-2l_f)!]/(J+1)!\times\{(J/2)!/[(J/2-L)!(J/2-l_i)!(J/2-l_f)!]\}^2, \tag{2-17}$$

and the Racah coefficient is

$$W^2[j_il_ij_fl_f;(1/2)L]=\left|\frac{(L+\kappa_i+\kappa_f+1)(\kappa_i+\kappa_f-L)}{4\kappa_i\kappa_f(2\kappa_i+1)(2\kappa_f+1)}\right|. \tag{2-18}$$

The radial matrix elements are

$$R_L(m)=(\kappa_i+\kappa_f)\int j_L(kr)(F_fG_i+G_fF_i)\,dr \tag{2-19}$$

and

$$R_L(e)=\int\{j_{L-1}(kr)\times[(\kappa_f-\kappa_i)(F_fG_i+G_fF_i)+L(FG_i-G_fF_i)+L(G_fG_i+F_fF_i)j_L(kr)\}dr \tag{2-20a}$$

$$R_L(e)=\int(1/kr)\{(F_fG_i-G_fF_i)L(L+1)j_L(kr)+(\kappa_f-\kappa_i)(F_fG_i+G_fF_i)[r(d/dr)+1]j_L(kr)\}\,dr. \tag{2-20b}$$

The radial Dirac eigenfunctions F and G are solutions of the equations

$$[(d/dr)+(\kappa/r)]G=(E-V+1)F, \quad (2\text{–}21a)$$

$$[-(d/dr)+(\kappa/r)]F=(E-V-1)G; \quad (2\text{–}21b)$$

they include a factor r and are normalized to satisfy the relation

$$\int(F^2+G^2)\,dr=1. \quad (2\text{–}22)$$

2.2. Wave Functions

2.2.1. Nonrelativistic Hydrogenic Bound-State Wave Functions; Screening

In a first approximation, the electrons in bound states are represented by single-particle wave functions in a point Coulomb potential (Burhop, 1935; Callan, 1961; Kostroun, *et al.*, 1971). These hydrogenic wave functions (discussed, e.g., by Bethe and Salpeter, 1957, Chap. 1) are of the form

$$\psi_{nlm}(r,\theta,\phi)=R_{nl}(r)Y_{lm}(\theta,\phi). \quad (2\text{–}23)$$

The principal, orbital angular momentum, and magnetic quantum numbers are n, l, and m, respectively; and Y_{lm} is a spherical harmonic. The radial eigenfunction is

$$R_{nl}(r)=A_{nl}\exp[-(Z/na)r]r^l\sum_{s=0}^{n-l-1}B_{nls}r^s, \quad (2\text{–}24)$$

where

$$B_{nls}=(-)^{s+1}\times\{[(n+l)!]^2/(2l+1+s)!s!(n-1-l-s)!\}\times(2Z/na)^s, \quad (2\text{–}25)$$

and

$$A_{nl}=-\{(n-l-1)!/2n[(n+l)!]^3\}^{1/2}\times(2Z/na)^{l+(3/2)}. \quad (2\text{–}26)$$

Here, $a=\hbar^2/me^2$ is the Bohr radius.

The wave functions (2–23) are the exact nonrelativistic result for a single electron bound in the field of a point charge $+Ze$. The wave functions approximately describe a single electron outside a closed atomic shell, or a hole in an otherwise filled shell, insofar as the field can be assumed to be effectively central and Z is replaced by an appropriate effective charge $Z^*=Z-\sigma$. The calculation of radiationless transition probabilities (and of analogous phenomena, such as the photoelectric effect) is simplified very much if the analytic hydrogenic wave functions can be used.

The choice of the screening constant σ is of critical importance. The problem has been discussed in general by Hartree (1957, Chap. 7) and in the present context by Callan (1961, 1963c) and Kostroun *et al.* (1971). In the Hartree recipe, the screening constant is derived from the ratio of the mean hydrogenic radius $\bar{r}_H$ to the mean radius $\bar{r}$ from a more realistic wave function:

$$\sigma=Z-\bar{r}_H/\bar{r}. \quad (2\text{–}27)$$

For this purpose, $\bar{r}$ is found from suitable self-consistent field (SCF) wave functions; considerably different results follow from the SCF wave functions used by different authors (Callan, 1963c). Effective charges Z^* derived from SCF wave functions of Löwdin and Appel (1956) have been tabulated by Callan (1963a) for the $2s$, $2p$, and $3d$ shells of atoms with $Z=21$ to 50, 74 to 80, 85, and 90. Best results, at least for the purpose of calculating K- and L-shell fluorescence yields, apparently are obtained if Z^* for bound states is evaluated (Kostroun *et al.*, 1971) through the recipe (2–27) with $\bar{r}$ as computed by Froese (1966).

A different approach to the evaluation of screening constants is sometimes taken in calculations of nuclear internal conversion coefficients, which in some features resemble the present problem. Here, σ is chosen so that a point nucleus of charge $Z^*=Z-\sigma$ binds a single hydrogenic electron in the state (n, l) with the same binding energy that is observed for an electron in the corresponding state in the actual atom of nuclear charge Z (see, e.g., O'Connell and Carroll, 1966). The screening constants determined by this method are much larger than those obtained from Slater's recipe.

It should be noted that the wave function for a bound state with small principal quantum number n is concentrated in a relatively small range of the radial distance r in the neighborhood of the mean radius $\bar{r}$. Over this small range, the radial dependence $\sim r^{-1}$ of the effective hydrogenic potential can be expected to differ not too much from the actual potential experienced by the electron in a real atom, especially if Z is large. On the other hand, the radial eigenfunction of an electron with large n is much more spread out in r, and the hydrogenic approximation differs substantially from more realistic wave functions, particularly in the location of the nodes (see Fig. 2–1). Radiationless transition amplitudes, which depend on the overlap of various bound-state and continuum wave functions, are sensitive to the details of the functions used and can be severely affected by this discrepancy. Thus, measurements of radiationless transitions constitute a sensitive means for testing atomic wave functions. [For a discussion of this problem in relation to photoionization, see Fano and Cooper (1968).]

Screened hydrogenic wave functions are not necessarily orthogonal because the screening constant σ depends on the quantum numbers n and l. This lack of orthogonality has been disregarded by some authors (Massey and Burhop, 1936; Callan, 1961) while others have attempted to avoid the difficulty through the use of a single effective charge Z^*, equal to the geometric mean of charges appropriate to various shells that enter into the problem (Asaad and Burhop, 1958). The difficulty is inherent in the single-electron wave function approach.

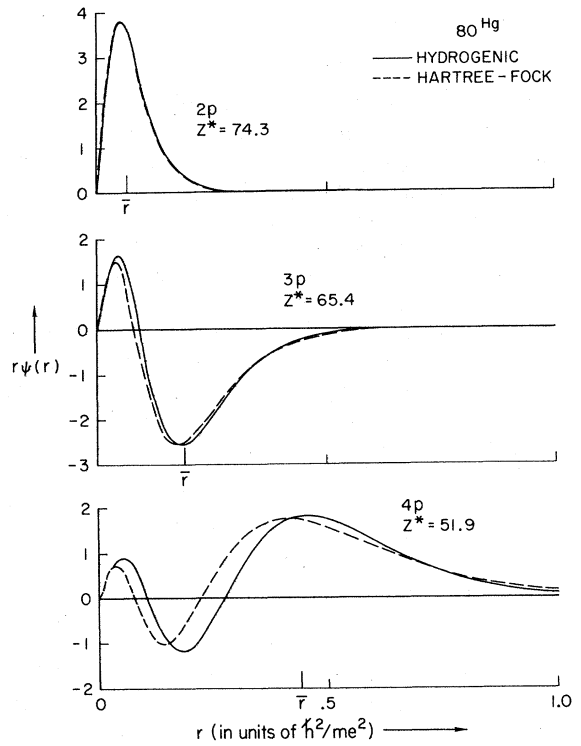

FIG. 2–1. Comparison of hydrogenic and Hartree–Fock $l=1$ radial eigenfunctions for mercury. The effective charge for the hydrogenic wave functions has been computed according to Hartree [Eq. 2–27)]. The mean SCF radii $\bar{r}$ and the Hartree–Fock wave functions are those of Mann (1968). [From Chen, Crasemann, and Kostroun (1971a), courtesy of American Institute of Physics.]

2.2.2. *Analytic Relativistic Wave Functions*

A Dirac electron of energy W in a Coulomb field $V=-Ze^2/r$ is described by

$$\psi_\kappa{}^\mu=\begin{pmatrix} g_\kappa(r)\chi_\kappa{}^\mu(\hat{r}) \\ if_\kappa(r)\chi_{-\kappa}{}^\mu(\hat{r}) \end{pmatrix}, \tag{2–28}$$

where the radial functions $u_1=rg(r)$ and $u_2=rf(r)$ satisfy the equations

$$du_1/dr=-(\kappa u_1/r)+[W+1+(\zeta/r)]u_2$$
$$du_2/dr=-[W-1+(\zeta/r)]u_1+(\kappa u_2/r). \tag{2–29}$$

Here, $\zeta=e^2Z=\alpha Z<1$ in relativistic units ($\hbar=c=m_e=1$); $\kappa=\mp[j+(1/2)]$ for $j=l\pm(1/2)$ [Eq. (2–15)] and μ is the eigenvalue of j_z.

Solutions of Eqs. (2–29) are discussed in the treatises of Bethe and Salpeter (1957, Sec. 14) and of Rose (1961, Chap. V) and are given explicitly for $1s$, $2s$, $2p_{1/2}$, and $2p_{3/2}$ bound states and for the continuum by Massey and Burhop (1936).

Unscreened relativistic hydrogenic wave functions have been used by Asaad (1967) to compute radial matrix elements (Slater integrals) for K- and L-shell radiationless transitions. The wave functions were expanded after the method of Layzer and Bahcall. The integrals could be put in the form $AZ(1+\alpha Z^2)$, the factor $(1+\alpha Z^2)$ taking account of relativistic effects.

Asaad (1960) has also applied the variational principle to obtain the Dirac wave functions of the K electrons of heavy atoms. Parameters were included to take account of Coulomb and spin–spin interactions and of the effect of the rest of the atom. The result can be interpreted to justify the use of screened hydrogenic wave functions, although the screening constant is somewhat larger than that given by Slater's rules.

An interesting approach in relativistic calculations of radiationless transition probabilities and related effects has been employed by Chattarji and Talukdar (1968) and by Talukdar and Chattarji (1970), who used screened Coulomb electronic wave functions, which are solutions of the Biedenharn symmetric Dirac–Coulomb Hamiltonian (Biedenharn and Swamy, 1964). This is a relativistic Hamiltonian having symmetry so that the radial parts of the spinor components of its solutions are formally nonrelativistic. The solutions form a complete canonical basis, unlike some other approximations, and their close correspondence to the nonrelativistic problem permits the use of many well-known results. The Biedenharn Hamiltonian differs from the exact Dirac–Coulomb Hamiltonian by a precisely known fine-structure term, so that no physical uncertainties result from its use. Substantial computational simplification is obtained from this approach. Large relativistic effects in $L_1-L_2M_{4,5}$ Coster–Kronig transitions at $32\leq Z\leq 41$, predicted by the calculations of Talukdar and Chattarji (1970), clearly need further investigation.

2.2.3. *Numerical Wave Functions*

Numerical integration of the wave equation permits the use of more realistic potentials at the expense of computational effort and a certain loss of elegance. Because electronic computers are virtually indispensable for this approach to the calculation of Auger transition probabilities, it was not until 1955 that Rubenstein and Snyder (1955a), using the University of Illinois ILLIAC digital computer, were able to carry out self-consistent-field calculations by the Hartree method without exchange. Asaad (1959) employed relativistic wave functions found by numerically integrating the pair of coupled Dirac differential equations (2–29) that contained a modified form of the Hartree-and-Hartree self-consistent-field electrostatic potential in place of the Coulomb point-charge potential. Listengarten (1961, 1962) used relativistic wave functions found by numerical solution of the system of Dirac radial differential equations for the statistical Thomas–Fermi–Dirac atom.

Mehlhorn (1968) very successfully used the numeri-

cal nonrelativistic Hartree-Slater wave functions for Ar ions computed by Herman and Skillman (1963). A relativistic version of the Herman-and-Skillman SCF wave functions, using a local approximation for exchange, has been introduced by Liberman, Waber, and Cromer (1965) and improved by Cowan *et al.* (1966); the potential of the earlier version was used by Scofield (1969) to calculate radiative transition rates. More recently, Bhalla and co-workers (1970a–f) computed K-shell Auger transition rates and fluorescence yields from relativistic Hartree–Slater wave functions.

The influence of chemical binding on the energy of K–LL Auger electrons from S, Si, and Al has been investigated by Coulson and Gianturco (1968) on the basis of nonrelativistic SCF wave functions. Changes in K and L fluorescence yields for various defect atomic configurations have been explored by Larkins (1971) for argon; the effect of multiple atomic vacancies was evaluated through a statistical weighting procedure.

An interesting approach was taken by McGuire (1969a, 1970a, 1971a, b): He computed radiationless and radiative transition probabilities to the K and L shells by first calculating the quantity $-rV(r)$ for ions through the approach of Herman and Skillman (1963). Then making a straight-line approximation to $-rV(r)$, he obtained a one-electron Schrödinger equation that could be solved exactly in terms of Whittaker functions for the radial part.

2.2.4. *Continuum Wave Functions*

If the nuclear charge is neglected, the ejected positive-energy electron with orbital angular momentum $l\hbar$ is described nonrelativistically by the free-particle wave function

$$\psi_{\infty l}=2(km/\hbar)^{1/2}(1/kr)f_e(kr), \qquad (2\text{–}30)$$

where

$$f_e(kr)=(\pi kr/2)^{1/2}J_{l+(1/2)}(kr), \qquad (2\text{–}31)$$

and $J_{l+1/2}(kr)$ is the ordinary Bessel function of half-integer order.

The solution of the Schrödinger equation in the Coulomb potential of an effective point charge Z^*e, normalized to represent one electron ejected per unit time [so that Eq. (2–5) for the transition probability applies] is the *Gordon wave function* (Gordon, 1928; Gaunt, 1930),

$$\psi_{\infty l}=(m/\hbar)^{1/2}[2^{l+1}/(2l+1)!]\times\exp[\pi Z^*/(2k)]k^{l+1/2}\times|\Gamma[l+1+(iZ^*/k)]|\,r^l e^{-ikr}\times{}_1F_1[l+1+(iZ^*/k);\,2l+2;\,2ikr]\times Y_{lm}(\theta,\phi), \qquad (2\text{–}32)$$

where ${}_1F_1(a;\,b;\,c)$ is the confluent hypergeometric function, and k is the wave number of the ejected electron. Since the work of Burhop (1935), this result has been used in most nonrelativistic calculations of radiationless transition probabilities employing analytic wave functions.

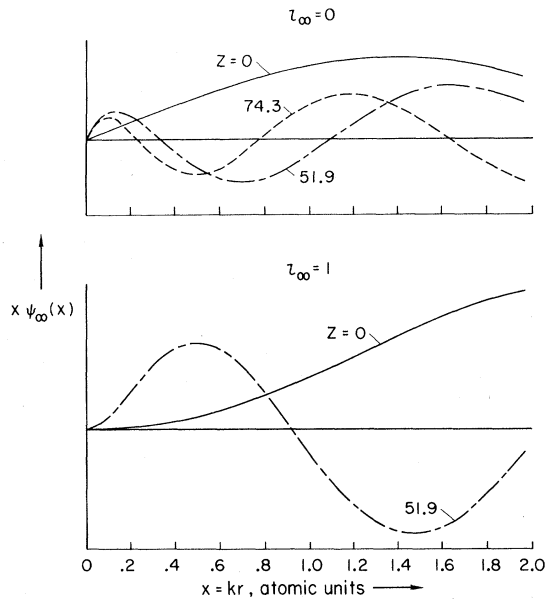

FIG. 2–2. Radial wave functions for s and p continuum electrons in the Coulomb field of an effective point charge Ze.

Screening of the continuum wave function greatly affects the radiationless transition probabilities. It is difficult to select an appropriate effective charge for the continuum electron that sees a steadily decreasing charge as it moves away from the nucleus. Kostroun, Chen, and Crasemann (1971) have shown that results can be obtained that agree very closely with experiment if Z^* in the continuum wave function is taken to be the geometric mean of the effective charge appropriate to the state from which the continuum electron originates and the effective charge pertaining to the next higher state. Thus, for the $K-L_{23}M_{23}$ transition, for example, the effective charge in the continuum wave function is taken to be $[Z^*(3p)\cdot Z^*(3d)]^{1/2}$ for the direct and $[Z^*(2p)Z^*(3s)]^{1/2}$ for the exchange matrix element. The effective charges $Z^*(n,\,l)$ are computed according to Hartree's recipe, Eq. (2–27), with SCF mean radii from Froese (1966).

The Coulomb continuum wave function (2–32) reduces, of course, to the function (2–30) in the limit $Z^*\to 0$; but for realistic effective charges, it differs very much from the free-particle solution in the region where the bound-state electronic wave functions are appreciable, the attractive Coulomb potential shortening the wavelength near the origin. This effect is illustrated in Fig. 2–2.

Coulomb continuum wave functions of the type given by Eq. (2–32) (Bethe and Salpeter, 1957, Sec. 4; Hull and Breit, 1957) generally contain confluent hypergeometric functions that lead to matrix elements in terms of ordinary hypergeometric functions of com-

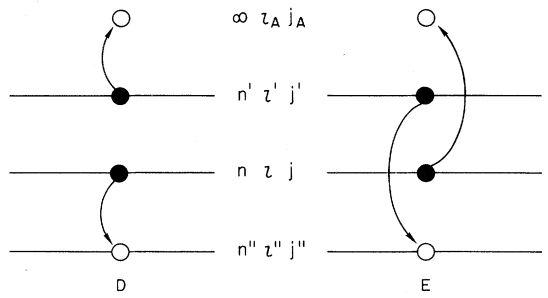

FIG. 2–3. Schematic representation of the direct (D) and exchange (E) Auger process, showing the notation for the principal, orbital-angular-momentum, and total-angular-momentum quantum numbers that characterize the pertinent electron states.

plex arguments (Sec. 2.3.1). To avoid tedious and complicated series expansions subject to truncation errors in the evaluation of these functions, Callan, Nikolai, and McDavid (1964) developed an elegant matrix method for simultaneously computing a number of the hypergeometric functions without truncation error. The required hypergeometric functions of complex arguments can also be constructed (Kostroun, Chen, and Crasemann, 1971) with the aid of Gauss' relations for contiguous functions (Abramowitz and Stegun, 1964, Chap. 15).

A useful form of the nonrelativistic Coulomb continuum wave function has been derived by Yost, Wheeler, and Breit (1936) and Breit and Yost (1935a, b) and employed in unpublished calculations by G. D. Archard (quoted by Asaad, 1965b, and by Mehlhorn and Asaad, 1966).

Numerical continuum wave functions have been used in some transition-rate calculations since the work of Rubenstein (1955a). Asaad (1959) asymptotically fitted numerical continuum wave functions for the Hartree–Hartree potential to an analytic relativistic free-particle solution to solve the problem of normalization to unit outgoing flux. Listengarten (1961, 1962) has calculated continuum wave functions by numerical integration of the relativistic wave equations with the Thomas–Fermi–Dirac atomic potential.

Continuum wave functions based on the best current SCF potentials, such as those of Mann (1968) and Froese (1966), have not yet been computed for use in calculations of radiationless transition probabilities. Much may be gained in future calculations by use of such functions or of numerical continuum functions based on local approximations for exchange (Cowan *et al.*, 1966).

2.3. Calculation of Radiationless Transition Probabilities

2.3.1. Evaluation of Radial Matrix Elements

Separation of the matrix element (2–2)

$$\int\int \psi_a^* \psi_b^* (e^2/r_{12}) \psi_c \psi_d \, d\tau_1 \, d\tau_2 \qquad (2\text{–}33)$$

into radial and angular factors is accomplished by expressing the Coulomb interaction potential in terms of scalar products of irreducible tensor operators (Condon and Shortley, 1953; de-Shalit and Talmi, 1963, Chap. 19–21; Kostroun, Chen, and Crasemann, 1971),

$$1/r_{12} = \sum_{\nu,\sigma} \gamma_\nu(r_1, r_2) C_{\nu\sigma}^*(\Omega_1) \cdot C_{\nu\sigma}(\Omega_2), \qquad (2\text{–}34)$$

where

$$\gamma_\nu(r_1, r_2) = r_1^\nu / r_2^{\nu+1}, \quad r_1 < r_2$$
$$= r_2^\nu / r_1^{\nu+1}, \quad r_2 < r_1 \qquad (2\text{–}35)$$

$$C_{\nu\sigma} = [4\pi/(2\nu+1)]^{1/2} Y_{\nu\sigma}(\Omega), \qquad (2\text{–}36)$$

the $Y_{\nu\sigma}$ being spherical harmonics.

The direct radial matrix elements then are of the form

$$\{(n''l'') \mid (nl)(n'l'), \nu, l_A\} = e^2 \iint_{r_1, r_2=0}^{\infty} \gamma_\nu R_{n''l''}(r_1) R_{nl}(r_1) R_{n'l'}(r_2) \times R_{\infty}{}^{l_A}(r_2) r_1^2 r_2^2 \, dr_1 \, dr_2. \qquad (2\text{–}37)$$

Here, the R's are radial wave functions that describe states characterized by the following principal and angular-momentum quantum numbers (Fig. 2–3):

$n''l''$	bound-state electron that is initially missing,
nl	electron that fills the initial vacancy,
$n'l'$	initial bound state of electron that is ejected,
∞l_A	positive-energy state of ejected electron.

Thus, for an L_1–$L_{2,3}M_{4,5}$ Coster–Kronig transition, $n''=2$, $l''=0$; $n=2$, $l=1$; $n'=3$, $l'=2$. The notation is essentially that of Asaad and Burhop (1958), which has become customary in the field. The quantum numbers $n''l''$ are often suppressed when there is no chance for confusion.

With nonrelativistic hydrogenic bound-state wave functions (Sec. 2.2.1) and the Gordon continuum wave function (Sec. 2.2.4), the radial matrix element (2–37) becomes (Kostroun *et al.*, 1971):

$$\{(n''l'') \mid (nl)(n'l'), \nu, l_A\} = (e^2/\hbar^2)(m/\hbar)^{1/2} A_{n''l''} A_{n'l'} A_{nl} \times \sum_{s''=0}^{n''-l''-1} \sum_{s'=0}^{n'-l'-1} \sum_{s=0}^{n-l-1} B_{n''l''s''} B_{n'l's'} B_{nls} \left\{ \frac{(l''+s''+l+s+2+\nu)!}{[(1/2)(c_1+c_2)]^{l''+s''+l+s+3+\nu}} \int_0^\infty \exp[-\tfrac{1}{2}c_3 x] x^{l'+s'+1-\nu} Q(x, \eta, l_A) \, dx - (l''+s''+l+s+2+\nu)! \sum_{j=1}^{l''+s''+l+s+3+\nu} \frac{\int_0^\infty \exp\{-[(c_1+c_2+c_3)/2]x\} x^{l''+s''+l'+s'+l+s+4-j} Q(x, \eta, l_A) \, dx}{[(1/2)(c_1+c_2)]^j (l''+s''+l+s+3+\nu-j)!} + (l''+s''+l+s+1-\nu)! \sum_{j=1}^{l''+s''+s+2-\nu} \frac{\int_0^\infty \exp\{-[(c_1+c_2+c_3)/2]x\} x^{l''+s''+l'+s'+l+s+4-j} Q(x, \eta, l_A) \, dx}{[(1/2)(c_1+c_2)]^j (l''+s''+l+s+2-\nu-j)!} \right\}, \qquad (2\text{–}38)$$

where

$$A_{nl}=-\{(n-l-1)!/2n[(n+l)!]^3\}^{1/2}(2Z/na\kappa)^{l+3/2},$$
$$B_{nls}=(-)^{s+1}\{[(n+l)!]^2/(2l+1+s)!s!(n-1-l-s)!\}(2Z/na\kappa)^s,$$
$$x=\kappa r, \qquad \kappa=[(E_{n''}-E_n-E_{n'})/13.602]^{1/2}, \qquad E \text{ in eV},$$
$$c_1=2Z''/n''a\kappa, \qquad c_2=2Z/na\kappa, \qquad c_3=2Z'/n'a\kappa, \qquad \eta=Z'/\kappa. \tag{2-39}$$

The Z's are effective charges, and the E's absolute values of the binding energies in the respective states, while a is the Bohr radius. The function Q, which occurs in the continuum wave function, is defined as

$$Q(x,\eta,l_A)\equiv[2^{l_A+1}/(2l_A+1)!]e^{\pi\eta/2}\,|\,\Gamma(l_A+1+i\eta)\,|\,\times x^{l_A}e^{-ix}{}_1F_1(l_A+1+i\eta;\,2l_A+2;\,2ix). \tag{2-40}$$

The integrals in Eq. (2–38), involving the confluent hypergeometric function ${}_1F_1(a;\,b;\,cx)$, can be evaluated analytically:

$$\int_0^\infty e^{-qx}x^pQ(x,\eta,l_A)\,dx=[2^{l_A+1}/(2l_A+1)]e^{\pi\eta/2}\,|\,\Gamma(l_A+1+i\eta)\,|\,[(p+l_A)!/(i+q)^{p+l_A+1}]$$
$$\times{}_2F_1[l_A+1+i\eta,\,p+l_A+1;\,2l_A+2;\,2i/(i+q)]. \tag{2-41}$$

The following general result is found for the radial matrix element:

$$\{(n''l'')\,|\,(nl)(n'l'),\nu,l_A\}=A_{n''l''}A_{n'l'}A_{nl}\sum_{s''=0}^{n''-l''-1}\sum_{s'=0}^{n'-l'-1}\sum_{s=0}^{n-l-1}B_{n''l''s''}B_{n'l's'}B_{nls}\left\{\frac{(l''+s''+l+s+2+\nu)!}{[(1/2)(c_1+c_2)]^{l''+s''+l+s+3+\nu}}\right.$$
$$\times P(l',s',l_A)-(l''+s''+l+s+2+\nu)!\sum_{j=1}^{l''+s''+l+s+3+\nu}\frac{P_j}{[(1/2)(c_1+c_2)]^j(l''+s''+l+s+3+\nu-j)!}$$
$$\left.+(l''+s''+l+s+1-\nu)!\sum_{j=1}^{l''+s''+l+s+2-\nu}\frac{P_j}{[(1/2)(c_1+c_2)]^j(l''+s''+l+s+2-\nu-j)!}\right\}, \tag{2-42}$$

where

$$P(l',s',l_A)=G(l_A,\eta)\{(l'+s'+l_A+1-\nu)!/(1/2)(c_3+i)^{l'+s'+l_A+2-\nu}\}$$
$$\times{}_2F_1\{l_A+1+i\eta,\,l'+s'+l_A+2-\nu;\,2l_A+2;\,2i/[(1/2)c_3+i]\}, \tag{2-43}$$
$$P_j=G(l_A,\eta)\{(l''+s''+l'+s'+l+s+l_A+4-j)!/[(1/2)(c_1+c_2+c_3)+i]^{l''+s''+l'+s'+l+s+l_A+5-j}\}$$
$$\times{}_2F_1(l_A+1+i\eta,\,l''+s''+l'+s'+l+s+l_A+5-j;\,2l_A+2;\,2i/[(1/2)(c_1+c_2+c_3)+i]), \tag{2-44}$$
$$G(l_A,\eta)=[2^{l_A+1}/(2l_A+1)!]e^{\pi\eta/2}\,|\,\Gamma(l_A+1+i\eta)\,|. \tag{2-45}$$

The remaining symbols in Eq. (2–42) have been defined earlier in this section. The expression is given in atomic units ($e=\hbar=m=1$), summarized here for convenience (Taylor, Parker, and Langenberg, 1969):

Atomic unit of length: $\hbar^2/me^2=0.52918\times10^{-8}$ cm (Bohr radius);

Atomic unit of time: $\hbar^3/me^4=2.4189\times10^{-17}$ sec (reciprocal of the circular frequency of the electron in the first Bohr orbit of hydrogen);

Atomic unit of energy: $me^4/\hbar^2=4.3598\times10^{-11}$ erg = 27.212 eV (potential energy of the electron in the first Bohr orbit, or twice the ground-state ionization energy of hydrogen).

The accuracy of the transition amplitude (2–42) is limited by the approximations implied in the use of hydrogenic wave functions and the neglect of relativity. In Sec. 2.2.3, reference is made to several calculations aimed at removing these limitations; such calculations usually involve numerical integrations and then do not yield analytical expressions for matrix elements.

A further limitation of the above approach to the calculation of radiationless transition amplitudes lies in the use of one-electron wave functions and the neglect of electron–electron correlations. A calculation with antisymmetric *two*-electron wave functions in j–j coupling, using second quantization, has recently been set up by Gautier (1969). An attempt to include the effect of electron correlation, using unrestricted Hartree–Fock wave functions, is being initiated by Callan (1969) and his group. Configuration interaction has been included in the calculations of Asaad (1965b) and of Mehlhorn and Asaad (1966) for light elements.

2.3.2. Representations: Coupling Schemes

Evaluation of the angular factors in the matrix elements (2–33) depends upon a choice of the appropiate angular-momentum coupling scheme. If spin–orbit coupling is neglected, the initial and final two-hole

states of the atom can be expressed for different values of the total angular momentum J in the (LSJM) representation of Russell–Saunders coupling. For the heavier atoms, this is not a good approximation because the spin–orbit interaction outweighs the electrostatic interaction, and inner-shell electron states are described more realistically by j–j rather than LS coupling. If one is interested in the relative intensities of the various radiationless transitions leading to a given final-state configuration, as in Auger-electron spectroscopy, it is important to choose the appropriate coupling scheme for each range of atomic numbers. Thus, calculations have been carried out in LS coupling (Rubenstein, 1955a; Callan, 1961; Kostroun, *et al.*, 1971), extreme j–j coupling (Asaad, 1959; Listengarten, 1961, 1962; Gautier, 1969; Chen, Crasemann, and Kostroun, 1971), and intermediate coupling (Asaad and Burhop, 1958; Mehlhorn, 1968). Asaad and Mehlhorn (1968) have even used a scheme in which the original inner-shell vacancy is described in j–j notation, and the final double vacancy in Russell–Saunders coupling; from this approach, expressions for line intensities in the L_2–MM and L_3–MM Auger-electron spectra were calculated in terms of radial integrals. However, if the purpose of the calculation is merely to determine the *total* radiationless transition probability in a certain final-state configuration, regardless of the term, to determine fluorescence yields, the choice of coupling scheme is immaterial as long as the initial vacancy is not in the final configuration. The total transition rate then is independent of the coupling, the wave functions in the various schemes being related by unitary transformations (Rubenstein, 1955a). An explicit formula relating radiationless transition probabilities in LS and in j–j coupling has been derived by Kostroun *et al.* (1971), who also identify the special class of X–XY type transitions for which LS and j–j coupling cannot be used interchangeably.

To simplify the present discussion, we restrict ourselves to LS coupling and follow the work of Kostroun (1968) and of Kostroun *et al.* (1971).

In ($LSJM$) representation, the antisymmetrized and properly normalized two-particle wave functions are of the form (de-Shalit and Talmi, 1963, Chaps. 19–21)

$$\psi_A(n_a l_a, n_b l_b; SLJM) = 2^{-1/2} \sum_{M_L M_S} (SM_S LM_L \mid JM) \times [\phi(n_a l_a n_b l_b LM_L) + (-)^{l_a+l_b-L+S} \phi(n_b l_b n_a l_a LM_L)] \times \chi[(1/2)(1/2)SM_s], \quad (2\text{–}46)$$

where

$$\phi(n_\alpha l_\alpha n_\beta l_\beta LM_L) = \sum_{m_\alpha m_\beta} (l_\alpha m_\alpha l_\beta m_\beta \mid LM_L) \phi_1(l_\alpha m_\alpha) \times \phi_2(l_\beta m_\beta) R_1(n_\alpha l_\alpha) R_2(n_\beta l_\beta), \quad (2\text{–}47)$$

$$\chi[(1/2)(1/2)SM_s] = \sum_{m_s m_{s'}} [(1/2) m_s (1/2) m_{s'} \mid SM_s] \times \chi_1(m_s) \chi_2(m_{s'}). \quad (2\text{–}48)$$

Here, $\phi_i(l_j m_j)$, $R_i(n_j l_j)$ and $\chi_i(m_{s'})$ are the single-particle angular, radial, and spin wave functions of electron i, with quantum numbers $n_j l_j m_j$ and $m_{s'}$.

The total transition probability (Sec. 2.1.1) into all possible states of L and S for a given final configuration of the atom then is

$$w = \sum_{L,S} [(2S+1)(2L+1)/2(2l''+1)] \times \sum_{l_A} |(1/\hbar) \langle n'' l_\infty'' l_A SLJM \mid e^2/r_{12} \mid n l n' l' SLJM \rangle|^2, \quad (2\text{–}49)$$

where the single-particle radial wave functions are suitably normalized; they are denoted by their quantum numbers as defined in Sec. 2.3.1. Equation (2–49) is summed over the magnetic quantum numbers of the final atom and the orbital angular momentum l_A of the ejected electron, and averaged over the quantum numbers of the initial vacancy.

Separation into radial and angular factors, as discussed in the preceding section, leads to

$$w = \sum_{S,L} [(2S+1)(2L+1)/2(2l''+1)] \times \sum_{l_A} |(1/2\hbar) \sum_{\nu} [d_\nu D_\nu \pm (-)^{l+l'} e_\nu E_\nu]|^2, \quad (2\text{–}50)$$

where the plus sign goes with even $L+S$, and the minus sign with odd $L+S$.

The functions D_ν and E_ν are the direct and exchange radial matrix elements $\{(n''l'')|(nl)(n'l'), \nu, l_A\}$ and $\{(n''l'')|(n'l')(nl), \nu, l_A\}$ discussed in Sec. 2.3.1. The angular factors d_ν and e_ν are

$$d_\nu = (-)^{l+l'+L} (l'' \,||\, C^\nu \,||\, l)(l_A \,||\, C^\nu \,||\, l') \begin{Bmatrix} l'' & l_A & L \\ l' & l & \nu \end{Bmatrix},$$

$$e_\nu = (-)^{l_A+l'+L} (l'' \,||\, C^\nu \,||\, l')(l_A \,||\, C^\nu \,||\, l) \begin{Bmatrix} l'' & l_A & L \\ l & l' & \nu \end{Bmatrix}. \quad (2\text{–}51)$$

Here, $(l \,||\, C^\nu \,||\, l')$ is the reduced matrix element of the spherical harmonic, multiplied by $[4\pi/(2\nu+1)]^{1/2}$, and

$$\begin{Bmatrix} l_1 & l_2 & L \\ l_3 & l_4 & S \end{Bmatrix}$$

is the 6-j symbol.

Expressions for Auger transition probilities in Russell–Saunders coupling have been calculated by Asaad and Burhop (1958) for K–LL transitions. Asaad (1965a) has also derived the form of the L_1–$L_{2,3}M_{4,5}$ Coster–Kronig transition probabilities. Kostroun, Chen, and Crasemann (1971) have listed all transition probabilities to the K shell in LS coupling, in terms of radial integrals, including final-state combinations of s, p, d, and f vacancies (see Table II.1A). Expressions for the total

TABLE II.IA. Auger transition probabilities to an initial 1*s* vacancy, in *LS* coupling, in terms of radial matrix elements $\{(nl)(n'l'), \nu, l_A\}$ (from Kostroun, Chen, and Crasemann, 1971).

Final-state configuration		Term	Transition probability[a]
ns	*n's*	$^1S_0; {}^3S_1$	$(1/2)(2J+1)\alpha \mid \{(ns)(n's), 0, 0\} \pm \{(n's)(ns), 0, 0\} \mid^2$
ns	*n'p*	$^1P_1; {}^3P_{012}$	$(1/2)(2J+1) \mid \{(ns)(n'p), 0, 1\} \pm (1/3)\{(n'p)(ns), 1, 1\} \mid^2$
np	*n'p*	$^1S_0; {}^3S_1$	$(1/6)(2J+1)\alpha \mid \{(np)(n'p), 1, 0\} \pm \{(n'p)(np), 1, 0\} \mid^2$
		$^1D_2; {}^3D_{123}$	$(1/15)(2J+1)\alpha \mid \{(np)(n'p), 1, 2\} \pm \{(n'p)(np), 1, 2\} \mid^2$
ns	*n'd*	$^1D_2; {}^3D_{123}$	$(1/2)(2J+1) \mid \{(ns)(n'd), 0, 2\} \pm (1/5)\{(n'd)(ns), 2, 2\} \mid^2$
np	*n'd*	$^1P_1; {}^3P_{012}$	$(1/9)(2J+1) \mid \{(np)(n'd), 1, 1\} \pm (3/5)\{(n'd)(np), 2, 1\} \mid^2$
		$^1F_3; {}^3F_{234}$	$(1/14)(2J+1) \mid \{(np)(n'd), 1, 3\} \pm (3/5)\{(n'd)(np), 2, 3\} \mid^2$
ns	*n'f*	$^1F_3; {}^3F_{234}$	$(1/2)(2J+1) \mid \{(ns)(n'f), 0, 3\} \pm (1/7)\{(n'f)(ns), 1, 3\} \mid^2$
np	*n'f*	$^1D_2; {}^3D_{123}$	$(1/10)(2J+1) \mid \{(np)(n'f), 1, 2\} \pm (3/7)\{(n'f)(np), 3, 2\} \mid^2$
		$^1G_4; {}^3G_{345}$	$(1/27)(4J+2) \mid \{(np)(n'f), 1, 4\} \pm (3/7)\{(n'f)(np), 3, 4\} \mid^2$
nd	*n'd*	$^1S_0; {}^3S_1$	$(1/10)(2J+1)\alpha \mid \{(nd)(n'd), 2, 0\} \pm \{(n'd)(nd), 2, 0\} \mid^2$
		$^1D_2; {}^3D_{123}$	$(1/35)(2J+1)\alpha \mid \{(nd)(n'd), 2, 2\} \pm \{(n'd)(nd), 2, 2\} \mid^2$
		$^1G_4; {}^3G_{345}$	$(1/35)(2J+1)\alpha \mid \{(nd)(n'd), 2, 4\} \pm \{(n'd)(nd), 2, 4\} \mid^2$
nd	*n'f*	$^1P_1; {}^3P_{012}$	$(1/50)(6J+3) \mid \{(nd)(n'f), 2, 1\} \pm (5/7)\{(n'f)(nd), 3, 1\} \mid^2$
		$^1F_3; {}^3F_{234}$	$(1/75)(4J+2) \mid \{(nd)(n'f), 2, 3\} \pm (5/7)\{(n'f)(nd), 2, 3\} \mid^2$
		$^1H_5; {}^3H_{456}$	$(1/33)(2J+1) \mid \{(nd)(n'f), 2, 5\} \pm (5/7)\{(n'f)(nd), 3, 5\} \mid^2$

[a] Here, we have $\alpha \equiv 1/2$ if $n = n'$, $\alpha \equiv 1$ if $n \neq n'$, and $\pm$ means $+$ for singlet and $-$ for triplet states.

Auger rates in *LS* coupling for an initial *s*, *p*, or *d* hole and final combinations of *s*, *p*, and *d* holes are listed in a report by McGuire (1969b), and total Auger rates in *LS* coupling for transitions involving final-state *f* holes have also been tabulated by McGuire (1970b).

The calculation of Auger transition probabilities to *L* subshells and of Coster–Kronig transitions is often more conveniently carried out in *j–j* coupling. The *j–j* wave functions are given in terms of the *LS* wave functions (de-Shalit and Talmi, 1963, Chaps. 19–21) by

$$\psi_A(n_a l_a j_a, n_b l_b j_b; JM) = \sum_{SL} [(2S+1)(2L+1)(2j_a+1)(2j_b+1)]^{1/2} \begin{Bmatrix} \frac{1}{2} & l_a & j_a \\ \frac{1}{2} & l_b & j_b \\ S & L & J \end{Bmatrix} \psi_A(n_a l_a; n_b l_b; SLJM), \quad (2\text{–}52)$$

where

$$\begin{Bmatrix} \frac{1}{2} & l_a & j_a \\ \frac{1}{2} & l_b & j_b \\ S & L & J \end{Bmatrix}$$

is the 9–*j* symbol. From the relation between the absolute squared values of the matrix elements of e^2/r_{12} in the two coupling schemes (see Kostroun, Chen, and Crasemann, 1971, Appendix B),

$$|\langle n_a' l_a' j_a', n_b' l_b' j_b'; JM \mid e^2/r_{12} \mid n_a l_a j_a, n_b l_b j_b; JM\rangle|^2 = \sum_{S,L,S',L'} [(2S+1)(2L+1)(2S'+1)(2L'+1)(2j_a'+1)$$

$$\times (2j_b'+1)(2j_a+1)(2j_b+1)] \begin{Bmatrix} \frac{1}{2} & l_a' & j_a' \\ \frac{1}{2} & l_b' & j_b' \\ \frac{1}{2} & L' & J \end{Bmatrix} \begin{Bmatrix} \frac{1}{2} & l_a & j_a \\ \frac{1}{2} & l_b & j_b \\ S' & L' & J \end{Bmatrix} \begin{Bmatrix} \frac{1}{2} & l_a' & j_a' \\ \frac{1}{2} & l_b' & j_b' \\ S & L & J \end{Bmatrix} \begin{Bmatrix} \frac{1}{2} & l_a & j_a \\ \frac{1}{2} & l_b & j_b \\ S & L & J \end{Bmatrix}$$

$$\times \langle n_a' l_a', n_b' l_b'; SLJM \mid e^2/r_{12} \mid n_a l_a, n_b l_b; SLJM\rangle \langle n_a' l_a', n_b' l_b'; S'L'JM \mid e^2/r_{12} \mid n_a l_a, n_b l_b; S'L'JM\rangle, \quad (2\text{–}53)$$

it can readily be shown, by summing both sides over j_a, j_b, l_b', j_b', J, and M that

$$w=(2j_a'+1)^{-1}\sum_J(2J+1)\sum_{l_b',j_b'}\sum_{j_a,j_b}|\langle n_a'l_a'j_a', n_b'l_b'j_b';J\,|\,e^2/r_{12}\,|\,n_al_aj_a, n_bl_bj_b;J\rangle|^2$$
$$=[2(2l_a'+1)]^{-1}\sum_{S,L}(2S+1)(2L+1)\sum_{l_b}|\langle n_a'l_a', n_b'l_b';SL\,|\,e^2/r_{12}\,|\,n_al_a, n_bl_b;SL\rangle|^2. \quad (2\text{–}54)$$

The total transition rate in j–j coupling, therefore, is

$$w=(2j_a'+1)^{-1}\sum_J(2J+1)\sum_{l_b'j_b'j_b}|\langle n_a'l_a'j_a', n_b'j_b';J\,|\,e^2/r_{12}\,|\,n_al_aj_a, n_bl_bj_b;J\rangle|^2. \quad (2\text{–}55)$$

Term intensities in j–j coupling have been obtained by Asaad (1963b) for an initial s or p hole and final combinations of s, p, and d holes. Expressions for transitions that involve final f holes have been obtained by McGuire (1970b) and by Crasemann, Chen, and Kostroun (1971). Auger transition probabilities in j–j coupling to $s_{1/2}$ and $p_{1/2}$ initial states are listed in Tables II.IB and II.IC in terms of radial integrals.

Of all transitions between given initial and final-state configurations, for which angular momentum and parity are conserved (see, e.g., Table II.I), only those that are energetically possible do occur. The requirement of energy conservation is

$$E_{n''l''}-E_{nl}-E_{n'l'}=E_{\infty l_A}>0, \quad (2\text{–}56)$$

where, as indicated in Fig. 2–3, $E_{n''l''}$ is the absolute value of the binding energy of the electron that is originally missing, while E_{nl} and $E_{n'l'}$ are the (absolute values of the) binding energies of electrons in the nl and $n'l'$ states *in an atom with an $n''l''$ vacancy*. The latter requirement is usually met, approximately, in calculations by taking $E_{n'l'}$ for an atom of the next higher atomic number, $Z+1$.

Calculations of Auger-electron energies $E_{\infty l_A}$ from Eq. (2–56) have met with only limited success, particularly for Coster–Kronig transitions where these energies are very small. The coupling, spin–orbit interaction, other relativistic effects, and even configuration interaction play a role. Perhaps the best results have been obtained by Mehlhorn (1968) in intermediate coupling for argon. For the purpose of calculating total Auger rates in order to find fluorescence and Auger yields, electron binding energies are best taken from the compilations of Bearden and Burr (1967) or of Siegbahn *et al.* (1967). Experimental measurements of Auger electron energies, and of cutoffs of the various transitions at certain atomic numbers, remain of the utmost importance.

2.3.3. *Survey of Results*

Published calculations of radiationless transition probabilities are listed in Table II.II in chronological order; extent of the calculations, types of wave functions employed, and other major characteristics of each approach are indicated. Many of these calculations were aimed at the interpretation of Auger–electron spectra and covered only a few elements. Among the earlier calculations, those of Callan (1961, 1963b) are the most extensive: K–LL transition probabilities were computed explicitly for $16\leq Z\leq 83$. Total Auger transition probabilities to the K shell were derived by combining these results with $(K\text{–}LX)/(K\text{–}LL)$ and $(K\text{–}XY)/(K\text{–}LL)$ ratios from unpublished work by Geoffrion, Bonenfant, and Nadeau (1959), based on unscreened hydrogenic wave functions. The results are compared in Fig. 2–4 with those of the more recent calculations of McGuire (1970a, b) and of Kostroun, Chen, and Crasemann (1971). Numerical results of the calculations are listed in Table II.III. Total K–LL Auger probabilities computed by these authors are compared in Fig. 2–5; the calculated $(K\text{–}LX)/(K\text{–}LL)$ and $(K\text{–}XY)/(K\text{–}LL)$ ratios are compared with experimental data from Auger-electron spectra in Fig. 2–6.

Walters and Bhalla (1971) computed K-shell Auger widths for $4\leq Z\leq 54$ using nonrelativistic numerical Hartree–Slater wave functions with Kohn–Sham (1954) and Gaspar (1956) exchange. They did not, however, take into account the higher matrix elements (e.g. K–LN and K–MN) included in the calculations of McGuire (1970a) and of Kostroun *et al.* (1971).

It is interesting that the rather large discrepancy between radiationless transition probabilities calculated by various authors does not result in comparable

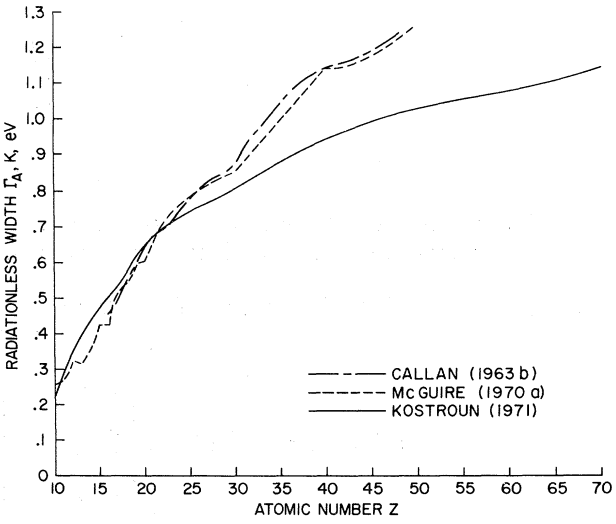

FIG. 2–4. Theoretical total Auger width of the atomic 1s level, as a function of atomic number. [From Kostroun, Chen, and Crasemann (1971), courtesy of American Institute of Physics.]

TABLE II.IB. Auger transition probabilities to an initial $s_{1/2}$ vacancy, in j–j coupling, in terms of radial matrix elements $\{(nl)(n'l'), \nu, l_A\}$. Here, J stands for the total angular momentum of the final two-hole configuration, and j_A is the total angular momentum of the Auger electron. The notation $\bar{l}$ (e.g., $\bar{p}$, $\bar{d}$) is used if $j=l-(1/2)$; in the absence of the bar, $j=l+(1/2)$. The constant α is equal to 1/2 if $n=n'$ and equal to unity if $n\neq n'$ (from Chen, Kostroun, and Crasemann, private communication).

Final-state configuration		J	j_A	Transition probability
ns	$n's$	0	1/2	$(1/2)\alpha \mid \{(ns)(n's),0,0\}+\{(n's)(ns),0,0\} \mid^2$
		1	1/2	$(3/2) \mid \{(ns)(n's),0,0\}-\{(n's)(ns),0,0\} \mid^2$
ns	$n'\bar{p}$	0	1/2	$(1/2) \mid \{(ns)(n'\bar{p}),0,1\}-(1/3)\{(n'\bar{p})(ns),1,1\} \mid^2$
		1	1/2	$(1/6) \mid \{(ns)(n'\bar{p}),0,1\}-(1/3)\{(n'\bar{p})(ns),1,1\} \mid^2$
		1	3/2	$(4/27) \mid \{(n'\bar{p})(ns),1,1\} \mid^2$
ns	$n'p$	1	1/2	$(4/27) \mid \{(n'p)(ns),1,1\} \mid^2$
		1	3/2	$(1/6) \mid 3\{(ns)(n'p),0,1\}+(1/3)\{(n'p)(ns),1,1\} \mid^2$
		2	3/2	$(5/2) \mid \{(ns)(n'p),0,1\}-(1/3)\{(n'p)(ns),1,1\} \mid^2$
ns	$n'\bar{d}$	1	3/2	$(3/2) \mid \{(ns)(n'\bar{d}),0,2\}-(1/5)\{(n'd)(ns),2,2\} \mid^2$
		2	3/2	$(1/10) \mid 5\{(ns)(n'\bar{d}),0,2\}-(1/5)\{(n'\bar{d})(ns),2,2\} \mid^2$
		2	5/2	$(12/125) \mid \{(n'\bar{d})(ns),2,2\} \mid^2$
ns	$n'd$	2	3/2	$(12/125) \mid \{(n'd)(ns),2,2\} \mid^2$
		2	5/2	$(1/10) \mid 5\{(ns)(n'd),0,2\}+(1/5)\{(n'd)(ns),2,2\} \mid^2$
		3	5/2	$(7/2) \mid \{(ns)(n'd),0,2\}-(1/5)\{(n'd)(ns),2,2\} \mid^2$
ns	$n'\bar{f}$	2	5/2	$(5/2) \mid \{(ns)(n'\bar{f}),0,3\}-(1/7)\{(n'\bar{f})(ns),3,3\} \mid^2$
		3	5/2	$(1/14) \mid 7\{(ns)(n'\bar{f}),0,3\}-(1/7)\{(n'\bar{f})(ns),3,3\} \mid^2$
		3	7/2	$(7/2) \mid (14/99)\{(n'\bar{f})(ns),3,3\} \mid^2$
ns	$n'f$	3	5/2	$(7/2) \mid (14/99)\{(n'f)(ns),3,3\} \mid^2$
		3	7/2	$(1/14) \mid 7\{(ns)(n'f),0,3\}+(1/7)\{(n'f)(ns),3,3\} \mid^2$
		4	7/2	$(9/2) \mid \{(ns)(n'f),0,3\}-(1/7)\{(n'f)(ns),3,3\} \mid^2$
$n\bar{p}$	$n'\bar{p}$	0	1/2	$(1/18)\alpha \mid \{(n\bar{p})(n'\bar{p}),1,0\}+\{(n'\bar{p})(n\bar{p}),1,0\} \mid^2$
		1	1/2	$(1/54) \mid \{(n\bar{p})(n'\bar{p}),1,0\}-\{(n'\bar{p})(n\bar{p}),1,0\} \mid^2$
		1	3/2	$(4/27) \mid \{(n\bar{p})(n'\bar{p}),1,2\}-\{(n'\bar{p})(n\bar{p}),1,2\} \mid^2$
$n\bar{p}$	$n'p$	1	1/2	$(4/27) \mid \{(n\bar{p})(n'p),1,0\}-\{n'p)(n\bar{p}),1,0\} \mid^2$
		1	3/2	$(1/54) \mid \{(n\bar{p})(n'p),1,2\}-\{(n'p)(n\bar{p}),1,2\} \mid^2$
		2	3/2	$(1/90) \mid \{(n\bar{p})(n'p),1,2\}-5\{(n'p)(n\bar{p}),1,2\} \mid^2$
		2	5/2	$(4/15) \mid \{(n\bar{p})(n'p),1,2\} \mid^2$
$n\bar{p}$	$n'\bar{d}$	1	1/2	$(4/27) \mid \{(n\bar{p})(n'\bar{d}),1,1\} \mid^2$
		1	3/2	$(1/6) \mid (1/3)\{(n\bar{p})(n'\bar{d}),1,1\}+(3/5)\{(n'\bar{d})(n\bar{p}),2,1\} \mid^2$
		2	3/2	$(1/10) \mid (1/3)\{(n\bar{p})(n'\bar{d}),1,1\}-(1/5)\{(n'\bar{d})(n\bar{p}),2,1\} \mid^2$
		2	5/2	$(12/5) \mid (1/3)\{(n\bar{p})(n'\bar{d}),1,3\}-(1/5)\{(n'\bar{d})(n\bar{p}),2,3\} \mid^2$
$n\bar{p}$	$n'd$	2	3/2	$(12/5) \mid (1/3)\{(n\bar{p})(n'd),1,1\}-(1/5)\{(n'd)(n\bar{p}),2,1\} \mid^2$
		2	5/2	$(1/10) \mid (1/3)\{(n\bar{p})(n'd),1,3\}-(1/5)\{(n'd)(n\bar{p}),2,3\} \mid^2$
		3	5/2	$(1/14) \mid (1/3)\{(n\bar{p})(n'd),1,3\}-(7/5)\{(n'd)(n\bar{p}),2,3\} \mid^2$
		3	7/2	$(8/21) \mid \{(n\bar{p})(n'd),1,3\} \mid^2$
$n\bar{p}$	$n\bar{f}$	2	3/2	$(4/15) \mid \{(n\bar{p})(n'\bar{f}),1,2\} \mid^2$
		2	5/2	$(5/2) \mid (1/15)\{(n\bar{p})(n'\bar{f}),1,2\}+(1/7)\{(n'\bar{f})(n\bar{p}),3,2\} \mid^2$
		3	5/2	$(1/14) \mid (1/3)\{(n\bar{p})(n'\bar{f}),1,2\}-(1/7)\{(n'\bar{f})(n\bar{p}),3,2\} \mid^2$
		3	7/2	$(24/7) \mid (1/3)\{(n\bar{p})(n'\bar{f}),1,4\}-(1/7)\{(n'\bar{f})(n\bar{p}),3,4\} \mid^2$
$n\bar{p}$	$n'f$	3	5/2	$(24/7) \mid (1/3)\{(n\bar{p})(n'f),1,2\}-(1/7)\{(n'f)(n\bar{p}),3,2\} \mid^2$
		3	7/2	$(1/14) \mid (1/3)\{(n\bar{p})(n'f),1,4\}-(1/7)\{(n'f)(n\bar{p}),3,4\} \mid^2$
		4	7/2	$(1/18) \mid (1/3)\{(n\bar{p})(n'f),1,4\}-(9/7)\{(n'f)(n\bar{p}),3,4\} \mid^2$
		4	9/2	$(40/81) \mid \{(n\bar{p})(n'f),1,4\} \mid^2$
np	$n'p$	0	1/2	$(1/9)\alpha \mid \{(np)(n'p),1,0\}+\{(n'p)(np),1,0\} \mid^2$
		1	1/2	$(5/27) \mid \{(np)(n'p),1,0\}-\{(n'p)(np),1,0\} \mid^2$
		1	3/2	$(2/135) \mid \{(np)(n'p),1,2\}-\{(n'p)(np),1,2\} \mid^2$
		2	3/2	$(2/45)\alpha \mid \{(np)(n'p),1,2\}+\{(n'p)(np),1,2\} \mid^2$
		2	5/2	$(1/15)\alpha \mid \{(np)(n'p),1,2\}+\{(n'p)(np),1,2\} \mid^2$
		3	5/2	$(7/15) \mid \{(np)(n'p),1,2\}-\{(n'p)(np),1,2\} \mid^2$
np	$n'\bar{d}$	0	1/2	$\mid (1/3)\{(np)(n'\bar{d}),1,1\}-(1/5)\{(n'\bar{d})(np),2,1\} \mid^2$
		1	1/2	$(1/15) \mid (5/3)\{(np)(n'\bar{d}),1,1\}-(3/5)\{(n'\bar{d})(np),2,1\} \mid^2$
		1	3/2	$(2/15) \mid (1/3)\{(np)(n'\bar{d}),1,1\}-(3/5)\{(n'\bar{d})(np),2,1\} \mid^2$
		2	3/2	$(2/5) \mid (1/3)\{(np)(n'\bar{d}),1,1\}-(1/5)\{(n'\bar{d})(np),2,1\} \mid^2$
		2	5/2	$(3/5) \mid (1/3)\{(np)(n'\bar{d}),1,3\}-(1/5)\{(n'\bar{d})(np),2,3\} \mid^2$
		3	5/2	$(3/35) \mid (7/3)\{(np)(n'\bar{d}),1,3\}-(1/5)\{(n'\bar{d})(np),2,3\} \mid^2$
		3	7/2	$(144/875) \mid \{(n'\bar{d})(np),2,3\} \mid^2$

TABLE II.IB. (*Continued*)

Final-state configuration		J	j_A	Transition probability
np	$n'd$	1	1/2	$(12/125) \mid \{(np)(n'd), 2, 1\} \mid^2$
		1	3/2	$(3/10) \mid \{(np)(n'd), 1, 1\} + (1/5)\{(n'd)(np), 2, 1\} \mid^2$
		2	3/2	$(21/10) \mid (1/3)\{(np)(n'd), 1, 1\} - (1/5)\{(n'd)(np), 2, 1\} \mid^2$
		2	5/2	$(4/35) \mid (1/3)\{(np)(n'd), 1, 3\} - (1/5)\{(n'd)(np), 2, 3\} \mid^2$
		3	5/2	$(8/35) \mid (1/3)\{(np)(n'd), 1, 3\} - (2/5)\{(n'd)(np), 2, 3\} \mid^2$
		3	7/2	$(3/70) \mid (5/3)\{(np)(n'd), 1, 3\} + (3/5)\{(n'd)(np), 2, 3\} \mid^2$
		4	7/2	$(81/14) \mid (1/3)\{(np)(n'd), 1, 3\} - (1/5)\{(n'd)(np), 2, 3\} \mid^2$
np	$n'\bar{f}$	1	3/3	$(27/10) \mid (1/3)\{(np)(n'f), 1, 2\} - (1/7)\{(n'\bar{f})(np), 3, 2\} \mid^2$
		2	3/2	$(27/70) \mid (7/9)\{(np)(n'\bar{f}), 1, 2\} - (1/7)\{(n'\bar{f})(np), 3, 2\} \mid^2$
		2	5/2	$(4/35) \mid (1/3)\{(np)(n'\bar{f}), 1, 2\} - (4/7)\{(n'\bar{f})(np), 3, 2\} \mid^2$
		3	5/2	$(8/35) \mid (1/3)\{(np)(n'\bar{f}), 1, 2\} - (1/7)\{(n'\bar{f})(np), 3, 2\} \mid^2$
		3	7/2	$(15/14) \mid (1/3)\{(np)(n'\bar{f}), 1, 4\} - (1/7)\{(n'\bar{f})(np), 3, 4\} \mid^2$
		4	7/2	$(1/14) \mid 3\{(np)(n'\bar{f}), 1, 4\} - (1/7)\{(n'\bar{f})(np), 3, 4\} \mid^2$
		4	9/2	$(7/60) \mid \{(n'\bar{f})(np), 3, 4\} \mid^2$
np	$n'f$	2	3/2	$(89/1060) \mid \{(n'f)(np), 3, 2\} \mid^2$
		2	5/2	$(6/35) \mid (5/3)\{(np)(n'f), 1, 2\} + (1/7)\{(n'f)(np), 3, 2\} \mid^2$
		3	5/2	$(18/7) \mid (1/3)\{(np)(n'f), 1, 2\} - (1/7)\{(n'f)(np), 3, 2\} \mid^2$
		3	7/2	$(2/21) \mid (1/3)\{(np)(n'f), 1, 4\} - (1/7)\{(n'f)(np), 3, 4\} \mid^2$
		4	7/2	$(10/63) \mid (1/3)\{(np)(n'f), 1, 4\} + (3/7)\{(n'f)(np), 3, 4\} \mid^2$
		4	9/2	$(2/7) \mid (7/9)\{(np)(n'f), 1, 4\} + (1/7)\{(n'f)(np), 3, 4\} \mid^2$
		5	9/2	$(22/3) \mid (1/3)\{(np)(n'f), 1, 4\} - (1/7)\{(n'f)(np), 3, 4\} \mid^2$
$n\bar{d}$	$n'\bar{d}$	0	1/2	$(1/25)\alpha \mid \{(n\bar{d})(n'\bar{d}), 2, 0\} + \{(n'\bar{d})(n\bar{d}), 2, 0\} \mid^2$
		1	1/2	$(3/125) \mid \{(n\bar{d})(n'\bar{d}), 2, 0\} - \{(n'\bar{d})(n\bar{d}), 2, 0\} \mid^2$
		1	3/2	$(6/125) \mid \{(n\bar{d})(n'\bar{d}), 2, 2\} - \{(n'\bar{d})(n\bar{d}), 2, 2\} \mid^2$
		2	3/2	$(2/125)\alpha \mid \{(n\bar{d})(n'\bar{d}), 2, 2\} + \{(n'\bar{d})(n\bar{d}), 2, 2\} \mid^2$
		2	5/2	$(3/125)\alpha \mid \{(n\bar{d})(n'\bar{d}), 2, 2\} + \{(n'\bar{d})(n\bar{d}), 2, 2\} \mid^2$
		3	5/2	$(3/875) \mid \{(n\bar{d})(n'\bar{d}), 2, 2\} - \{(n'\bar{d})(n\bar{d}), 2, 2\} \mid^2$
		3	7/2	$(144/875) \mid \{(n\bar{d})(n'\bar{d}), 2, 4\} - \{(n'\bar{d})(n\bar{d}), 2, 4\} \mid^2$
$n\bar{d}$	$n'd$	1	1/2	$(12/125) \mid \{(n\bar{d})(n'd), 2, 0\} - \{(n'd)(n\bar{d}), 2, 0\} \mid^2$
		1	3/2	$(3/250) \mid \{(n\bar{d})(n'd), 2, 2\} - \{(n'd)(n\bar{d}), 2, 2\} \mid^2$
		2	3/2	$(3/1750) \mid 3\{(n\bar{d})(n'd), 2, 2\} - 7\{(n'd)(n\bar{d}), 2, 2\} \mid^2$
		2	5/2	$(4/875) \mid 4\{(n\bar{d})(n'd), 2, 2\} - \{(n'd)(n\bar{d}), 2, 2\} \mid^2$
		3	5/2	$(32/875) \mid \{(n\bar{d})(n'd), 2, 2\} - \{(n'd)(n\bar{d}), 2, 2\} \mid^2$
		3	7/2	$(27/1750) \mid \{(n\bar{d})(n'd), 2, 4\} - \{(n'd)(n\bar{d}), 2, 4\} \mid^2$
		4	7/2	$(1/350) \mid \{(n\bar{d})(n'd), 2, 4\} - 9\{(n'd)(n\bar{d}), 2, 4\} \mid^2$
		4	9/2	$(8/35) \mid \{(n\bar{d})(n'd), 2, 4\} \mid^2$
$n\bar{d}$	$n'\bar{f}$	1	1/2	$(12/125) \mid \{(n\bar{d})(n'\bar{f}), 2, 1\} \mid^2$
		1	3/2	$(3/10) \mid (1/5)\{(n\bar{d})(n'\bar{f}), 2, 1\} + (3/7)\{(n'\bar{f})(n\bar{d}), 3, 1\} \mid^2$
		2	3/2	$(109/111) \mid (1/5)\{(n\bar{d})(n'\bar{f}), 2, 1\} - (1/7)\{(n'\bar{f})(n\bar{d}), 3, 1\} \mid^2$
		2	5/2	$(325/152) \mid (1/5)\{(n\bar{d})(n'\bar{f}), 2, 3\} - (1/7)\{(n'\bar{f})(n\bar{d}), 3, 3\} \mid^2$
		3	5/2	$(7/162) \mid (23/25)\{(n\bar{d})(n'\bar{f}), 2, 3\} + (23/70)\{(n'\bar{f})(n\bar{d}), 3, 3\} \mid^2$
		3	7/2	$(27/70) \mid (1/5)\{(n\bar{d})(n'\bar{f}), 2, 3\} + (5/21)\{(n'\bar{f})(n\bar{d}), 3, 3\} \mid^2$
		4	7/2	$(55/97) \mid (1/5)\{(n\bar{d})(n'\bar{f}), 2, 3\} - (1/7)\{(n'\bar{f})(n\bar{d}), 3, 3\} \mid^2$
		4	9/2	$(1217/240) \mid (1/5)\{(n\bar{d})(n'\bar{f}), 2, 5\} - (1/7)\{(n'\bar{f})(n\bar{d}), 3, 5\} \mid^2$
$n\bar{d}$	$n'f$	2	3/2	$(144/35) \mid (1/5)\{(n\bar{d})(n'f), 2, 1\} - (1/7)\{(n'f)(n\bar{d}), 3, 1\} \mid^2$
		2	5/2	$(6/35) \mid (1/5)\{(n\bar{d})(n'f), 2, 3\} - (1/7)\{(n'f)(n\bar{d}), 3, 3\} \mid^2$
		3	5/2	$(2/7) \mid (1/5)\{(n\bar{d})(n'f), 2, 3\} - (3/7)\{(n'f)(n\bar{d}), 3, 3\} \mid^2$
		3	7/2	$(2/21) \mid \{(n\bar{d})(n'f), 2, 3\} - (1/7)\{(n'f)(n\bar{d}), 3, 3\} \mid^2$
		4	7/2	$(927/649) \mid (1/5)\{(n\bar{d})(n'f), 2, 3\} - (1/7)\{(n'f)(n\bar{d}), 3, 3\} \mid^2$
		4	9/2	$(2/7) \mid (1/5)\{(n\bar{d})(n'f), 2, 5\} - (1/7)\{(n'f)(n\bar{d}), 3, 5\} \mid^2$
		5	9/2	$(2/33) \mid (1/5)\{(n\bar{d})(n'f), 2, 5\} - (11/7)\{(n'f)(n\bar{d}), 3, 5\} \mid^2$
		5	11/2	$(16/55) \mid \{(n\bar{d})(n'f), 2, 5\} \mid^2$
nd	$n'd$	0	1/2	$(3/50)\alpha \mid \{(nd)(n'd), 2, 0\} + \{(n'd)(nd), 2, 0\} \mid^2$
		1	1/2	$(21/250) \mid \{(nd)(n'd), 2, 0\} - \{(n'd)(nd), 2, 0\} \mid^2$
		1	3/2	$(12/875) \mid \{(nd)(n'd), 2, 2\} - \{(n'd)(nd), 2, 2\} \mid^2$
		2	3/2	$(24/875)\alpha \mid \{(nd)(n'd), 2, 2\} + \{(n'd)(nd), 2, 2\} \mid^2$
		2	5/2	$(36/875)\alpha \mid \{(nd)(n'd), 2, 2\} + \{(n'd)(nd), 2, 2\} \mid^2$
		3	5/2	$(108/875) \mid \{(nd)(n'd), 2, 2\} - \{(n'd)(nd), 2, 2\} \mid^2$
		3	7/2	$(4/875) \mid \{(nd)(n'd), 2, 4\} - \{(n'd)(nd), 2, 4\} \mid^2$
		4	7/2	$(4/175)\alpha \mid \{(nd)(n'd), 2, 4\} + \{(n'd)(nd), 2, 4\} \mid^2$
		4	9/2	$(1/35)\alpha \mid \{(nd)(n'd), 2, 4\} + \{(n'd)(nd), 2, 4\} \mid^2$
		5	9/2	$(11/35) \mid \{(nd)(n'd), 2, 4\} - \{(n'd)(nd), 2, 4\} \mid^2$

TABLE II.IB (*Continued*)

Final-state configuration		J	j_A	Transition probability
nd	$n'\bar{f}$	0	1/2	$(3/2) \mid (1/5)\{(nd)(n'\bar{f}),2,1\}-(1/7)\{(n'\bar{f})(nd),3,1\}\mid^2$
		1	1/2	$(1109/1035) \mid (7/25)\{(nd)(n'\bar{f}),2,1\}-(1/7)\{(n'\bar{f})(nd),3,1\}\mid^2$
		1	3/2	$(12/35) \mid (1/5)\{(nd)(n'f),2,1\}-(2/7)\{(n'\bar{f})(nd),3,1\}\mid^2$
		2	3/2	$(203/296) \mid (1/5)\{(nd)(n'\bar{f}),2,1\}-(1/7)\{(n'\bar{f})(nd),3,1\}\mid^2$
		2	5/2	$(1481/1440) \mid (1/5)\{(nd)(n'\bar{f}),2,3\}-(1/7)\{(n'\bar{f})(nd),3,3\}\mid^2$
		3	5/2	$(12/35) \mid (3/5)\{(nd)(n'\bar{f}),2,3\}-(1/7)\{(n'\bar{f})(nd),3,3\}\mid^2$
		3	7/2	$(4/35) \mid (1/5)\{(nd)(n'\bar{f}),2,3\}-(5/7)\{(n'\bar{f})(nd),3,3\}\mid^2$
		4	7/2	$(4/7) \mid (1/5)\{(nd)(n'\bar{f}),2,3\}-(1/7)\{(n'\bar{f})(nd),3,3\}\mid^2$
		4	9/2	$(5/7) \mid (1/5)\{(nd)(n'\bar{f}),2,5\}-(1/7)\{(n'\bar{f})(nd),3,5\}\mid^2$
		5	9/2	$(5/77) \mid (11/5)\{(nd)(n'\bar{f}),2,5\}-(1/7\{(n'\bar{f})(nd),3,5\}\mid^2$
		5	11/2	$(38/239) \mid \{(n'\bar{f})(nd),3,5\}\mid^2$
nd	$n'f$	1	1/2	$(106/1515) \mid \{(n'f)(nd),3,1\}\mid^2$
		1	3/2	$(24/7) \mid (3/5)\{(nd)(n'f),2,1\}+(1/7)\{(n'f)(nd),3,1\}\mid^2$
		2	3/2	$(81/35) \mid (1/5)\{(nd)(n'f),2,1\}-(1/7)\{(n'f)(nd),3,1\}\mid^2$
		2	5/2	$(32/105) \mid (1/5)\{(nd)(n'f),2,3\}-(1/7)\{(n'f)(nd),3,3\}\mid^2$
		3	5/2	$(8/21) \mid (1/5)\{(nd)(n'f),2,3\}+(2/7)\{(n'f)(nd),3,3\}\mid^2$
		3	7/2	$(9/14) \mid (1/3)\{(nd)(n'f),2,3\}+(1/7)\{(n'f)(nd),3,3\}\mid^2$
		4	7/2	$(55/14) \mid (1/5)\{(nd)(n'f),2,3\}-(1/7)\{(n'f)(nd),3,3\}\mid^2$
nd	$n'f$	4	9/2	$(8/77) \mid (1/5)\{(nd)(n'f),2,5\}-(1/7)\{(n'f)(nd),3,5\}\mid^2$
		5	9/2	$(32/77) \mid (1/5)\{(nd)(n'f),2,5\}+(3/14)\{(n'f)(nd),3,5\}\mid^2$
		5	11/2	$(79/146) \mid (7/25)\{(nd)(n'f),2,5\}+(1/7)\{(n'f)(nd),3,5\}\mid^2$
		6	11/2	$(581/59) \mid (1/5)\{(nd)(n'f),2,5\}-(1/7)\{(n'f)(nd),3,5\}\mid^2$
$n\bar{f}$	$n'\bar{f}$	0	1/2	$(3/98)\alpha \mid \{(n\bar{f})(n'\bar{f}),3,0\}+\{(n'\bar{f})(n\bar{f}),3,0\}\mid^2$
		1	1/2	$(7/320) \mid \{(n\bar{f})(n'\bar{f}),3,0\}-\{(n'\bar{f})(n\bar{f}),3,0\}\mid^2$
		1	3/2	$(41/1465) \mid \{(n\bar{f})(n'\bar{f}),3,2\}-\{(n'\bar{f})(n\bar{f}),3,2\}\mid^2$
		2	3/2	$(17/1215)\alpha \mid \{(n\bar{f})(n'\bar{f}),3,2\}+\{(n'\bar{f})(n\bar{f}),3,2\}\mid^2$
		2	5/2	$(17/810)\alpha \mid \{(n\bar{f})(n'\bar{f}),3,2\}+\{(n'\bar{f})(n\bar{f}),3,2\}\mid^2$
		3	5/2	$(53/7575) \mid \{(n\bar{f})(n'\bar{f}),3,2\}-\{(n'\bar{f})(n\bar{f}),3,2\}\mid^2$
		3	7/2	$(33/566) \mid \{(n\bar{f})(n'f),3,4\}-\{(n'\bar{f})(n\bar{f}),3,4\}\mid^2$
		4	7/2	$(7/600)\alpha \mid \{(n\bar{f})(n'\bar{f}),3,4\}+\{(n'\bar{f})(n\bar{f}),3,4\}\mid^2$
		4	9/2	$(29/1990)\alpha \mid \{(n\bar{f})(n'\bar{f}),3,4\}+\{(n'\bar{f})(n\bar{f}),3,4\}\mid^2$
		5	9/2	$(11/8300) \mid \{(n\bar{f})(n'\bar{f}),3,4\}-\{(n'\bar{f})(n\bar{f}),3,4\}\mid^2$
		5	11/2	$(38/239) \mid \{(n\bar{f})(n'\bar{f}),3,6\}-\{(n'\bar{f})(n\bar{f}),3,6\}\mid^2$
$n\bar{f}$	nf	1	1/2	$(106/1515) \mid \{(n\bar{f})(n'f),3,0\}-\{(n'f)(n\bar{f}),3,0\}\mid^2$
		1	3/2	$(53/6060) \mid \{(n\bar{f})(n'f),3,2\}-\{(n'f)(n\bar{f}),3,2\}\mid^2$
		2	3/2	$(29/1990) \mid \{(n\bar{f})(n'f),3,2\}-(9/5)\{(n'f)(n\bar{f}),3,2\}\mid^2$
		2	5/2	$(51/8200) \mid (5/2)\{(n\bar{f})(n'f),3,2\}-\{(n'f)(n\bar{f}),3,2\}\mid^2$
		3	5/2	$(51/164) \mid \{(n\bar{f})(n'f),3,2\}-\{(n'f)(n\bar{f}),3,2\}\mid^2$
		3	7/2	$(4/305) \mid \{(n\bar{f})(n'f),3,4\}-\{(n'f)(n\bar{f}),3,4\}\mid^2$
		4	7/2	$(13/2180) \mid \{(n\bar{f})(n'f),3,4\}-(11/3)\{(n'f)(n\bar{f}),3,4\}\mid^2$
		4	9/2	$(39/18400) \mid 6\{(n\bar{f})(n'f),3,4\}-\{(n'f)(n\bar{f}),3,4\}\mid^2$
		5	9/2	$(5/262) \mid \{(n\bar{f})(n'f),3,4\}-\{(n'f)(n\bar{f}),3,4\}\mid^2$
		5	11/2	$(8/725) \mid \{(n\bar{f})(n'f),3,6\}-\{(n'f)(n\bar{f}),3,6\}\mid^2$
		6	11/2	$(17/14300) \mid \{(n\bar{f})(n'f),3,6\}-13\{(n'f)(n\bar{f}),3,6\}\mid^2$
		6	13/2	$(134/671) \mid \{(n\bar{f})(n'f),3,6\}\mid^2$
nf	$n'f$	0	1/2	$(2/49)\alpha \mid \{(nf)(n'f),3,0\}+\{(n'f)(nf),3,0\}\mid^2$
		1	1/2	$(53/1010) \mid \{(nf)(n'f),3,0\}-\{(n'f)(nf),3,0\}\mid^2$
		1	3/2	$(7/600 \mid \{(nf)(n'f),3,0\}-\{(n'f)(nf),3,0\}\mid^2$
		2	3/2	$(7/360)\alpha \mid \{(nf)(n'f),3,2\}+\{(n'f)(nf),3,2\}\mid^2$
		2	5/2	$(13/446)\alpha \mid \{(nf)(n'f),3,2\}+\{(n'f)(nf),3,2\}\mid^2$
		3	5/2	$(59/920) \mid \{(nf)(n'f),3,2\}-\{(n'f)(nf),3,2\}\mid^2$
		3	7/2	$(131/20600) \mid \{(nf)(n'f),3,4\}-\{(n'f)(nf),3,4\}\mid^2$
		4	7/2	$(5/262)\alpha \mid \{(nf)(n'f),3,4\}+\{(n'f)(nf),3,4\}\mid^2$
		4	9/2	$(13/545)\alpha \mid \{(nf)(n'f),3,4\}+\{(n'f)(nf),3,4\}\mid^2$
		5	9/2	$(19/184) \mid \{(nf)(n'f),3,4\}-\{(n'f)(nf),3,4\}\mid^2$
		5	11/2	$(21/10300) \mid \{(nf)(n'f),3,6\}-\{(n'f)(nf),3,6\}\mid^2$
		6	11/2	$(43/3015)\alpha \mid \{(nf)(n'f),3,6\}+\{(n'f)(nf),3,6\}\mid^2$
		6	13/2	$(101/6070)\alpha \mid \{(nf)(n'f),3,6\}+\{(n'f)(nf),3,6\}\mid^2$
		7	13/2	$(165/661/ \mid \{(nf)(n'f),3,6\}-\{(n'f)(nf),3,6\}\mid^2$

TABLE II.IC. Auger transition probabilities to an initial $p_{1/2}$ vacancy, in j–j coupling, in terms of radial matrix elements $\{(nl)(n'l'), \nu, l_A)\}$. Here, J stands for the total angular momentum of the final two-hole configuration, and j_A is the total angular momentum of the Auger electron. The notation $\bar{l}$ (e.g., $\bar{p}, \bar{d}$) is used if $j=l-(1/2)$; in the absence of the bar, $j=l+(1/2)$. The constant α is equal to 1/2 if $n=n'$ and equal to unity if $n\neq n'$ (from Chen, Kostroun, and Crasemann, private communication).

Final-state configuration		J	j_A	Transition probability
ns	$n's$	0	1/2	$(1/18)\alpha \mid \{(ns)(n's),1,1\}+\{(n's)(ns),1,1\} \mid^2$
		1	1/2	$(1/54) \mid \{(ns)(n's),1,1\}-\{(n's)(ns),1,1\} \mid^2$
		1	3/2	$(4/27) \mid \{(ns)(n's),1,1\}-\{(n's)(ns),1,1\} \mid^2$
ns	$n'\bar{p}$	0	1/2	$(1/2) \mid (1/3)\{(ns)(n'\bar{p}),1,0\}-\{(n'\bar{p})(ns),0,0\} \mid^2$
		1	1/2	$(1/6) \mid (1/3)\{(ns)(n'\bar{p}),1,0\}-3\{(n'\bar{p})(ns),0,0\} \mid^2$
		1	3/2	$(4/27) \mid \{(ns)(n'\bar{p}),1,2\} \mid^2$
ns	$n'p$	1	1/2	$(4/27) \mid \{(ns)(n'p),1,0\} \mid^2$
		1	3/2	$(1/6) \mid (1/3)\{(ns)(n'p),1,2\}+(3/5)\{(n'p)(ns),2,2\} \mid^2$
		2	3/2	$(1/10) \mid (1/3)\{(ns)(n'p),1,2\}-(1/5)\{(n'p)(ns),2,2\} \mid^2$
		2	5/2	$(12/5) \mid (1/3)\{(ns)(n'p),1,2\}-(1/5)\{(n'p)(ns),2,2\} \mid^2$
ns	$n'\bar{d}$	1	1/2	$(4/27) \mid \{(ns)(n'\bar{d}),1,1\}-\{(n'd)(ns),1,1\} \mid^2$
		1	3/2	$(1/54) \mid \{(ns)(n'\bar{d}),1,1\}-\{(n'd)(ns),1,1\} \mid^2$
		2	3/2	$(1/90) \mid \{(ns)(n'\bar{d}),1,1\}-5\{(n'\bar{d})(ns),1,1\} \mid^2$
		2	5/2	$(4/15) \mid \{(ns)(n'\bar{d}),1,3\} \mid^2$
ns	$n'd$	2	3/2	$(4/15) \mid \{(ns)(n'd),1,\} \mid^2$
		2	5/2	$(1/10) \mid (1/3)\{(ns)(n'd),1,3\}+(5/7)\{(n'd)(ns),3,3\} \mid^2$
		3	5/2	$(1/14) \mid (1/3)\{(ns)(n'd),1,3\}-(1/7)\{(n'd)(ns),3,3\} \mid^2$
		3	7/2	$(24/7) \mid (1/3)\{(ns)(n'd),1,3\}-(1/7)\{(n'd)(ns),3,3\} \mid^2$
ns	$n'\bar{f}$	2	3/2	$(12/5) \mid (1/3)\{(ns)(n'\bar{f}),1,2\}-(1/5)\{(n'\bar{f})(ns),2,2\} \mid^2$
		2	5/2	$(1/10) \mid (1/3)\{(ns)(n'\bar{f}),1,2\}-(1/5)\{(n'\bar{f})(ns),2,2\} \mid^2$
		3	5/2	$(5/70) \mid (1/3)\{(ns)(n'\bar{f}),1,2\}-(7/5)\{(n'\bar{f})(ns),2,2\} \mid^2$
		3	7/2	$(8/21) \mid \{(ns)(n'\bar{f}),1,4\} \mid^2$
ns	$n'f$	3	5/2	$(8/21) \mid \{(ns)(n'f),1,2\} \mid^2$
		3	7/2	$(5/70) \mid (1/3)\{(ns)(n'f),1,4\}+(7/9)\{(n'f)(ns),4,4\} \mid^2$
		4	7/2	$(1/18) \mid (1/3)\{(ns)(n'f),1,4\}-(1/9)\{(n'f)(ns),4,4\} \mid^2$
		4	9/2	$(40/9) \mid (1/3)\{(ns)(n'f),1,4\}-(1/9)\{(n'f)(ns),4,4\} \mid^2$
$n\bar{p}$	$n'\bar{p}$	0	1/2	$(1/2)\alpha \mid \{(n\bar{p})(n'\bar{p}),0,1\}+\{(n'\bar{p})(n\bar{p}),0,1\} \mid^2$
		1	1/2	$(3/2) \mid \{(n\bar{p})(n'\bar{p}),0,1\}-\{(n'\bar{p})(n\bar{p}),0,1\} \mid^2$
$n\bar{p}$	$n'p$	1	3/2	$(3/2) \mid \{(n\bar{p})(n'p),0,1\}-(1/5)\{(n'p)(n\bar{p}),2,1\} \mid^2$
		2	3/2	$(1/10) \mid 5\{(n\bar{p})(n'p),0,1\}-(1/5)\{(n'p)(n\bar{p}),2,1\} \mid^2$
		2	5/2	$(12/125) \mid \{(n'p)(n\bar{p}),2,3\} \mid^2$
$n\bar{p}$	$n'\bar{d}$	1	1/2	$(4/27) \mid \{(n'\bar{d})(n\bar{p}),1,0\} \mid^2$
		1	3/2	$(1/6) \mid 3\{(n\bar{p})(n'\bar{d}),0,2\}+(1/3)\{(n'\bar{d})(n\bar{p}),1,2\} \mid^2$
		2	3/2	$(5/2) \mid \{(n\bar{p})(n'\bar{d}),0,2\}-(1/3)\{(n'\bar{d})(n\bar{p}),1,2\} \mid^2$
$n\bar{p}$	$n'd$	2	5/2	$(5/2) \mid \{(n\bar{p})(n'd),0,2\}-(1/7)\{(n'd)(n\bar{p}),3,2\} \mid^2$
		3	5/2	$(1/14) \mid 7\{(n\bar{p})(n'd),0,2\}-(1/7)\{(n\,d)(n\bar{p}),3,2\} \mid^2$
		3	7/2	$(24/343) \mid \{(n'd)(n\bar{p}),3,4\} \mid^2$
$n\bar{p}$	$n'\bar{f}$	2	3/2	$(24/25) \mid \{(n'\bar{f})(n\bar{p}),2,1\} \mid^2$
		2	5/2	$(1/10) \mid 5\{(n\bar{p})(n'\bar{f}),0,3\}+(1/5)\{(n'\bar{f})(n\bar{p}),2,3\} \mid^2$
		3	5/2	$(7/2) \mid \{(n\bar{p})(n'\bar{f}),0,3\}-(1/5)\{(n'\bar{f})(n\bar{p}),2,3\} \mid^2$
$n\bar{p}$	$n'f$	3	7/2	$(7/2) \mid \{(n\bar{p})(n'f),0,3\}-(1/9)\{(n'f)(n\bar{p}),4,3\} \mid^2$
		4	7/2	$(9/2) \mid \{(n\bar{p})(n'f),0,3\}-(1/81)\{(n'f)(n\bar{p}),4,3\} \mid^2$
		4	9/2	$(79/1440) \mid \{(n'f)(n\bar{p}),4,5\} \mid^2$
np	$n'p$	0	1/2	$(1/25)\alpha \mid \{(np)(n'p),3,1\}+\{(n'p)(np),2,1\} \mid^2$
		1	1/2	$(3/125) \mid \{(np)(n'p),2,1\}-\{(n'p)(np),2,1\} \mid^2$
		1	3/2	$(6/125) \mid \{(np)(n'p),2,1\}-\{(n'p)(np),2,1\} \mid^2$
		2	3/2	$(2/125)\alpha \mid \{(np)(n'p),2,1\}+\{(n'p)(np),2,1\} \mid^2$
		2	5/2	$(3/125)\alpha \mid \{(np)(n'p),2,3\}+\{(n'p)(np),2,3\} \mid^2$
		3	5/2	$(3/875) \mid \{(np)(n'p),2,3\}-\{(n'p)(np),2,3\} \mid^2$
		3	7/2	$(144/875) \mid \{(np)(n'p),2,3\}-\{(n'p)(np),2,3\} \mid^2$
np	$n'\bar{d}$	0	1/2	$\mid (1/5)\{(np)(n'\bar{d}),2,0\}-(1/3)\{(n'\bar{d})(np),1,0\} \mid^2$
		1	1/2	$(1/15) \mid (3/5)\{(np)(n'\bar{d}),2,0\}-(5/3)\{(n'\bar{d})(np),1,0\} \mid^2$
		1	3/2	$(2/15) \mid (3/5)\{(np)(n'\bar{d}),2,2\}-(1/3)\{(n'\bar{d})(np),1,2\} \mid^2$
		2	3/2	$(2/5) \mid (1/5)\{(np)(n'\bar{d}),2,2\}-(1/3)\{(n'\bar{d})(np),1,2\} \mid^2$
		2	5/2	$(3/5) \mid (1/5)\{(np)(n'\bar{d}),2,2\}-(1/3)\{(n'\bar{d})(np),1,2\} \mid^2$
		3	5/2	$(3/35) \mid (1/5)\{(np)(n'\bar{d}),2,2\}-(7/3)\{(n'\bar{d})(np),1,2\} \mid^2$
		3	7/2	$(144/875) \mid \{(np)(n'\bar{d}),2,4\} \mid^2$

TABLE II.IC (*Continued*)

Final-state configuration		J	j_A	Transition probability
np	$n'd$	1	1/2	$(12/125) \mid \{(np)(n'd), 2, 0\} \mid^2$
		1	3/2	$(3/10) \mid (1/5)\{(np)(n'd), 2, 2\} + (3/7)\{(n'd)(np), 3, 2\} \mid^2$
		2	3/2	$(27/70) \mid (1/5)\{(np)(n'd), 2, 2\} - (1/7)\{(n'd)(np), 3, 2\} \mid^2$
		2	5/2	$(64/35) \mid (1/5)\{(np)(n'd), 2, 2\} - (1/7)\{(n'd)(np), 3, 2\} \mid^2$
		3	5/2	$(8/35) \mid (2/5)\{(np)(n'd), 2, 2\} + (1/7)\{(n'd)(np), 3, 2\} \mid^2$
		3	7/2	$(3/70) \mid (3/5)\{(np)(n'd), 2, 4\} + (5/7)\{(n'd)(np), 3, 4\} \mid^2$
		4	7/2	$(1/14) \mid (1/5)\{(np)(n'd), 2, 4\} - (1/7)\{(n'd)(np), 3, 4\} \mid^2$
		4	9/2	$(40/7) \mid (1/5)\{(np)(n'd), 2, 4\} - (1/7)\{(n'd)(np), 3, 4\} \mid^2$
np	$n'\bar{f}$	1	1/2	$(12/125) \mid \{(np)(n'\bar{f}), 2, 1\} - \{(n'\bar{f})(np), 2, 1\} \mid^2$
		1	3/2	$(3/250) \mid \{(np)(n'\bar{f}), 2, 1\} - \{(n'\bar{f})(np), 2, 1\} \mid^2$
		2	3/2	$(27/70) \mid (1/5)\{(np)(n'\bar{f}), 2, 1\} - (7/15)\{(n'\bar{f})(np), 2, 1\} \mid^2$
		2	5/2	$(4/35) \mid (4/5)\{(np)(n'\bar{f}), 2, 3\} - (1/5)\{(n'\bar{f})(np), 2, 1\} \mid^2$
		3	5/2	$(32/35) \mid (1/5)\{(np)(n'\bar{f}), 2, 3\} - (1/5)\{(n'\bar{f})(np), 2, 3\} \mid^2$
		3	7/2	$(27/70) \mid (1/5)\{(np)(n'\bar{f}), 2, 3\} - (1/5)\{(n'\bar{f})(np), 2, 3\} \mid^2$
		4	7/2	$(229/3205) \mid (1/5)\{(np)(n'\bar{f}), 2, 3\} - (9/5)\{(n'\bar{f})(np), 2, 3\} \mid^2$
		4	9/2	$(8/35) \mid \{(np)(n'\bar{f}), 2, 5\} \mid^2$
np	$n'f$	2	3/2	$(13/79) \mid \{(np)(n'f), 2, 1\} \mid^2$
		2	5/2	$(6/35) \mid (1/5)\{(np)(n'f), 2, 3\} + (5/9)\{(n'f)(np), 4, 3\} \mid^2$
		3	5/2	$(2/7) \mid (1/5)\{(np)(n'f), 2, 3\} + (1/9)\{(n'f)(np), 4, 3\} \mid^2$
		3	7/2	$(419/176) \mid (1/5)\{(np)(n'f), 2, 3\} + (1/9)\{(n'f)(np), 4, 3\} \mid^2$
		4	7/2	$(10/63) \mid (3/5)\{(np)(n'f), 2, 3\} + (1/9)\{(n'f)(np), 4, 3\} \mid^2$
np	$n'f$	4	9/2	$(2/63) \mid (3/5)\{(np)(n'f), 2, 5\} + (7/9)\{(n'f)(np), 4, 5\} \mid^2$
		5	9/2	$(63/1040) \mid (1/5)\{(np)(n'f), 2, 5\} + (1/9)\{(n'f)(np), 4, 5\} \mid^2$
		5	11/2	$(749/103) \mid (1/5)\{(np)(n'f), 2, 5\} + (1/9)\{(n'f)(np), 4, 5\} \mid^2$
$n\bar{d}$	$n'\bar{d}$	0	1/2	$(1/9)\alpha \mid \{(n\bar{d})(n'\bar{d}), 1, 1\} + \{(n'\bar{d})(n\bar{d}), 1, 1\} \mid^2$
		1	1/2	$(5/27 \mid \{(n\bar{d})(n'\bar{d}), 1, 1\} - \{(n'\bar{d})(n\bar{d}), 1, 1\} \mid^2$
		1	3/2	$(2/135) \mid \{(n\bar{d})(n'\bar{d}), 1, 1\} - \{(n'\bar{d})(n\bar{d}), 1, 1\} \mid^2$
		2	3/2	$(2/45)\alpha \mid \{(n\bar{d})(n'\bar{d}), 1, 1\} + \{(n'\bar{d})(nd), 1, 1\} \mid^2$
		2	5/2	$(3/45)\alpha \mid \{(n\bar{d})(n'\bar{d}), 1, 3\} + \{(n'\bar{d})(n\bar{d}), 1, 3\} \mid^2$
		3	5/2	$(21/45) \mid \{(n\bar{d})(n'\bar{d}), 1, 3\} - \{(n'\bar{d})(n\bar{d}), 1, 3\} \mid^2$
$n\bar{d}$	$n'd$	1	3/2	$(27/10) \mid (1/3)\{(n\bar{d})(n'd), 1, 1\} - (1/7)\{(n'd)(n\bar{d}), 3, 1\} \mid^2$
		2	3/2	$(3/70) \mid (7/3)\{(n\bar{d})(n'd), 1, 1\} - (3/7)\{(n'd)(n\bar{d}), 3, 1\} \mid^2$
		2	5/2	$(4/35) \mid (1/3)\{(n\bar{d})(n'd), 1, 3\} - (4/7)\{(n'd)(n\bar{d}), 3, 3\} \mid^2$
		3	5/2	$(8/35) \mid (1/3)\{(n\bar{d})(n'd), 1, 3\} - (1/7)\{(n'd)(n\bar{d}), 3, 3\} \mid^2$
		3	7/2	$(15/14) \mid (1/3)\{(n\bar{d})(n'd), 1, 3\} - (1/7)\{(n'd)(n\bar{d}), 3, 3\} \mid^2$
		4	7/2	$(1/14) \mid 3\{(n\bar{d})(n'd), 1, 3\} - (1/7)\{(n'd)(n\bar{d}), 3, 3\} \mid^2$
		4	9/2	$(40/343) \mid \{(n'd)(n\bar{d}), 3, 5\} \mid^2$
nd	$n'd$	0	1/2	$(3/48)\alpha \mid \{(nd)(n'd), 3, 1\} + \{(n'd)(nd), 3, 1\} \mid^2$
		1	1/2	$(15/686) \mid \{(nd)(n'd), 3, 1\} - \{(n'd)(nd), 3, 1\} \mid^2$
		1	3/2	$(48/1715) \mid \{(nd)(n'd), 3, 1\} - \{(n'd)(nd), 3, 1\} \mid^2$
		2	3/2	$(24/1715)\alpha \mid \{(nd)(n'd), 3, 1\} + \{(n'd)(nd), 3, 1\} \mid^2$
		2	5/2	$(36/1715)\alpha \mid \{(nd)(n'd), 3, 3\} + \{(n'd)(nd), 3, 3\} \mid^2$
		3	5/2	$(12/1715) \mid \{(nd)(n'd), 3, 3\} - \{(n'd)(nd), 3, 3\} \mid^2$
		3	7/2	$(20/343) \mid \{(nd)(n'd), 3, 3\} - \{(n'd)(nd), 3, 3\} \mid^2$
		4	7/2	$(4/343)\alpha \mid \{(nd)(n'd), 3, 3\} + \{(n'd)(nd), 3, 3\} \mid^2$
		4	9/2	$(5/343)\alpha \mid \{(nd)(n'd), 3, 5\} + \{(n'd)(nd), 3, 5\} \mid^2$
		5	9/2	$(5/3773) \mid \{(nd)(n'd), 3, 5\} - \{(n'd)(nd), 3, 5\} \mid^2$
		5	11/2	$(600/3773) \mid \{(nd)(n'd), 3, 5\} - \{(n'd)(nd), 3, 5\} \mid^2$
$n\bar{d}$	$n'\bar{f}$	1	1/2	$(12/125) \mid \{(n'\bar{f})(n\bar{d}), 2, 0\} \mid^2$
		1	3/2	$(3/10) \mid \{(n\bar{d})(n'\bar{f}), 1, 2\} + (1/5)\{(n'\bar{f})(n\bar{d}), 2, 2\} \mid^2$
		2	3/2	$(21/10) \mid (1/3)\{(n\bar{d})(n'\bar{f}), 1, 2\} + (1/5)\{(n'\bar{f})(n\bar{d}), 2, 2\} \mid^2$
		2	5/2	$(4/35) \mid (1/3)\{(n\bar{d})(n'\bar{f}), 1, 2\} - (1/5)\{(n'\bar{f})(n\bar{d}), 2, 2\} \mid^2$
		3	5/2	$(8/35) \mid (1/3)\{(n\bar{d})(n'\bar{f}), 1, 2\} + (2/5)\{(n'\bar{f})(n\bar{d}), 2, 2\} \mid^2$
		3	7/2	$(27/70) \mid (5/9)\{(n\bar{d})(n'\bar{f}), 1, 4\} + (1/5)\{(n'\bar{f})(n\bar{d}), 2, 4\} \mid^2$
		4	7/2	$(238/1753) \mid (1/3)\{(n\bar{d})(n'\bar{f}), 1, 4\} - (1/5)\{(n'\bar{f})(n\bar{d}), 2, 4\} \mid^2$
$n\bar{d}$	$n'f$	2	5/2	$(30/7) \mid (1/3)\{(n\bar{d})(n'f), 1, 2\} - (1/9)\{(n'f)(n\bar{d}), 4, 2\} \mid^2$
		3	5/2	$(19/67) \mid L(n\bar{d})(n'f), 1, 2\} - (1/9)\{(n'f)(n\bar{d}), 4, 2\} \mid^2$

TABLE II.IC (*Continued*)

Final-state configuration		J	j_A	Transition probability
		3	7/2	$(2/21) \mid (1/3)\{(n\bar{d})(n'f), 1, 4\} - (5/9)\{(n'f)(n\bar{d}), 4, 4\} \mid^2$
		4	7/2	$(10/63) \mid (1/3)\{(n\bar{d})(n'f), 1, 4\} - (1/9)\{(n'f)(n\bar{d}), 4, 4\} \mid^2$
		4	9/2	$(14/9) \mid (1/3)\{(n\bar{d})(n'f), 1, 4\} - (1/9)\{(n'f)(n\bar{d}), 4, 4\} \mid^2$
		5	9/2	$(101/124) \mid \{(n\bar{d})(n'f), 1, 4\} - (1/33)\{(n'f)(n\bar{d}), 4, 4\} \mid^2$
		5	11/2	$(22/245) \mid \{(n'f)(n\bar{d}), 4, 6\} \mid^2$
nd	$n'\bar{f}$	0	1/2	$(3/2) \mid (1/7)\{(nd)(n'\bar{f}), 3, 0\} - (1/5)\{(n'\bar{f})(nd), 2, 0\} \mid^2$
		1	1/2	$(15/14) \mid (1/7)\{(nd)(n'\bar{f}), 3, 0\} - (7/25)\{(n'\bar{f})(nd), 2, 0\} \mid^2$
		1	3/2	$(12/35) \mid (2/7)\{(nd)(n'\bar{f}), 3, 2\} - (1/5)\{(n'\bar{f})(nd), 2, 2\} \mid^2$
		2	3/2	$(24/35) \mid (1/7)\{(nd)(n'f), 3, 2\} - (1/5)\{(n'f)(nd), 2, 2\} \mid^2$
		2	5/2	$(36/35) \mid (1/7)\{(nd)(n'\bar{f}), 3, 2\} - (1/5)\{(n'\bar{f})(nd), 2, 2\} \mid^2$
		3	5/2	$(12/35) \mid (1/7)\{(nd)(n'\bar{f}), 3, 2\} - (3/5)\{(n'\bar{f})(nd), 2, 2\} \mid^2$
		3	7/2	$(4/35) \mid (5/7)\{(nd)(n'\bar{f}), 3, 4\} - (1/5)\{(n'\bar{f})(nd), 2, 4\} \mid^2$
		4	7/2	$(2977/521) \mid (1/7)\{(nd)(n'\bar{f}), 3, 4\} - (1/5)\{(n'\bar{f})(nd), 2, 4\} \mid^2$
		4	9/2	$(1057/148) \mid (1/7)\{(nd)(n'\bar{f}), 3, 4\} - (1/5)\{(n'\bar{f})(nd), 2, 4\} \mid^2$
		5	9/2	$(5/77) \mid (1/7)\{(nd)(n'\bar{f}), 3, 4\} - (11/5)\{(n'\bar{f})(nd), 2, 4\} \mid^2$
		5	11/2	$(7/44) \mid \{(nd)(n'\bar{f}), 3, 6\} \mid^2$
nd	$n'f$	1	1/2	$(191/2730) \mid \{(nd)(n'f), 3, 0\} \mid^2$
		1	3/2	$(3/7) \mid (1/7)\{(nd)(n'f), 3, 2\} + (1/3)\{(n'f)(nd), 4, 2\} \mid^2$
		2	3/2	$(5/7) \mid (1/7)\{(nd)(n'f), 3, 2\} - (1/9)\{(n'f)(nd), 4, 2\} \mid^2$
		2	5/2	$(339/178) \mid (1/7)\{(nd)(n'f), 3, 2\} - (1/9)\{(n'f)(nd), 4, 2\} \mid^2$
		3	5/2	$(8/21) \mid (2/7)\{(nd)(n'f), 3, 2\} + (1/9)\{(n'f)(nd), 4, 2\} \mid^2$
		3	7/2	$(9/14) \mid (1/7)\{(nd)(n'f), 3, 4\} + (5/27)\{(n'f)(nd), 4, 4\} \mid^2$
		4	7/2	$(26/89) \mid (1/7)\{(nd)(n'f), 3, 4\} - (1/9)\{(n'f)(nd), 4, 4\} \mid^2$
		4	9/2	$(273/73) \mid (1/7)\{(nd)(n'f), 3, 4\} - (1/9)\{(n'f)(nd), 4, 4\} \mid^2$
		5	9/2	$(32/77) \mid (3/14)\{(nd)(n'f), 3, 4\} + (1/9)\{(n f)(nd), 4, 4\} \mid^2$
		5	11/2	$(46/85) \mid 1/7)\{(nd)(n'f), 3, 6\} + (7/45)\{(n'f)(nd), 4, 6\} \mid^2$
		6	11/2	$(81/1390) \mid (1/7)\{(nd)(n'f), 3, 6\} - (1/9)\{(n'f)(nd), 4, 6\} \mid^2$
		6	13/2	$(1351/138) \mid (1/7)\{(nd)(n'f), 3, 6\} - (1/9)\{(n'f)(nd), 4, 6\} \mid^2$
$n\bar{f}$	$n'\bar{f}$	0	1/2	$(3/50)\alpha \mid \{(n\bar{f})(n'\bar{f}), 2, 1\} + \{(n'\bar{f})(n\bar{f}), 2, 1\} \mid^2$
		1	1/2	$(21/250) \mid \{(n\bar{f})(n'\bar{f}), 2, 1\} - \{(n'\bar{f})(n\bar{f}), 2, 1\} \mid^2$
		1	3/2	$(12/875) \mid \{(n\bar{f})(n'\bar{f}), 2, 1\} - \{(n'\bar{f})(nf), 2, 1\} \mid^2$
		2	3/2	$(31/1130)\alpha \mid \{(n\bar{f})(n'\bar{f}), 2, 1\} + \{(n'\bar{f})(n\bar{f}), 2, 1\} \mid^2$
		2	5/2	$(36/875)\alpha \mid \{(n\bar{f})(n'\bar{f}), 2, 3\} + \{(n'\bar{f})(n\bar{f}), 2, 3\} \mid^2$
		3	5/2	$(10/81) \mid \{(n\bar{f})(n'\bar{f}), 2, 3\} - \{(n'\bar{f})(n\bar{f}), 2, 3\} \mid^2$
		3	7/2	$(4/875) \mid \{(n\bar{f})(n'\bar{f}), 2, 3\} - \{(n'\bar{f})(n\bar{f}), 2, 3\} \mid^2$
		4	7/2	$(4/175)\alpha \mid \{(n\bar{f})(n'\bar{f}), 2, 3\} + \{(n'\bar{f})(n\bar{f}), 2, 3\} \mid^2$
		4	9/2	$(1/35)\alpha \mid \{(n\bar{f})(n'\bar{f}), 2, 5\} + \{(n'\bar{f})(n\bar{f}), 2, 5\} \mid^2$
		5	9/2	$(11/35) \mid \{(n\bar{f})(n'\bar{f}), 2, 5\} - \{(n'\bar{f})(n\bar{f}), 2, 5\} \mid^2$
$n\bar{f}$	$n'f$	1	3/2	$(27/7) \mid (1/5)\{(n\bar{f})(n'f), 2, 1\} - (1/9)\{(n'f)(n\bar{f}), 4, 1\} \mid^2$
		2	3/2	$(5/7) \mid (9/25)\{(n\bar{f})(n'f), 2, 1\} - (1/9)\{(n'f)(n\bar{f}), 4, 1\} \mid^2$
		2	5/2	$(32/105) \mid (1/5)\{(n\bar{f})(n'f), 2, 3\} - (5/18)\{(n'f)(n\bar{f}), 4, 3\} \mid^2$
		3	5/2	$(8/21) \mid (1/5)\{(n\bar{f})(n'f), 2, 3\} - (1/9)\{(n'f)(n\bar{f}), 4, 3\} \mid^2$
		3	7/2	$(466/261) \mid (1/5)\{(n\bar{f})(n'f), 2, 3\} - (1/9)\{(n'f)(n\bar{f}), 4, 3\} \mid^2$
		4	7/2	$(26/89) \mid (1/15)\{(n\bar{f})(n'f), 2, 3\} - (1/9)\{(n'f)(n\bar{f}), 4, 3\} \mid^2$
$n\bar{f}$	$n'f$	4	9/2	$(8/77) \mid (1/5)\{(n\bar{f})(n'f), 2, 5\} - (2/3)\{(n'f)(n\bar{f}), 4, 5\} \mid^2$
		5	9/2	$(32/77) \mid (1/5)\{(n\bar{f})(n'f), 2, 5\} - (1/9)\{(n'f)(n\bar{f}), 4, 5\} \mid^2$
		5	11/2	$(631/595) \mid (1/5)\{(n\bar{f})(n'f), 2, 5\} - (1/9)\{(n'f)(n\bar{f}), 4, 5\} \mid^2$
		6	11/2	$(67/1150) \mid (13/5)\{(n\bar{f})(n'f), 2, 5\} - (1/9)\{(n'f)(n\bar{f}), 4, 5\} \mid^2$
		6	13/2	$(11/91) \mid \{(n\bar{f})(n'f), 4, 7\} \mid^2$
nf	$n'f$	0	1/2	$(2/81)\alpha \mid \{(nf)(n'f), 4, 1\} + \{(n'f)(nf), 4, 1\} \mid^2$
		1	1/2	$(12/625) \mid \{(nf)(n'f), 4, 1\} - \{(n'f)(nf), 4, 1\} \mid^2$
		1	3/2	$(19/970) \mid \{(nf)(n'f), 4, 1\} - \{(n'f)(nf), 4, 1\} \mid^2$
		2	3/2	$(1/85)\alpha \mid \{(nf)(n'f), 4, 1\} + \{(n'f)(nf), 4, 1\} \mid^2$
		2	5/2	$(26/1475)\alpha \mid \{(nf)(n'f), 4, 3\} + \{(n'f)(nf), 4, 3\} \mid^2$
		3	5/2	$(97/12100) \mid \{(nf)(n'f), 4, 3\} - \{(n'f)(nf), 4, 3\} \mid^2$
		3	7/2	$(71/2050) \mid \{(nf)(n'f), 4, 3\} - \{(n'f)(nf), 4, 3\} \mid^2$
		4	7/2	$(3/210)\alpha \mid \{(nf)(n'f), 4, 3\} + \{(n'f)(nf), 4, 3\} \mid^2$
		4	9/2	$(7/485)\alpha \mid \{(nf)(n'f), 4, 5\} + \{(n'f)(nf), 4, 5\} \mid^2$

TABLE II.IC (*Continued*)

Final-state configuration	J	j_A	Transition probability
	5	9/2	$(251/75400) \mid \{(nf)(n'f), 4, 5\} - \{(n'f)(nf), 4, 5\} \mid^2$
	5	11/2	$(42/695) \mid \{(nf)(n'f), 4, 5\} - \{(n'f)(nf), 4, 5\} \mid^2$
	6	11/2	$(101/11700)\alpha \mid \{(nf)(n'f), 4, 5\} + \{(n'f)(nf), 4, 5\} \mid^2$
	6	13/2	$(13/1290)\alpha \mid \{(nf)(n'f), 4, 7\} + \{(n'f)(nf), 4, 7\} \mid^2$
	7	13/2	$(47/70000) \mid \{(nf)(n'f), 4, 7\} - \{(n'f)(nf), 4, 7\} \mid^2$
	7	15/2	$(17/113) \mid \{(nf)(n'f), 4, 7\} - \{(n'f)(nf), 4, 7\} \mid^2$

variations in theoretical K-shell fluorescence yields (Sec. 3.4), because of concomitant discrepancies, in the same direction, in radiative transition probabilities (Sec. 2.4). However the *total* K-level widths calculated via the different approaches show considerable spread (Sec. 2.5).

The K-shell fluorescence yields calculated by various authors are compared with experiment in Sec. 3.4 and are listed in Table III.IV.

Only a few calculations of radiationless transition probabilities to the L shells and Coster–Kronig transition probabilities have been performed, as can be seen from Table II.II. The first comprehensive calculations of L-shell Coster–Kronig, Auger, and radiative rates and fluorescence yields were made by McGuire (1971a, b), who lists results for $12 \leq Z \leq 90$. The calculations are based on an approximate nonrelativistic Herman-and-Skillman potential; Auger transition probabilities are computed in LS coupling, while Coster–Kronig transition probabilities are computed in j–j coupling. Fluorescence yields of the L_2 and L_3 subshells and L_2–L_3X Coster–Kronig transition probabilities for $26 \leq Z \leq 93$ have been calculated by Chen, Crasemann, and Kostroun (1971a) from nonrelativistic screened hydrogenic wave functions; corresponding L_1-shell quantities were computed through the same approach by Crasemann, Chen, and Kostroun (1971). Results of these calculations are compared with measured quantities in Sec. 4.7. It is seen that generally good agreement is obtained for L-subshell fluorescence yields, but some puzzling discrepancies exist among Coster–Kronig transition probabilities (Chen *et al.*, 1971).

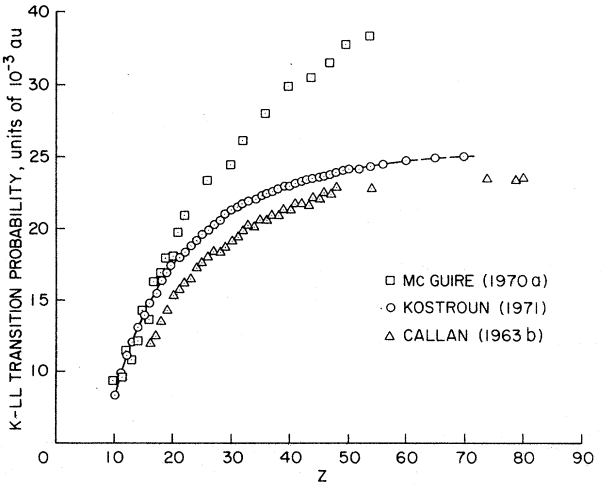

FIG. 2–5. Calculated K–LL transition probabilities *vs.* atomic number. Not indicated is the result of Bhalla and Ramsdale (1970a) who find a total relativistic K–LL transition probability of 47.6×10^{-3} a.u. for $Z = 81$. [From Kostroun, Chen, and Crasemann (1971), courtesy of American Institute of Physics.]

2.4. Radiative Transition Probabilities

2.4.1. Calculations

In the earliest calculations of K-fluorescence yields, Burhop (1935) calculated the number of K series x-ray quanta emitted per second by evaluating only the electric dipole matrix element for transitions to the $1s$ level and using Einstein's formula for the A coefficient:

$$w_{fi} \cong (\omega^3/3\hbar c^3) \mid \langle e\mathbf{r} \rangle \mid^2. \qquad (2\text{–}57)$$

With unscreeened hydrogenic wave functions, employed

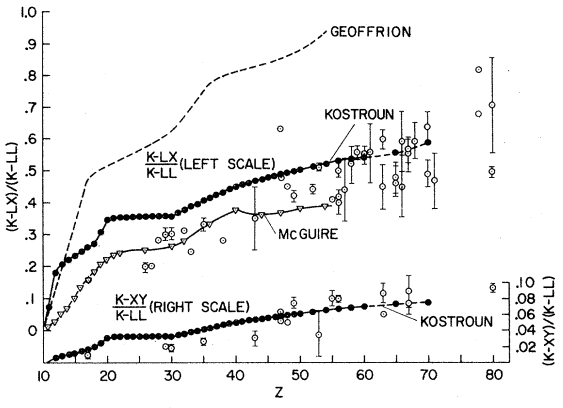

FIG. 2–6. Theoretical and experimental $(K$–$LX)/(K$–$LL)$ and $(K$–$XY)/(K$–$LL)$ Auger transition-probability ratios as functions of atomic number. Calculated ratios are from Geoffrion, Bonenfant, and Nadeau (1959), McGuire (1970a), and Kostroun, Chen, and Crasemann (1971). Measured relative intensities of the K Auger-electron groups are those assembled by Erman, Rossi, Bonacalza, and Mistel (1964), except for the following: the Zn ratios are from Bellicard, Moussa, and Haynes (1956), the Co ratios are from Bellicard, Moussa, and Haynes (1957), the Te data are from Casey and Albridge (1969), while the Ce and Nd ratios are as reported by D'Yakov and Rogachev (1962). [From Kostroun, Chen, and Crasemann (1971), courtesy of American Institute of Physics.]

TABLE II.II. Summary of Auger transition-probability calculations.

Reference	Transitions	R/NR[a]	Wave functions	Coupling	Z	Remarks
Pincherle (1935)	K–LL, K–LX, K–LY; L_1–$L_{23}M_{45}$, L_1–$L_{23}N_1$	NR	Unscreened hydrogenic bound-state; unscreened Coulomb continuum			Individual transition probabilities found independent of Z
Burhop (1935)	K–LL, K–LM	NR	Slater-screened hydrogenic bound-state; Gordon continuum (plane-wave continuum for K–LM)	j–j	1–60	Established basic approach for nonrelativistic calculations
Massey (1936)	K–LL	R	Slater-screened hydrogenic	j–j	79	First relativistic calculation, based on Møller formula
Ramberg (1937)	K–LL, K–LX, K–XY	NR	Numerical for Thomas-Fermi field	j–j	79	
Rubenstein (1955a)	K–LL, K–LX, K–XY, L–XY, M–XY	NR	Numerical Hartree self-consistent field without exchange	LS	18, 36, 47	
Asaad (1958)	K–LL, K–LM	NR	Screened hydrogenic	Intermediate	25–80	
Asaad (1959)	K–LL	R	Numerical for Hartree and Hartree potential; continuum fitted to Gordon at large r	j–j	80	
Geoffrion (1959)	K–$L_{23}L_{23}$ K–$M_{45}M_{45}$	NR	Unscreened hydrogenic			Extended calculations of Pincherle (1935); results independent of Z; unpublished
Listengarten (1961)	K–LL	R	Numerical for Thomas–Fermi–Dirac potential	j–j	81	
Callan (1961, 1963b)	K–LL	NR	Hartree-screened hydrogenic, Gordon continuum	LS	16–83	Combined results with $(K$–$LX)/(K$–$LL)$ and $(K$–$XY)/(K$–$LL)$ ratios of Geffrion (1959)
Listengarten (1962)	K–LL	R	Same as Listengarten (1961)	j–j	65, 92	
Asaad (1963a)	K–LL	NR	Transition amplitudes of Callan (1961, 1963b)	Intermediate	12–41 44–80	
Asaad (1963b)	...	...	...	j–j	...	Tables of transition probabilities in terms of radial integrals, final vacancies through $d_{5/2}/d_{5/2}$
Asaad (1965a)	L_1–$L_{23}M_{45}$	NR	Transition amplitudes of Callan (1961, 1963b)	LS, Intermediate	29–50 76–90	Initial LS, final intermediate coupling
Asaad (1965b)	K–LL	NR	Transition amplitudes of Rubenstein (1955a), Burhop (1935), and Callan (1961)	Intermediate	12–80	Includes configuration interaction

TABLE II.II (*Continued*)

Reference	Transitions	R/NR[a]	Wave functions	Coupling	Z	Remarks
Assad (1968)	L_2–MM, L_3–MM	NR	Transition amplitudes of Rubenstein (1955a)	j–j (LS)	18	Express initial vacancy in j–j and final double vacancy in LS coupling. List transition amplitudes in terms of radial integrals
Mehlhorn (1968)	L_1–$L_{23}M_1$ L_1–$L_{23}M_{23}$ L_1–MM	NR	Hartree–Fock-Slater (Herman and Skillman) for Ar *ions*	Intermediate	18	Configuration interaction included
Chattarji (1968)	K–L_1L_1	R	Screened hydrogenic, solutions of Biedenharn Dirac-Coulomb Hamiltonian	j–j	72–80	
Talukdar (1970)	L_1–L_2M_{45}	R	Same as Chattarji (1968)	j–j	32–41	Calculation yields large relativistic corrections
McGuire (1969a)	K–LL, K–LM	NR	Exact solutions of wave equation for approximation to Herman–Skillman HFS $-rV(r)$ for ions	LS	4–18	Revised in McGuire (1970a) K fluorescence yields
McGuire (1970a)	K–LL, K–LM	NR	Same as McGuire (1969a) but closer approximation	LS	18–54	Includes revision of results of McGuire (1969a)
Bhalla (1970a–c) Bhalla and Ramsdale (1970a), Bhalla et al. (1970a, b)	K–LL, K–LM, K–MM	R	Numerical Hartree–Fock–Slater	j–j	21–93	Term intensities as well as K fluorescence yields are calculated
McGuire (1971a)	L–XY through L–NO	NR	Same as McGuire (1970a)	LS j–j	11–90	Auger, Coster–Kronig, and radiative transition rates to L_1, L_2, L_3 subshells; Coster–Kronig in j–j, others in LS coupling
Kostroun (1971)	K–XY through K–MN	NR	Slater-screened bound-state hydrogenic; specially screened continuum	LS	10–70	Emphasis on total K Auger rates, fluorescence yields
McGuire (1971b)	L–XY through L–NN	NR	Same as McGuire (1970a)	j–j	18–90	Individual-term electron transition rates
Walters (1971)	K–XY through K–MM	NR	Hartree–Fock-Slater with Kohn–Sham and Gaspar exchange	LS	5–54	Total Auger rates and K fluorescence yields
Chen (1971a)	L_2–XY and L_3–XY through L–$N_{67}N_{67}$	NR	Same as Kostroun (1971)	j–j	26–93	L_2 and L_3 Auger rates, ω_2, ω_3, and Coster-Kronig rates
Crasemann (1971)	L_1–XY through L_1–$N_{67}N_{67}$	NR	Same as Kostroun (1971)	j–j	33–85	L_1 Auger rates, ω_1, f_{12}, f_{13}

[a] NR = nonrelativistic; R = relativistic.

TABLE II.III. Calculated total K-level Auger transition rates, in units of eV/$\hbar$.

Element	Callan (1963b)	McGuire (1970a)	Kostroun (1971)
$_{10}$Ne		0.258	0.231
$_{11}$Na		0.268	0.289
$_{12}$Mg		0.325	0.358
$_{13}$Al		0.316	0.400
$_{14}$Si		0.358	0.438
$_{15}$P		0.428	0.475
$_{16}$S	0.46	0.425	0.508
$_{17}$Cl	0.50	0.515	0.536
$_{18}$Ar	0.56	0.544	0.576
$_{19}$K	0.60	0.597	0.611
$_{20}$Ca	0.66	0.603	0.650
$_{21}$Sc	0.68	0.672	0.671
$_{22}$Ti	0.70	0.716	0.692
$_{23}$V	0.72		0.710
$_{24}$Cr	0.75		0.725
$_{25}$Mn	0.78		0.740
$_{26}$Fe	0.81	0.803	0.754
$_{27}$Co	0.83		0.768
$_{28}$Ni	0.84		0.780
$_{29}$Cu	0.86		0.791
$_{30}$Zn	0.88	0.854	0.802
$_{31}$Ga	0.93		0.818
$_{32}$Ge	0.96		0.833
$_{33}$As	0.99		0.848
$_{34}$Se	1.02		0.861
$_{35}$Br	1.05		0.875
$_{36}$Kr	1.08	1.03	0.888
$_{37}$Rb	1.10		0.902
$_{38}$Sr	1.11		0.912
$_{39}$Y	1.13		0.928
$_{40}$Zr	1.14	1.14	0.939
$_{41}$Nb	1.15		0.950
$_{42}$Mo	1.16		0.959
$_{43}$Tc	1.17		0.968
$_{44}$Ru	1.18	1.16	0.977
$_{45}$Rh	1.19		0.985
$_{46}$Pd	1.21		0.993
$_{47}$Ag	1.22	1.20	1.000
$_{48}$Cd	1.24		1.007
$_{49}$In			1.016
$_{50}$Sn		1.26	1.024
$_{52}$Te			1.038
$_{54}$Xe			1.051
$_{56}$Ba			1.064
$_{58}$Ce			1.074
$_{60}$Nd			1.082
$_{65}$Tb			1.102
$_{70}$Yb			1.133

in the simplest theories (Pincherle, 1935; Geoffrion, Bonenfant, and Nadeau, 1959), Eq. (2–57) leads to the prediction that the K-shell radiative transition probability is proportional to the fourth power of the atomic number:

$$w_{fi}(K) \propto Z^4. \tag{2–58}$$

For electric dipole transitions only, an electron that radiatively fills a K vacancy must come from an np state. On these grounds, Callan (1963b) computed K x-ray emission rates semiempirically using the equation

$$w_{fi}(K) = \sum_n A_n Z^4, \tag{2–59}$$

with the A_n being empirical coefficients for the $np \rightarrow 1s$ transitions, suitably modified for the filling of shells. The results agree well (to $\sim$50%) with available experimental results and compare favorably with the most recent and elaborate theoretical work.

Relativistic calculations of x-ray emission rates have been carried out by Massey and Burhop (1936) and by Laskar (1955, 1958) with screened hydrogenic wave functions. These calculations are based on a Coulomb potential, as are those of Payne and Levinger (1956), Taylor and Payne (1960), and Babushkin (1967). Asaad (1959) used a self-consistent-field potential for a relativistic calculation of $2p_{1/2} \rightarrow 1s$ and $2p_{3/2} \rightarrow 1s$ radiative transition rates in Hg. Laskar and Raffray (1967) computed radiative $E1$, $M1$, and $E2$ transition probabilities to the K, L_1, L_2, and L_3 shells using Slater-screened hydrogenic wave functions and second-quantization formalism; they included the effect of retardation. While these authors report that they have performed the calculations for $50 \leq Z \leq 100$, they include only the numerical results for Pb in their publication.

In a very comprehensive calculation of radiative transition rates to the K and L shells, Scofield (1969) computed the total radiative decay rates and the rates of emission of a number of x-ray lines for elements with atomic numbers $13 \leq Z \leq 92$. The atomic electrons were taken to be in single-particle states in a central potential given by the relativistic Hartree–Slater theory. All multipoles of the radiation field and all transitions from occupied atomic states were included. The electrons were treated relativistically and the effect of retardation was included. The basic formalism employed in these calculations is discussed in Sec. 2.1.3. Scofield's paper includes tabulated K x-ray emission rates for 30 elements with $13 \leq Z \leq 92$, and lists transition probabilities from the L_1 through the $O_{2,3}$ subshells. It also lists radiative transition probabilities to the L_1, L_2, and L_3 levels from subshells through $O_{4,5}$ for 21 elements with atomic numbers $13 \leq Z \leq 92$. Very similar calculations by Rosner and Bhalla (1970) lead to transition probabilities that agree with those of Scofield (1969) to at least three significant figures in most cases. The paper of Rosner and Bhalla (1970) contains one table, listing total radiative transition rates to the K shell, all three L subshells together, and all M subshells combined, for 10 elements with $21 \leq Z \leq 93$. Only transitions from initial states as high as N_7 are taken into consideration.

McGuire (1970a) has calculated radiative transition probabilities to the K shell through his original approach based on the Harman-and-Skillman Hartree–Slater

potential, discussed in Sec. 2.2.3. Radiative transition rates to the K shell have been computed by Walters and Bhalla (1971) from nonrelativistic numerical Hartree–Slater wave functions with Kohn–Sham and Gaspar exchange. Magnetic dipole L_2–L_3 radiative Coster–Kronig transition probabiliies for seven elements with $70 \leq Z \leq 93$ have been calculated from screened relativistic hydrogenic wave functions by Chen *et al.* (1971a).

2.4.2. *Summary of Results and Comparisons With Experiment*

The more comprehensive published calculations of K x-ray emission rates are those of Callan (1963b), Babushkin (1967), Scofield (1969), McGuire (1970a), Rosner and Bhalla (1970), and Walters and Bhalla (1971). Of these, the approaches of Babushkin, Scofield, and Rosner and Bhalla are based on relativistic wave functions.

Total K x-ray emission rates calculated by various authors are listed in Table II.IV. Relative K x-ray intensities have recently been measured by a number of investigators and compared primarily with the calculations of Scofield (1969), who has published the most comprehensive results. Ebert and Slivinski (1969) find measured relative K decay rates for $62 \leq Z \leq 92$ in excellent agreement with Scofield's results, and Nelson and Suanders (1969) note equally good agreement of $K\alpha_2/K\alpha_1$ ratios for 36 elements between $_{51}$Sb and $_{95}$Am. Also, $K\beta_3/K\beta_1$ ratios for elements of medium atomic numbers (but not of high Z) agree well with the calculations (Salem, Saunders, and Nelson, 1970). However, measured $K\beta/K\alpha$ ratios appear to exceed Scofield's theoretical ratios, according to work by Slivinski and Ebert (1969) and by Hansen, Freund, and Fink (1970a, b); the discrepancy is as large as 20% at low Z (Slivinski and Ebert, 1969), and of the order of 7% if one extrapolates the theoretical ratio to $Z=96$ (Hansen, 1971). Schult (1971) has measured the K x-ray intensity ratios $K\alpha_2/K\alpha_1$, $K\beta_1/K\alpha_1$, $K\beta_2/K\beta_1$, $K\beta_3/K\beta_1$, $K\beta_4/K\beta_1$, and $K\beta_5/K\beta_1$ for eight elements from $_{63}$Eu to $_{92}$U and compared them with the calculations of Rosner and Bhalla (1970). With a Ge(Li) x-ray spectrometer, dePinho (1971) has determined the intensities of $K\alpha_2$, $K\beta_3$, $K\beta_1$, $K\beta_5$, $K\beta_2$, and $K\beta_4$ x-ray lines relative to the $K\alpha_1$ intensity of nine elements between $_{79}$Au and $_{92}$U and compared these ratios with Scofield's (1969) calculations. The recent work on K x-ray intensity ratios has been reviewed by Nelson, Saunders, and Salem (1970) and is the subject of a thesis by Hansen (1971).

In Fig. 2–7, measured $K\beta/K\alpha$ x-ray intensity ratios are compared with theoretical predictions, and a similar comparison of $K\alpha_2/K\alpha_1$ ratios is indicated in Fig. 2–8.

Goldberg (1962) and recently Venugopala Rao, Palms, and Wood (1971) investigated L x-ray intensities at high Z. The latter authors used Si(Li) detectors to perform measurements over the range $65 \leq Z \leq 94$ and made a critical comparison of experimental results with the calculations of Scofield (1969) and of Rosner and Bhalla (1970). Venugopala Rao *et al.* (1971) arrived basically at the following conclusions:

(a) Measured intensity ratios of x-ray transitions originating from higher shells to transitions originating

TABLE II.IV. Calculated total K x-ray emission rates, in units of eV/$\hbar$.

Element	Callan (1963b)	McGuire (1970a)	Scofield (1969)
$_{10}$Ne		0.0049	0.0048
$_{11}$Na		0.0079	0.0071
$_{12}$Mg		0.0116	0.0100
$_{13}$Al		0.0158	0.0138
$_{14}$Si		0.0242	0.0202
$_{15}$P		0.0354	0.0288
$_{16}$S	0.05	0.0433	0.0398
$_{17}$Cl	0.06	0.0653	0.0540
$_{18}$Ar	0.09	0.0811	0.0717
$_{19}$K	0.11	0.109	0.0933
$_{20}$Ca	0.13	0.140	0.119
$_{21}$Sc	0.16	0.193	0.150
$_{22}$Ti	0.19	0.242	0.186
$_{23}$V	0.23		0.228
$_{24}$Cr	0.28		0.276
$_{25}$Mn	0.32		0.333
$_{26}$Fe	0.38	0.506	0.396
$_{27}$Co	0.44		0.469
$_{28}$Ni	0.51		0.551
$_{29}$Cu	0.59		0.643
$_{30}$Zn	0.67	0.928	0.747
$_{31}$Ga	0.82		0.864
$_{32}$Ge	1.00		0.996
$_{33}$As	1.20		1.142
$_{34}$Se	1.44		1.305
$_{35}$Br	1.77		1.486
$_{36}$Kr	2.10	2.13	1.686
$_{37}$Rb	2.34		1.905
$_{38}$Sr	2.61		2.144
$_{39}$Y	2.89		2.405
$_{40}$Zr	3.20	3.44	2.688
$_{41}$Nb	3.53		2.995
$_{42}$Mo	3.89		3.328
$_{43}$Tc	4.27		3.687
$_{44}$Ru	4.69	5.07	4.075
$_{45}$Rh	5.13		4.493
$_{46}$Pd	5.60		4.940
$_{47}$Ag	6.10	6.65	5.423
$_{48}$Cd	6.64		5.940
$_{49}$In			6.494
$_{50}$Sn		8.70	7.089
$_{52}$Te			8.402
$_{54}$Xe			9.894
$_{56}$Ba			11.57
$_{58}$Ce			13.44
$_{60}$Nd			15.52
$_{65}$Tb			21.75
$_{70}$Yb			29.65

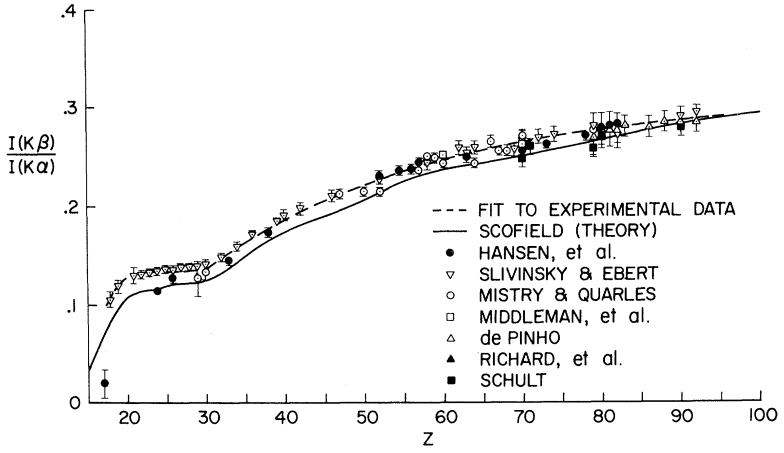

FIG. 2–7. $K\beta/K\alpha$ x-ray intensity ratio as a function of atomic number. Experimental data are from Hansen, Freund, and Fink (1970a) and Hansen (1971a); Ebert and Slivinsky (1969) and Ebert (private communication); Mistry and Quarles (1971), and Quarles (private communication, 1971); Middleman, Ford and Hofstadter (1970); de Pinho (1971); Richard, Bonner, Furuta, and Morgan (1970); and Schult (private communication and 1971). The solid curve is the theoretical $K\beta/K\alpha$ ratio from the work of Scofield (1969), and the broken curve is a best fit to the experimental points. [From Venugopala Rao, Chen, and Crasemann (1972), courtesy of American Institute of Physics.]

from lower shells generally exceed Scofield's theoretical ratios. This discrepancy is observed for $K\beta/K\alpha$ ratios as well as for the ratios $s_2=I(L_2N+L_2O+\cdots)/I(L_2M)$ and $s_3=I(L_3N+L_3O+\cdots)/I(L_3M)$.

(b) Intensity ratios that involve neighboring subshells generally agree well with theory. Examples are $K\alpha_2/K\alpha_1$ and $L\alpha_2/L\alpha_1$.

To illustrate these trends, the ratio s_2 is plotted in Fig. 2–9 and the intensity ratio $L\alpha_1/L\alpha_2$ is indicated in Fig. 2–10, as functions of atomic number.

Salem, Tsutsui, and Rabbani (1971) have most recently measured the x-ray intensity ratios $L\beta_3/L\beta_4$, $L\gamma_1/L\beta_1$, $L\alpha_2/L\alpha_1$, $L\beta_{2,15}/L\alpha_1$, $L\beta_5/L\alpha_1$, $L\beta_6/L\alpha_1$, and $L\gamma_2/L\beta_4$ for several elements between $_{57}$La and $_{92}$U; the results substantially confirm the above conclusions.

Intensity ratios of L x rays from elements with lower atomic numbers have been measured by Wyckoff and Davidson (1965) and by Nix (1972). There is a definite need for additional experimental work on this subject, in order to provide a basis for comparison with recent theoretical results. M x-ray intensities have not yet been measured; some theoretical results have been published by Bhalla (1970c).

So far, only allowed (electric dipole) radiative transitions have been discussed in this section. One forbidden x-ray transition, KL_1, has recently been observed by several experimenters: Boehm (1970), Smither, Freedman, and Porter (1970), Schult (1971), and Venugopala Rao, Wood, and Palms (1971). Observed intensities for this magnetic dipole transition are in reasonable agreement with the transition probabilities calculated by Scofield (1969) and Rosner and Bhalla (1970).

2.5. Atomic Level Widths

2.5.1. Principles

The energy width Γ of an atomic state is related to the mean life τ of the state through a definition based on the Heisenberg uncertainty principle:

$$\Gamma\tau=\hbar. \tag{2–60}$$

The decay probability (per unit time) of a state is therefore $1/\tau=\Gamma/\hbar$. If we denote the radiative decay probability of a state i by $\Gamma_R(i)/\hbar$, the radiationless (Auger) decay probability by $\Gamma_A(i)/\hbar$, and the Coster-Kronig decay probability by $\Gamma_{CK}(i)/\hbar$, we have for

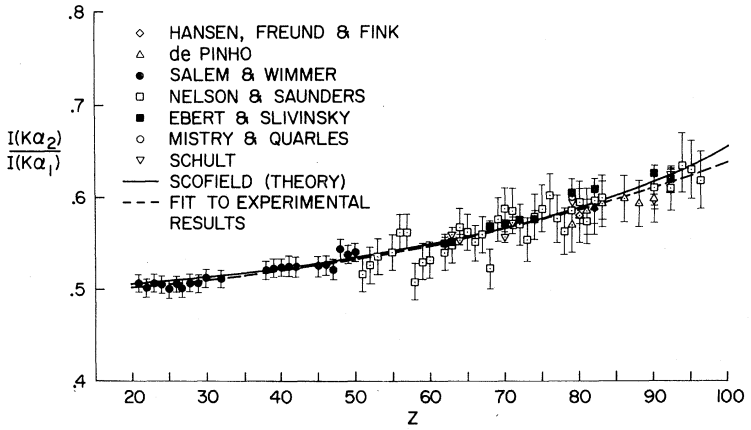

FIG. 2–8. $K\alpha_2/K\alpha_1$ x-ray intensity ratio as a function of atomic number. The measured points are from Hansen, Freund, and Fink (1970a); de Pinho (1971); Salem and Wimmer (1970) Nelson and Saunders (1969); Ebert and Slivinsky (1969) and Ebert (private communication); Mistry and Quarles (1971) and Quarles (1971); and Schult (private communication and 1971). The solid curve indicates the theoretical ratio computed by Scofield (1969), and the broken curve is a least-squares fit to the experimental data. [From Venugopala Rao, Chen, and Crasemann, (1972), courtesy of American Institute of Physics.]

the total width

$$\Gamma(i)=\Gamma_R(i)+\Gamma_A(i)+\Gamma_{CK}(i). \qquad (2\text{–}61)$$

The fluorescence yield of the state i is

$$\omega_i=\Gamma_R(i)/\Gamma(i)=\Gamma_R(i)/[\Gamma_R(i)+\Gamma_A(i)+\Gamma_{CK}(i)]. \qquad (2\text{–}62)$$

Level decay probabilities (or level widths divided by $\hbar$) are commonly given in units of electron volts over $\hbar$ (eV/$\hbar$), or in atomic units (a.u.) or milli-atomic-units (m a.u.) of inverse time, with the corresponding level widths Γ in eV, atomic units of energy, or ergs. These units are related as follows:

Transition probability:

$$1 \text{ a.u.}=4.1341\times10^{16} \text{ sec}^{-1}=27.212 \text{ eV}/\hbar.$$

Width:

$$1 \text{ a.u.}=4.3598\times10^{-11} \text{ erg}=27.212 \text{ eV}. \qquad (2\text{–}63)$$

Information on the widths of atomic levels is based on measurements of the linewidths of x-ray emission lines, measurements of absorption edges, and of absorption lines. The basic theory of natural linewidths, following Dirac's radiation theory, was formulated by Weisskopf and Wigner (1930). In a sophisticated study based on modern quantum electrodynamics, Arnous and Heitler (1953) later concluded that the "classical line shape" of Weisskopf and Wigner is an excellent approximation to the exact result.

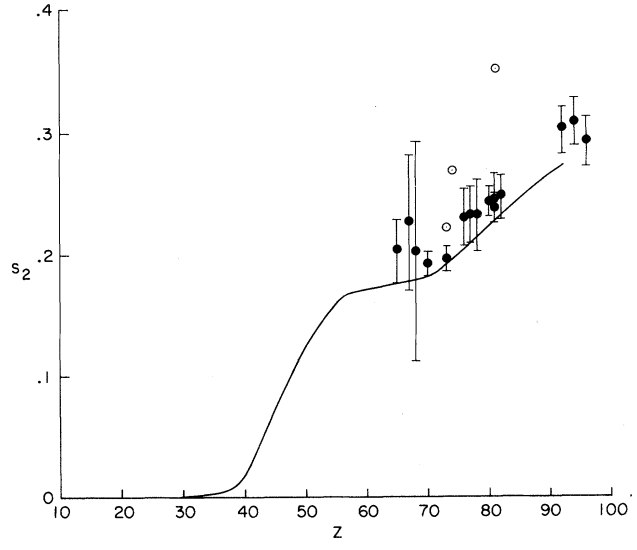

FIG. 2–9. The x-ray intensity ratio $s_2=I(L_2N+L_2O+\cdots)/I(L_2M)$, as a function of atomic number. Solid points represent results obtained by $K\alpha_2$–L x-ray coincidence measurements; open circles indicate ratios calculated from the results of Goldberg (1962). The curve is based on theoretical estimates of Scofield (1969) which do not include p-shell electron contributions. Data in this figure include results summarized by Venugopala Rao, Palms, and Wood (1971) and those obtained by McGeorge and Fink (1971a) for $Z=92$, 94, and 96, and by Mohan (1971) for $Z=78$ and 81.

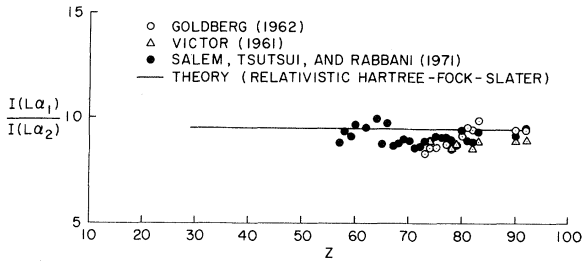

FIG. 2–10. The $L\alpha_1/L\alpha_2$ x-ray intensity ratio as a function of atomic number. In the experimental work, the L_3 vacancies were created by electron bombardment of target elements. Errors are estimated at 5%–6% in the work of Salem, Tsutsui, and Rabbani (1971) and 15%–25% in the work of Goldberg (1962) and of Victor (1961).

According to the quantum-mechanical result, a radiative transition between an initial state A and a final state B has the spectral distribution

$$I(\omega)d\omega=\frac{\Gamma(A)+\Gamma(B)}{2\pi\hbar}\times\frac{d\omega}{(\omega_{AB}-\omega)^2+\{[\Gamma(A)+\Gamma(B)]/(2\hbar)\}^2}, \qquad (2\text{–}64)$$

where $\omega_{AB}=(E_A-E_B)/\hbar$ is the mean circular frequency of the line.

As is apparent from Eq. (2–64), the width of a spectral line is the sum of the widths of the initial and final states. Thus, the atomic K-level width, for example, can be determined by correcting measured $K\alpha_1$ and $K\alpha_2$ x-ray linewidths for instrumental contributions and subtracting L_3 and L_2 level widths, respectively.

2.5.2. K-Level Widths

Information on atomic level widths is scarce and widely scattered, but more extensive data are available on the 1*s* shell than on higher levels. Early measurements of $K\alpha$ line widths were performed by Allison (1933), Richtmyer and Barnes (1934), Ingelstam (1936), and Parratt (1936). Somewhat later, Gokhale (1952) and Brogren (1954) worked on the problem, and an extensive set of $K\alpha_1$ and $K\alpha_2$ linewidth measurements for $Z>50$ was most recently performed by Nelson, John, and Saunders (1969).

Leisi *et al.* (1961) combined $K\alpha$ linewidth information with measurements of L_2 and L_3 level widths and found that for $Z>40$, K-level widths are well represented by the expression

$$\Gamma(K)=1.73\times Z^{3.93}\times10^{-6} \text{ eV} \qquad (2\text{–}65)$$

within the errors of measurement, as illustrated in Fig. 2–11.

In the theoretical calculation of level widths, it is necessary to take account of all radiative and non-

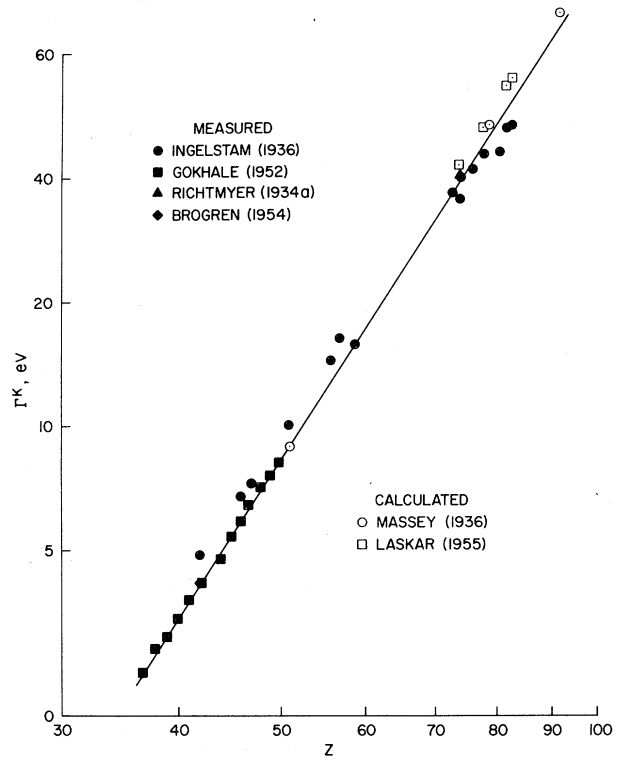

FIG. 2–11. K-level width as a function of atomic number. The straight line represents Eq. (2–65). [After Leisi, Brunner, Perdrisat, and Scherrer (1961), courtesy of Birkhäuser Publishing Co.]

radiative transitions that deexcite a state. An early calculation of this type was performed by Ramberg and Richtmyer (1937) for the K, L, M, and N levels of Au. Recent calculations of $\Gamma(K)$ by Callan (1963b), McGuire (1970a), and Kostroun *et al.* (1971) are compared with the semiempirical K widths of Leisi *et al.* (1961) in Fig. 2–12.

The relation of level widths to the natural width of γ-ray internal conversion lines has been discussed by Mladjenović (1954) and by Geiger, Graham, and Merritt (1963). [See also Sevier (1972), Chap. 6.]

2.5.3. L-Level Widths

Information on L-level widths has been derived from measurements of absorption edges, and absorption and emission line shapes by Leisi *et al.* (1961), on the basis of original data of Richtmyer, Barnes, and Ramberg (1934), Parratt (1938), Beeman and Friedman (1939), and Bearden and Snyder (1941).

Calculated L level widths are plotted against atomic number in Fig. 2–13.

There is a pronounced need for new data on atomic level widths for the purpose of testing theoretical results.

3. K-SHELL FLUORESCENCE YIELDS

The experimental determination of K-shell fluorescence yields ω_K has been a notable endeavor, because of the importance of these quantities in numerous contexts and because it is only now becoming possible to calculate fluorescence yields from theory with any degree of confidence. Consequently, a great amount of effort has been devoted to this line of research by many investigators. In this chaper, we attempt to classify the methods that have been employed in determining ω_K and to compare their potential reliability. Furthermore, from the vast body of experimental data reported in the literature, we select by critical evaluation a limited list of ω_K values that can be considered highly reliable. These values form the basis for a comparison with theory and for a list of recommended values.

3.1. Experimental Methods

For the determination of the K-shell fluorescence yield ω_K (or the Auger yield a_K), the K x-ray or the K Auger-electron emission rate and the number of primary K-shell vacancies must be measured. Vacancies in the K shell are produced by charged-particle impact, photoionization, internal conversion, or orbital-electron capture, and by higher-order effects in nuclear decay. Methods for determining ω_K vary according to the ionization process, the target material, or the decay scheme of the radionuclide, the detectors, and the requirements for necessary corrections. Table III.I is a compilation of methods reported in the literature; these are discussed below.

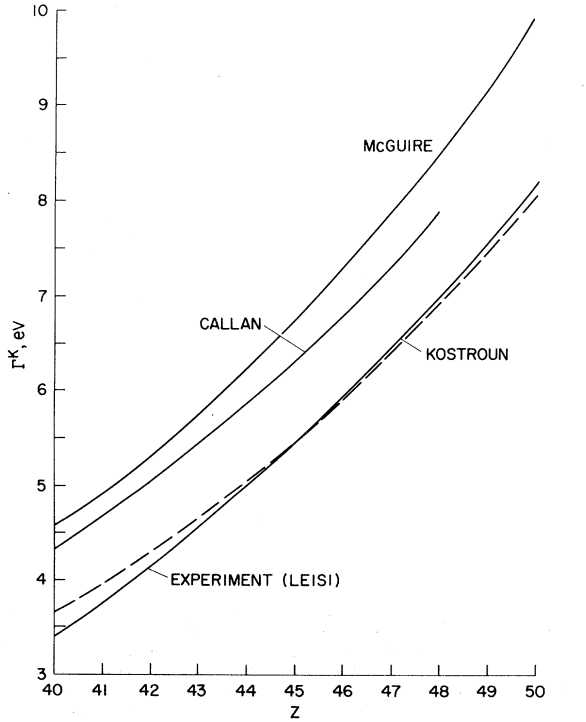

FIG. 2–12. Theoretical K-level widths after Callan (1963b), McGuire (1970), and Kostroun, Chen, and Crasemann (1971), compared with the semiempirical relation of Leisi, Brunner, Perdrisat, and Scherrer (1961).

3.1.1. Fluorescent-Excitation Methods

Gaseous Targets. In this method (No. 1 in Table III.I), a proportional counter is used to measure photoelectric absorption of the exciting radiation and the intensity of fluorescent x rays. (The characteristics of proportional counters are discussed, e.g., by Gold and Bennett, 1965.) Two peaks are normally observed in the spectrum, as shown in Fig. 3–1: The photopeak, of intensity I_A, appears at a pulse height that corresponds to the energy of the monochromatic exciting radiation; it is due to events in which target atoms that have been photoelectrically ionized in their K shells are de-excited by Auger transitions. A second peak, of intensity I_R, results from K-ionized target atoms that are de-excited radiatively, when the emitted K x ray escapes from the counter gas without interacting. This second "escape" peak appears at lower energy than the photopeak; the energy difference is the K x-ray energy. The fluorescence yield ω_K is essentially

$$\omega_K = I_R/(I_A+I_R). \qquad (3\text{–}1)$$

The primary vacancies can be created through photoionization of the target-gas atoms by means of a beam of x rays or low-energy γ rays. Crone (1936), Heintze (1955), Bailey and Swedlund (1967), and Pahor *et al.* (1968, 1969, 1971a–c) have used exciting radiation produced by an x-ray tube; electron-capturing nuclides were employed as radiation sources by West and Rothwell (1950), Bertolini, Bisi, and Zappa (1953), Harrison, Crawford, and Hopkins (1955), Frey, Johnston, and Hopkins (1959), Godeau (1961), and Watanabe, Schnopper, and Cirillo (1962).

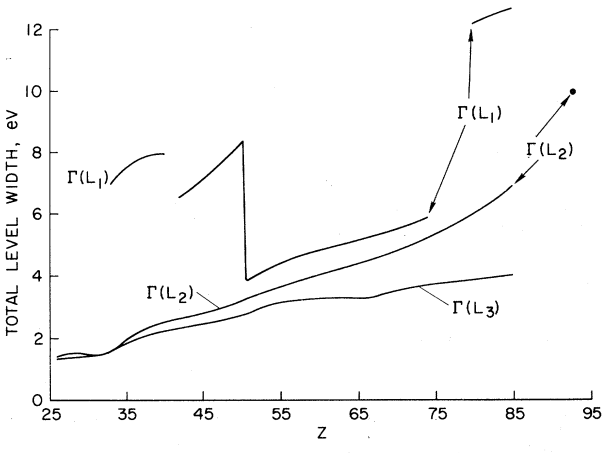

FIG. 2–13. Total L_1-, L_2-, and L_3-level widths, as functions of atomic number. Sharp discontinuities in $\Gamma(L_1)$ occur where intense Coster–Kronig transitions become energetically possible or impossible. Because electron binding energies in atoms with inner vacancies are subject to considerable uncertainties, the exact atomic numbers at which width discontinuities occur are not always certain. Only in some cases can these discontinuities be located with the aid of Coster–Kronig and Auger-electron spectra. [From Crasemann, Chen, and Kostroun (1971), courtesy of American Institute of Physics.]

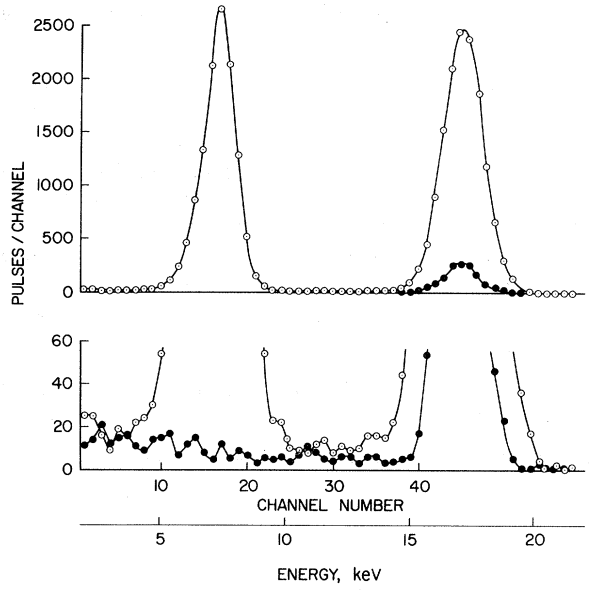

FIG. 3–1. Pulse height distribution from a wall-less multiwire counter filled with CH_4 and nonradioactive GeH_4 admixture. The background spectrum (solid circles) is taken without GeH_4 admixture. [After Pahor, Kodre, Hribar, and Moljk (1969), courtesy of Springer-Verlag.]

The wall effect introduces errors at low counting-gas pressures: if the trajectory of an electron takes it to the wall, a part of the ionization is lost and a reduced pulse is produced. This problem can be avoided by using a wall-less multiwire proportional counter with surrounding ring counter, as shown in Fig. 3–2 (Drever and Moljk, 1957; Pahor *et al.*, 1968, 1969, 1971a–c).

Corrections must be taken into account for the following effects: (1) absorption of fluorescent K x rays in the counter gas (nonescape). This correction requires the numerical solution of multiple integrals that depend on counter dimensions, absorption coefficients, and pressure of the counting-gas mixture. For example, Heintze (1955) found values between 0.947 ± 0.006 and 0.694 ± 0.022 for the escape probability in a conventional argon-filled single-wire counter. The nonescape correction can also be determined experimentally by repeating measurements at various gas pressures and extrapolating to zero pressure. In any case, an uncertainty of at least 1% remains and contributes to the error of the final result. (2) Absorption of the exciting radiation in higher shells of target atoms, often described in terms of the so-called "K jump" in the photoelectric cross section (Compton and Allison, 1935; Blokhin, 1957; Henke *et al.*, 1967; McMaster *et al.*, 1969). This correction is usually estimated from photoelectric absorption coefficients for the various atomic shells. For example, values from 1.147 to 1.177 are reported for the K-jump correction of Ge (Blokhin, 1957; Pahor *et al.*, 1969); this uncertainty results in a possible systematic error of 3%, not included in the quoted error in ω_K for Ge as determined by Pahor *et al.* (1969). The magnitude of the K-jump correction

TABLE III.I. Methods that have been used for the determination of K-shell fluorescence yields.

No.	Method	Mode of production of primary vacancies	Target or source	Detectors[a]	Atomic numbers to which applied	Quoted accuracy (percent)	Presently estimated ultimate accuracy of the method (percent)
1	Fluorescent excitation of gaseous targets	X rays	Gaseous	ic, pc, mw	10–54	0.5–22	3
2	Fluorescent excitation of solid targets	X rays	Solid	ic, ppl, pc, NaI (Tl)	4–56	1.4–26	3
3	Auger- and conversion-electron spectroscopy	Internal conversion, electron capture	Solid	$s\pi$, sl, sd, NaI(Tl)	43–93	0.2–9.0	1
4	Auger-electron, x- and β-ray spectroscopy	Electron capture	Solid	sd, NaI(Tl)	80	1.7	2
5	Auger-electron and K x-ray spectroscopy	Electron capture	Gaseous	pc, mw	17, 31	0.4–5.6	1
6	Auger-electron and K x-ray spectroscopy	Electron capture	Solid	pc, d, Si(Li)	12–49 78, 92	0.9–37 0.8	5 1
7	K x-ray and γ-ray or conversion-electron spectroscopy	Electron capture leading to metastable states	Solid	pc, NaI(Tl) anthracene, sc	27–49	5.9–8.9	5
8	Determination of K x-ray emission rate and disintegration rate	Electron capture	Solid	pc, NaI(Tl)	23–54	0.8–10.0	1
9	Measurement of (K x-ray)–(γ-ray) or (K x-ray)–(K conversion-electron) coincidences	Electron capture, internal conversion	Solid	pc, NaI(Tl), Ge(Li), Si(Li)	22–52	1.3–9.0	2
10	Cloud-chamber technique	X rays	Gaseous	cc	8–54	3–75	15
11	Change of ionization at K edge	X rays	Gaseous Solid	ic phc	22–53	Not quoted	20
12	Photographic emulsion technique	Electron capture	Solid	ppl	84	5.6	15
13	Charged-particle excitation	e^-, p, α, heavy ions	Gaseous Solid	pc, Si(Li), Ge(Li)	6–18	11–17	15

[a] The following abbreviations are used: cc, cloud chamber; ic, ionization chamber; pc, proportional counter; d, double proportional counter; mw, multiwire proportional counter; phc, photocathode; ppl, photographic film or plate; sc, semiconductor; sd, double-focusing spectrometer; sl, lens spectrometer; $s\pi$, 180° spectrometer.

increases with higher Z up to 1.29 for uranium (McMaster *et al.*, 1969). (3) Secondary electrons or x rays emitted from the counter walls and wires. This correction is essentially negligible for wall-less multiwire proportional counters contained in pressure vessels of low-Z material. (4) Background subtraction and the resolution of photopeak and escape peak.

Solid Targets. Method No. 2 is based on the excitation of solid targets by x-ray irradiation. The K-shell fluorescence yield is proportional to the ratio of intensities of the fluorescent K x rays, I_K and the incident exciting radiation, I:

$$\omega_K \propto I_K/I. \tag{3–2}$$

Target thickness should be optimized so that the probability of ionization is as high as possible and self-absorption of the fluorescent x rays in the target is low.

Various detectors have been used in measurements of this type. Early work was performed with photographic films (Lay, 1934) or ionization chambers (Kossel, 1923; Bothe, 1925; Balderston, 1926; Harms, 1927; Compton, 1929; Haas, 1932; Berkey, 1934; Arends,

1935; Martin, Bower, and Laby, 1935; Backhurst, 1936; Stephenson, 1937; Fairbrother, Parkyn, and O'Connor, 1957). Roos (1954, 1955, 1957) employed a NaI(Tl) scintillation spectrometer, placing target foils at three distances from the crystal. Nichols (1956) used two NaI(Tl) detectors; he oriented the target foil at 45° with respect to the beam axis, placing one detector on the beam axis and the other at right angles to it. Some authors have used proportional counters (Fig. 3–3) to measure both the exciting and fluorescent x rays (Davidson and Wyckoff, 1962; Bailey and Swedlund, 1967; Dick and Lucas, 1970). Others have placed the target foils directly in the window of a proportional counter (Patronis, Braden, and Wyly, 1957; Bertrand, Charpak, and Suzor, 1959; Suzor and Charpak, 1959). Konstantinov, Perepelkin, and Sazonova (1964) mounted target foils between two proportional counters, as illustrated in Fig. 3–4; the foils were coated with radioactive source material for exciting radiation.

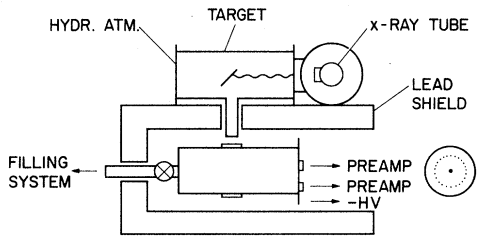

FIG. 3–2. Experimental arrangement for the passage of monoenergetic x rays through a wall-less counter, according to Pahor, Kodre, and Moljk (1968). (Courtesy of North-Holland Publishing Co.)

Corrections for the following effects are most important in this method: (1) Absorption of the exciting radiation in the detector window; (2) Self-absorption of fluorescent K x rays in the sample. (These two effects are not independent, and are related to the amount of absorption of the exciting radiation in the target foil. The necessary corrections are usually calculated by numerical integration of multiple integrals.) (3) Detection efficiencies for exciting and fluorescent radiation, including solid angles. Considerable errors arise from these corrections; these can be reduced to a few percent only under the most favorable conditions. Additional uncertainties of 1%–5% can arise from absorption coefficients of the solid target material for the primary and fluorescent radiation; these coefficients are usually adopted from the literature, e.g., from Storm and Israel (1970).

3.1.2. *Excitation Due to Radioactive Decay*

Auger- and Conversion-Electron Spectroscopy With High-Resolution Spectrometers. The principle of this method (No. 3) is the determination of the ratio of K Auger-electron intensity I_A and K conversion-electron

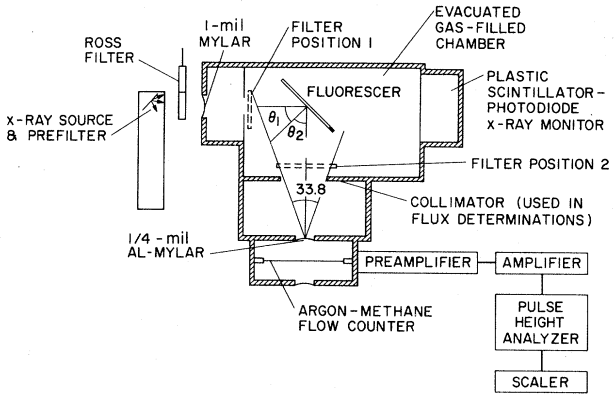

FIG. 3–3. Apparatus for fluorescence-yield measurements employed by Bailey and Swedlund (1967).

intensity I_e. The K Auger yield a_K satisfies the proportionality relation

$$a_K \propto I_A/I_e. \qquad (3\text{–}3)$$

The most suitable radioactive nuclides for this method decay through a highly converted γ transition. Different techniques have been used for source preparation: simple drop deposition (Steffen, Huber, and Humbel, 1949; Broyles, Thomas, and Haynes, 1953; Pruett and Wilkinson, 1954; Ketelle, Thomas, and Brosi, 1956; Hoffman and Dropesky, 1958), electroplating (Wapstra, 1953), glow discharge (Forrest and Easterday, 1958), sublimation (Laberrigue-Frolow, Radvanyi, and Langevin, 1956; Graham and Merritt, 1961), and vacuum evaporation (Bergström and Thulin, 1950; Haber *et al.*, 1952; Broyles, Thomas, and Haynes, 1953; Nall, Baird, and Haynes, 1960; Graham *et al.*, 1961; Ravier, Marguin, and Moussa, 1961; Suter and Reyes-Suter, 1961; Foin, Gizon, and Oms, 1968; Oms, Foin, and Baudry, 1968). Self-absorption of Auger electrons in the source must be minimized by using exceedingly thin

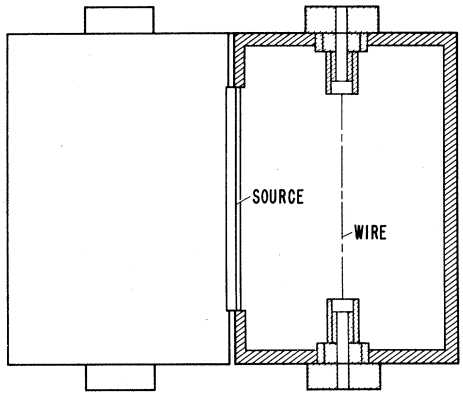

FIG. 3–4. Arrangement for fluorescence-yield measurements with two proportional counters, according to Konstantinov, Perepelkin, and Sazonova (1964). The radioactive source providing the exciting x rays is placed between the counters. (Courtesy of Columbia Technical Translations.)

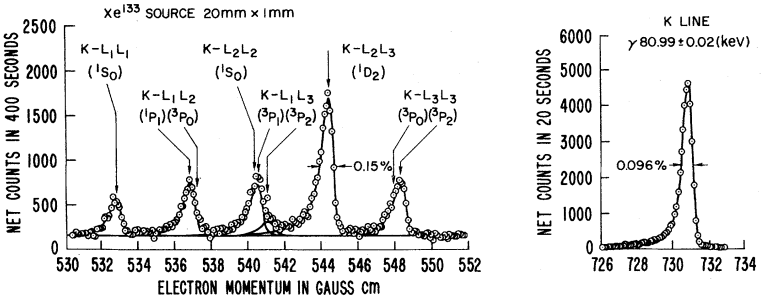

FIG. 3–5. The K–LL Auger spectrum emitted by ^{133}Cs following β decay of ^{133}Xe. The 80.99-keV K-conversion line in ^{133}Cs shown at the right gives rise to essentially all the K x rays and Auger-electron lines from this nuclide as measured with the Chalk River high-resolution (0.07%) spectrometer. [After Graham, Brown, Ewan, and Uhler (1961), courtesy of National Research Council of Canada, Ottawa, Canada.]

sources, and low-Z backings must be employed to reduce backscattering; both effects contribute toward a "degradation tail" on the low-energy side of the electron spectrum. Suitable sources can be prepared by evaporation in vacuum of carrier-free or very-high-specific-activity material, or by deposition under a retarding potential in an electromagnetic mass separator.[4]

Measurements of this type are usually performed with high-resolution magnetic lens spectrometers (Steffen, Huber, and Humbel, 1949; Kondaiah, 1951; Huber *et al.*, 1952; Broyles, Thomas, and Haynes, 1953; Wapstra, 1953; Azuma, 1954; Mladjenović and Slätis, 1955; Ketelle, Thomas, and Brosi, 1956; Laberrigue-Frolow, Radvanyi, and Langevin, 1956; Forrest and Easterday, 1958), 180°-spectrometers (Steffen, Huber, and Humbel, 1949; Pruett and Wilkinson, 1954; Hoffman and Dropesky, 1958), and double-focusing spectrometers (Bergström and Thulin, 1950; Broyles, Thomas, and Haynes, 1953; Gray, 1956; Brabetz *et al.*, 1959; Nall, Baird, and Haynes, 1960; Erman and Sujkowski, 1961; Graham and Merritt, 1961; Graham *et al.*, 1961; Monnand and Moussa, 1961; Ravier, Marguin, and Moussa, 1961; Suter and Reyes-Suter, 1961; Foin, Gizon, and Oms, 1968; Oms, Foin, and Baudry, 1968). Measurements can also be carried out with silicon semiconductor detectors. In any case, high resolution is the essential condition for obtaining accurate results (Fig. 3–5).

Corrections must be applied to allow for the effects of self-absorption, scattering, and backscattering of Auger and conversion electrons and for absorption in the detector window. If only the K–LL Auger-electron groups are measured, the Auger-electron intensity ratios $(K\text{–}LX)/(K\text{–}LL)$ and $(K\text{–}XY)/(K\text{–}LL)$ must be taken into account. If the source nuclei undergo electron capture, a part of the measured number of K vacancies arises from K capture. To allow for this contribution, it is necessary to know P_K, the fraction of nuclei decaying by K capture, as well as the total and K-shell internal conversion coefficients. The pertinent factors can be determined by x–γ and x–x coincidence measurements with NaI(Tl) or Ge(Li) detectors (Pruett and Wilkinson, 1954; Foin, Gizon, and Oms, 1968).

Auger-Electron, X-Ray, and β-Ray Spectroscopy. In this method (No. 4), the ratio $R_{A\beta}$ of K Auger-electron intensity to β-particle intensity is measured with a high-resolution magnetic spectrometer, and the ratio $R_{R\beta}$ of K x-ray intensity and β-particle intensity is determined with NaI(Tl) counters and by $4\pi\beta$–γ coincidence counting, using a suitable nuclide as tracer (Park and Christmas, 1967). The fluorescence yield is

$$\omega_K = R_{R\beta}/(R_{R\beta}+R_{A\beta}). \qquad (3\text{–}4)$$

Only nuclides that decay by both electron capture and β^- emission, such as ^{204}Tl, are suitable for this method. The sources must be prepared on thin films by evaporation in vacuum.

Corrections must be applied for several effects: (1) Self-absorption and self-scattering of electrons due to finite source thickness; (2) Electron backscattering from the source backing; (3) Absorption of electrons in the detector window; and (4) $(K\text{–}LX)/(K\text{–}LL)$ and $(K\text{–}XY)/K\text{–}LL)$ Auger-electron intensity ratios, if only K–LL Auger-electron groups are measured.

Auger-Electron and X-Ray Spectroscopy With Gaseous Radioactive Sources. With radioactive gases, two sets of measurements are performed: First, with a high-Z counting gas at high pressure, the total intensity I_{RA}

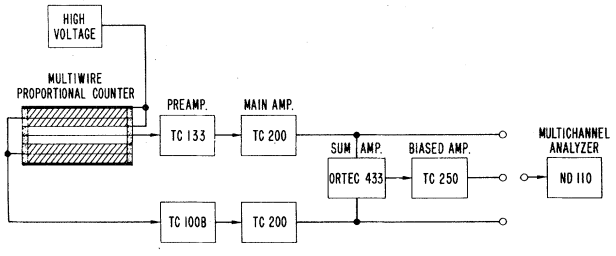

FIG. 3–6. Block diagram of electronic apparatus for measuring Auger-electron spectra with a multiwire proportional counter, as employed by Freund, Genz, Siberts, and Fink (1969) with $^{71}GeH_4$ gas. The shaded region represents the ring-counter volume. (Courtesy of North-Holland Publishing Co.)

[4] Even direct deposition of a retarded ion beam at only 1.0 kV results in excessive source self-absorption for electrons below 4 keV, due to penetration of the ions into the backing. This fact was demonstrated by Krisciokaitis and Haynes (1967) in studies of K and L Auger spectra from ^{113}Sn sources. In these experiments, sources were made by deposition of mass-separated 1.0-keV ^{113}Sn ions onto a filament and subsequent vacuum-evaporation of the radioactive material.

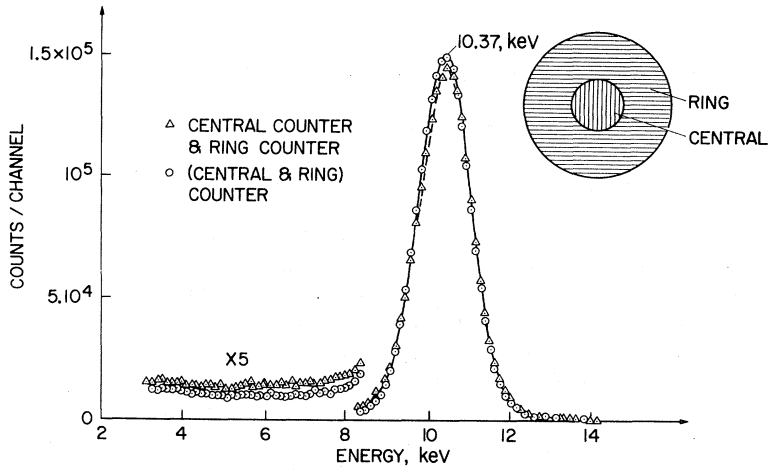

FIG. 3–7. Comparison of K Auger-electron spectra of Ga following ^{71}Ge decay, measured with a multiwire counter filled with 0.3 atm of propane. [From Freund, Genz, Siberts, and Fink, (1969a), courtesy of North-Holland Publishing Co.]

of K x rays and K Auger electrons is determined with high efficiency. Next, with a low-Z counting gas at low pressure, the absorption of K x rays is drastically reduced and essentially only the K Auger-electron intensity I_A is measured. The K fluorescence yield can then be found from the relation

$$\omega_K \propto (I_{RA}-I_A)/I_{RA}. \tag{3-5}$$

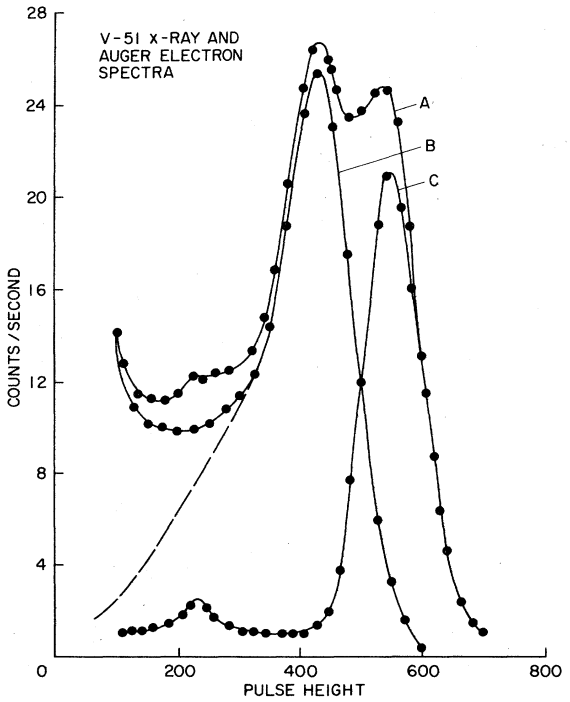

FIG. 3–8. K Auger-electron and K x-ray spectra of ^{51}V, measured with a solid ^{51}Cr source in a single-wire proportional counter (Frey, Johnston, and Hopkins, 1959). Curve A is the total spectrum, curve B is the x-ray spectrum obtained with a 1.54 mg/cm^2 Al absorber. Spectrum C was obtained by subtracting curve B from A. The dashed portion of curve B is an estimation of low-energy "tailing."

Proportional counters have been used to measure the intensities (Fig. 3–6).

Corrections must be made to account for the following factors: (1) Counter efficiencies for K x rays and K Auger electrons; (2) Loss of degraded K Auger electrons due to a definite energy cutoff; and (3) Secondary radiations emitted from counter walls. This latter correction can be determined by variation of length and diameter of a single-wire proportional counter (Spernol, 1967). No correction is necessary if a wall-less multiwire proportional counter which is surrounded by a ring counter is used (Drever and Moljk, 1957; Pahor and Moljk, 1967; Freund *et al.*, 1969; Pahor, Kodre, and Moljk, 1970). Appropriate corrections for degradation tails of the K peak can be made accurately (Fig. 3–7). The corresponding contributions to the error in the final result are less than 1.5%. Errors from other sources can be kept to less than 0.5% (Freund *et al.*, 1969a). This method (No. 5) can be one of the most accurate.

Auger-Electron and X-ray Spectroscopy With Solid Radioactive Sources. The total intensity of K x rays and K Auger electrons, I_{RA}, is measured with an uncovered solid source placed in the active volume of a gas counter. The source is then covered with a foil of sufficient thickness to absorb all Auger electrons, and only the K x-ray intensity I_R is measured (Harrison, Crawford, and Hopkins, 1955; Frey, Johnston, and Hopkins, 1959; Rightmire, Simanton, and Kohman, 1959). The fluorescence yield is proportional to the ratio of the two intensities (Fig. 3–8):

$$\omega_K \propto I_R/I_{RA}. \tag{3-6}$$

Single-wire proportional counters have been used to measure the intensities. Attempts have also been made to use this method with solid sources mounted internally between double-chambered proportional counters and to deduce the fluorescence yield with the aid of Eq. (3–5) (Konstantinov, Sokolova, and Sazonova, 1961; Kramer *et al.*, 1962).

The most serious corrections required by this method are for: (1) Self-absorption of K Auger electrons. This effect can be large. For example, the correction for self-absorption of K Auger electrons from ^{54}Mn sources prepared by evaporation of a liquid drop amounts to as much as 50%; by electrospraying, 23%; by electrodeposition, 15%; and by vacuum evaporation, 2–4% (Bambynek and Reher, 1967b); (2) Absorption of K x rays in the sandwich foils. The correction required amounts to 0.5%–3.0%, depending on type and thickness of the foil; and (3) Degradation tails. The required corrections are very difficult and have not been made in measurements with solid sources; (4) The contribution from K x rays which is always present in the measurement of K Auger-electron intensities, because of x-ray scattering and photoelectrons ejected from the walls and internal parts of the counter. This effect simulates a higher electron intensity and has not been taken into account in experiments with solid sources; and (5) Change in geometry. In so-called 2π or 4π geometry for solid sources, a loss of K x rays emitted at small angles (e.g., $<2°$) reduces the effective geometry appreciably (up to 4%), leading to a lower value for the K x-ray intensity. No corrections for such losses have been made.

Because of the indicated difficulties, methods for measuring ω_K at low Z on the basis of K Auger-electron intensity determinations from solid sources should be considered with reservations.

Recently, a considerable improvement for high-Z elements was made by Hansen *et al.* (1972), who took advantage of the capability of a "windowless," cooled Si(Li) detector to measure K Auger electrons and K x rays simultaneously from a carrier-free radioactive source. The fluorescence yield is given by

$$\omega_K = 1/(1+I_A/I_R), \tag{3–6a}$$

where I_A and I_R are the K Auger-electron and K x-ray intensities, respectively. This approach does not require knowledge of conversion coefficients, branching ratios, and solid angles, but it does require the determination of the relative efficiencies for detection of K Auger electrons and K x rays, corrections for self-absorption and scattering, and small corrections for summing effects. In the high-Z region, the method can be made very accurate, because radiative transitions dominate very much over Auger transitions.[5]

K X-Ray and γ-Ray or Conversion-Electron Spectroscopy. In this method (No. 7), the intensity of the K x rays and of the conversion electrons or γ rays is measured. Nuclides that have a metastable state with a converted γ transition are suitable. Sources prepared by drop evaporation have been used. Sen and Durosinmi-Etti (1966) employed a surface-barrier electron detector and a NaI(Tl) x-ray and γ-ray detector. Schmolz and Hoffman (1968) used two anthracene crystals to measure K x rays and two NaI(Tl) crystals to count γ rays. Wilken (1968) used a proportional counter to determine the conversion-electron intensity and a NaI(Tl) detector for the γ rays.

Corrections must take into account: (1) Self-absorption, (2) Solid angles, (3) Detector efficiencies, and (4) K x rays and K Auger electrons originating from electron capture. Furthermore, the pertinent internal conversion coefficients must be known.

Determination of K X-Ray Emission Rate and Disintegration Rate. This method (No. 8) requires determination of the K x-ray emission rate I_K, preferably with a large proportional counter filled to a sufficient pressure to absorb all K x rays (Fig. 3–9). In addition, the disintegration rate D must be determined, preferably by means of a coincidence technique as used in the absolute standardization of radioactive sources. The value $P_K\omega_K$ is found from the relationship

$$P_K\omega_K = I_K/D, \tag{3–7}$$

where P_K is the fraction of disintegrations proceeding by K capture.

The method is described in detail by Taylor and Merritt (1963). To check the K x-ray emission rate, a second fairly independent approach can be used (Bambynek, 1967a; Bambynek and Reher, 1968a; Bambynek, De Roost, and Funck, 1968b; Bambynek and Reher, 1970), utilizing a medium solid-angle arrangement with a proportional counter or a thin NaI(Tl) crystal as detector (Bambynek, Lerch, and Spernol, 1966; Bambynek, 1967c). The detection system for determining the disintegration rate by the $4\pi\beta$–γ coincidence method has been described by Campion (1959). It consists of a 4π flow-type pillbox proportional counter placed between two NaI(Tl) detectors (Fig. 3–10). A calibrated γ spectrometer (Vaninbroukx and Grosse, 1966) has been used as a second fairly independent system to determine the disintegration rate (Bambynek, 1967a; Bambynek and Reher, 1968a; Bambynek, De Roost, and Funck, 1968b; Bambynek and Reher, 1970).

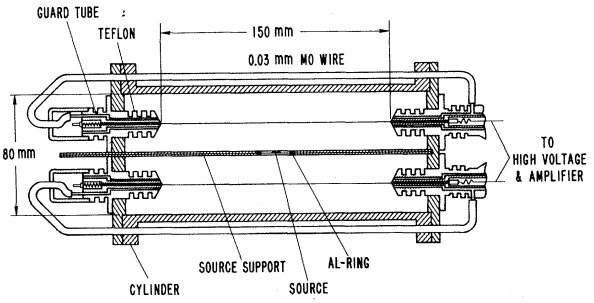

FIG. 3–9. A large 4π proportional counter for the measurement of K x rays (Bambynek, 1965). The counter is operated under high pressure of up to 50 atm inside a stainless-steel tube not shown in the figure.

[5] This method can also be applied directly to the determination of K conversion coefficients by the absolute e^-/γ ("AEG") method (Hamilton *et al.*, 1966).

Radioactive sources have been prepared for experiments of this type by drop evaporation (Taylor and Merritt, 1963; Legrand, 1965; Leistner and Friedrich, 1965; Troughton, 1967; Dobrilović *et al.*, 1970), electrodeposition (Petel and Houtermans, 1967), and evaporation in vacuum (Bambynek, 1967a; Bambynek and Reher, 1968; Bambynek, De Roost, and Funck, 1968; Bambynek and Reher, 1970). Sources were mounted on thin metallized plastic foils for determining disintegration rates, then were sandwiched between absorber foils that stop all Auger electrons, in order to measure K x-ray emission rates in a high-pressure proportional counter.

The principal corrections that must be applied in the K x-ray measurements are for (1) Self-absorption in the sources, (2) Foil absorption, determined by varying foil thickness, (3) X-ray counter efficiency (normally near unity), checked by varying gas pressure, and (4) The effect of γ rays and β^+ particles, if present. The corrections in the determination of the disintegration rate by the coincidence method are small and well-understood, and involve only parameters that can be determined experimentally as an integral part of the measurement. Thus, the disintegration-rate measurements make only a small contribution to the errors in the $P_K\omega_K$ values.

This method has been applied in laboratories specializing in the standardization of radionuclides. Several of the most reliable values have been measured by this method.

Coincidence Methods. With nuclides that decay by electron capture, feeding a γ transition in the daughter nucleus, coincidences can be measured between K x rays and γ rays. One finds

$$P_K\omega_K = C_{K(\gamma)}/(C_\gamma \epsilon_K), \qquad (3\text{–}8)$$

where $C_{K(\gamma)}$ is the (K x-ray)–(γ-ray) coincidence counting rate, C_γ is the singles γ rate, P_K is the fraction of decays proceeding by K capture to the level in the daughter nucleus that decays by the γ transition under consideration, and ϵ_K is the overall efficiency of the x-ray counter (Fig. 3–11). Most sources for such experiments have been prepared by drop evaporation; Grotheer, Hammer, and Hoffman (1969) used molecular plating. Different combinations of detectors have been employed: proportional counters for the K x rays and NaI(Tl) detectors for the γ rays (Hagedoorn and Konijn, 1957; Konijn, Hagedoorn, and van Nooijen,

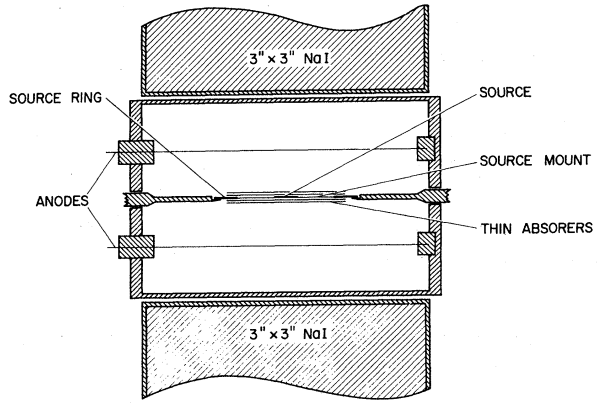

FIG. 3–10. Coincidence counting system for the determination of disintegration rates. [After Taylor and Merritt (1963), courtesy of Nuclear Energy Information Center, Warsaw, Poland.]

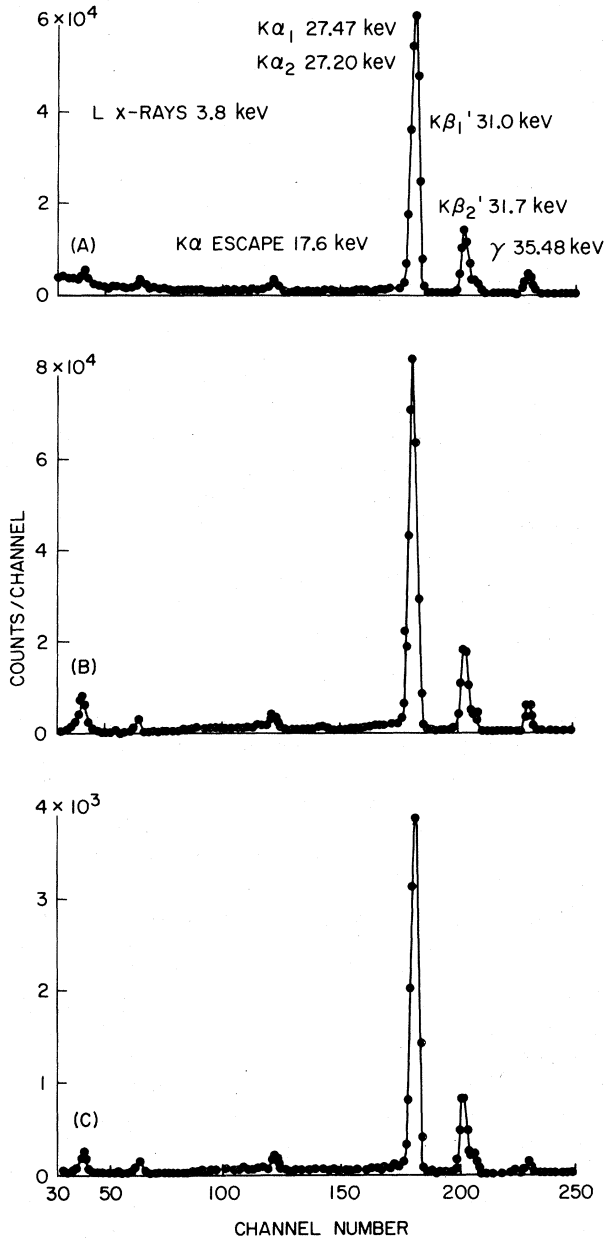

FIG. 3–11. Spectrum of Te x rays and γ rays following the decay of ^{125}I. *A*, single spectrum, *B*, spectrum in coincidence with $K\alpha$ and $K\beta$ x rays, *C*, spectrum in coincidence with 35.48-keV γ rays. [Karttunen, Freund, and Fink (1969), courtesy of North-Holland Publishing Co.]

1958; Konijn, van Nooijen, and Hagedoorn, 1958; Hagedoorn and Wapstra, 1960; Mukerji and McGouch, 1967; Mukerji, McGouch, and Cole, 1967), or proportional counters (Rubinson and Gopinathan, 1968), NaI(Tl) detectors (Welker and Perlman, 1965; Mukerji, McGouch, and Cole, 1967; Hammer, 1968; Grotheer, Hammer, and Hoffmann, 1969), and Ge(Li) detectors (Karttunen, Freund, and Fink, 1969) for both radiations.

Principal corrections must be applied for the following effects: (1) Self-absorption and absorption of K x rays in the materials between the source and the sensitive volume of the detector; (2) Efficiency of the K x-ray detector, including solid angle; (3) Detection of γ rays in the K x-ray detector; (4) Contribution of positrons, if present; and (5) Sum and accidental coincidences. Values of P_K and P_{β^+} must be taken from the literature (Fink, 1968) or computed from theory (Behrens and Jänecke, 1969; Zyryanova, 1968).

It is also possible to determine ω_K from coincidence measurements of the K x-ray spectrum gated by K conversion electrons (Kyles *et al.*, 1970; Hansen, 1971 and Hansen *et al.*, 1972). One has

$$\omega_K = C_{R(e)}/(C_e \epsilon_R), \tag{3-8a}$$

where $C_{R(e)}$ is the counting rate of K x rays gated by K conversion electrons, C_e is the number of K conversion electrons counted in the gate, and ϵ_R is the over-all efficiency of the x-ray counter. The method is suited for a variety of cases, because many nuclides undergo β- or α-decay to an excited state, followed by a K-converted γ transition.

Kyles *et al.* (1970) employed a proportional counter for detecting K conversion electrons and a thin NaI(Tl) detector for K x rays, while Hansen (1971, Hansen *et al.*, 1971, 1972) used cooled Si(Li) and Ge(Li) detectors. Corrections must be made for: (1) Self-absorption and absorption of K x rays in the materials between the source and sensitive volume of the detector; (2) Detection efficiency of the K x-ray detector, and (3) Contribution of K x rays from K–K vacancy cascades, if these are present.

Instead of utilizing coincidences between x rays and conversion electrons, it should also be possible to determine ω_K from coincidences between K Auger electrons and K conversion electrons from a single γ transition which does not exhibit cascading of K vacancies from K capture or other coincident transitions that undergo K-shell conversion. This approach, suggested by Hansen (1971), has not yet been applied; it should lead to accurate results at high Z, where ω_K can be determined to $\sim$1% through a 10% measurement of a_K:

$$\omega_K = 1 - C_{A(e)}/(C_e \epsilon_A). \tag{3-8b}$$

Here, $C_{A(e)}$ is the counting rate of K Auger electrons gated by K conversion electrons, C_e is the gate counting rate of K conversion electrons, and ϵ_A is the over-all detection efficiency of the Auger-electron counter.

3.1.3. *Inner-Shell Vacancies Produced by Charged-Particle Impact*

Electrons. In this method (No. 13), a beam of monoenergetic electrons of 0.2–20 keV energy impinges on a target and produces vacancies in the K shell. Both solid targets (Hink and Päschke, 1971) and gaseous targets (Tawara, Harrison, and de Heer, 1972) have been used. The intensity I_K of the generated x rays is measured with a suitable flow proportional counter equipped with a thin entrance window (Hink, Scheit, and Ziegler, 1970a, b). The number of incident electrons n_e is measured by means of a Faraday cup. The ratio I_K/n_e is proportional to the K x-ray emission cross section $\sigma_K(E)$ of the target material for electrons of energy E, which is equal to the product of the K-shell fluorescence yield ω_K and the K-shell ionization cross section:

$$\omega_K \sigma_I(E) = \sigma_K(E).$$

Principal corrections are those required for: (1) Energy loss of the incident electrons in the target material; (2) Self-absorption of x rays in the target; (3) Absorption of x rays in the entrance window of the counter; (4) Solid angle; (5) Efficiency of the proportional counter; and (6) Bremsstrahlung background.

Values of $\sigma_I(E)$ have been deduced from the classical calculations of Gryzinski (1965) by Hink and Päschke (1971).

It is possible to determine the fluorescence yield from measurements of both the K x-ray emission cross section (Tawara, Harrison, and de Heer, 1972) and the K Auger-electron ejection cross section (Glupe and Mehlhorn, 1967; Glupe, 1971).

Protons. Protons have been used to produce K-shell vacancies in experiments from which the fluorescence yield ω_K could be deduced (Khan, Potter, and Worley, 1965; Brandt and Laubert, 1969; Garcia, 1970). [See also contributions to the International Conference on Inner-Shell Vacancy Phenomena, Atlanta, 1972; *Proceedings* to be published by North-Holland Publishing Co., Amsterdam.] However, no ω_K values determined by this method have yet been reported.

Heavier Ions. Ionization of the K shell can also be caused by impact of heavier ions. Saris and Onderdelinden (1970) have determined cross sections for Ne K x-ray emission in Ne^+–Ne collisions. The deduced fluorescence yield depends strongly on the energy of the incident ions. The production of multiple vacancies is a prominent feature of heavy-ion impact (Knudsen *et al.*, 1971; Brandt, 1972).

3.1.4. *Other Methods*

There are some obsolete methods which today are only of historical interest.

Cloud-Chamber Technique. Gaseous targets are irradiated by monoenergetic x rays. From the total number of single photoelectron tracks and the number of Auger-electron tracks in a cloud chamber, ω_K can

be deduced. By this method, Auger (1925) first established the existence of radiationless transitions.

Jump of Photoionization Current at the K Edge. The current in an ionization chamber is determined when the energy of exciting x rays is just on the high-energy side of the K absorption edge of the target element, and when it is just on the low-energy side of the absorption edge. Gaseous targets were employed (Martin, 1927; Stockmeyer, 1932), or solid target material was evaporated in vacuum onto a photocathode (Rumsh and Shchemelev, 1962).

Photographic Emulsion Technique. Germain (1950) determined the fluorescence yield of Po by using electron-sensitive photographic plates soaked in a solution containing ^{211}At. From the observed number of α tracks with and without Auger tracks, ω_K was deduced.

3.2. Criteria for Best Methods to Determine ω_K

3.2.1. Measurements

When using radioactive sources, it is important that the purity of the sources be checked in every case, since the presence of an unexpected weak radioactive impurity can give rise to an appreciable contribution to the K x-ray and Auger-electron intensities. Only a few investigators report a detailed check of source purity. Great care should be taken in the preparation of thin, uniform sources, especially when low-energy radiations are to be measured. Self-absorption is often unexpectedly large, and is difficult to estimate.

In published reports, all corrections should be stated explicitly and described in detail, with an indication of the uncertainty that each correction contributes to the final result.

3.2.2. Estimation of Errors

The treatment of statistical and stematic uncertainties should be clearly stated. Systematic errors should be added arithmetically to the standard deviation (Garfinkel and Newbery, 1968); in any case, it should be clearly explained how the confidence limits were estimated.

It is most advisable that two or more independent methods be used, on order to eliminate hidden systematic errors.

3.2.3. Conclusion

Of all methods described above, the three best ones are based on (1) measurements with gaseous radioactive sources in proportional counters, preferably of the wall-less multiwire type, (2) measurements of the K x-ray emission rate and the disintegration rate, and (3) for high Z, simultaneous measurements of K Auger electrons and K x rays from a weightless radioactive source, with a "windowless" cooled Si(Li) detector. With these methods, an accuracy of better than 1% might be reached in favorable circumstances. In addition, the method of using Auger- and conversion-electron measurements with high-resolution spectrometers could also attain high accuracy for high-Z elements, if sources are carefully prepared.

3.3. Evaluation of Most Reliable ω_K Values

A list of all published, experimentally determined K fluorescence yields is maintained by the authors and available on request. From these, we have selected those values that can with certainty be judged reliable, because they were derived from measurements performed with pure and carefully prepared sources, and all necessary corrections were carefully determined and clearly described. Unfortunately, in the majority of publications the information is less than complete. It is therefore probable that we have omitted some "good" results from the list of selected ω_K.

3.3.1. Measurements Employing Electron-Capture Transitions

In many measurements, the quantity $P_K\omega_K$ has been determined (Sec. 3.1.2): We have re-evaluated ω_K found through such measurements reported by Taylor and Merritt (1963), Bambynek (1967a), Petel and Houtermans (1967), Troughton (1967), Bambynek, De Roost, and Funck (1968), Bambynek and Reher (1968), Hammer (1968), Rubinson and Gopinathan (1968), Grotheer, Hammer and Hoffmann (1969), Karttunen, Freund, and Fink (1969), Bambynek and Reher (1970), and Dobrilović *et al.* (1970). The re-evaluation was based on use of a uniform value of P_K for each given nuclear transition. All capture transitions employed in these measurements are allowed. We have calculated the capture probabilities P_K from a least-squares fit of experimental values of $(P_L/P_K)/(q_{L_1}/q_K)^2$ (Behrens and Bühring, 1968). These values were multiplied by the neutrino-energy dependent factor $(q_{L_1}/q_K)^2$ for individual cases. This procedure avoids exchange and overlap corrections (Bahcall 1962, 1963a–c, 1965; Faessler *et al.*, 1970; Martin and Blichert-Toft, 1970; Vatai, 1970). To allow for M capture, P_{M_1}/P_{L_1} ratios were derived from the g_{M_1}/g_{L_1} ratios of Bahcall (1963b) for $Z\leq 37$ and of Renier *et al.* (1968) for $Z>37$; the latter are interpolations between ratios of Bahcall (1963b) and of Robinson (1965). No correction was applied for exchange and overlap. Allowance was made for the energy dependence $(q_{M_1}/q_{L_1})^2$ of individual transitions. Capture of M_2 electrons was taken into account with P_{M_2}/P_{M_1} ratios tabulated by Behrens and Jänecke (1969). As Bahcall (1963b) pointed out, M_2 capture has only a very small effect due to near-cancellation by the P_{L_2}/P_{L_1} ratio. The small contribution of capture from higher shells was estimated with the aid of interpolated and extrapolated $(4s+5s+\cdots)/3s$ ratios as reported by Robinson (1965). Table III.II contains the measured $P_K\omega_K$ values, calculated K-capture probabilities P_K, and newly calculated values of the fluorescence yield ω_K.

TABLE III.II. Fluorescence yields ω_K calculated from measured $P_K\omega_K$ values on the basis of a uniform capture probability P_K for each transition.

Nuclide	Level (keV) in daughter nucleus	$P_K\omega_K$	Reference	P_K	Element	ω_K
^{51}Cr	320	0.227	Taylor (1963)	0.895	V	0.253
^{54}Mn	835	0.257	Taylor (1963)	0.893	Cr	0.287
	835	0.2514	Bambynek (1967a)	0.893	Cr	0.282
	835	0.2500	Petel (1967)	0.893	Cr	0.280
	835	0.2492	Hammer (1968)	0.893	Cr	0.279
	835	0.2511	Dobrilović (1970)	0.893	Cr	0.281
^{57}Co	136	0.3044	Rubinson (1968)	0.891	Fe	0.342
^{58}Co	810, 1675	0.3054[a]	Bambynek (1968b)	0.893	Fe	0.342
^{65}Zn	0, 1115	0.400[a]	Taylor (1963)	0.887	Cu	0.451
	0, 1115	0.3894[a]	Bambynek *et al.* (1968)	0.887	Cu	0.439
	1115	0.3927	Hammer (1968)	0.884	Cu	0.444
^{84}Sr	880, 1910	0.5782	Gehrling (1971)	0.883	Kr	0.655
^{85}Sr	514	0.5959	Grotheer (1969)	0.877	Rb	0.679
	514	0.586	Bambynek (1970)	0.877	Rb	0.668
^{88}Y	2734	0.6290	Grotheer (1969)	0.877	Sr	0.717
	1836, 2734	0.6130	Bambynek (1972)	0.877	Sr	0.699
^{125}I	35	0.685	Karttunen (1969)	0.799	Te	0.857
^{131}Cs	0	0.754	Troughton (1967)	0.837	Xe	0.900

[a] Mean P_K value from all possible transitions.

3.3.2. *Reevaluation of Errors*

The errors of ω_K, quoted by various authors, are not strictly comparable because they were determined on the basis of differing principles. In order to find comparable errors, we have reestimated the uncertainties of those fluorescence yields selected as "most reliable." The following procedure was used: Contributions to the final error, made by uncertainties in the various corrections, were added to the standard deviation. In general, we have used errors of corrections as quoted by the authors, but when these errors were not given, we assigned an uncertainty of 10%. If the standard deviation was not stated, we used 0.8%. The squared reciprocals of these re-evaluated errors were employed as weights in the calculation of mean values from the selected "most reliable" experimental results.

3.3.3. *Semiempirical Fits*

Several attempts have been made to fit experimentally determined K-shell fluorescence yields to semiempirical formulas. The basis for early attempts of this kind was the theoretically deduced result that, in first approximation, the radiative transition probability P_R calculated from unscreened hydrogenic wave functions is proportional to the fourth power of the atomic number and the radiationless transition probability P_A is constant (Wentzel, 1927):

$$P_R = aZ^4; \qquad P_A = b. \tag{3-9}$$

Hence we have

$$\omega_K = (1+\alpha Z^{-4})^{-1}; \tag{3-10}$$

the constant $\alpha = b/a$ is of the order of 10^6 (Backhurst, 1936; Burhop, 1952). Similar relations have been used by Haas (1932), who replaced Z by $Z-1$, and by Arends (1935) who introduced a multiplicative constant of order unity; this approach was also used by Gray (1956). A modification was proposed by Burhop (1955) to allow for screening and relativistic effects:

$$[\omega_K/(1-\omega_K)]^{1/4} = A+BZ+CZ^3. \tag{3-11}$$

Many authors have fitted experimentally determined fluorescence yields to this formula (Burhop, 1955; Laberrigue-Frolow, Radvanyi, and Langevin, 1956; Hagedoorn and Wapstra, 1960; Bailey and Swedlund, 1967; Grotheer, Hammer, and Hoffmann, 1969).

A more general *ansatz* would be a polynomial that includes all the relations mentioned above:

$$[\omega_K/(1-\omega_K)]^{1/4} = B_0 + \sum_{i=1}^{p} B_i Z^i. \tag{3-12}$$

The constants B_i calculated by the various authors are listed in Table III.III.

By examining the Auger widths computed by Callan (1963c), Bailey and Swedlund (1967) found that the Auger transition rate is more nearly proportional to Z than constant. Consequently, the exponent on the left-hand side of Eq. (3-11) should be one-third rather than one-fourth (Bailey and Swedlund, 1967; Grotheer, Hammer, and Hoffmann, 1969). Furthermore, Grotheer, Hammer, and Hoffmann (1969) calculated "best fit" values using an exponent of 1/3.5 and "several parameters."

Recently, Byrne and Howarth (1970) approximated

TABLE III.III. Constants calculated by fitting experimentally determined K-shell fluorescence yields to two semiempirical equations.

Reference	B_0	B_1	B_3	B_5
	A. $[\omega_K/(1-\omega_K)]^{1/4}=B_0+B_1Z+B_3Z^3+B_5Z^5$.			
Wentzel (1927)		0.0316		
Haas (1932)	−0.0334	0.0334		
Arends (1935)		0.0558		-6.05×10^{-10}
Backhurst (1936)		0.0314		
Burhop (1955)	−0.044	0.0346	-1.35×10^{-6}	
Gray (1956)		0.0316		-1.61×10^{-10}
Laberrigue-Frolow (1956)	−0.0217	0.03318	-1.14×10^{-6}	
Hagedoorn (1960)	−0.064±0.021	0.0340±0.0008	$-(1.03\pm0.14)\times10^{-6}$	
Bailey (1967)[a]	0.0408	0.0315	0.828×10^{-6}	
Grotheer (1969)	0.1268	0.02743	-6.577×10^{-8}	
Present work	0.015±0.010	0.0327±0.0005	$-(0.64\pm0.07)\times10^{-6}$	
	B. $[\omega_K/(1-\omega_K)]^{1/3}=B_0+B_1Z+B_3Z^3$.			
Bailey (1967)[a]	−0.1019	0.03377	1.177×10^{-6}	
Grotheer (1969)	−0.1624	0.03821	-7.156×10^{-8}	

[a] For $Z\geq13$.

ω_K by an eighth-order polynomial and made separate fits for the ranges $Z<13$, $13\leq Z\leq65$, and $Z>65$. Unfortunately, these authors did not report their constants. They compared the fitted data, which they regard as a set of "best experimental ω_K values," with those deduced from some of the earliest theoretical calculations, using the simple formula

$$\omega_K=(1+\alpha Z^{-m})^{-1}. \tag{3–13}$$

From the set of the so-called best experimental data, Byrne and Howarth obtained the constants $\alpha=(1.16\pm0.07)\times10^5$ and $m=3.36\pm0.02$. These figures were interpreted as evidence that the Auger transition probability is approximately proportional to $Z^{1/2}$, as Steffen, Huber, and Humbel (1949) had already pointed out. Such Z dependence corresponds to an exponent 1/3.5 in Eq. (3–12).

Our list of selected "most reliable" values of ω_K is included in Table III.IV. In order to check the result of Byrne and Howarth, we fitted these ω_K values to Eq. (3–13) and found $\alpha=5.45\times10^5$ and $m=3.85$ instead. This lack of agreement, especially for the constant m, does not support the hypothesis of a $Z^{1/2}$ dependence of the Auger transition probability.

We therefore performed a detailed polynomial regression analysis (Crow, Davis, and Maxfield, 1960). Two different analyses were carried out: First, the selected most reliable experimental ω_K values (Table III.IV) were fitted to the relation (3–12). Second, the same experimental values were fitted to a relation with an exponent 1/3.5:

$$[\omega_K/(1-\omega_K)]^{1/3.5}=C_0+\sum_{i=1}^{p}C_iZ^i. \tag{3–14}$$

The following procedure was used in the stepwise regression analysis: Starting with a linear relation, powers of the independent variable Z were generated to calculate polynomials of successively increasing degrees. For each polynomial of degree p, some statistical quantities were calculated: The regression coefficient B_i $(i=1, 2, \cdots, p)$; the standard deviation of the regression coefficient B_i, $s(B_i)$; the t values $t_i=B_i/s(B_i)$ which were used to test the null hypothesis for the regression coefficients; the confidence coefficients S_i, which indicate the statistical confidence with which B_i is different from zero; the multiple correlation coefficient r and the residual standard deviation of the fit, s_{res}. Now, the term with the lowest t value was discarded. A new set of regression coefficients and the other statistical quantities mentioned above were calculated for this reduced polynomial, and the null hypothesis for the new regression coefficients was tested. Again the term with the lowest t value was eliminated from the polynomial. This procedure was continued until only one term remained. We have analyzed polynomials up to the seventh degree in ascendant and descendant order.

A detailed study of the results indicates that an equation with linear and cubic terms yields the statistically most reliable approximation to the experimental points ($r=99.564\%$, $s_{\text{res}}=2.64\%$, $S_{\min}=99.999\%$).

From the same type of analysis using Eq. (3–14) with the exponent 1/3.5, it was found that the statistically most reliable equation is a polynomial with terms of powers 1 and 4 ($r=99.486\%$, $s_{\text{res}}=3.70\%$, $S_{\min}=97.7\%$). Comparison of these results with a fit by Eq. (3–11), which employs an exponent of 1/4, leads to the conclusion that the latter yields the statistically better approximation to the experimental data. Consequently, Eq. (3–11) was chosen for the present work.

TABLE III.IV. Selected "most reliable" experimental, recommended empirical, and theoretical K-shell fluorescence yields.

		Selected "most reliable" experimental values			Fitted values[b]	Total uncertainty[c]	Theoretical ω_K		
Z	Element	ω_K	Method[a]	Reference	ω_K	$\Delta\omega_K$	McGuire (1970a)	Kostroun (1971)	Walters (1971)
5	B						0.00056		0.0008
6	C						0.0026		0.0024
7	N						0.0060		0.0047
8	O						0.0094		0.0077
9	F						0.0133		0.0115
10	Ne						0.0182	0.0204	0.0164
11	Na						0.0260	0.0240	0.0224
12	Mg						0.0336	0.0272	0.0301
13	Al	0.0381	2	Konstantinov (1964)					
		0.0379	2	Bailey (1967)					
		*0.0380[d]			0.0357	0.0028	0.0412	0.0333	0.0398
14	Si	0.043	1	Pahor (1971a)[e]	0.0470	0.0082	0.0592	0.0441	0.0514
15	P	0.060	1	Pahor (1968)	0.0604	0.0100	0.0743	0.0572	0.0653
16	S	0.082	1	Pahor (1971a)[e]	0.0761	0.0100	0.0899	0.0727	0.0818
17	Cl	0.0970	2	Bailey (1967)					
		0.095	5	Pahor (1967)					
		0.103	1	Pahor (1971a)[e]					
		*0.0955			0.0942	0.0051	0.108	0.0915	0.1004
18	Ar	0.129	1	Heintze (1955)					
		0.122	1	Bailey (1967)					
		0.119	1	Bailey (1967)					
		0.121	1	Pahor (1971a)[e]					
		0.122	13	Tawara (1972)[e]					
		*0.122			0.115	0.006	0.126	0.111	0.1215
19	K				0.138	0.013	0.149	0.132	0.1448
20	Ca				0.163	0.016	0.177	0.155	0.1708
21	Sc	0.190	2	Bailey (1967)	0.190	0.016	0.205	0.183	0.1991
22	Ti	0.221	2	Bailey (1967)	0.219	0.018	0.233	0.212	0.2273
23	V	0.253[f]	8	Taylor (1963)					
		0.250	2	Bailey (1967)					
		*0.253			0.250	0.007		0.243	0.2608
24	Cr	0.287[f]	8	Taylor (1963)					
		0.282[f]	8	Bambynek (1967a)					
		0.280[f]	8	Petel (1967)					
		0.279[f]	9	Hammer (1968)					
		0.281[f]	8	Dobrilović (1970)[e]					
		*0.283			0.282	0.007		0.276	0.2939
25	Mn	0.303	2	Bailey (1967)	0.314	0.023		0.310	0.3276
		0.322	6	Dobrilović (1972)[e]					
		*0.313							
26	Fe	0.347	2	Bailey (1967)					
		0.342[f]	9	Rubinson (1968)					
		0.342[f]	8	Bambynek *et al.* (1968)					
		*0.342			0.347	0.008	0.364	0.344	0.3624
27	Co	0.366	2	Bailey (1967)	0.381	0.027		0.379	0.3977
28	Ni				0.414	0.028		0.414	0.4329
29	Cu	0.451[f]	8	Taylor (1963)					
		0.439[f]	8	Bambynek and Peher (1968)					

TABLE III.IV (*Continued*)

		Selected "most reliable" experimental values			Fitted values[b]	Total uncertainty[c]	Theoretical ω_K		
Z	Element	ω_K	Method[a]	Reference	ω_K	$\Delta\omega_K$	McGuire (1970a)	Kostroun (1971)	Walters (1971)
		0.444[f]	9	Hammer (1968)					
		*0.443			0.445	0.009		0.448	0.4678
30	Zn				0.479	0.030	0.499	0.482	0.5014
31	Ga	0.528	5	Freund (1969)					
		0.529	5	Pahor (1970)					
		*0.528			0.510	0.008		0.514	0.5338
32	Ge	0.554[g]	1	Pahor (1969)[e]	0.540	0.026	0.558	0.545	0.5650
33	As	0.588	1	Pahor (1971b)[e]	0.567	0.031		0.574	0.5947
		0.589	9	Chew (1972)					
34	Se				0.596	0.032		0.602	0.6230
35	Br				0.622	0.032		0.629	0.6498
36	Kr	0.660	1	Heintze (1955)					
		0.666	1	Pahor (1971c)[e]					
		0.655[f]	9	Gehrling (1971)[e]	0.646	0.030	0.659	0.655	0.6754
		*0.660							
37	Rb	0.679[f]	9	Grotheer (1969)					
		0.668[f]	8	Bambynek (1970)					
		*0.669			0.669	0.008		0.679	0.6987
38	Sr	0.717[f]	9	Grotheer (1969)	0.691	0.026		0.702	0.7211
		0.699[f]	8	Bambynek (1972)[e]					
		*0.702							
39	Y				0.711	0.031		0.722	0.7420
40	Zr				0.730	0.032	0.740	0.741	0.7611
41	Nb				0.748	0.032		0.759	0.7788
42	Mo				0.764	0.032		0.776	0.7951
43	Tc				0.779	0.032		0.792	0.8093
44	Ru				0.793	0.031	0.806	0.807	0.8236
45	Rh				0.807	0.031		0.820	0.8367
46	Pd				0.819	0.030		0.833	0.8491
47	Ag	0.834	3	Foin (1968)	0.830	0.025	0.842	0.844	0.8605
48	Cd				0.840	0.029		0.855	0.8707
49	In				0.850	0.029		0.865	0.8803
50	Sn				0.859	0.028	0.871	0.874	0.8889
51	Sb				0.867	0.028			0.8971
52	Te	0.857[f]	9	Karttunen (1969)	0.875	0.028		0.890	0.9046
53	I				0.882	0.028			0.9112
54	Xe	0.880	1	Heintze (1955)					
		0.900[f]	8	Troughton (1967)					
		*0.894			0.889	0.020	0.902	0.904	0.9176
55	Cs	0.873	3	Erman (1961)					
		0.898	3	Graham *et al.* (1961)					
		*0.889			0.895	0.012			
56	Ba				0.901	0.026		0.916	
57	La				0.906	0.026			
58	Ce				0.911	0.026		0.926	
59	Pr				0.915	0.025			
60	Nd				0.920	0.024		0.935	
61	Pm				0.924	0.024			
62	Sm				0.928	0.023			

TABLE III.IV (*Continued*)

		Selected "most reliable" experimental values			Fitted values[b]	Total uncertainty[c]	Theoretical ω_K		
Z	Element	ω_K	Method[a]	Reference	ω_K	$\Delta\omega_K$	McGuire (1970a)	Kostroun (1971)	Walters (1971)
63	Eu	0.925	3	Monnand (1961)	0.931	0.015			
64	Gd				0.934	0.022			
65	Tb				0.937	0.022		0.952	
66	Dy	0.943	3	Graham and Merritt (1961)	0.940	0.016			
67	Ho				0.943	0.021			
68	Er				0.945	0.021			
69	Tm				0.948	0.020			
70	Yb				0.950	0.020		0.963	
71	In				0.952	0.020			
72	Hf				0.954	0.019			
73	Ta				0.956	0.019			
74	W				0.957	0.019			
75	Re				0.959	0.018			
76	Os				0.961	0.018			
77	Ir				0.962	0.018			
78	Pt	0.967	6	Hansen (1972)	0.963	0.013			
79	Au				0.964	0.017			
80	Hg	0.952	3	Nall (1960)					
		0.970	4	Park (1967)					
		*0.958			0.966	0.020			
82	Pb	0.972	6	Hansen (1972)	0.968	0.013			
92	U	0.970	6	Hansen (1972)	0.976	0.013			

[a] Methods are identified by numbers explained in Table III.I.

[b] These values were calculated from Eq. (3.11). The constants $A=0.015\pm0.010$, $B=0.0327\pm0.0005$, and $C=-(0.64\pm0.07)\times10^{-6}$ were determined by fitting the selected "most reliable" experimental values to this equation.

[c] The total uncertainty takes into account the uncertainty of the constants A, B, and C, and uncertainties due to systematic errors in the measurements.

[d] Asterisks identify weighted-mean values of ω_K.

[e] Values communicated too late to be included in the least-squares fit.

[f] These values, based on $P_K\omega_K$ results, have been recalculated using uniform capture probabilities P_K as listed in Table III.III.

[g] Corrected for 0.993 K x-ray efficiency.

[h] Revised with a K-jump correction of 1.147, interpolated from Blokhin (1957). A. Moljk, private communication (1971).

[i] No experimental values are listed for $Z<13$ because for the lightest elements ω_K appears to depend significantly on the chemical state.

Semiempirical values of the K-shell fluorescence yield ω_K for $4\leq Z\leq 80$, $Z=82$, and $Z=93$ were calculated by fitting the selected "most reliable" measured values to Eq. (3–11); the results are listed in Table III.IV in the column labeled "fitted values." The uncertainty $\Delta\omega_K$ of these fitted values is listed in the following column. Because of the importance of $\Delta\omega_K$, we describe in some detail how this uncertainty was calculated.

For atomic numbers for which at least one "most reliable" measured value is available, the over-all uncertainty $\Delta\omega_K$ depends (1) on the uncertainty Δ_{fit} arising from the statistical error in the fitting procedure, and (2) on an uncertainty Δ_{sys} due to residual systematic effects that remain after suitable correction factors have been applied. The error Δ_{fit} of a ω_K value calculated from the semiempirical Equation (3–11) is given by

$$\Delta_{\text{fit}}=S_{\text{res}}[4R^3/(1+R^4)^2][\tilde{\mathbf{X}}(e_{ij})\mathbf{X}]^{1/2}, \quad (3\text{–}15)$$

where R stands for $A+BZ+CZ^3$. The matrix (e_{ij}) is the inverse of the matrix of the system of normal equations, $\mathbf{X}$ is a vector with the components $(1, Z, Z^3)$, and $\mathbf{X}$ is its transpose. The residual standard deviation S_{res} is

$$S_{\text{res}}=[(\omega_{\text{obs}}-\omega_{\text{cal}})^2/(n-m)]^{1/2}. \quad (3\text{–}16)$$

Here, ω_{obs} denotes the measured value of ω_K, while ω_{cal} is the value calculated from the semiempirical equation (3–11); n is the number of experimental points, and m is the number of parameters.

If more than one reliable measured value is available for a given atomic number, a mean value $\bar{\omega}=(\sum p_i\omega_i)/\sum p_i$ is calculated; the weights p_i are the squared

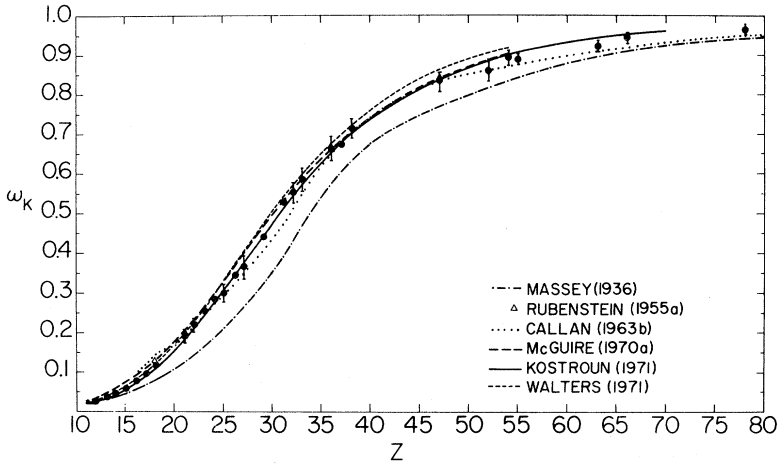

FIG. 3–12. Theoretical K-shell fluorescence yield as a function of atomic number, according to various authors: Massey and Burhop (1936), Rubenstein (1955a), Callan (1963b), McGuire (1970a), Kostroun, Chen, and Crasemann (1971), and Walters and Bhalla (1971). Experimental data are those listed in Table III.IV.

reciprocals of reevaluated errors. These mean values and weights were used to calculate the errors

$$e_1=\{[\sum p_i(\omega_{\text{obs}}-\bar{\omega})^2]/[(\nu-1)\sum p_i]\}^{1/2},$$

$$e_2=(\sum p_i)^{-1/2}, \quad (3\text{–}17)$$

where ν is the number of measured points for a given Z. The errors e_1 and e_2 represent the "external" and "internal" consistency of the measurements. Following Topping (1963), we chose

$$\Delta_{\text{sys}}=\max(e_1, e_2). \quad (3\text{–}18)$$

If there is only one measurement for a given Z, the error assigned by the experimenter is used.

The over-all uncertainty was calculated from the relation

$$\Delta\omega_K=[(\Delta_{\text{fit}})^2+(\Delta_{\text{sys}})^2]^{1/2}. \quad (3\text{–}19)$$

In order to estimate $\Delta\omega_K$ for atomic numbers for which no measurements are available, a plot of $\Delta\omega_K/\omega_K$ vs. Z was constructed with points based on single measurements per Z. For atomic numbers lacking measurements, $\Delta\omega_K/\omega_K$ was read from this curve and 0.5% was added, somewhat arbitrarily.

3.4. Comparison of Experimental and Theoretical K-Shell Fluorescence Yields

Of late, it has been possible to calculate K-shell fluorescence yields from first principles. Progress in this area can be attributed to several factors: (1) The availability of fast computers has made it possible to include all of the many transitions that contribute to the total Auger width of the K level; (2) Advances have been made in developing more realistic wave functions, both by improvements in the screening of hydrogenic wave functions and by the development of better self-consistent-field numerical wave functions (Sec. 2.2); (3) More accurate binding energies have become available (Bearden and Burr, 1967; Siegbahn *et al.*, 1967; Lotz, 1970; Carlson, Nestor, Malik, and Tucker, 1969), which is important because radiationless transition probabilities are very sensitive to the continuum-electron energy, and (4) For the first time, comprehensive and generally quite accurate computations of radiative transition probabilities have been performed (Sec. 2.4). Moreoever, ω_K is the *ratio* of radiative and total level widths, and calculations that yield larger Auger transition probabilities seem, as a rule, also to predict larger radiative probabilities. Thus, in spite of rather large differences among some of the calculated widths (Figs. 2–4, 2–5, and 2–12), fluorescence yields computed in recent work are mutually quite consistent (Fig. 3–12).

The theoretical K-shell fluorescence yields calculated by McGuire (1970a), Kostroun *et al.*, (1971), and Walters and Bhalla (1971) are included in Table III.IV. Above $Z\cong 50$, the theoretical values of ω_K are slightly higher than values derived from the best fit of Eq. (3–11) to the selected experimental results (Fig. 3–13), because relativistic effects have been neglected in all of these calculations, resulting in an underestimation of the Auger width. Furthermore, Walters and Bhalla have neglected K–LN and K–MN Auger transitions, causing their ω_K values to fall above those computed by Kostroun *et al.* However, general agreement between theoretical results and fitted values is good; it can be expected that the slight remaining systematic discrepancies will be removed in the near future.

4. L-SHELL YIELDS

A complete quantitative description of the decay of an excited state of an atom with an L vacancy by radiative and nonradiative transitions requires the measurement of at least six of the nine quantities characterizing the L shell [see Eqs. (1–16)] as discussed in Sec. 1.3. The methods to be discussed in this chapter are used primarily in the measurement of L

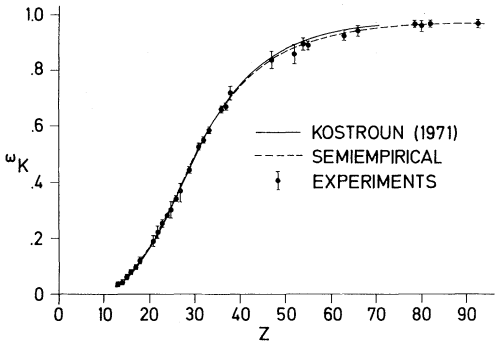

FIG. 3–13. Theoretical K-shell fluorescence yield according to Kostroun, Chen, and Crasemann (1971), as a function of atomic number. The data points are "most reliable" critically evaluated experimental results from Table III.IV. The dashed curve represents values of ω_K derived from a best fit of Eq. (3–11) to the selected experimental results.

x-ray fluorescence yields (ω_1, ω_2, and ω_3) and Coster–Kronig yields (f_{12}, f_{13}, and f_{23}). The availability of efficient high-resolution x-ray detectors has recently facilitated the measurement of all six quantities for suitable atomic numbers. Two basic requirements to obtain such detailed information are (1) the controlled production of primary L-subshell vacancies, and (2) high-resolution spectrometry of photons or electrons resulting from the decay of these vacancies.

The primary vacancies are produced by fluorescent excitation, charged-particle bombardment, or selection of suitable transitions following radioactive decay or the filling of a K-shell vacancy. The distribution of these vacancies in the three L subshells depends very much upon the nature of the process. Selection of a specific primary distribution for the study of L-shell yields depends upon the experimental techniques. An ideal choice is a case in which vacancies are produced in only one subshell. Next in order of preference are distributions in which vacancies in one subshell are preponderant.

Recent innovations in detector technology have resulted in high-resolution techniques with which low-energy photons and electrons involved in L-subshell transitions can be observed with high efficiency over a considerable range of high-Z values. Among these are the current generation of semiconductor detectors to study x rays of energy as low as 1–2 keV and the electrostatic spectrometers and ESCA techniques to study electrons. This capacity to observe x-ray and electron transitions characteristic of individual L subshells, coupled with knowledge of the primary vacancy distribution, has in the past few years resulted in considerable progress in the determination of L-shell yields.

The following sections are devoted to a detailed study of the primary L-subshell vacancy distributions encountered in various excitation mechanisms, and of experimental techniques for the measurement of L-shell yields. An exhaustive summary of available results on L-shell yields is presented in the form of tables, and criteria for accuracy and reliability are discussed.

4.1. Primary L-Subshell Fluorescent Excitation

Although historically, direct fluorescent excitation is an important method for creating primary vacancies for measuring L-shell fluorescence yields (Lay, 1934; Küstner and Arends, 1935; Ross *et al.*, 1955), more accurate methods now exist. The measurement of an L-shell fluorescence yield by direct photoexcitation requires that accurate photoelectric cross-section values for individual subshells—either experimental or theoretical—be available for determining the number of primary vacancies. Recently, considerable new work in the area of photoelectric excitation has been performed. Bearden (1966) has conducted a thorough series of x-ray absorption-coefficient measurements for many elements. These measurements and those of Deslattes (1959) as well as many other experiments form a reliable body of modern data on x-ray absorption coefficients. Guttman and Wagenfeld (1967) have published a short summary of theoretical calculations of x-ray absorption coefficients. They used hydrogenlike wave functions and included dipole, dipole–octupole, Compton, and quadrupole terms in their calculations. The results of the theoretical work are in excellent agreement with measured values. The authors assert that, away from absorption edges, agreement is better than 5%, and that their calculations are considerably better than those appearing in the *International Tables of X-Ray Crystallography* by McGillavry and Lansdale (1965).

The availability of good absorption coefficients and the good agreement between theory and experiment that has recently been attained suggests some interesting possibilities. In other sections of this paper, tables of available fluorescence yields for the individual L subshells are presented. If the theoretical calculations are really as good as the cited comparisons imply, then the L-subshell vacancy distribution for any particular practical application could be obtained reliably from theory. The average L-shell fluorescence yield for a particular case could then be calculated, using the subshell fluorescence-yield tables. Unfortunately, this procedure cannot be carried out as yet, since most of the existing tables of absorption cross sections contain only a sum of the values of the absorption coefficients for all of the atomic shells. For example, Guttman and Wagenfeld (1967) list total absorption coefficients that include cross sections for all the K, L, M, and N shells. We strongly recommend that future tables specify individual values of the cross sections for each of the atomic shells and subshells used to obtain the total absorption coefficient, as in the recent work of Rakavy and Ron (1967) and of McGuire (1970d). If this were done, great flexibility in computing average fluorescence yields for many practical applications involving photoelectric excitation would become available.

4.2. Primary L-Subshell Excitation by Charged-Particle Bombardment

The problem of creating primary vacancies for fluorescence-yield measurements by charged-particle bombardment has been discussed in a review paper by Fink *et al.* (1966). They pointed out that theoretical methods must be used to determine the rate at which atomic vacancies are created by a beam of charged particles, and referenced theoretical work. In the past six years, no new experimental measurements of fluorescence yields using charged-particle bombardment have appeared in the literature. Nevertheless, because of considerable theoretical activity in recent years, it is worthwhile to re-examine the possibility of using charged-particle bombardment as a means for vacancy production in fluorescence-yield measurements.

Recent developments in plasma physics and astrophysics have revived interest in the study of the ionization of atoms by electron collision. A considerable amount of experimental and theoretical work has been done in this field, much of which is summarized in comprehensive review articles by Moisewitch and Smith (1968) and Kieffer and Dunn (1966). As with photoelectric cross sections, here too a lack of cross sections for individual subshells exists. Although considerable progress has been made in understanding the ionization of atoms by electron impact, it is unlikely that these developments will have significant application to the determination of fluorescence yields. The use of energetic electrons for the creation of primary vacancies in fluorescence-yield experiments is severely limited by experimental factors. Electron beams with sufficiently high energies to ionize inner shells with large probability also produce bremsstrahlung that makes it difficult to observe the characteristic radiation emitted by atoms.

For heavy charged-particle bombardment, the situation is quite different. A number of experiments have recently been performed with the object of measuring ionization cross sections of atoms for various species of bombarding particles. In these experiments, known values of the fluorescence yields were used to calculate ionization cross sections from the observed intensities of characteristic x rays (Khan, Potter, and Worley, 1966; Bissinger *et al.*, 1970; Garcia, 1970a; Richard *et al.*, 1970). However, the state of our knowledge of theoretical ionization cross sections for protons (if not for heavier incident ions) is such that serious consideration should be given to initiating fluorescence-yield measurements using energetic protons. Following the theoretical work of Bang and Hansteen (1959), who first considered the effect of the deflection of the incident particle by the nucleus in an ionizing collision, Garcia (1970b) has improved the theory to a point where it is considered reliable for the calculation of ionization probabilities and vacancy distributions created by proton impact. Furthermore, improvements in the resolving power of solid-state x-ray detectors make it possible to observe and resolve the characteristic x rays produced by the incident proton beam. It should therefore be possible to measure a number of fluorescence yields of various shells and subshells with this method. In the case of heavier incident particles, the theory has not yet been worked out in sufficient detail to make the measurement of fluorescence yields practical. The creation of multiple vacancies is a complicating factor in charged-particle excitation experiments.

4.3. Primary L-Subshell Excitation Due to Radioactive Decay

Radioactive decay of nuclei, in particular orbital electron capture and internal conversion, provides a readily accessible means for producing primary L-subshell vacancies.

4.3.1. L-Shell Orbital Electron Capture

The probability of orbital electron capture from any one of the L subshells depends upon the nature and energy of the transition. Early theoretical estimates of capture probabilities (P_K and P_{L_i}) were made by Band, Zyryanova, and Chen-Zhui (1956), Band, Zyryanova, and Suslov (1958), Brysk and Rose (1958), and Winter (1968). More recent calculations, which include P_M, are reported in the work of Behrens and Bühring (1968), Zyryanova and Suslov (1968), Behrens and Jänecke (1969), and of Martin and Blichert-Toft (1970). In the case of allowed and non-unique first forbidden transitions, vacancies appear predominantly in the L_1 subshell, the ratio P_{L_2}/P_{L_1} being less than 0.15 for decay energies well above the L-shell binding energies. The number of L_3-subshell vacancies produced is negligible. Thus, such pure L-capture decays effectively provide a source of L_1-subshell vacancies. However, such cases are few; a list of some of the known pure L-capture transitions and of the corresponding primary L-vacancy distributions is presented in Table IV.I. In the majority of experimentally accessible cases, the K-capture process predominates, giving rise to additional L-vacancy production (as discussed in Sec. 4.4), and a knowledge of the P_L/P_K capture ratio is then necessary to predict the L-subshell vacancy distribution. Selected values of theoretical P_L/P_K and P_{L_2}/P_{L_1} capture ratios for decay energies Q_{EC} much larger than the K-shell binding energy are presented in Table IV.II.

There is no experimental work in which the distribution of L-subshell vacancies due to L-shell orbital electron capture has been investigated. There is only indirect evidence to support theoretical estimates in that measured ratios of P_L/P_K for allowed and first-forbidden transitions agree with theory within a few percent over a wide range of Z (Fink, 1968).

TABLE IV.I. Primary L-vacancy distributions produced in the disintegration of radioactive nuclides that decay by orbital electron capture from the L and higher shells only.

Parent nucleus	Daughter nucleus (level in keV)	Spin and parity	Decay energy Q_{EC} (keV)	N_1	N_2	N_3
^{44}Ti	^{44}Sc (146.3)	$0^+\rightarrow1^+$	13.7	0.996	0.004	...
^{181}W	^{181}Ta (158.8)	$9/2^+\rightarrow11/2^-$	31.2	0.938	0.062	...
^{181}W	^{181}Ta (136.3)	$9/2^+\rightarrow9/2^+$	63.7	0.939	0.061	...
^{193}Pt	^{193}Ir (0)	$3/2^-, 1/2^-\rightarrow3/2^+$	60.8	0.931	0.069	...
^{195}Au	^{195}Pt (211.2)	$3/2^+\rightarrow3/2^-$	15.8	0.886	0.114	...
^{194}Hg	^{194}Au (0)	$0^+\rightarrow1^-$	81	0.927	0.073	...
^{202}Pb	^{202}Tl (0)	$0^+\rightarrow2^-$	50	0.906	0.080	0.014
^{205}Pb	^{205}Tl (0)	$5/2^-\rightarrow1/2^+$	35	0.872	0.082	0.046
^{207}Bi	^{207}Pb (2339)	$9/2^-\rightarrow7/2^-$	61	0.919	0.081	...

4.3.2. *L-Shell Internal Conversion*

The theory of primary L-vacancy production by internal conversion in the L subshells has been studied more extensively than by the electron-capture process discussed above. Theoretical L-subshell conversion coefficients α_{L_i}, which indicate the relative probabilities of L-vacancy creation, have been calculated by several authors, and published tables are available of α_{L_i} for transitions of pure multipolarity as a function of transition energy and atomic number (Rose, 1958; Sliv and Band, 1958; Bhalla, 1967; Pauli, 1967; Hager and Seltzer, 1968; Dragoun, Pauli, and Schmutzler, 1969). The use of tabulated values is limited to pure transitions or cases in which the multipolarity admixture is accurately known from experiment. Some of the known pure L-conversion transitions are listed in Table IV.III with the corresponding primary L-vacancy distributions. If the transition energy is large enough to permit K conversion, which is often the case, the filling of K vacancies by L electrons gives rise to L vacancies (as discussed in Sec. 4.4, below) and a knowledge of the K conversion coefficient is necessary. An interesting class is that of low-energy $E2$ transitions fed by even-even alpha-emitting heavy nuclei. These transitions are converted predominantly in the L_2 and L_3 subshells, where the ratio $N_1:N_2:N_3$ is typically 3:100:100; such transitions are therefore useful for the study of the filling of L_2- and L_3-subshell vacancies. In these cases, there are few if any alternative ways of producing L_2- and L_3-subshell vacancies, such as electron capture or the filling of a K-shell vacancy by an L electron. Some known transitions of this type are listed in Table IV.III with the resultant primary L-vacancy distributions.

For many individual transitions, $L_1:L_2:L_3$ conversion-electron ratios, as well as K/L ratios, have been measured; this work has been summarized by Hamilton *et al.* (1966) and by Dingus and Rud (1968). Cascades of two or three transitions often occur in radioactive decay, e.g., electron capture followed by internal conversion, or two transitions that both undergo internal conversion. In such cases, the estimation of primary L-vacancy distributions becomes less certain.

TABLE IV.II. Capture ratios P_L/P_K and P_{L_2}/P_{L_1} for selected atomic numbers, based on theoretical capture probabilities from the work of Zyryanova and Suslov (1968a) with exchange correction after Bahcall (1963b). The decay energy is assumed to be very large compared to K- and L-electron binding energies.

Z	P_L/P_K	P_{L_2}/P_{L_1}
50	0.1289	0.0246
60	0.1400	0.0376
70	0.1539	0.0546
80	0.1712	0.0768
90	0.1937	0.1064
100	0.2236	0.1470

TABLE IV.III. Primary L-subshell vacancy distributions produced in nuclear transitions that are internally converted in the L and higher shells only.

Nuclide	Transition: Initial and final spin and parity	Transition: Energy (keV)	Primary L-vacancy distribution: N_1	N_2	N_3
^{151}Eu	$7/2^+\rightarrow5/2^+$	21.6	0.837	0.102	0.061
^{163}Dy	$5/2^+\rightarrow5/2^-$	25	0.366	0.258	0.376
^{191}Ir	$11/2^-\rightarrow5/2^+$	41.8	0.506	0.484	0.010
^{192}Ir	$1^+\rightarrow4^+$	58	0.098	0.478	0.424
^{194}Ir	$(0, 1^-)\rightarrow1^-$	43	0.902	0.088	0.010
^{210}Bi	$0^-\rightarrow1^-$	46.5	0.903	0.090	0.007
^{226}Ra	$2^+\rightarrow0^+$	67.8	0.016	0.539	0.445
^{228}Th	$2^+\rightarrow0^+$	57.5	0.017	0.530	0.453
^{231}Pa	$7/2^-\rightarrow3/2^-$	58.5	0.019	0.537	0.444
^{234}U	$2^+\rightarrow0^+$	43.5	0.018	0.513	0.469
^{236}U	$2^+\rightarrow0^+$	45.3	0.018	0.520	0.462
^{240}Pu	$2^+\rightarrow0^+$	42.9	0.020	0.520	0.460
^{248}Cm	$2^+\rightarrow0^+$	43.4	0.020	0.542	0.438

4.4. Primary L-Subshell Excitation Through Transitions to the K Shell

The class of L-subshell vacancies that appears at the second stage of a cascade of events beginning with the creation of a K-shell vacancy is discussed in this section. The two well-known phenomena involved are $K\alpha$ x-ray emission and K Auger-electron emission.

The important radiative transitions to the K shell are listed by Bearden (1967) for $3 \leq Z \leq 95$. The transitions of interest here are $K-L_2$ and $K-L_3$, in which L_2 or L_3 electrons fill a vacancy in the K shell, leaving the atom in an L_2- or L_3-ionized state, while the difference in binding energies is emitted as a $K\alpha_2$ or $K\alpha_1$ x ray, respectively. Radiative $K-L_1$ transitions are forbidden by the electric-dipole selection rule, $\Delta l = \pm 1$, where $(\Delta l)\hbar$ is the orbital angular-momentum change. However, the $K-L_1$ radiative transition probability does not completely vanish and contributes a few L_1 vacancies. For example, $\sim 0.05\%$ of all L vacancies produced during radiative transitions at $Z=80$ are in the L_1 subshell. The theoretical ratio of the intensity of $K-L_1$ transitions to that of all $K-L$ transitions, $I(KL_1)/I(KL)$, is plotted as a function of Z in Fig. 4–1. The x-ray intensity ratio $I(K\alpha_2)/I(K\alpha_1)$ is equal to the ratio of L_2- to L_3 subshell primary vacancies produced during K x-ray emission and is plotted as a function of Z in Fig. 2–8. The ratio $I(K\beta)/I(K\alpha)$ is equal to the ratio of higher shell (M, N, $\cdots$) vacancies to L-shell vacancies created in K x-ray emission and is plotted as a function of Z in Fig. 2–7. Values of these ratios from a best fit to the data are listed in Table IV.IV.

Nonradiative transitions filling K vacancies with

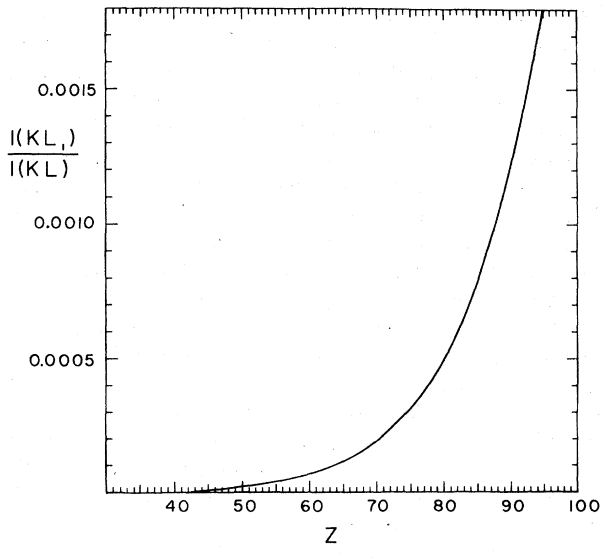

FIG. 4–1. Ratio of the intensity of radiative K–L_1 transitions to the intensity of all radiative K–L transitions, as a function of atomic number. The graph is based on the theoretical radiative decay rates of Scofield (1969).

TABLE IV.IV. X-ray intensity ratios derived from a least-squares fit to available experimental data. From Venugopala Rao, Chen, and Crasemann (1972).

Z	$\frac{I(K\alpha_2)}{I(K\alpha_1)}$	$\frac{I(K\beta)}{I(K\alpha)}$	Z	$\frac{I(K\alpha_2)}{I(K\alpha_1)}$	$\frac{I(K\beta)}{I(K\alpha)}$
20	0.503	0.128	58	0.545	0.241
22	0.504	0.133	60	0.548	0.246
24	0.505	0.133	62	0.552	0.250
26	0.507	0.134	64	0.555	0.254
28	0.508	0.135	66	0.559	0.257
30	0.510	0.135	68	0.563	0.261
32	0.512	0.148	70	0.567	0.264
34	0.514	0.158	72	0.571	0.267
36	0.516	0.168	74	0.575	0.270
38	0.518	0.177	76	0.579	0.272
40	0.520	0.185	78	0.583	0.275
42	0.522	0.193	80	0.588	0.277
44	0.525	0.201	82	0.592	0.279
46	0.527	0.208	84	0.597	0.281
48	0.530	0.214	86	0.602	0.283
50	0.533	0.220	88	0.607	0.285
52	0.536	0.226	90	0.612	0.287
54	0.539	0.231	92	0.617	0.288
56	0.542	0.236	94	0.622	0.290

L-shell electrons fall into two categories: (a) $K-LL$ transitions, in which one electron from an L subshell fills the K vacancy while the excess energy is carried away by another L-subshell electron, and (b) $K-LX$ transitions, in which an outer shell (M, N, $\cdots$) electron is ejected. In both cases, the atom is left in a doubly ionized state; only in case (a), both vacancies are in the L shell.

The average number n_{KL_i} of primary L_i vacancies created in the filling of a K-shell vacancy by an electron from an L_i subshell can be written as the sum of two parts, $n_{KL_i}(R)$ due to radiative transitions and $n_{KL_i}(A)$ due to Auger transitions:

$$n_{KL_i} = n_{KL_i}(R) + n_{KL_i}(A). \tag{4–1}$$

The number $n_{KL_i}(R)$ is proportional to the probability that a $K-L_i$ radiative transition takes place:

$$n_{KL_i}(R) = \omega_K [I(KL_i)/I_K(R)]. \tag{4–2}$$

Here, $I(KL_i)$ is the $K-L_i$ x-ray intensity, and $I_K(R)$ is the total intensity of K x rays. As mentioned earlier, $I(KL_1)$ is negligible because $K-L_1$ electric dipole radiative transitions are forbidden. For L_2 and L_3 subshells, we can express this quantity in terms of K x-ray intensity ratios in the following way:

$$n_{KL_2}(R) = \omega_K \left[\frac{I(K\alpha_2)}{I(K\alpha_1)}\right]\left\{\left[1+\frac{I(K\alpha_2)}{I(K\alpha_1)}\right]\left[1+\frac{I(K\beta)}{I(K\alpha)}\right]\right\}^{-1},$$

$$n_{KL_3}(R) = \omega_K \left\{\left[1+\frac{I(K\alpha_2)}{I(K\alpha_1)}\right]\left[1+\frac{I(K\beta)}{I(K\alpha)}\right]\right\}^{-1}. \tag{4–3}$$

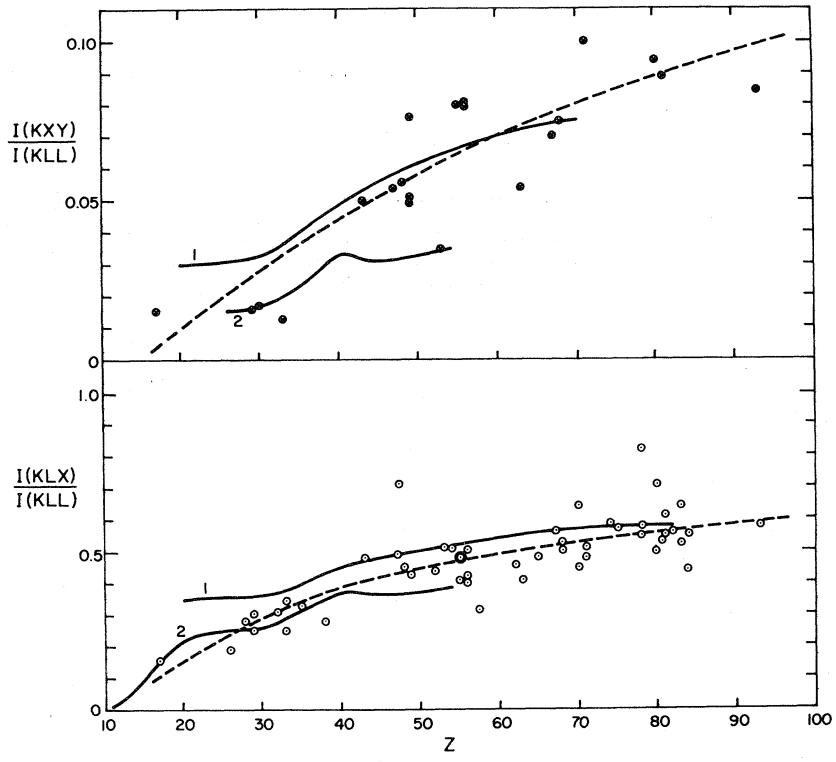

FIG. 4–2. Auger-electron intensity ratios $I(KXY)/I(KLL)$ and $I(KLX)/I(KLL)$ as functions of atomic number. Experimental data are compared with theoretical ratios according to Venugopala Rao, Chen, and Crasemann (1972) (curve 1) and McGuire (1970a and private communication) (curve 2). The broken curves are best fits to the measured ratios.[From Venugopala Rao, Chen, and Crasemann (1972), courtesy of American Institute of Physics.]

The quantity $n_{KL_i}(A)$ is proportional to the sum of the probabilities for producing an L_i vacancy in $K-LL$ and $K-LX$ type Auger transitions and can be expressed in terms of experimentally measured Auger-electron intensity ratios, as follows:

$$n_{KL_i}(A)=(1-\omega_K)\left[b_i+\frac{I(K-L_iX)}{I(K-LL)}\right]\times\left[1+\frac{I(K-LX)}{I(K-LL)}+\frac{I(K-XY)}{I(K-LL)}\right]^{-1}. \quad (4\text{–}4)$$

Here, b_i denotes the probability per $K-LL$ transition of producing an L_i vacancy. For the three L subshells, we have

$$b_1=\frac{2I(K-L_1L_1)+I(K-L_1L_2)+I(K-L_1L_3)}{I(K-LL)},$$

$$b_2=\frac{2I(K-L_2L_2)+I(K-L_1L_2)+I(K-L_2L_3)}{I(K-LL)},$$

$$b_3=\frac{2I(K-L_3L_3)+I(K-L_1L_3)+I(K-L_2L_3)}{I(K-LL)}. \quad (4\text{–}5)$$

It should be noted that the effect of Coster–Kronig transitions is not included in these definitions.

Much theoretical effort has been directed toward calculating the relative intensities of the individual $K-LL$ Auger lines and of the main $K-LL$, $K-LX$, and $K-XY$ Auger groups (Sec. 2.3). Partial summaries of experimental data on K Auger-electron intensities have been compiled by Gray (1956), Wapstra, Nijgh, and van Lieshout (1959), Listengarten (1960), Graham, Bergström, and Brown (1962), Hörnfeldt (1962), Dionisio (1964), Erman, *et al.* (1964), and Bergström and Nordling (1964). The available theoretical and experimental ratios of prominent K Auger-transition rates have recently been summarized by Venugopala Rao, Chen, and Crasemann (1972). These authors conclude that no reasonable agreement exists between theoretical estimates and experimental data on K Auger rates for $Z<55$, where the Auger effect dominates in the production of L vacancies.[6] There is, however, fairly reasonable agreement between theory and experiment as far as radiative rates are concerned. Thus, Venugopala Rao *et al.* (1972) believe that the best estimates of n_{KL_i} are obtained from a fit to the available experimental information. The intensities of $K-LX$ and $K-XY$ Auger-electron groups relative to the $K-LL$ group intensity are presented in Fig. 4–2. The probability b_i of producing an L_i-subshell vacancy per $K-LL$ transition is plotted in Figs. 4–3, 4–4, and 4–5. In Fig. 4–6 the intensity ratios $I(KL_iX)/I(KLL)$ are indicated. Values of these ratios derived from a best fit to the experimental data are listed in Table IV.V. Using these fitted values and those in Table IV.IV, the average vacancy distributions n_{KL_i} were calculated; they are listed in Table IV.VI.

[6] However, Chase, Kelly, and Kohler (1971) recently have had considerable success in calculating the Auger spectrum of Ne through Brueckner–Goldstone many-body perturbation theory.

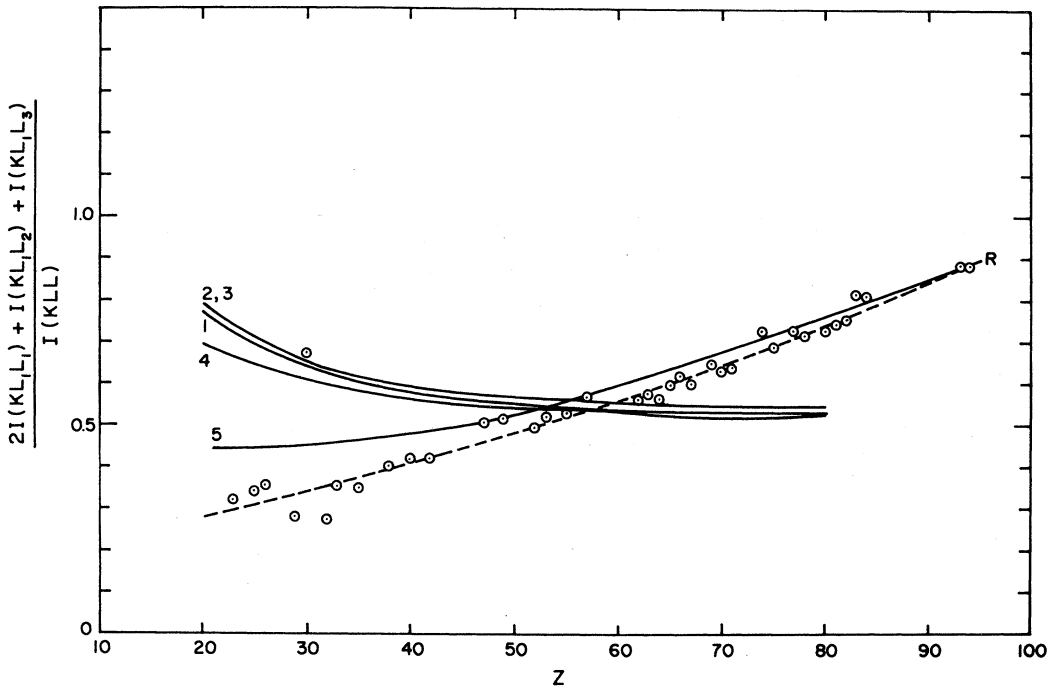

FIG. 4–3. The probability b_1 of L_1-vacancy production per K–LL Auger transition, as a function of atomic number. The points are experimental ratios. Solid curves indicate theoretical ratios: 1. Venugopala Rao, Chen, and Crasemann (1972); 2. nonrelativistic calculations in j-j coupling by Asaad (1963*a*); 3. nonrelativistic calculation in intermediate coupling by Asaad (1963a); 4. nonrelativistic calculations in intermediate coupling with configuration mixing by Asaad (1965b) and by Mehlhorn and Asaad (1966); 5. relativistic calculation in j-j coupling by Ramsdale (1969). The broken curve is a least-squares fit to the experimental points. [From Venugopala Rao, Chen, and Crasemann (1972), courtesy of American Institute of Physics.]

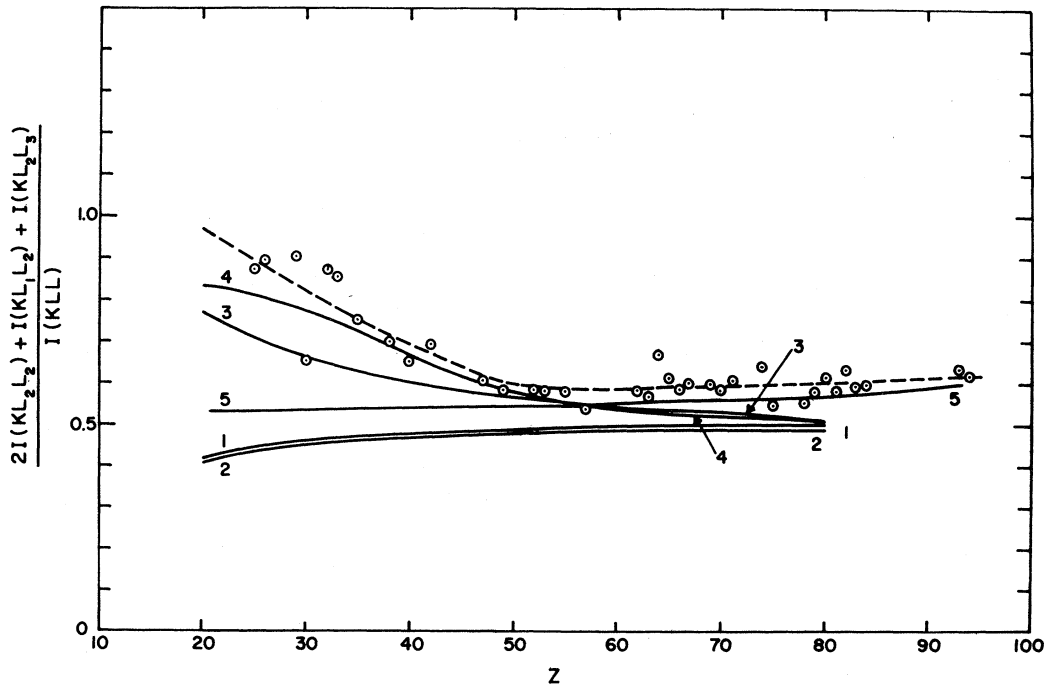

FIG. 4–4. The probability b_2 of L_2-vacancy production per K–LL Auger transition, as a function of atomic number. The points indicate experimental ratios. Solid curves are theoretical ratios, keyed as in Fig. 4–3. The broken curve is a least-squares fit to the experimental points. [From Venugopala Rao, Chen, and Crasemann (1972), courtesy of American Institute of Physics.]

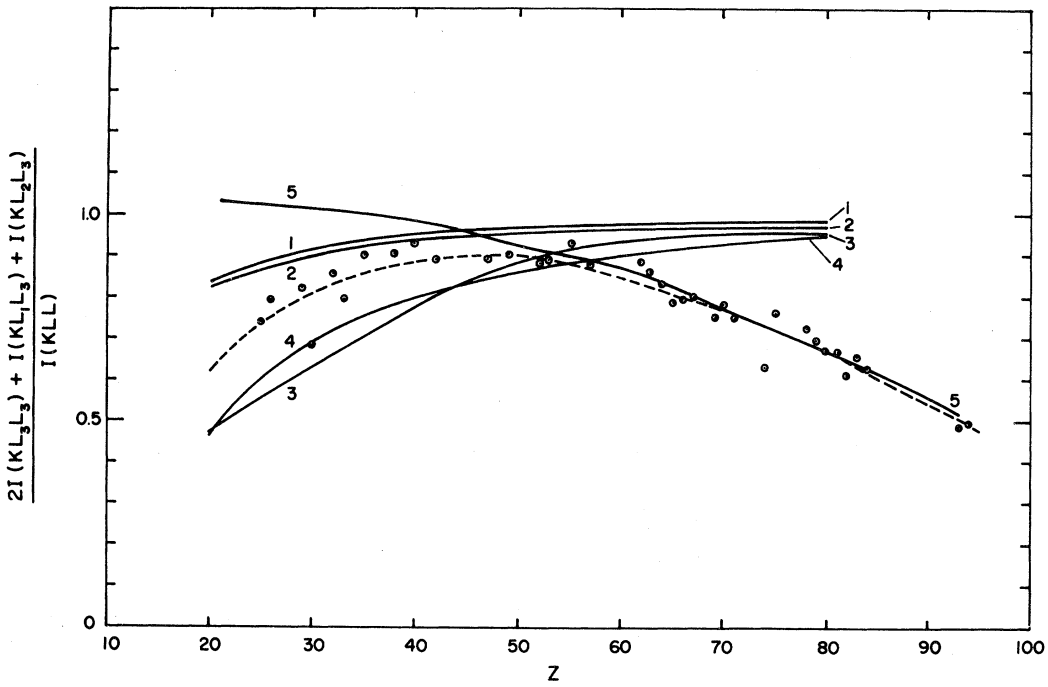

FIG. 4–5. The probability b_3 of L_3-vacancy production per K–LL Auger transition, as a function of atomic number. The points represent measured ratios. Theoretical ratios are indicated by solid curves, keyed as in Fig. 4–3. The broken curve is a least-squares fit to the experimental points. [From Venugopala Rao, Chen, and Crasemann (1972), courtesy of American Institute of Physics.]

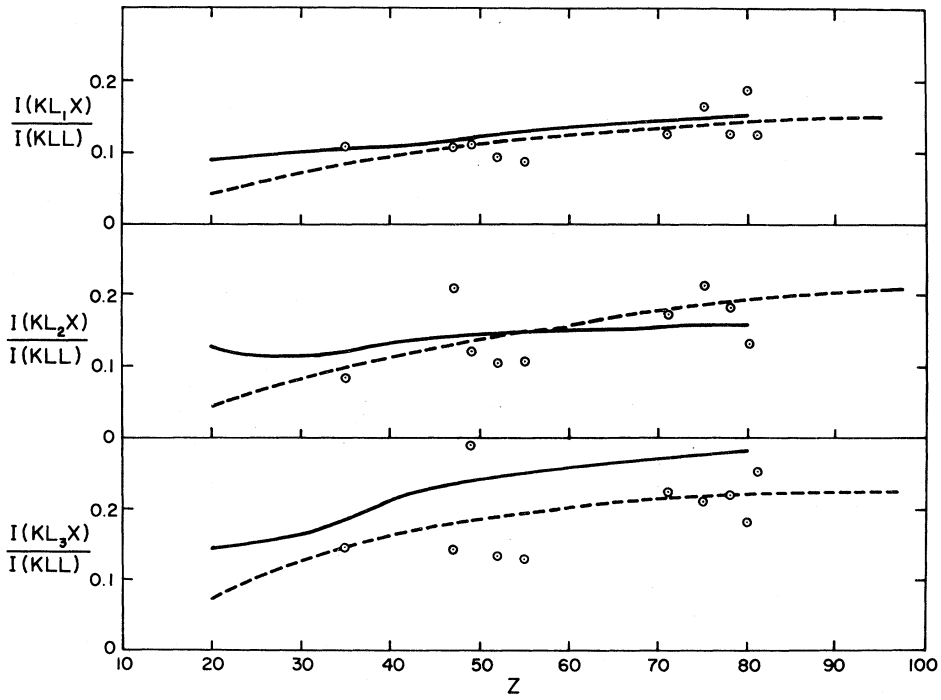

FIG. 4–6. Auger-electron intensity ratios $I(KL_iX)/I(KLL)$. The solid curves represent theoretical predictions of Venugopala Rao, Chen, and Crasemann (1972); the broken curves are best fits to the data. [From Venugopala Rao, Chen, and Crasemann (1972), courtesy of American Institute of Physics.]

TABLE IV.V. Auger-electron intensity ratios derived from a best fit to experimental data. From Venugopala Rao, Chen, and Crasemann (1972).

Z	b_1[a]	b_2[a]	b_3[a]	KL_1X/KLL	KL_2X/KLL	KL_3X/KLL	KLX/KLL	KXY/KLL
20	0.301	1.041	0.658	0.046	0.042	0.074	0.161	0.0096
22	0.308	0.987	0.705	0.054	0.048	0.087	0.189	0.0135
24	0.317	0.940	0.743	0.062	0.054	0.098	0.215	0.0173
26	0.326	0.900	0.774	0.070	0.060	0.109	0.239	0.0210
28	0.336	0.864	0.800	0.078	0.065	0.119	0.262	0.0246
30	0.348	0.831	0.821	0.085	0.071	0.128	0.284	0.0280
32	0.360	0.801	0.839	0.091	0.075	0.138	0.304	0.0314
34	0.372	0.774	0.854	0.098	0.081	0.144	0.323	0.0347
36	0.386	0.748	0.866	0.105	0.085	0.152	0.342	0.0379
38	0.399	0.724	0.877	0.111	0.089	0.158	0.359	0.0410
40	0.413	0.701	0.886	0.116	0.094	0.165	0.375	0.0440
42	0.428	0.679	0.893	0.122	0.097	0.170	0.390	0.0470
44	0.442	0.658	0.900	0.127	0.101	0.176	0.404	0.0498
46	0.457	0.638	0.905	0.133	0.104	0.180	0.417	0.0526
48	0.472	0.619	0.909	0.138	0.107	0.185	0.430	0.0553
50	0.489	0.603	0.908	0.142	0.111	0.189	0.442	0.0579
52	0.507	0.590	0.903	0.146	0.114	0.193	0.453	0.0604
54	0.522	0.588	0.890	0.151	0.116	0.196	0.463	0.0629
56	0.536	0.588	0.876	0.154	0.119	0.200	0.473	0.0653
58	0.550	0.588	0.862	0.159	0.122	0.202	0.483	0.0677
60	0.565	0.588	0.847	0.163	0.124	0.206	0.492	0.0699
62	0.581	0.587	0.832	0.166	0.126	0.208	0.500	0.0721
64	0.597	0.588	0.815	0.170	0.128	0.211	0.508	0.0743
66	0.614	0.588	0.798	0.173	0.130	0.212	0.515	0.0764
68	0.630	0.588	0.782	0.176	0.132	0.214	0.522	0.0784
70	0.646	0.590	0.764	0.179	0.134	0.215	0.528	0.0804
72	0.664	0.591	0.745	0.182	0.135	0.218	0.535	0.0923
74	0.682	0.593	0.725	0.185	0.137	0.219	0.540	0.0841
76	0.701	0.594	0.705	0.187	0.138	0.220	0.546	0.0859
78	0.719	0.596	0.685	0.190	0.140	0.222	0.551	0.0877
80	0.739	0.598	0.663	0.192	0.142	0.223	0.556	0.0894
82	0.759	0.600	0.641	0.195	0.142	0.223	0.560	0.0911
84	0.779	0.603	0.618	0.197	0.143	0.225	0.565	0.0927
86	0.800	0.605	0.595	0.199	0.145	0.225	0.569	0.0942
88	0.822	0.608	0.570	0.201	0.145	0.226	0.572	0.0958
90	0.844	0.612	0.544	0.203	0.145	0.226	0.576	0.0972
92	0.867	0.615	0.518	0.205	0.147	0.227	0.579	0.0987
94	0.891	0.619	0.490	0.207	0.148	0.228	0.583	0.100

[a] The quantity b_i is the probability, per K–LL Auger transition, that an L_i vacancy is produced.

In Fig. 4–7 the vacancy numbers n_{KL_i} are plotted as a function of Z. Also shown is the total number of primary L vacancies produced in all three subshells as a result of the decay of a K-vacancy state, i.e.,

$$n_{KL}=\sum_i n_{KL_i}. \tag{4–6}$$

Earlier summaries of n_{KL_i} were published in the form of graphs by Robinson and Fink (1955, 1960), Wapstra, Nijgh, and van Lieshout (1959), and Listengarten (1960).

Table IV.VI lists L vacancies produced in radiative and nonradiative decay of K-vacancy states. It must be noted that the nonradiative decay of a K-vacancy state leads to double-vacancy states. The decay rate of double-L vacancy states may depend upon which of the two L vacancies remains a "spectator vacancy," as discussed by Krisciokaitis and Haynes (1967); this can be studied by observing L x rays in coincidence with K Auger electrons. Multiple-vacancy effects are discussed further in Sec. 5.2.

4.5. Experimental Techniques for the Determination of L-Shell Yields

The techniques available for L-shell yield measurements in which L x-ray emission rates are studied can be divided broadly into two categories: single-spectrum methods and coincidence methods. In singles-spectrum methods, the emission rates are usually measured relative to some other events, such as conversion electrons or γ rays, that can be normalized to known pri-

TABLE IV.VI. Average number of primary L_i-subshell vacancies produced by transitions to the K shell: $n_{KL_i}(A)$ due to Auger transitions and $n_{KL_i}(R)$ due to radiative transitions. Also listed is the total number of primary L vacancies produced by Auger transitions $[n_{KL}(A)]$, by radiative transitions $[n_{KL}(R)]$, and by all transitions (n_{KL}) to the K shell. From Venugopala Rao, Chen, and Crasemann (1972).

Z	$n_{KL_1}(A)$	$n_{KL_2}(A)$	$n_{KL_2}(R)$	$n_{KL_3}(A)$	$n_{KL_3}(R)$	$n_{KL}(A)$	$n_{KL}(R)$	n_{KL}
20	0.253	0.790	0.048	0.534	0.096	1.577	0.144	1.721
22	0.235	0.672	0.065	0.514	0.129	1.421	0.194	1.615
24	0.220	0.578	0.083	0.489	0.165	1.287	0.248	1.535
26	0.205	0.498	0.103	0.457	0.203	1.160	0.306	1.466
28	0.188	0.423	0.123	0.418	0.242	1.029	0.365	1.394
30	0.172	0.358	0.142	0.377	0.279	0.907	0.421	1.328
32	0.156	0.302	0.159	0.337	0.311	0.795	0.470	1.265
34	0.140	0.254	0.175	0.296	0.340	0.690	0.515	1.205
36	0.129	0.217	0.188	0.262	0.365	0.608	0.553	1.161
38	0.133	0.180	0.200	0.229	0.387	0.522	0.587	1.109
40	0.100	0.153	0.211	0.200	0.405	0.453	0.616	1.069
42	0.090	0.127	0.220	0.175	0.421	0.392	0.641	1.033
44	0.0808	0.108	0.227	0.153	0.433	0.342	0.660	1.002
46	0.0727	0.0913	0.234	0.133	0.443	0.297	0.677	0.974
48	0.0659	0.0783	0.240	0.118	0.452	0.262	0.692	0.954
50	0.0592	0.0670	0.245	0.103	0.460	0.229	0.705	0.934
52	0.540	0.0582	0.249	0.0904	0.465	0.203	0.714	0.917
54	0.0489	0.0512	0.253	0.0790	0.469	0.179	0.722	0.901
56	0.0444	0.0455	0.256	0.0693	0.473	0.159	0.729	0.888
58	0.0407	0.0408	0.259	0.0611	0.475	0.143	0.734	0.877
60	0.0373	0.0365	0.261	0.0539	0.477	0.128	0.738	0.866
62	0.0342	0.0327	0.264	0.0476	0.479	0.115	0.743	0.858
64	0.0320	0.0299	0.266	0.0427	0.479	0.105	0.745	0.850
66	0.0297	0.0271	0.268	0.0381	0.480	0.0949	0.748	0.843
68	0.0277	0.0248	0.270	0.0343	0.479	0.0868	0.749	0.836
70	0.0257	0.0225	0.272	0.0304	0.480	0.0786	0.752	0.831
72	0.0240	0.0206	0.274	0.0273	0.479	0.0719	0.753	0.825
74	0.0230	0.0193	0.275	0.0250	0.478	0.0673	0.753	0.820
76	0.0212	0.0175	0.277	0.0221	0.478	0.0608	0.755	0.816
78	0.0206	0.0166	0.278	0.0205	0.477	0.0577	0.755	0.813
80	0.0193	0.0153	0.280	0.0183	0.476	0.0529	0.756	0.809
82	0.0185	0.0144	0.281	0.0168	0.475	0.0497	0.756	0.806
84	0.0177	0.0135	0.284	0.0153	0.474	0.0465	0.758	0.805
86	0.0168	0.0126	0.285	0.0138	0.473	0.0432	0.758	0.801
88	0.0160	0.0117	0.286	0.0124	0.472	0.0401	0.758	0.798
90	0.0150	0.0108	0.288	0.0110	0.470	0.0368	0.758	0.795
92	0.0147	0.0104	0.289	0.0102	0.469	0.0353	0.758	0.793
94	0.0150	0.0105	0.290	0.0099	0.467	0.0354	0.757	0.792

mary vacancy distributions. The same principle is basically utilized in coincidence methods, except that known primary distributions of vacancies or single subshell vacancies are isolated by gating on conversion electrons, K x rays, γ rays, or α particles.

Among the variety of detectors available for observing L x rays, bent-crystal diffraction spectrometers are best suited for studying L x-ray spectra with highest resolution, but they are not suitable for coincidence arrangements because of low efficiency. The currently available Si(Li) and Ge(Li) low-energy photon spectrometers with resolution as good as 170 eV FWHM at 6.4 keV are the most efficient and can be used with care to energies as low as 2.5 keV. Below 2.5 keV, proportional-counter systems are best suited. Typical L x-ray spectra measured with Si(Li) detectors are shown in Figs. 4–8 to 4–11. The L x-ray spectrum in Fig. 4–12 was recorded with a diffraction spectrometer; its usefulness for isolating individual transitions is apparent.

Instead of studying L x rays, one can study L Auger electrons; high-resolution Auger spectra can provide information on Auger and Coster–Kronig yields. A typical L Auger-electron spectrum at $Z=92$ is shown in Fig. 4–13. Low-energy electron spectrometers, such as electrostatic spectrometers (Blauth, 1957; Mehlhorn, 1960; Siegbahn, 1967), double-focussing magnetic spectrometers (Nall, Baird, and Haynes, 1960; Albridge and Hollander, 1961; Sujkowski and Mellin, 1961) and magnetic lens spectrometers (Risch, 1958) tend to have low transmission.

However, it should be pointed out that both electron

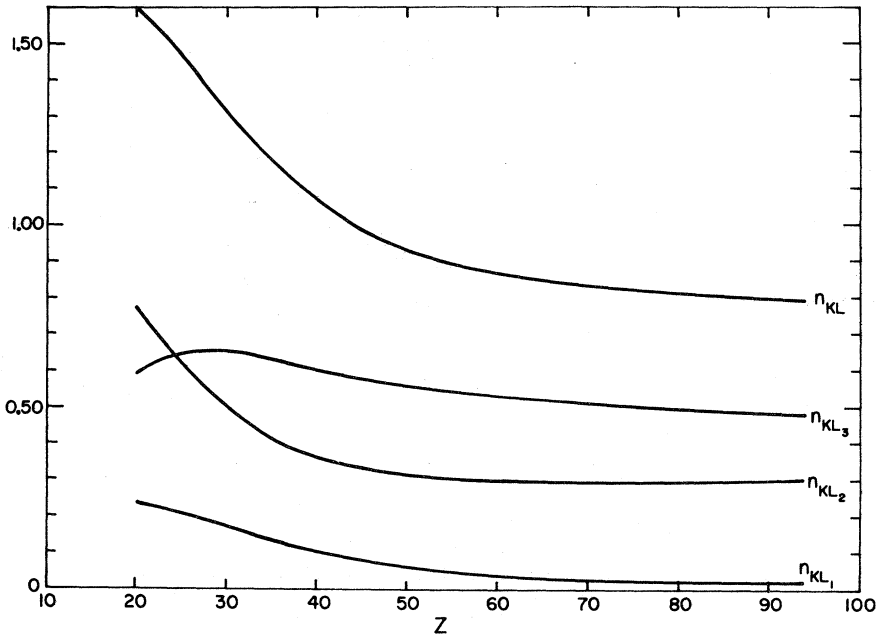

FIG. 4–7. Average numbers n_{KL_i} of primary L_i-subshell vacancies produced in the decay of one K vacancy through radiative transitions and through Auger transitions of the types K–L_iL_j and K–L_iX. (Not included are additional L vacancies produced through Coster–Kronig transitions of the type L_i–L_jX.) Also shown in $n_{KL}=\Sigma\, n_{KL_i}$. [Based on results of Venugopala Rao, Chen, and Crasemann (1972), courtesy of American Institute of Physics.]

spectrometers and diffraction spectrometers are best suited for studying the rates of individual transitions to the L shell, while efficient multichannel devices, such as semiconductor detectors, proportional and scintillation counters, are most suitable for measuring total L-shell yields. Often a judicious combination of these detectors leads to the measurement of L-shell yields which are otherwise inaccessible. In what follows, we first outline the basic principles employed in measuring L-shell yields and then proceed to describe details of the individual techniques and their applications.

If one measures the total number of L x rays, I_L, arising from a known number n_L of primary L vacancies present in an event, such as a radioactive transition or fluorescent excitation, then the average fluorescence yield $\bar{\omega}_L$ is given directly by the relation

$$\bar{\omega}_L = I_L/n_L. \tag{4–7}$$

Historically, this has been the quantity measured most

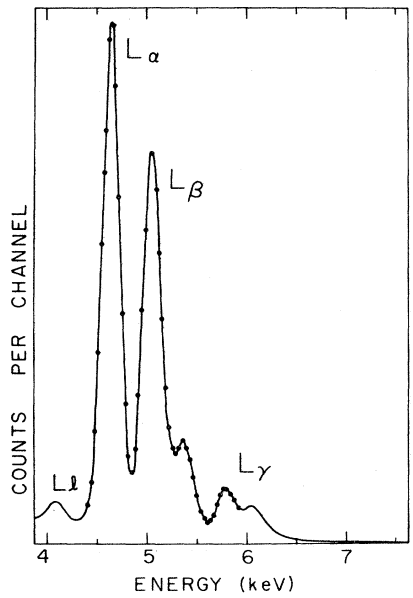

FIG. 4–8. Lanthanum L x-ray spectrum generated in the decay of ^{139}Ce, measured with a Si(Li) detector of 180-eV resolution FWHM at 6.4 keV. (R. W. Fink, private communication)

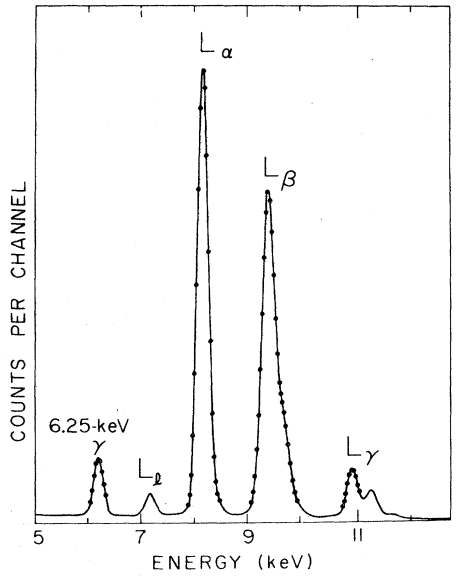

FIG. 4–9. Tantalum L x rays emitted in the decay of ^{181}W, measured with a Si(Li) spectrometer of 180-eV resolution FWHM at 6.4 keV. (R. W. Fink, private communication)

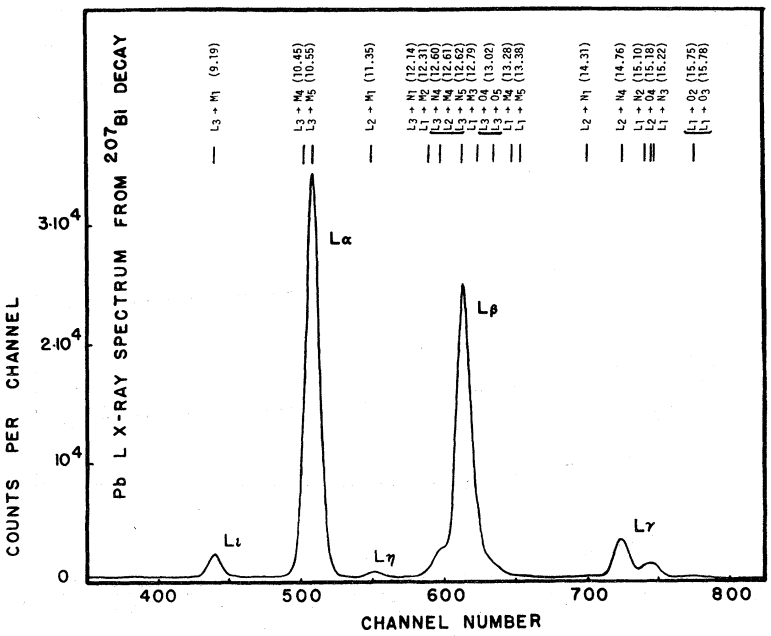

FIG. 4–10. Lead L x-ray spectrum from the decay of ^{207}Bi, measured with a KeVex Si(Li) spectrometer of 155-eV resolution FWHM at 5.9 keV. Prominent transitions and their energies are indicated. [From Venugopala Rao, Palms, and Wood (1971), courtesy of American Institute of Physics.]

often (Sec. 4.5). The production of primary vacancies in the three L subshells has been described in Secs. 4.1–4.4. The total vacancy number n_L in a sample is given by

$$n_L=\sum_i n_i^L,$$

$$n_i^L=n_{L_i}+n_K n_{KL_i}. \tag{4-8}$$

Here, n_{L_i} is the number of primary vacancies directly produced in the L_i subshell by processes such as L-shell internal conversion or L-shell electron capture. By n_{KL_i}, we denote the number of primary vacancies produced by transitions of an L_i-subshell electron to the K shell (Sec. 4.4), and n_K is the total number of K vacancies in the sample.

The normalized primary vacancy distribution is denoted by N_i^L:

$$N_i^L=n_i^L/\sum_i n_i^L; \qquad \sum_i N_i^L=1. \tag{4-9}$$

The superscript L will be omitted in the remainder of this chapter when no ambiguity arises.

To obtain specific information on individual subshells we need to know, first, how many of the n_L primary vacancies belong to each of the three L subshells and, second, how many of the I_L x rays are characteristic of each individual subshell. It is possible to derive the primary vacancy distribution from principles described in Secs. 4.1–4.4, but it is not always experimentally feasible to count the number of x rays characteristic of each of the three L subshells. A study of L x-ray spectra measured with Si(Li) x-ray spectrometers reveals that only two of the resolved photopeaks are characteristic of a single L subshell, namely, Ll and $L\alpha$ x rays that arise from transitions to the L_3 subshell (see Figs. 4–8 to 4–11). At high Z, the high-energy end of the L x-ray spectrum is characteristic of the L_1 subshell even though complete resolution of the corresponding photopeaks is not achieved. Since detectors can resolve high-Z L x-ray spectra into components Ll, $L\alpha$, $L\eta$, $L\beta$, and $L\gamma$, we formulate a basic set of equations, consistent with the definitions of Sec. 1.3, that relate L-shell yields to the counting rates measured in a typical experiment.

We shall assume that the L x-ray counting rates have been corrected for photopeak detection efficiency, detector solid angle, source self-absorption, attenuation suffered by the radiation on its path between source and detector, and any summing effects in the detector.

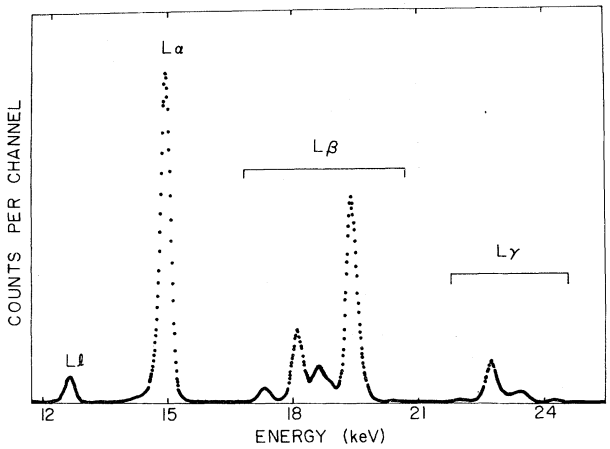

FIG. 4–11. Curium L x rays emitted in the decay of ^{249}Cf, measured with a Si(Li) detector of 180-eV resolution FWHM at 6.4 keV. (R. W. Fink, private communication)

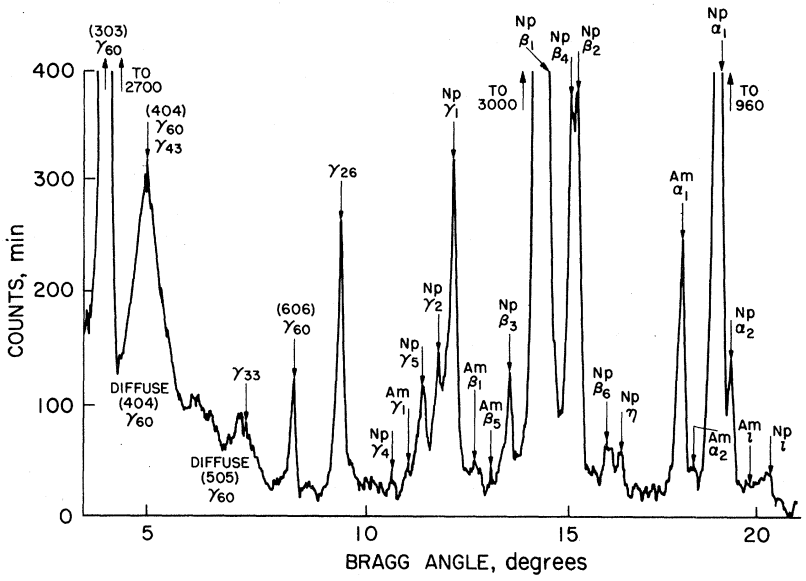

FIG. 4–12. Spectrum of x rays and low-energy γ rays emitted in the decay of ^{241}Am. Chart record from a 10-inch quartz bent-crystal spectrometer. The detector was a sodium iodide scintillation spectrometer. [From Day (1955), courtesy of American Institute of Physics.]

The problems involved in these corrections and the impact of semiconductor detectors on x-ray spectroscopy in general are discussed by various authors (Hollander, 1966; Freund *et al.*, 1969b; Palms, Venugopala Rao, and Wood, 1969; Campbell, Goble, and Smith, 1970; Hollstein, 1970; Walter, 1970).

Let p be the probability of exciting an L vacancy in an event such as radioactive decay or fluorescent excitation. If I_L is the intensity of L x rays counted in D events per unit time (e.g., disintegrations per second), and I_{Ll}, $I_{L\alpha}$, $I_{L\eta}$, $I_{L\beta}$, and $I_{L\gamma}$ are the intensities of the corresponding Ll, $L\alpha$, $L\eta$, $L\beta$, and $L\gamma$ x rays, the

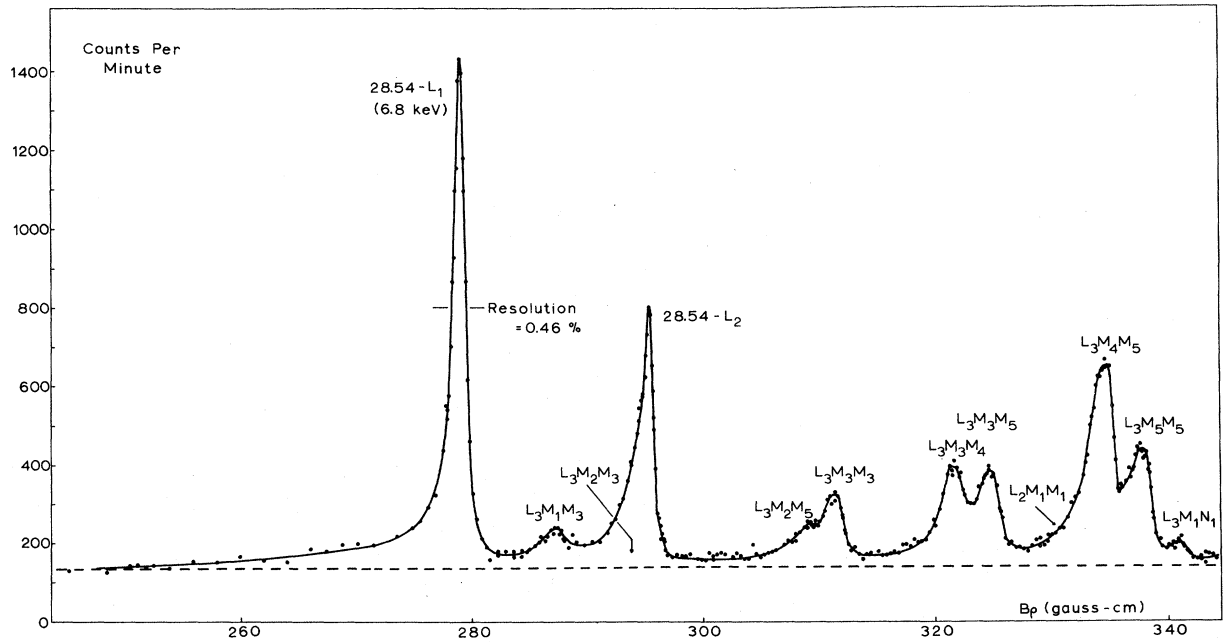

FIG. 4–13. Spectrum of ^{233}U L Auger electrons and low-energy internal conversion electrons, measured with an iron-free double-focusing β-ray spectrometer. [From Zender, Pou, and Albridge (1969), courtesy of Springer-Verlag.]

following relations can be established between the L-shell yields and the intensities:

$$
\begin{aligned}
I_L &= Dp\tilde{\omega}_L = Dp(N_1\nu_1 + N_2\nu_2 + N_3\nu_3), \\
I_{Ll,\alpha} &= DpV_3\omega_3/(1+s_3) \\
&= [Dp/(1+s_3)] \\
&\quad \times [N_1(f_{13}+f_{12}f_{23}) + N_2 f_{23} + N_3]\omega_3, \\
I_{L\eta,\beta,\gamma} - s_3 I_{Ll,\alpha} &= Dp(V_1\omega_1 + V_2\omega_2) \\
&= Dp[N_1(\omega_1 + f_{12}\omega_2) + N_2\omega_2], \\
I_{L\eta,\beta} - s_3 I_{Ll,\alpha} &= Dp[V_1\omega_1/(1+s_1) + V_2\omega_2/(1+s_2)] \\
&= Dp[N_1\omega_1/(1+s_1) \\
&\qquad + (N_1 f_{12} + N_2)\omega_2/(1+s_2)], \\
I_{L\gamma} &= Dp\{[V_1 s_1/(1+s_1)]\omega_1 \\
&\qquad + [V_2 s_2/(1+s_2)]\omega_2\} \\
&= Dp\{[N_1 s_1\omega_1/(1+s_1)] \\
&\quad + [(N_1 f_{12} + N_2)s_2\omega_2/(1+s_2)]\}. \qquad (4\text{–}10)
\end{aligned}
$$

Here, we have

$$
\begin{aligned}
I_L &= I_{Ll} + I_{L\alpha} + I_{L\eta} + I_{L\beta} + I_{L\gamma}, \\
I_{Ll,\alpha} &= I_{Ll} + I_{L\alpha}, \qquad I_{L\eta,\beta} = I_{L\eta} + I_{L\beta}, \\
I_{L\eta,\beta,\gamma} &= I_{L\eta} + I_{L\beta} + I_{L\gamma}.
\end{aligned}
$$

The quantity p in the above equations can be found from detailed knowledge of the events under consideration. If the events are pure L-capture decays, p is the L-capture probability P_L. In a pure L-conversion process, p is the conversion-electron ratio $\alpha_L/(1+\alpha_t)$. If the events correspond to the decay of K vacancies, p is the number n_{KL}. If all these processes are present simultaneously, as can be the case in a singles-spectrum study, p is a function of all the above quantities. In terms of the total number of primary vacancies n_L, the fraction p is $p = n_L/D$.

The quantities s_1, s_2, and s_3, which appear in Eqs. (4–10), are intensity ratios of resolved L x-ray peaks arising from transitions to the L_1, L_2, and L_3 subshells, respectively. They are actually radiative decay branching ratios for the individual L subshells, as defined in the works of Holmes and Kostroun (1970) and Venugopala Rao, Palms, and Wood (1971). For the L_1 subshell, we have

$$
\begin{aligned}
s_1 &= \frac{I(L_1N) + I(L_1O) + \cdots}{I(L_1M)} \\
&= \frac{\text{Intensity of } L\gamma \text{ x rays originating from } L_1 \text{ vacancies}}{\text{Intensity of } L\beta \text{ x rays originating from } L_1 \text{ vacancies}}, \qquad (4\text{–}11)
\end{aligned}
$$

where $I(L_1X)$ is the intensity of radiative transitions by X-shell electrons filling L_1 vacancies. Similarly, we have

$$
\begin{aligned}
s_2 &= \frac{I(L_2N) + I(L_2O) + \cdots}{I(L_2M)} \\
&= \frac{\text{Intensity of } L\gamma \text{ x rays originating from } L_2 \text{ vacancies}}{\text{Intensity of } L\eta \text{ and } L\beta \text{ x rays originating from } L_2 \text{ vacancies}}, \qquad (4\text{–}12)
\end{aligned}
$$

and

$$
\begin{aligned}
s_3 &= \frac{I(L_3N) + I(L_3O) + \cdots}{I(L_3M)} \\
&= \frac{\text{Intensity of } L\beta \text{ x rays originating from } L_3 \text{ vacancies}}{\text{Intensity of } Ll \text{ and } L\alpha \text{ x rays originating from } L_3 \text{ vacancies}}. \qquad (4\text{–}13)
\end{aligned}
$$

It should be emphasized that the definition of these branching ratios takes into account the fact that currently available semiconductor x-ray detectors have limited resolution. Obviously, studies of L x-ray spectra based on work with bent-crystal diffraction spectrometers capable of finer resolution need not be confined to the use of such gross ratios of groups of x rays.

It is clear from Eqs. (4–10) that a simple study of the singles spectrum cannot provide significant information on any one subshell. If the resolution of the L x-ray detector permits, it is possible to analyze the $L\gamma$ x-ray photopeak into its two parts, one corresponding to the L_2 subshell ($L^2\gamma$) and the other corresponding to the L_1 subshell ($L^1\gamma$). Then the last of Eqs. (4–10) can be split into two parts:

$$
\begin{aligned}
I_{L^1\gamma} &= DpV_1\omega_1[s_1/(1+s_1)], \qquad (4\text{–}14) \\
I_{L^2\gamma} &= DpV_2\omega_2[s_2/(1+s_2)]. \qquad (4\text{–}15)
\end{aligned}
$$

Equation (4–14) contains only the two unknown

quantities s_1 and ω_1, corresponding to the L_1 subshell. Hence, a determination of one of these quantities is possible if the other is known, as demonstrated in the work of Venugopala Rao, Palms, and Wood (1971), and of Chu *et al.* (1971).

If one uses coincidence techniques and selects only certain kinds among C_0 total counts, then he can choose a specific primary distribution of L vacancies. The above set of equations can be suitably modified to fit the conditions of a coincidence experiment. We denote the L x-ray intensity coincidence-gated by a photon or electron by $I_{L(g)}$. In particular, $I_{L\alpha(g)}$ means the intensity of $L\alpha$ x rays gated by g. The counting rate of gating events is written C_g and replaces D in the above equations. With these modifications, we can write the set of equations applicable to any coincidence experiment as follows:

$$I_{L(g)}=C_g p\bar{\omega}_L, \tag{4–16}$$

$$I_{Ll,\alpha(g)}=C_g pV_3\omega_3/(1+s_3), \tag{4–17}$$

$$I_{L\eta,\beta,\gamma(g)}-s_3I_{Ll,\alpha(g)}=C_g p(V_1\omega_1+V_2\omega_2), \tag{4–18}$$

$$I_{L\eta,\beta(g)}-s_3I_{Ll,\alpha(g)}=C_g p\{[V_1\omega_1/(1+s_1)]+[V_2\omega_2/(1+s_2)]\}, \tag{4–19}$$

$$I_{L\gamma(g)}=C_g p\{[V_1\omega_1s_1/(1+s_1)]+[V_2\omega_2s_2/(1+s_2)]\}. \tag{4–20}$$

These equations are similar in form to Eqs. (4–10) for singles experiments, except that the V_i's refer to the specific distribution of L-subshell vacancies selected in a given coincidence experiment. In Table IV.VII we list the ideal cases in which primary vacancies occur in only one subshell. Only the first two cases have been utilized experimentally to date.

TABLE IV.VII. Ideal cases in which primary vacancies occur in one L subshell only.

Event	Primary L-subshell vacancy distribution		
	N_1	N_2	N_3
$K\alpha_1$ x-ray emission	0	0	1
$K\alpha_2$ x-ray emission	0	1	0
L_1-electron internal conversion	1	0	0

4.5.1. ($K\alpha$ X-Ray)–(L X-Ray) Coincidence Methods

Since the final state of the atom in the transition resulting in $K\alpha_1$ x-ray emission is an L_3 vacancy state, $K\alpha_1$ x rays can be used to signal the formation of L_3 vacancies. The appropriate relations for coincidence rates are obtained by substituting $p=1$, $N_3=1$, $N_1=N_2=0$, and $g=K\alpha_1$ in the general equations (4–16)–(4–20), with the results

$$I_{L(K\alpha_1)}=C_{K\alpha_1}\omega_3, \tag{4–21}$$

$$I_{L\beta(K\alpha_1)}/I_{Ll,\alpha(K\alpha_1)}=s_3. \tag{4–22}$$

Similarly, if $K\alpha_2$ x rays are used to signal the formation of L_2 vacancies, we have $p=1$, $N_2=1$, $N_1=N_3=0$, and $g=K\alpha_2$:

$$I_{L(K\alpha_2)}=C_{K\alpha_2}\nu_2=C_{K\alpha_2}(\omega_2+f_{23}\omega_3), \tag{4–23}$$

$$I_{Ll,\alpha(K\alpha_2)}(1+s_3)=C_{K\alpha_2}f_{23}\omega_3, \tag{4–24}$$

$$I_{L\gamma(K\alpha_2)}/[I_{L\beta,\eta(K\alpha_2)}-s_3I_{Ll,\alpha(K\alpha_2)}]=s_2. \tag{4–25}$$

Thus, not only the fluorescence yields ω_2 and ω_3, but also the Coster–Kronig yield f_{23} and the radiative branching ratios s_2 and s_3 can be measured if high-resolution detectors are used to observe both L and K x rays. Currently available resolution permits measurement of these quantities for $Z\geq 75$. Below $Z=75$, the $L\eta$ x-ray photopeak is not clearly resolved from the $L\alpha$ photopeak, and appropriate care must be taken in evaluating the relative intensities. If the three main L x-ray groups are not resolved, as with scintillation spectrometers, only ν_2 and ω_3 can be measured. If the $K\alpha$ x rays are not resolved into $K\alpha_1$ and $K\alpha_2$ components, but separated from the $K\beta$ peak, then coincidence measurements can only determine the average fluorescence yield ω_{KL}, defined as the number of L x rays which follow emission of a K x ray. The relevant equations are found by substituting

$$N_1=0,\quad p=1,\quad N_2=I_{K\alpha_2}/I_{K\alpha},\quad N_3=I_{K\alpha_1}/I_{K\alpha},\quad \bar{\omega}_L=\omega_{KL}$$

into the general equation (4–16):

$$I_{L(K\alpha)}=C_{K\alpha}\{[(I_{K\alpha_2}/I_{K\alpha})\nu_2]+[(I_{K\alpha_1}/I_{K\alpha})\omega_3]\}=C_{K\alpha}\omega_{KL}. \tag{4–26}$$

There is an obvious advantage in using resolved $K\alpha_1$ and $K\alpha_2$ x rays as signals for the formation of L_3 and L_2 vacancies, respectively. An important remaining consideration is the directional correlation between $K\alpha_1$ and L x rays, which occur in cascade. For example, a coincidence measurement of ω_3 with the counters at 180° to each other yields a result that is 3% higher than if coincidence rates are averaged over all angles. This difference is reduced by the finite solid angles subtended by the detectors. The effect of directional correlations and the current status of experiments on directional correlations are considered in detail in Sec. 4.5.5.

Fluorescence-yield measurements based on ($K\alpha$)–(L x-ray) coincidences, performed before the advent of high-resolution x-ray detectors, have been reviewed earlier (Fink *et al.*, 1966). Poor detector resolution notwithstanding, special techniques were employed to signal the formation of L_2 vacancies (Venugopala Rao and Crasemann, 1965b) and L_3 vacancies (Jopson *et al.*, 1964a). Price, Mark, and Swift (1968) were the first to exploit high resolution at K x-ray energies. They used a Ge(Li) spectrometer to detect well-resolved

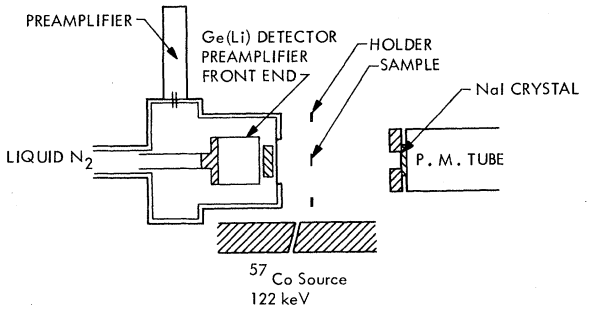

Experimental setup for L-subshell yield measurements.

FIG. 4–14. Experimental arrangement for measurement of L-shell fluorescence yields, after Price, Mark, and Swift (1968). (Courtesy of University of California Lawrence Livermore Laboratory, Livermore, and the U. S. Atomic Energy Commission under whose auspices work was performed.)

$K\alpha_1$ and $K\alpha_2$ x rays, while a cleaved NaI(Tl) crystal was employed to detect the coincident unresolved group of L x rays. Initial K vacancies were produced through photoelectric excitation, by well-collimated γ rays from ^{57}Co striking a thin foil target. Figure 4–14 illustrates the target-detector geometry. Measurements were performed on 15 elements with $71 \leq Z \leq 92$. Because the L x-ray detector could not resolve L x-ray spectra into component groups, only ν_2 and ω_3 were measured. Even with a high-resolution L x-ray detector, the use of thin foils would not permit the study of Coster–Kronig transitions that transfer vacancies from the L_2 to the L_3 subshell: some L-series x rays from the L_2 subshell can ionize the L_3 subshell. For example,

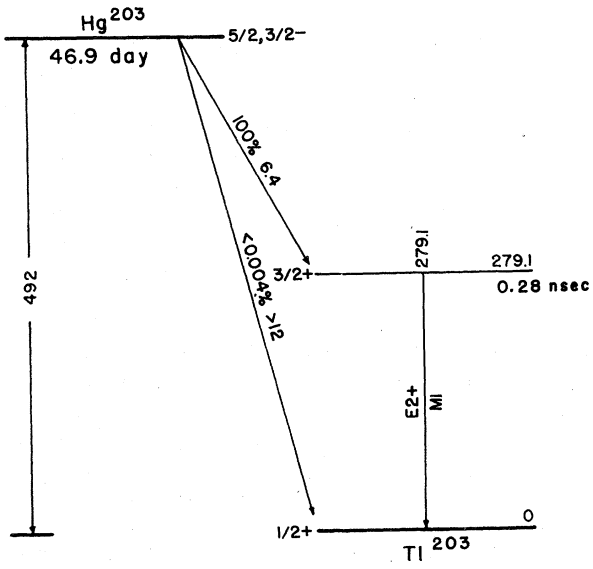

FIG. 4–15. Decay scheme of ^{203}Hg. [From Wood, Palms, and Venugopala Rao (1969), courtesy of American Institute of Physics.]

$L_{\gamma 1}$ x rays from L_2–N_4 transitions have an energy large enough to eject an L_3-subshell electron. Source self-excitation of L_3 vacancies then prevents an accurate determination of the number of L_3 vacancies that result from Coster–Kronig transfers from the L_2 subshell.

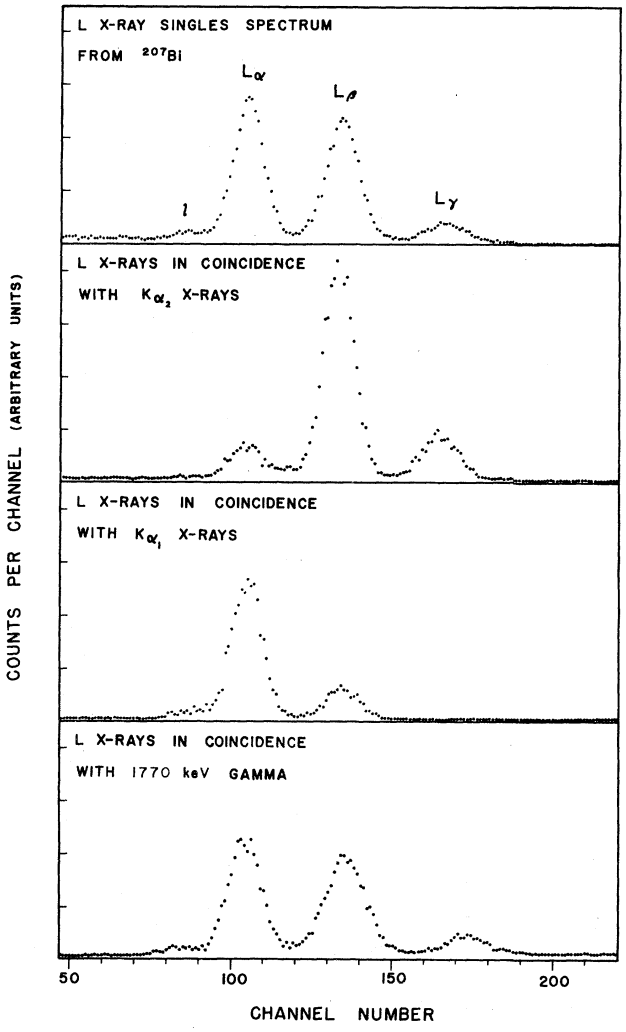

FIG. 4–16. Typical Pb L x-ray spectra in coincidence with $K\alpha_1$ and $K\alpha_2$ x rays, measured with a Si(Li) spectrometer. The presence of $L\alpha$ components in coincidence with $K\alpha_2$ x rays demonstrates the Coster–Kronig transfer of vacancies from the L_2 to the L_3 subshell. [From Venugopala Rao, Wood, Palms, and Fink (1969), courtesy of American Institute of Physics.]

The difficulty of self-excitation of L_3 vacancies is substantially eliminated if one uses high specific activity radioactive sources and becomes negligible with weightless carrier-free sources. Ideal for such experiments are radioactive nuclides with simple decay schemes, e.g., the electron-capturing ^{204}Tl, or ^{203}Hg feeding the internally converted 279-keV transition in ^{203}Tl (Fig. 4–15).

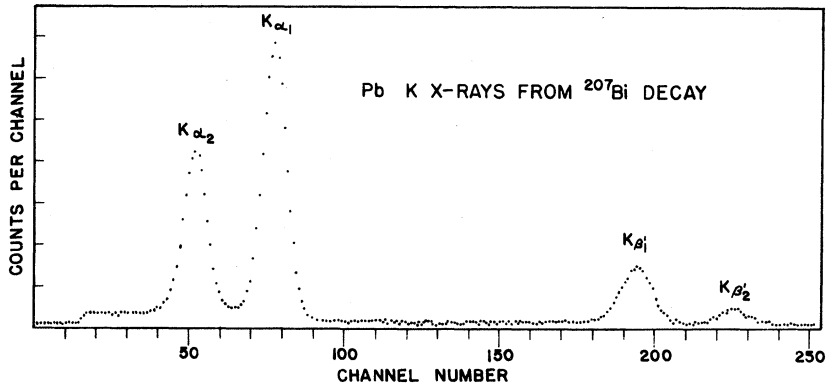

FIG. 4–17. Lead K x-ray spectrum, measured with a Ge(Li) spectrometer of 470-eV FWHM resolution at 14.4 keV. [From Venugopala Rao, Wood, Palms, and Fink (1969), courtesy of American Institute of Physics.]

With radioactive isotopes as sources of K and L vacancies, coincidence measurements have been performed with high resolution for both K x rays and L x rays by Venugopala Rao *et al.* (1969), Wood, Palms, and Venugopala Rao (1969), Mohan *et al.* (1970a), Holmes and Kostroun (1970), McGeorge, Freund, and Fink (1970), and McGeorge and Fink (1971b), in the range of $65 \leq Z \leq 96$. Typical sets of L x-ray spectra observed in coincidence with $K\alpha_1$ and $K\alpha_2$ x rays in the electron-capture decay of ^{207}Bi are shown in Fig. 4–16.

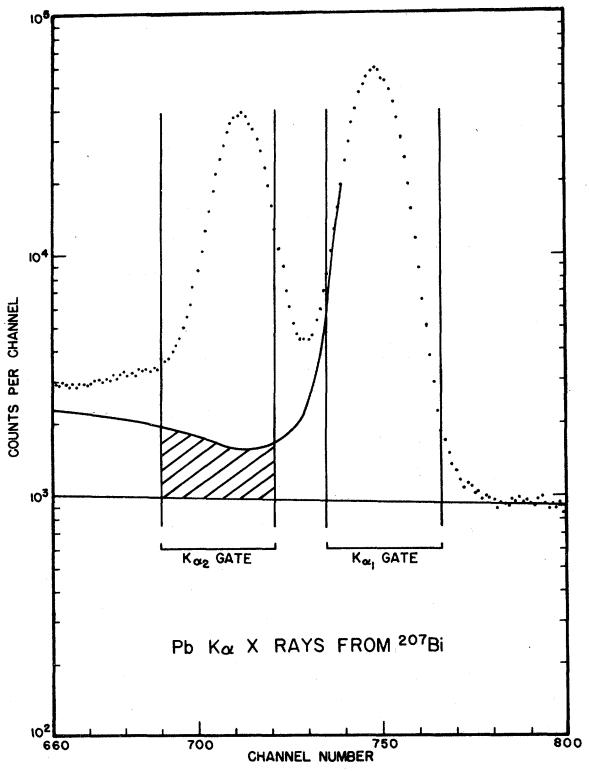

FIG. 4–18. Typical positions of single-channel analyzer windows to select $K\alpha_1$ and $K\alpha_2$ gate pulses for coincidence experiments. The crosshatched area represents the contribution of $K\alpha_1$ x rays to the $K\alpha_2$ gate. [From Venugopala Rao, Wood, Palms, and Fink (1969), courtesy of American Institute of Physics.]

In spite of the fact that detectors are available that separate $K\alpha_1$ and $K\alpha_2$ photopeaks clearly at Z as low as 65 (Fig. 4–17), a serious problem arises in gating on one of these photopeaks. For example, when a single-channel analyzer window is set on the $K\alpha_2$ peak, as many as 6% of the events admitted through the window can be due to $K\alpha_1$ x rays, as illustrated in Fig. 4–18. Experimental procedures to take this effect into account have been outlined by Venugopala Rao *et al.* (1969). Holmes and Kostroun (1970) have solved this problem by computing the shape of the low-energy photopeak tail by Monte–Carlo calculations. Unless suitable corrections of this type are made, an excessive value for f_{23} is found.

A complication occurs in measurements with radioactive isotopes the decay of which involves a cascade of two transitions, both giving rise to K and L vacancies. A case in point is that of ^{159}Dy, where K capture is followed by K conversion (Fig. 4–19). Gating on $K\alpha_1$ x rays, one then observes not only the ensuing L_3 x rays, but all L x rays arising from the transition in cascade. This cascade effect has been accounted for by McGeorge, Freund, and Fink (1970) in their work on ^{159}Dy by measuring coincidences with $K\beta$ x rays.

An interesting variation of the methods discussed in this section consists in observing $K\alpha$ x rays in coincidence with $L\alpha$ x rays, as done by Wood, Palms, and

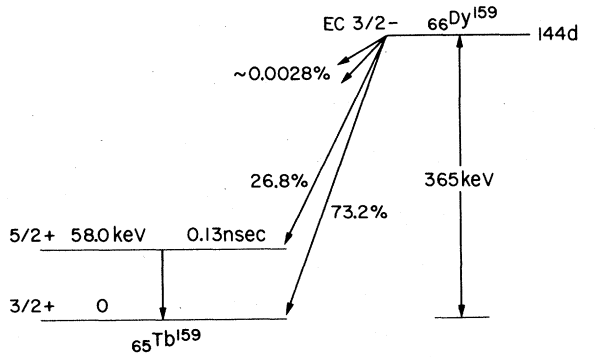

FIG. 4–19. Partial ^{159}Dy decay scheme, after McGeorge, Freund, and Fink (1970). (Courtesy of American Institute of Physics.)

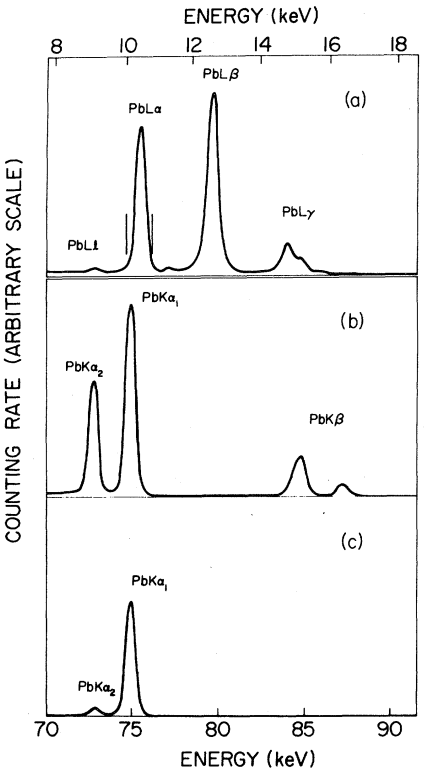

FIG. 4–20. (a) Lead L x-ray spectrum measured with a Si(Li) detector. The position of the single-channel analyzer window selecting $L\alpha$ x-ray gates is shown. (b) Lead K x-ray singles spectrum measured with a Ge(Li) detector. (c) Lead K x-ray spectrum in coincidence with $L\alpha$ x rays. The presence of $K\alpha_2$ x rays indicates the Coster–Kronig transfer of vacancies from the L_2 to the L_3 subshell. [From Wood, Palms, and Venugopala Rao (1972), courtesy and American Institute of Physics.]

Venugopala Rao (1972) to measure f_{23} at $Z=82$. This approach is based upon the following considerations: A radioactive source is chosen in which K and L vacancies are formed during the decay. The radiative filling of L_3-subshell vacancies results in the emission of L_3-subshell characteristic x rays (mostly $L\alpha$). The K x-ray spectrum coincident with these $L\alpha$ x rays contains (a) $K\alpha_1$ x rays, because some of the L_3 vacancies are formed originally as a result of $K\alpha_1$ x-ray emission, and (b) $K\alpha_2$ x rays, because some of the L_3 vacancies are the result of Coster–Kronig transfers from the L_2 subshell in which some vacancies were originally formed during the emission of $K\alpha_2$ x rays. The ratio of coincidence counting rates of $K\alpha_2$ and $K\alpha_1$ x rays, $C_{K\alpha_2(L\alpha)}$ and $C_{K\alpha_1(L\alpha)}$, is related to the L_2–L_3X Coster–Kronig transition probability by

$$C_{K\alpha_2(L\alpha)}/C_{K\alpha_1(L\alpha)}=(C_{K\alpha_2}/C_{K\alpha_1})f_{23}.$$

Here, $C_{K\alpha_2}/C_{K\alpha_1}$ is the ratio of singles $K\alpha_2$ and $K\alpha_1$ x-ray counting rates. The coincidence counting rate $C_{K\alpha_1(L\alpha)}$ must be corrected for directional correlation effects between $K\alpha_1$ and $L\alpha$ x rays. A typical coincidence spectrum is shown in Fig. 4–20.

4.5.2. (*Conversion-Electron*)–(*L X-Ray*) *Coincidence Methods*

The number of internal-conversion electrons emitted during a nuclear transition is equal to the number of vacancies produced in corresponding atomic shells. Hence, a coincidence arrangement in which conversion electrons are used to signal the formation of L vacancies is ideally suited for measuring L-shell yields. In particular, if L conversion electrons are selected, L vacancies are counted directly. Semiconductor electron detectors are best suited for such measurements. While individual L-subshell electrons cannot be separated with such detectors, the method is helpful in choosing a primary L-vacancy distribution that is known experimentally or theoretically. Ideally, a nuclear transition is chosen that is not preceded or followed by nuclear events in which L vacancies are produced. If K conversion electrons are present, they indicate the formation of K vacancies which lead to the formation of additional L vacancies (Sec. 4.4).

Since in most cases vacancies are present in all the L subshells, only a mean L-shell fluorescence yield $\bar{\omega}_L$ is obtained if the L x-ray spectrum is not resolved. For example, L conversion of the 58.5-keV transition in ^{231}Pa fed in the decay of ^{232}Th has been used to measure $\bar{\omega}_L$ by employing a NaI(Tl) detector for L x rays and an electrostatic spectrometer for conversion electrons, in a fast–slow coincidence arrangement (Boyer and Barat, 1968). L-subshell yields of Tl and Pb have been measured by studying the L internal conversion of the 279-keV transition following ^{203}Hg decay (Wood, Palms, and Venugopala Rao, 1969) and of the 1064-keV transition in ^{207}Bi decay (Venugopala Rao *et al.*, 1969) with a fast coincidence arrangement containing two cooled high-resolution Si(Li) L x-ray detectors. Figure 4–21 shows the spectrum of thallium L x rays in coincidence with L conversion electrons from the 279-keV transition. By observing the $L_{l+\alpha}$, $L_{\eta+\beta}$, and L_γ x-ray yields separately and utilizing information on L_2- and L_3-subshell yields from (K x-ray)–(L x-ray) coincidence measurements, all three L_1 subshell yields (ω_1, f_{12}, and f_{13}) can be evaluated.

Appropriate relations connecting coincidence rates and L-shell yields are found by making the following substitutions in the general equations (4–16)–(4–20):

$$p=1, \qquad g=e_L, \qquad N_1:N_2:N_3=\alpha_{L1}/\alpha_L:\alpha_{L2}/\alpha_L:\alpha_{L3}/\alpha_L.$$

Here, e_L symbolizes L conversion electrons; it is assumed that no other source of L vacancies exists. Then C_{e_L} represents the L conversion-electron gate counting rate and $I_{L(e_L)}$ denotes the intensity of L x rays in coincidence with C_{e_L}.

If K instead of L conversion electrons are used, the following relation applies:

$$pN_i=n_{KL_i}.$$

No experiments have been reported in which (K con-

version-electron)–(L x-ray) coincidences were observed with high resolution. The use of L conversion electrons for signalling L vacancy formation is preferable because uncertainties in estimating n_{KL_i} are avoided. But at low Z, K vacancies are mostly filled by Auger transitions leading to double-vacancy states (see Sec. 4.4), and in such cases (K conversion-electron)–(L x-ray) coincidences can be used advantageously to study the decay of double-vacancy states.

4.5.3. (γ-Ray)–(L X-Ray) Coincidence Method

When two transitions are in cascade through a short-lived intermediate state, the (L x-ray)–(γ-ray) coincidence method can be applied, because L vacancies created during the internal conversion of one transition are in time coincidence with γ rays from the other transition. In addition, this method can be used to advantage whenever orbital electron capture leads to an excited state that decays through prompt γ-ray emission. Primary L vacancies produced in transitions in cascade with the gating γ ray can be due to one or more of the four processes discussed in Secs. 4.3 and 4.4, i.e., electron capture, internal conversion, K x-ray emission, and K Auger-electron emission. Accurate knowledge of the primary vacancy distribution is of crucial importance. A typical situation is illustrated by the example of the decay of ^{207}Bi (Fig. 4–22).

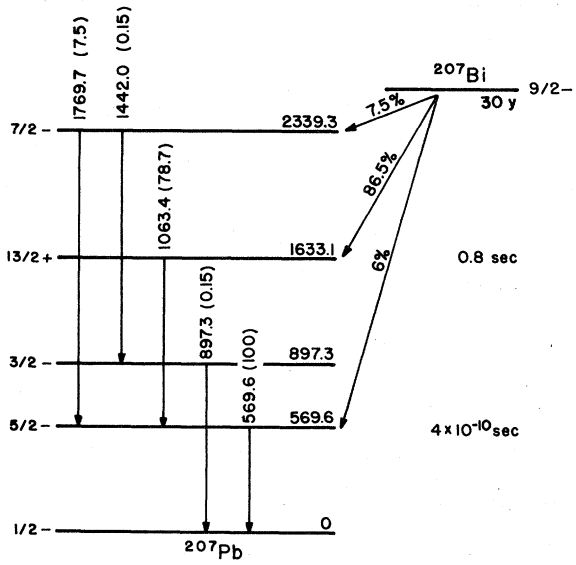

FIG. 4–22. Decay scheme of ^{207}Bi. [From Venugopala Rao, Wood, Palms, and Fink (1969), courtesy of American Institute of Physics.]

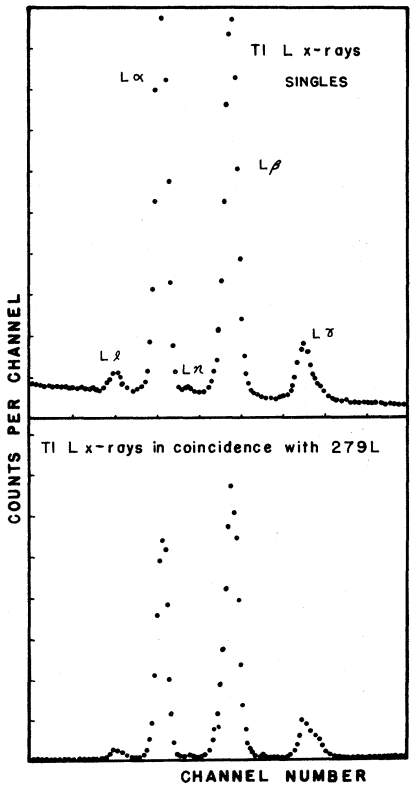

FIG. 4–21. Thallium L x-ray singles spectrum and L x-ray spectrum in coincidence with L conversion electrons from the 279-keV transition fed in the decay of ^{203}Hg. [From Wood, Palms, and Venugopala Rao (1969), courtesy of American Institute of Physics.]

In an ideal case for this method, a pure L-capture decay leads to an excited state that decays to the ground state by a prompt γ transition. These conditions are met, for example, by ^{181}W decaying to the 136- and 159-keV levels of ^{181}Ta by pure L capture (Fig. 4–23).

When several γ rays are present, as for example in the decay of ^{207}Bi and ^{195}Au, experimental care is required to single out L x rays that are truly coincident with a γ ray, because the gating window set on the corresponding photopeak can admit events that arise from the Compton distribution of higher energy γ rays. The unwanted contribution can be found by a standard nuclear spectroscopy technique of observing true coincidences with the window set on the continuum above the desired photopeak.

The appropriate equations relating L-shell yields and coincidence rates are the general equations (4–16)–(4–20), with g indicating the γ ray used for gating. Both p and N_i must be calculated for each case. Assuming that L_2- and L_3-subshell yields can be determined through (K x-ray)–(L x-ray) coincidence measurements, one can measure L_1-subshell yields. The method has been employed successfully with Pb, Tb, and Ta (Venugopala Rao *et al.*, 1969; McGeorge, Freund, and Fink, 1970; Mohan *et al.*, 1970a). Earlier work based on this principle includes that of Jopson, Mark, and Swift (1962), Halley and Engelkemeir (1964), and Venugopala Rao and Crasemann (1965a

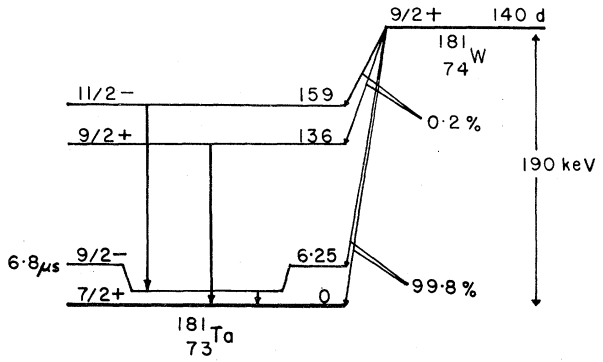

FIG. 4–23. Decay scheme of ^{181}W. [From Mohan, Fink, Wood, Palms, and Venugopala Rao (1970a), courtesy of American Institute of Physics.]

and 1966), who counted unresolved L x rays and hence determined only average yields.

4.5.4. (α-Particle)–(L X-Ray) Coincidence Method

With high-Z α-emitting elements, single nuclear transitions for L-shell vacancy creation can be selected through (α)–(L x-ray) coincidences. The principle is similar to that of the (γ-ray)–(L x-ray) coincidence method described above: a known primary vacancy distribution is chosen by means of the coincidence requirement. The method is useful if the number of L_i-subshell vacancies is proportional to the subshell conversion coefficients α_{L_i} of a single γ transition (Sec. 4.3). There are two restrictions: (1) the α-decay-fed nuclear level must decay to the ground state, and (2) this decay must take place by a γ transition converted in the L shell or a higher shell; K conversion must not occur.

Requirement (1) limits the application to low-lying levels in high-Z nuclides, for which requirement (2) is always fulfilled owing to the high K-shell binding energies. For example, for even–even nuclei with $Z>86$, the first excited state tends to be $\sim$50 keV above the ground state, whereas the K-shell binding energy is $\geq$100 keV.

In order to determine the L-subshell quantities of interest, namely, ω_i and f_{ij}, the (α-particle)–(L x-ray) coincidence method can be combined with the (γ-ray)–(L x-ray) coincidence method discussed in Sec. 4.5.3; it is restricted to high-Z nuclides by the requirements noted above. In even–even nuclides, low-energy $E2$ ground-state transitions occur, leading to a primary vacancy distribution $N_1:N_2:N_3\cong 0:1:1$. In odd-A nuclides, dipole ($E1$, $M1$) transitions take place. Thus, the results from $E2$ transitions give information on the L_2 and L_3 subshells, and the results from dipole transitions furnish information on L_1-subshell quantities. Consequently, to determine all six L-subshell quantities for a given element, both even-A and odd-A nuclides must be studied.

Appropriate equations for the simple case of an α-particle group feeding a ground-state transition that is converted in the L or higher shells only are found by making the following substitutions in the general equations (4–16)–(4–20):

$$g=\alpha, \qquad p=\alpha_L/(1+\alpha_t).$$

The result is

$$I_{L(\alpha)}=C_\alpha[\alpha_L/(1+\alpha_t)]\bar{\omega}_L$$
$$=C_\alpha[\alpha_L/(1+\alpha_t)](N_1\nu_1+N_2\nu_2+N_3\nu_3). \quad (4\text{–}27)$$

The method has been applied in principle by Halley and Engelkemeir (1964) to measure average fluorescence yields of the Ra, Th, U, Pu, and Cm daughters of even–even α emitters. Byrne *et al.* (1968) used this method together with a high-resolution measurement of the intensity ratio of L x rays that are characteristic of the L_3 subshell to those characteristic of the L_2 subshell, and measured the L_2-shell yields of ^{240}Pu, ^{236}U, and ^{234}U, daughters of the even–even α emitters ^{244}Cm, ^{240}Pu, and ^{238}Pu. If the small number of primary vacancies in the L_1 subshell is neglected, Eq. (4–27) simplifies to

$$I_{L(\alpha)}=C_\alpha p[N_2\omega_2+(N_3+N_2f_{23})\omega_3]. \quad (4\text{–}28)$$

Following the notation of Byrne *et al.* (1968), we define

$$I_{L(\alpha)}/C_\alpha=F,$$
$$(N_3+N_2f_{23})\omega_3/N_2\omega_2=I_3^L/I_2^L=F_3',$$
$$N_3/N_2=C_3', \quad (4\text{–}29)$$

where I_i^L is the number of L x rays characteristic of the L_i subshell. Byrne *et al.* (1968) measured the quantities F and F_3', while the quantities p and C_3' were calculated from available information. In terms of these four quantities, ω_2 and f_{23} are given by the relations

$$\omega_2=[F(1+C_3'\nu)]/[p(1+F_3')];$$
$$f_{23}=(\omega_2/\omega_3)F_3'-C_3'. \quad (4\text{–}30)$$

It is necessary to assume a value for ω_3, which is a serious limitation of this method.

4.5.5. Directional Correlation Effects in Coincidence Measurements

The existence of directional correlations[7] in some cascade transitions of characteristic x rays is implied by the general theory of directional correlations of multipole radiations, as outlined by Frauenfelder and Steffen (1965). The directional correlation function $W(k_1, k_2)=W(\theta)$ is defined so that $W(\theta)\,d\Omega_1\,d\Omega_2$ is the probability that an atom decaying through the cascade

[7] We follow the convention that the term *directional correlation* pertains to the correlation of directions only, while *angular correlation* comprises polarization correlation as well, requiring that the linear or circular polarization of one or both radiations be measured.

TABLE IV.VIII. $M2$ and $E1$ admixtures in $K\alpha_1$ x rays and in prominent L_3X transitions. The quantity δ^2 is defined as the $M2/E1$ transition-probability ratio. After Scofield (private communication, 1971).

Z	$\delta^2(K\alpha_1)$	$\delta^2(Ll)$	$\delta^2(L\alpha_1)$	$\delta^2(L\beta_6)$	$\delta^2(L\beta_2)$
50	4.52×10^{-4}	6.78×10^{-6}	1.09×10^{-5}	1.04×10^{-5}	1.40×10^{-5}
60	9.84×10^{-4}	1.58×10^{-5}	2.51×10^{-5}	2.54×10^{-5}	3.39×10^{-5}
70	1.93×10^{-3}	3.37×10^{-5}	5.04×10^{-5}	5.27×10^{-5}	6.98×10^{-5}
80	3.49×10^{-3}	5.64×10^{-5}	9.11×10^{-5}	9.78×10^{-5}	1.29×10^{-4}
90	6.02×10^{-3}	9.20×10^{-5}	1.53×10^{-4}	1.67×10^{-4}	2.19×10^{-4}
100	1.00×10^{-2}	1.39×10^{-4}	2.43×10^{-4}	2.66×10^{-4}	3.51×10^{-4}

$I_i \rightarrow I \rightarrow I_f$ emits the two x rays R_1 and R_2 in the directions k_1 and k_2 into the solid angles $d\Omega_1$ and $d\Omega_2$; θ is the angle between k_1 and k_2 and I_i, I, and I_f are the angular momenta of the initial, intermediate, and final states, respectively. We have

$$W(\theta) = \sum_{k \text{ even}} A_{kk} P_k(\cos\theta), \qquad (4\text{–}31)$$

where the $P_k(\cos\theta)$ are Legendre polynomials of order k, and the coefficients A_{kk} are functions of the angular momenta I_i, I, and I_f and of the multipolarities of the emitted radiations. Each coefficient A_{kk} consists of a factor $A_k(1)$ that depends only on the first transition of the cascade, and a factor $A_k(2)$ that depends only on the second transition. Allowing for transitions of mixed character, we can express these factors as

$$A_k(1) = [F_k(L_1 L_1 I_i I) + 2\delta_1 F_k(L_1 L_1' I_i I) + \delta_1^2 F_k(L_1' L_1' I_i I)]/(1+\delta_1^2)$$
$$A_k(2) = [F_k(L_2 L_2 I_f I) + 2\delta_2 F_k(L_2 L_2' I_f I) + \delta_2^2 F_k(L_2' L_2' I_f I)]/(1+\delta_2^2). \qquad (4\text{–}32)$$

Here, L_1, L_1' and L_2, L_2' are the multipolarities of the x rays emitted in the first and second transitions, respectively. The mixing ratios δ_i are defined so that δ_i^2 is the ratio of total L_i'-pole to L_i-pole intensity. Mixing ratios, including other definitions of δ found in the literature, are discussed by Rose and Brink (1967). Tabulations of the coefficients F_k have been published by several authors (Ferentz and Rosenzweig, 1955; Wapstra, Nijgh, and van Lieshout, 1959; Frauenfelder and Steffen, 1965). The A_k vanish if $I=\frac{1}{2}$. For pure multipole transitions, the mixing ratio is zero and A_{kk} is the product of the two functions $F_k(L_1 L_1 I_i I)$ and $F_k(L_2 L_2 I_f I)$.

Directional correlations in x-ray cascades were first discussed by Moellering and Jensen (1956), who treated the special case of L_l-$K\alpha_1$ and L_η-$K\alpha_2$ cascades. These authors derived the dependence of the (L_l+L_η)–$K\alpha$ directional correlation on the natural width Γ of the intermediate level as compared with the magnitude Δ of the $2p$-level splitting due to spin-orbit interaction, viz.,

$$W(\theta) = \{[(11/3)\Delta^2 + 3\Gamma^2]/(\Delta^2+\Gamma^2)\} + [(\Delta^2+3\Gamma^2)/(\Delta^2+\Gamma^2)]\cos^2\theta, \qquad (4\text{–}33)$$

where the statistical average over $K\alpha_1$ and $K\alpha_2$ has been taken. In the limit $\Delta \ll \Gamma$, the result is as though the $2p$ level were not split,

$$W(\theta) = 1 + \cos^2\theta, \qquad (4\text{–}34)$$

and in the limit $\Gamma \ll \Delta$, ordinarily approached in x-ray transitions, the correlation is given by

$$W(\theta) = 1 + (3/11)\cos^2\theta. \qquad (4\text{–}35)$$

Theoretical x-ray directional correlations have also been discussed by Babushkin (1965b). Among cascades that include K x rays, only those that include $K\alpha_1$ x rays result in anisotropic directional correlations; for $K\alpha_2$ emission the spin $I=\frac{1}{2}$ of the $2p_{1/2}$ intermediate state produces $W(\theta)=1$.

The possible admixtures of other multipolarities must, however, be considered in interpreting measured correlation coefficients. The theoretical work by Scofield (1969) and Rosner and Bhalla (1970) on radiative transition probabilities including higher multipole contributions permits the estimation of the mixing ratios. Table IV.VIII lists Scofield's mixing ratios for $E1$ and $M2$ admixtures, defined as the ratio of $M2$ multipole transition rate to $E1$ transition rate, for prominent transitions involved in (K x-ray)–(L x-ray) cascades. Theoretical estimates of the corresponding directional coefficients A_{22} are presented in Table IV.IX (Scofield, private communication).

Recent experiments have confirmed the existence of anisotropic directional correlations between K and L x rays. The quantity usually quoted in experimental work is the asymmetry coefficient D:

$$D = [C(180°)/C(90°)] - 1. \qquad (4\text{–}36)$$

Here, $C(\theta)$ is the coincidence counting rate with the detectors at an angle θ to each other. Beste (1968) has found an average anisotropy of $(8\pm6)\%$ between

TABLE IV.IX. Directional correlation coefficients A_{22} for $K\alpha_1$–L x-ray cascades corresponding to the $M2/E1$ mixing ratios listed in Table IV.VIII.

Z	$K\alpha_1$–Ll ($K\rightarrow L_3\rightarrow M_1$)	$K\alpha_1$–$L\alpha_{1,2}$ ($K\rightarrow L_3\rightarrow M_{4,5}$
50	0.266	0.0284
60	0.273	0.0302
70	0.281	0.0325
80	0.291	0.0354
90	0.303	0.0390
100	0.317	0.0433

K and L x rays in lanthanum. Konstantinov and Sazonova (1968) have measured the directional correlation of K and L x rays in terbium and found $D=0.16$. Price, Mark, and Swift (1968) measured D for five elements: Ta, Pt, Au, Ac, and Pa. The measurements referred to so far were based on the use of proportional counters and NaI(Tl) crystals for the detection of L x rays, without sufficient energy resolution to distinguish between different L x-ray components.

Wood, Palms, and Venugopala Rao (1969) have employed high-resolution detectors for both K and L x rays to measure the directional correlation in the case of Tl. Catz and Coryell (1969), Catz (1970) and Catz and Macias (1971a) have utilized high resolution for the detection of L x rays, while NaI(Tl) detectors were employed for K x rays (except at low Z), to study (K x-ray)–(L x-ray) cascades in Ta, Tl, and Pb. Because these authors could not resolve $K\alpha_2$ from $K\alpha_1$ x rays, they corrected the data for the effect of L_2–L_3X Coster–Kronig transitions. The effect of finite solid angles subtended by the detectors was taken into account in all these measurements.

The work of Catz *et al.* (1969, 1970) has demonstrated the necessity to consider admixtures of magnetic quadrupole radiation to the predominantly electric dipole x-ray transitions. It is found that $M2$ contributions to L x-ray transitions are slightly higher than predicted by Scofield's calculations. Such disagreement might lead one to question the accuracy of theoretically predicted relative intensities of some L x-ray transitions, or to consider the possibility that the angular correlation is perturbed. Additional high-resolution work is needed.

In Table IV.X, currently available experimental results on K and L x-ray directional correlations are summarized.

In most experimental arrangements used to measure L_3-subshell fluorescence yields by the $K\alpha_1$–L x-ray coincidence method, the detectors are oriented at 180° to each other. Because of directional correlation effects, coincidence rates measured at 180° must be multiplied by the factor $(1+A_{22}f_\Omega)^{-1}$, where f_Ω is the finite-solid-angle correction:

$$f_\Omega=(1/2)\cos\theta_m(1+\cos\theta_m). \qquad (4\text{–}37)$$

Here, θ_m is the half-angle subtended by the detector. The correction can be substantial. For a fractional solid angle of 0.05, the value of f_Ω is approximately 0.85.

Directional correlations between γ rays and L x rays have not yet been investigated sufficiently. Halley and Engelkemeir (1964) studied this effect in the case of γ rays emitted in $4^+\rightarrow 2^+$ transitions and L x rays from internal conversion of the ensuing $2^+\rightarrow 0^+$ transitions (e.g., 99-keV γ rays and L x rays in the decay of ^{238}Pu), and found that L x-ray emission is isotropic with respect to the direction of γ-ray emission to within $\pm 2\%$.

Benoist (1954) has pointed out that an anisotropic directional correlation may exist between α particles and L x rays emitted in transitions to the L_3 subshell; the maximum possible anisotropy is $\sim 7\%$. Falk-Vairant *et al.* (1954) have studied the directional correlation of α particles and L x rays in the decay of ^{230}Th and found L x-ray emission to be isotropic with respect to the direction of α emission, within experimental errors ($\pm 4\%$).

4.5.6. *Singles Spectrum Methods*

Several methods by which L x-ray emission rates from a radioactive source can be measured by studying singles spectra only have been used successfully to determine average L-shell fluorescence yields $\bar{\omega}_L$. If it is possible to study the L x-ray spectra at high resolution, individual subshell yields can be determined using Eqs. (4–10). In each of these methods, which are described below, the primary L-subshell vacancy distribution is determined by measuring another accompanying radiation (e.g., conversion electrons, α particles, K x rays, γ rays).

In K and L orbital electron-capture decay of a nucleus, the ratio of L x-ray to K x-ray emission rates is related to the electron-capture probability ratio

TABLE IV.X. Measured directional correlation coefficients A_{22}.

Element	Cascade	A_{22} (multiples of 10^{-2})	Reference
$_{60}$Nd	$K\alpha_1$–Ll	15±4	Catz (1971b)
	$K\alpha_1$–$L\alpha$	2.7±0.3	
	$K\alpha_1$–$L\beta$	0.1±0.5	
$_{65}$Tb	$K\alpha$–Ll	14±5	Catz (1971b)
	$K\alpha$–$L\alpha$	2.6±0.5	
	$K\alpha$–$L\beta$	−0.1±0.5	
$_{73}$Ta	$K\alpha$–$L\alpha$	2.48±0.41	Catz (1971a)
	$K\alpha$–$L\beta$	−0.12±0.46	
$_{81}$Tl	$K\alpha$–Ll	26±5	Wood (1969)
	$K\alpha$–$L\alpha$	5.0±3.0	
$_{81}$Tl	$K\alpha$–Ll	21.8±2.0	Catz (1971a)
	$K\alpha$–$L\alpha$	3.63±0.32	
	$K\alpha$–$L\beta$	1.31±0.36	
$_{82}$Pb	$K\alpha$–Ll	23.32±2.06	Catz (1970)
	$K\alpha$–$L\alpha$	4.13±0.36	
	$K\alpha$–$L\beta$	1.22±0.43	

P_L/P_K as follows:

$$I_L/I_K=[(P_L/P_K)+n_{KL}](\bar{\omega}_L/\omega_K). \quad (4\text{–}38)$$

This relation can be used, in principle, to find $\bar{\omega}_L$ in cases in which only ground-state transitions are present, as in ^{131}Cs and ^{204}Tl (Fink and Robinson, 1966; Schmied and Fink, 1957; Hohmuth and Winter, 1964; Venugopala Rao and Crasemann, 1965a).

Internal conversion of nuclear γ rays in K and L shells similarly provides an indication of vacancy numbers; an example is the 279-keV transition in ^{203}Tl. The ratio of L to K x-ray intensities is related to the ratio of L- and K-shell conversion coefficients α_L and α_K as follows:

$$I_L/I_K=[(\alpha_L/\alpha_K)+n_{KL}](\bar{\omega}_L/\omega_K). \quad (4\text{–}39)$$

A knowledge of experimental or theoretical conversion-electron intensities is necessary (Winkenbach, 1958; Ramaswamy, 1962; Zimmerli and Flammersfeld, 1963; Wilken, 1968; Kloppenburg, 1969).

Halley and Engelkemeir (1964) have measured the total number of L x rays and of α particles emitted by ^{232}U. The α-particle number served to monitor the total number of L vacancies produced during internal conversion of the 57.9-keV transition in ^{228}Th fed by α decay of ^{232}U. An average L-shell fluorescence yield $\bar{\omega}_L$ was derived from the relation

$$I_L/I_\alpha=[\alpha_L/(1+\alpha_t)]f\bar{\omega}_L, \quad (4\text{–}40)$$

where f is the fraction of α particles populating the 57.9-keV state, and α_t is the total internal-conversion coefficient of the transition. Fink (1957) has measured the emission rates of L x rays and α particles from ^{210}Pb (RaD) to calculate the Bi L-shell yield.

All the above methods involve the use of detectors which do not resolve L x rays characteristic of single subshells; thus only $\bar{\omega}_L$ can be measured. Only in special circumstances can an individual L subshell yield be obtained by assuming information on other subshells (Winkenbach, 1958; Zimmerli and Flammersfeld, 1963; Wilken, 1968). Venugopala Rao, Palms, and Wood (1971) have studied the Pb L x-ray spectrum from the decay of ^{207}Bi with Si(Li) detectors with a resolution of 155 eV at 5.9 keV. They analyzed the $L\gamma$ x-ray peak and determined the number of $L\gamma$ x rays characteristic of the L_1 and L_2 subshells. Using Eq. (4–14), they found the L_1-subshell fluorescence yield ω_1. Such high-resolution L x-ray spectra could be analyzed to find individual subshell yields at higher Z (e.g., in the trans-uranium region), provided the primary vacancy distribution is known. Thus, Chu *et al.* (1972) have studied the Cm L x-ray spectrum from the decay of ^{249}Cf and deduced individual L subshell yields. At low Z, where sufficient resolution cannot yet be attained, measurement of $\bar{\omega}_L$ only is possible, provided very thin and uniform sources (i.e., vacuum-evaporated or mass-separated carrier-free, solids-free sources) are used (Nix, 1972).

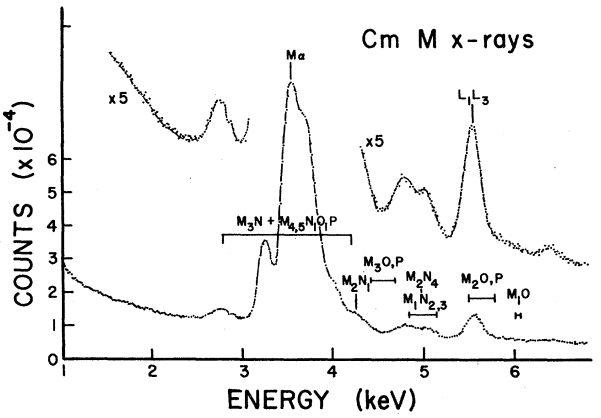

FIG. 4–24. Curium M x-ray spectrum, measured with a Si(Li) detector of resolution 180-eV FWHM at 6.4 keV. [From Karttunen, Freund, and Fink (1971), courtesy of North-Holland Publishing Co.]

Singles-spectrum studies have also been utilized with L vacancies produced by photon bombardment; known photoionization cross sections (Sec. 4.1) were employed to estimate the primary L-vacancy numbers (Konstantinov, Sazonova, and Perepelkin, 1960; Konstantinov, Sokolova, and Sazonova, 1961; Konstantinov, Perepelkin, and Sazonova, 1964; Konstantinov and Sazonova, 1965; Bailey and Swedlund, 1967). The accuracy of the results depends crucially upon the accuracy of the partial cross sections used by the cited investigators.

Pahor and Hribar (private communication) have excited the L_3 subshell of xenon with K x rays of vanadium and studied the proportional-counter spectrum which contains a full-energy peak due to Auger events and an escape peak due to the escape of L_3 characteristic x rays from the counter. With known transition probabilities and "L_3-jump" of the photoelectric cross section, the L_3-subshell fluorescence yield of xenon could be determined from the intensity ratio of the full-energy and escape peaks.

The advantages of Si(Li) detectors were utilized in a recent experiment by Karttunen, Freund, and Fink (1971), in which the radiative L_1–L_3 Coster–Kronig transition was detected with ^{241}Am and ^{249}Cf sources. The transition energies are 4.82 and 5.53 keV, respectively, and the corresponding x rays fall into the region of M x rays. The singles M x-ray spectrum from ^{249}Cf decay is shown in Fig. 4–24. The identification of the L_1–L_3 x ray was confirmed by looking at the coincident spectrum gated by $L\alpha$ x rays. The radiative component $f_{13}(R)$ of the Coster–Kronig yield f_{13} was found by measuring the intensity of L_1–L_3 x rays relative to the intensity of L_1-subshell characteristic x rays:

$$I(L_1L_3)/I(L_1X)=f_{13}(R)/\omega_1. \quad (4\text{–}41)$$

In a case in which no L_1-subshell characteristic x rays can be sufficiently resolved, L_3 subshell characteristic

x rays (e.g., $L\alpha$) could be used for comparison, using the relation

$$I(L_1L_3)/(I(L\alpha)=N_1f_{13}(R)/V_3\omega_3. \quad (4\text{–}42)$$

The L_1–L_3 radiative transition has been observed previously in the low-Z region ($Z=11$, 12, 13, and 16) by optical spectroscopy (Tomboulian, 1948).

4.5.7. Diffraction Spectrometry

There is a definite need for high-resolution studies of L x-ray intensities. It is clear from Eqs. (4–10)–(4–20) that an accurate knowledge of the radiative decay branching ratios s_1, s_2, and s_3 is required to gain information on L-shell yields. Furthermore, the experimental study of relative intensities of L x-ray transitions to individual L subshells is useful in testing theoretical estimates of the radiative decay rate of L-shell vacancies (Sec. 2.4).

Bent-crystal spectrometers are best suited for studying the individual transitions. However, much of the recent work on L emission lines has not been focused on intensity measurements, but rather on the measurement of wavelengths and identification of new transitions (Nigam, Garg, and Kapoor, 1968; Deodhar and Varma, 1969; Gokhale and Shukla, 1970).

Barton, Robinson, and Perlman (1951) were the first to use a bent quartz crystal spectrometer to measure L x-ray intensities; with a proportional counter as detector, they measured x rays produced in the decay of ^{241}Am and ^{242}Cm. This transmission-type spectrometer, designed by Barton (1950) and later modified by Browne (1952) by replacing quartz with topaz and the proportional counter with a scintillation counter, was utilized by Jaffe *et al.* (1955) and Day (1957) to measure precise relative intensities of Np L x rays. The instrument is of the Cauchois approximate-focussing type (Cauchois, 1932) and has a resolution of ~40 eV FWHM at 17 keV. Corrections are required for source self-absorption because of the necessity to use intense radioactive sources, and for the reflectivity of the crystal. Using a bent-crystal spectrometer and photographic recordings, Frilley, Gokhale, and Valadares (1951), and Ewan (1952) measured the relative intensities of the L x rays of Bi following the disintegration of RaD. Bent-crystal spectrometers have also been employed to obtain relative intensities of L-series lines from transuranium elements, in order to supplement data for L_2-subshell yields (Salgueiro *et al.*, 1961; Byrne *et al.*, 1968). Photographic film was used to detect the x rays.

Peed *et al.* (1957) have employed a Bragg spectrograph to measure the L x-ray spectrum of polonium. Goldberg (1962) has measured the relative intensities of L x-ray lines from 13 heavy elements ($73\leq Z\leq 92$) with a transmission-type bent mica crystal spectrometer equipped with a NaI(Tl) detector; L vacancies were produced by electron bombardment. Goldberg's work also contains a survey of previous high-resolution measurements of L x-ray intensities. Most recently, L x-ray intensity measurements by diffraction spectroscopy were carried out by Salem, Tsutsui, and Rabbani (1971) for 27 elements in the range $57\leq Z\leq 92$.

The use of solid-state detectors in combination with bent-crystal spectrometers promises to yield valuable information for the calculation of L-subshell yields, in spite of the low efficiency encountered in these measurements. Transmission spectrometers in general suffer severe sensitivity losses below 25 keV, because of x-ray absorption by the crystal. This disadvantage is overcome in the recent work of Wehring and Wyman (1968), who designed and constructed a bent-crystal spectrometer of the Johansson type for the measurement of fission-fragment K x rays; such a device would be very useful for measuring L x-ray intensities at high Z.

The measurement of x-ray line widths constitutes an important application of diffraction spectrometry. The natural widths of the $K\alpha_1$ and $K\alpha_2$ x-ray lines yield important information on the L_2 and L_3 subshells (Sec. 2.5). The natural width of an x ray is the sum of the widths of the two atomic levels between which the transition takes place; hence, the fluorescence yields of the L_2 and L_3 subshells can be expressed as follows:

$$\omega_2=\Gamma_R(L_2)/[\Gamma(K\alpha_2)-\Gamma(K)], \quad (4\text{–}43)$$

$$\omega_3=\Gamma_R(L_3)/[\Gamma(K\alpha_1)-\Gamma(K)]. \quad (4\text{–}44)$$

With the aid of theoretical estimates of the radiative widths $\Gamma_R(L_2)$ and $\Gamma_R(L_3)$ and the total width $\Gamma(K)$, the experimentally measured natural widths of the $K\alpha_2$ and $K\alpha_1$ lines can be used to calculate ω_2 and ω_3.

Gokhale (1952) has used a transmission-type spectrometer with photographic recording to measure $\Gamma(K\alpha_2)$ and $\Gamma(K\alpha_1)$ for elements from ^{37}Rb through ^{50}Sn. His work also contains references to earlier work. More recently, Nelson, John, and Saunders (1969, 1970) have measured these widths for $Z>50$.

Shacklett and DuMond (1957) and Merril and DuMond (1960, 1961) measured L x-ray linewidths. The latter authors compared the widths of $L\beta_1$ (L_2–M_4) x rays and $L\alpha_2$ (L_3–M_5) x rays for $74<Z<95$, and found that the $L\alpha_2$ widths lie on a straight line, within experimental accuracy, while the $L\beta_1$ widths are best represented by a line with a kink at $Z=90$, the slope for $Z>90$ being considerably greater than for $74<Z<90$. This behavior is explained by the additional decay modes for L_2 vacancies, in the form of Coster–Kronig transitions of the type L_2–L_3M_5, that become energetically possible for $Z>90$. The width of some L levels has also been measured by Parratt (1959) and is discussed by Blokhin (1957) and Sevier (1972).

The study of L x-ray satellites is a further important application of diffraction spectrometry; it can lead to the measurement of Coster–Kronig yields. In fact,

Coster–Kronig transitions were originally discovered in tracing the origin of $L\alpha$ and $L\beta_2$ satellites (Coster and Kronig, 1935). Quantitative estimates of the Coster–Kronig yield f_{13} at high Z have been made by Ferreira (1955), Ferreira *et al.* (1965), and Salgueiro, Campos, and Ferreira (1965), with the aid of a bent mica crystal spectrometer and photographic recording. The $L\alpha$ x-ray satellites arise from the following sequence of events:

(a) The atom is initially ionized in the L_1 subshell.

(b) By a Coster–Kronig transition of the L_1–$L_3M_{4,5}$ type, the atom goes into a doubly ionized state, with one vacancy in the L_3 subshell and another in the $M_{4,5}$ subshells.

(c) The vacancy in the L_3 subshell is then filled through a radiative transition predominantly from the $M_{4,5}$ subshells. The emitted x ray has a slightly higher energy than the ordinary $L\alpha$ x ray (which is emitted in a singly ionized state) because of decreased screening; it appears as a satellite to the main line.

Coster–Kronig transitions of the type L_2–L_3M, if energetically possible, can also lead to such satellites.

If the sample under investigation has a primary vacancy distribution given by N_i, the ratio of intensities of the satellite, $I(L\alpha)_s$, to that of the main line or diagram line, $I(L\alpha)$, is

$$\frac{I(L\alpha)_s}{I(L\alpha)}=\frac{[N_1(f_{13}+f_{12}f_{23})+N_2f_{23}]\omega_3'(1+s_3)s_3'}{[N_3+N_1(f_{13}+f_{12}f_{23})+N_2f_{23}]\omega_3(1+s_3')s_3}. \tag{4-45}$$

Here, s_3' is the branching ratio defined as in Sec. 4.5, but for the doubly ionized state, and ω_3' is the L_3 fluorescence yield for the doubly ionized state. With plausible assumptions on f_{23}, ω_3', and s_3', one can find f_{13} (Ferreira, 1965). Furthermore, L_3-subshell yields can be studied in the presence of a "spectator" vacancy.

4.5.8. Methods Involving X-Ray and Auger-Electron Spectroscopy

In certain cases in which only one primary vacancy distribution (N_i) in the L subshells is experimentally accessible, information on the quantities ω_i and f_{ij} can be gained by supplementing the x-ray intensities with Auger-electron intensities. The quantities to be measured are the total number $I_i(R)$ of all x rays characteristic of the L_i subshell, and the total number $I_i(A)$ of all Auger-electrons characteristic of the subshell. In terms of intensities of individual transitions, we have

$$I_i(R)=\sum_j I(L_iX_j), \qquad I_i(A)=\sum_{j,k} I(L_i{-}X_jY_k). \tag{4-46}$$

The measured intensities are normalized in one of the following ways:

(a) Normalization is made to the γ-ray intensity or L_i conversion-electron intensities, respectively, if the vacancies arise from conversion (Ross *et al.*, 1955).

(b) The K x-ray and K–LL Auger-electron groups, respectively, are used for normalization when the vacancies arise from electron-capture decay. Accurate knowledge of ω_K is required.

(c) The Auger-electron and L x-ray absolute intensities are measured or calculated if the primary vacancies are generated by charged-particle bombardment (Päschke, 1963).

Knowledge of the total number of primary L vacancies, n_L, relative to the normalizing events is necessary in addition to knowledge of the distribution N_i of primary vacancies. The following equations relate the measured intensities and L-subshell yields:

$$\omega_1=I_1(R)/n_LN_1, \qquad a_1=I_1(A)/n_LN_1; \tag{4-47}$$

$$\omega_3=\frac{I_3(R)/I_3(A)}{1+[I_3(R)/I_3(A)]}, \qquad a_3=\{1+[I_3(R)/I_3(A)]\}^{-1}. \tag{4-48}$$

The remaining L-shell yields can be evaluated from the following equations if f_{12} or f_{13} is known (at high Z, where these techniques are useful, f_{12} is small):

$$\omega_2=I_2(R)/[n_L(N_2+f_{12}N_1)],$$
$$a_2=I_2(A)/[n_L(N_2+f_{12}N_1)]; \tag{4-49}$$

$$f_{12}+f_{13}=1-\{[I_1(R)+I_1(A)]/n_LN_1\}; \tag{4-50}$$

$$f_{23}=1-\{[I_2(R)+I_2(A)]/n_L(N_2+f_{12}N_1)\}. \tag{4-51}$$

High-resolution techniques are obviously necessary to measure the intensities of x rays or Auger electrons characteristic of each L_i subshell.

Ross *et al.* (1955) originally employed this method with a radioactive source of ^{210}Pb [RaD] of 4 mg/cm^2 thickness; they used a curved-crystal spectrometer for L x-ray analysis and the published L Auger-electron intensities from the work of Bashilov and Chervinskaya (1964).

Päschke (1963) used 55-keV electrons to excite an 8-μg/cm^2 gold film, simultaneously detecting L Auger electrons in a 180° magnetic spectrometer (resolution 0.5%) and L x rays with a NaI(Tl) detector. This approach requires a knowledge of ω_K and of theoretical L-subshell electron excitation cross sections and is therefore limited by the accuracy of these quantities. Considerable progress has been achieved both in low-energy Auger-electron spectrometry (in resolution and source techniques) and x-ray spectrometry (through use of semiconductor photon spectrometers).

High-resolution electron spectrometry with radioactive sources has been possible with energy resolutions of 0.18% at 11 keV; for example in ^{210}Pb [RaD] decay

(Haynes, Velinsky, and Velinsky, 1967). An iron-free magnetic $\pi\sqrt{2}$ spectrometer and very thin sources were used to meet the requirements for quantitative electron counting, namely, negligible tailing and line-broadening due to self-absorption. This permits the assignment of the most important individual Auger transition intensities; the three sums $\sum I(L_i-X_jY_k)$ can be derived. High-resolution studies of L Auger-electron transitions have also been performed by Zender, Pou, and Albridge (1969) on uranium, by Toburen and Albridge (1967) on platinum, and by Gizon, Gizon, and Valentin (1968) on lutetium; intensities were obtained for a number of resolved single lines and unresolved line groups. Assignment of the large number of possible transitions to given intensity groups is difficult, and ambiguities exist even in spectra measured with the best resolution. Reliable calculations of L Auger-electron intensities, which would help in estimating unresolved lines, are only beginning to become available for high-Z elements. Therefore, the intensities $I_i(A)$, although they are gross figures, may contain large errors.

High-resolution L x-ray spectra are best measured with curved-crystal spectrometers, which have the highest resolution and hence facilitate transition identification (Sec. 4.5.7). An alternative procedure is to measure the L x-ray spectrum with Si(Li) or Ge(Li) semiconductor detectors. [For characteristics of semiconductor radiation detectors, see, e.g., Mayer (1966) or Goulding and Stone (1970).] Although their energy resolution is inferior to that of curved-crystal spectrometers, the spectrum reveals a detailed structure for atomic numbers above $Z\approx 70$ (c.f., e.g., Figs. 4–8–4–11.) Thus, if source absorption is negligible and detector efficiencies are well known, intensity sums can be obtained more reliably through spectrum-resolving techniques combined with information on transition energies (Bearden, 1967a). Care must be taken in deriving the exact energies: L_3 transitions are close doublets of diagram lines and nondiagram transitions that occur in atoms with more than one vacancy; L_3M_i transitions in the presence of an $M_{3,4,5}$ vacancy must be considered. The associated energy shifts are 50 to 100 eV for $Z\geq 80$.

A typical example of x-ray spectrometry with solid-state detectors is found in the work of Freund and Fink (1969) on ^{210}Pb [RaD] decay; 10 subgroups or lines were resolved in the Bi L x-ray spectrum by means of graphical curve-resolving methods. Additional information is needed to identify components in unresolved doublets or multiplets that do not feed the same subshell (e.g., in the $L\beta$ x-ray group). Since at least one transition ($L_i\rightarrow X_j$) for each of the three subshells can be cleanly resolved, ratios of the type $I(L_iX_k)/I(L_iX_j)$ are of interest for unfolding multiplets. These ratios can be obtained from (a) diffraction spectrometry data, (b) coincidence experiments (see definition of s_i in Sec. 4.5), or (c) from theory (Sec. 2.4).

4.6. Experimental L-Shell Yields

In the preceding sections, methods for the measurement of L-shell yields have been discussed. A summary of requirements for the experimental determination of pertinent L-shell quantities is contained in Table IV.XI.

Experimental L-shell yields published up to May 1968 have been summarized in two previous review articles (Fink *et al.*, 1966; Venugopala Rao, 1968). Up-to-date tabulations are presented in the present section; special attention has been paid to identifying measured values with appropriate quantities as defined in Sec. 1.4.

Experimental L-subshell fluorescence yields ω_i are listed in Table IV.XII. Some results based on arbitrary assumptions regarding other L-shell yields have been excluded.

In Table IV.XIII, measured Coster–Kronig yields f_{ij} are listed. Average fluorescence yields ν_1, ν_2, and ω_L are collected in Table IV.XIV, which includes measured yields ω_{KL}. These are the average fluorescence yields for the particular distribution of primary vacancies that results from $K\alpha$ x-ray emission.

4.7. Comparison With Theory

Only two sets of theoretical L-shell yields have been published to date; these are due to McGuire (1970c, 1971a, b), and Chen, Crasemann, and Kostroun (1971), and Crasemann, Chen, and Kostroun (1971). The approaches taken in these computations have been discussed in Chap. 2 (see especially Sec. 2.3.3).

Calculated subshell fluorescence yields ω_1 are compared in Fig. 4–25 with the scant available experimental information. Agreement between the calculations of McGuire (1971a) and of Crasemann *et al.* (1971) is good, especially in view of the fact that very different wave functions were used in the two approaches. Much more experimental information will have to be available before a meaningful comparison of theory and experiment becomes possible.

TABLE IV.XI. Requirements for the experimental determination of L-shell yields.

Quantity	Prerequisites
$\bar{\omega}_L$	Knowledge of total number of L x rays or L Auger electrons, and of the total number of primary L vacancies
ω_{KL}	Selection of vacancies from $K\alpha$ x-ray emission
ν_i	Selection of vacancies from a single L subshell
ω_i	Resolution and identification (usually by coincidence techniques) of characteristic L-subshell x rays or Auger electrons, and selection of vacancies from a single L subshell
ω_i, ν_i, f_{ij}	Knowledge of primary vacancy distribution; at least partial resolution of L x rays or Auger electrons characteristic of individual L subshells

TABLE IV.XII. Experimental L-subshell fluorescence yields ω_i.

Z	Element	ω_1	ω_2	ω_3	Method	Reference
54	Xe			0.10±0.01	L x-ray escape in ppc.	Pahor (1971)
56	Ba	0.06		0.05±0.01	L Auger spectrum	Burford (1958)
65	Tb	0.18	0.165±0.018[a]	0.188±0.016	K–L x-ray coinc. and singles x-ray spectrum	McGeorge (1970, 1971a)
67	Ho			0.22±0.03	K–L x-ray coinc.	Jopson (1964a)
			0.170±0.055	0.169±0.030	K–L x-ray coinc.	Holmes (1970)
68	Er			0.21±0.03	K–L x-ray coinc.	Jopson (1964a)
			0.185±0.060	0.172±0.032	K–L x-ray coinc.	Holmes (1970)
70	Yb			0.20±0.02	K–L x-ray coinc.	Jopson (1964a)
			0.188±0.011[a]	0.183±0.011	K–L x-ray coinc.	Mohan (1970b)
71	Lu			0.22±0.03	K–L x-ray coinc.	Jopson (1964a)
				0.251±0.035	K–L x-ray coinc.	Price (1968)
72	Hf			0.22±0.03	K–L x-ray coinc.	Jopson (1964a)
				0.228±0.025	K–L x-ray coinc.	Price (1968)
73	Ta		0.25±0.02	0.27±0.01	K–L x-ray coinc.	Rao (1965b)
				0.25±0.03	K–L x-ray coinc.	Jopson (1964a)
				0.191	Fluorescent excitation of L_3 subshell	Küstner (1935)
			0.257±0.013[a]	0.228±0.013	K–L x-ray coinc.	Mohan (1970a)
				0.254±0.025	K–L x-ray coinc.	Price (1968)
74	W			0.207	Fluorescent excitation of L_3 subshell	Küstner (1935)
				0.272±0.037	K–L x-ray coinc.	Price (1968)
75	Re			0.284±0.043	K–L x-ray coinc.	Price (1968)
76	Os			0.290±0.030	K–L x-ray coinc.	Price (1968)
77	Ir			0.244	Fluorescent excitation of L_3 subshell	Küstner (1935)
77	Ir			0.262±0.036	K–L x-ray coinc.	Price (1968)
78	Pt			0.262	Fluorescent excitation of L_3 subshell	Küstner (1935)
				0.31±0.04	K–L x-ray coinc.	Jopson (1964a)
				0.317±0.029	K–L x-ray coinc.	Price (1968)
			0.331±0.021	0.291±0.018	K–L x-ray coinc.	Mohan (1971)
79	Au			0.276	Fluorescent excitation of L_3 subshell	Küstner (1935)
				0.31±0.04	K–L x-ray coinc.	Jopson (1964a)
				0.317±0.025	K–L x-ray coinc.	Price (1968)
80	Hg		0.39±0.03	0.40±0.02	K–L x-ray coinc.	Rao (1965b)
				0.32±0.05	K–L x-ray coinc.	Jopson (1964a)
				0.367±0.050	K–L x-ray coinc.	Price (1968)
			0.319±0.010[a]	0.300±0.010	K–L x-ray coinc.	Palms (1970)
81	Tl			0.37±0.07	K–L x-ray coinc.	Jopson (1964a)
				0.386±0.053	K–L x-ray coinc.	Price (1968)
			0.319±0.010	0.306±0.010	K–L x-ray coinc.	Wood (1969)
		0.07±0.02			(L-electron) (L x-ray) coinc.	Wood (1969)
			0.373±0.025	0.330±0.021	K–L x-ray coinc.	Mohan (1971)
82	Pb			0.337	Fluorescent excitation of L_3 subshell	Küstner (1935)
		0.07±0.02	0.363±0.015	0.315±0.013	K–L x-ray coinc., (γ-ray)–(L x-ray coinc., (L-electron)–(L x-ray) coinc.	Rao (1969)
		0.09±0.02			Singles L x-ray spectrum	Rao (1971)
82	Pb			0.32	Fluorescent excitation of L_3 subshell	Stephenson (1937)
				0.35±0.05	K–L x-ray coinc.	Jopson (1964a)
				0.354±0.028	K–L x-ray coinc.	Price (1968)
83	Bi			0.367	Fluorescent excitation of L_3 subshell	Küstner (1935)
				0.36	L Auger spectrum, fluorescent excitation of L_3 subshell	Risch (1958)

TABLE IV.XII (*Continued*)

Z	Element	ω_1	ω_2	ω_3	Method	Reference
				0.37±0.05	K–L x-ray coinc.	Jopson (1964a)
				0.362±0.029	K–L x-ray coinc.	Price (1968)
		0.12±0.01	0.32±0.04	0.40±0.05	L Auger and L x-ray singles spectra	Ross (1955)
		0.095±0.005	0.38±0.02	0.340±0.018	L Auger and L x-ray singles spectra	Freund (1969a), Fink (1971)
90	Th			0.42	Fluorescent excitation of L_3 subshell	Stephenson (1937)
				0.517±0.042	K–L x-ray coinc.	Price (1968)
91	Pa			0.46±0.05	L x-ray coinc.	Boyer (1968)
92	U			0.44	Fluorescent excitation of L_3 subshell	Stephenson (1937)
				0.500±0.040	K–L x-ray coinc.	Price (1968)
96	Cm		0.552±0.032	0.515±0.034	K–L x-ray coinc.	McGeorge (1971c)
		0.28±0.06	0.55±0.02	0.63±0.02	x-ray singles spectra	Chu (1972)

[a] Revised for admixture of $L\eta$ x rays in $L\alpha$ photopeak (McGeorge, 1971a).

In Fig. 4–26, calculated and measured fluorescence yields ω_2 are indicated. Theoretical results are seen to agree quite well, not only with measured values that are available for $Z \geq 65$, but with semiempirical yields for $37 \leq Z \leq 50$, derived from $K\alpha_2$ line widths measured by Gokhale (1952), semiempirical K-level widths after Leisi *et al.* (1961), and the theoretical L_2 radiative widths of Scofield (1969 and private communication). Also for ω_3 (Fig. 4–27), good agreement is found between calculations, especially those of Chen *et al.* (1971a), and measured values at high Z or values derived from measured widths at lower Z.

Theoretical L-subshell fluorescence yields ω_i are listed in Table IV.XV.

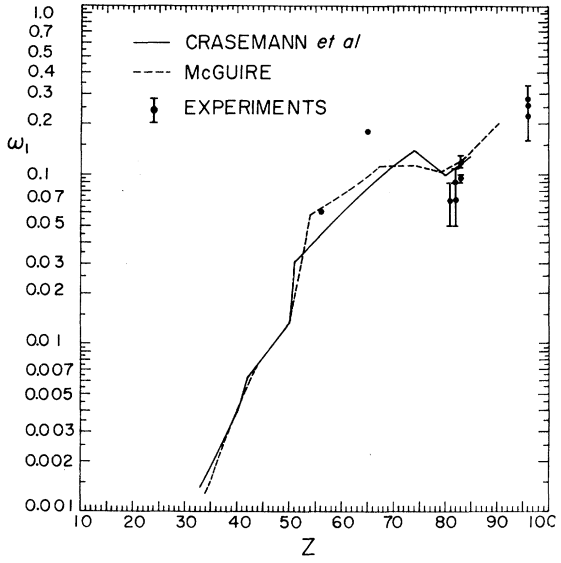

FIG. 4–25. L_1-subshell fluorescence yield ω_1 as a function of atomic number. The theoretical curves are due to Crasemann, Chen, and Kostroun (1971) and McGuire (1971a).

L-shell Coster–Kronig transition probabilities f_{ij} display abrupt discontinuities at atomic numbers where energy thresholds are located for certain intense groups of Coster–Kronig transitions, notably near $Z=41$, 50, and 75 for f_{12} and f_{13} (Figs. 4–28 and 4–29) and near $Z=30$ and 91 for f_{23} (Fig. 4–30). Discontinuities in L level widths are consequently produced (Fig. 2–13). The exact location of these discontinuities is somewhat uncertain, because electron binding

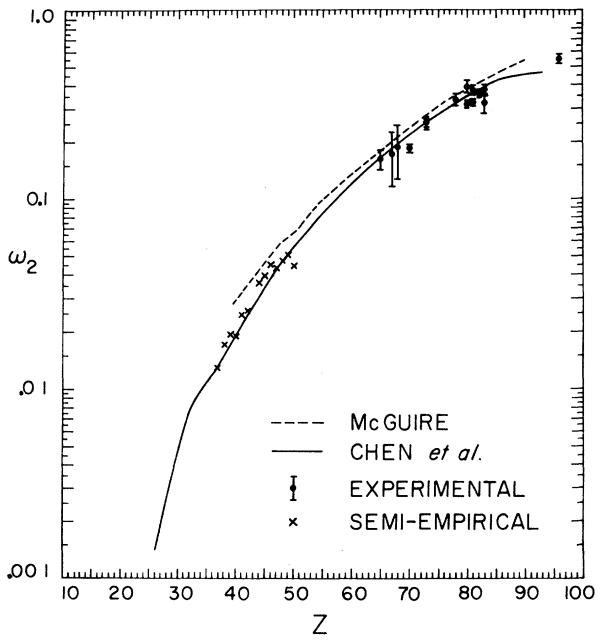

FIG. 4–26. L_2-subshell fluorescence yield ω_2 as a function of atomic number. The theoretical curves are due to Chen, Crasemann, and Kostroun (1971a) and McGuire (1971a). Dots indicate experimental data; crosses represent fluorescence yields derived from measured x-ray emission line widths and the theoretical x-ray emission rates of Scofield (1969).

TABLE IV.XIII. Measured L-shell Coster–Kronig yields.

Z	Element	f_{12}	f_{13}	f_{23}	Reference
56	Ba	0.66±0.07			Burford (1958)
65	Tb	0.41±0.36	0.43±0.28	0.066±0.014[a]	McGeorge (1970)
67	Ho			0.205±0.034	Holmes (1970)
68	Er			0.225±0.025	Holmes (1970)
70	Yb			0.142±0.009[a]	Mohan (1970b)
73	Ta			0.20±0.04	Rao (1965b)
			0.19		Ferreira (1965)
		<0.14	<0.36	0.148±0.010[a]	Mohan (1970a)
74	W		0.27±0.03		Ferreira (1965)
75	Re		0.30±0.04		Salgueiro (1965)
77	Ir		0.46±0.06		Ferreira (1965)
78	Pt		0.50±0.05		Ferreira (1965)
79	Au	0.25±0.13	0.51±0.13	(0.22)[b]	Päschke (1963)
			0.61±0.07		Ferreira (1965)
80	Hg	0.74±0.04		0.22±0.04	Nall (1960)[c]
				0.08±0.02	Rao (1965b)
				0.188±0.010	Palms (1970)
81	Tl		0.76±0.10		Ferreira (1965)
			0.57±0.10		Persson (1961)
		0.17±0.05	0.56±0.07	0.25±0.13	Sujkowski (1961)[d]
		0.14±0.03	0.56±0.05	0.169±0.010	Wood (1969)
				0.159±0.013	Mohan (1971)
82	Pb	0.15±0.04	0.57±0.03	0.164±0.016	Rao (1969)
				0.156±0.010	Rao (1971)
		0.17±0.05	0.61±0.08		Rao (1971)
				$+0.14$	
83	Bi	0.19±0.05	0.58±0.05	0.06	Ross (1955)
				-0.06	
		0.18±0.02	0.58±0.02	(0.164)[b]	Freund and Fink (1969); Fink (1971)
92	U			0.23±0.12[e]	McGeorge and Fink (1971b)
				$+0.05$	
93	Np	(0.10±0.04)[b]	0.55±0.09	0.02	Akalayev (1964)
				-0.02	
94	Pu			0.22±0.08[f]	Salgueiro (1961)
				0.24±0.08	McGeorge and Fink (1971b)
96	Cm			0.188±0.019	McGeorge and Fink (1971b)
		0.038±0.022	0.68±0.04		McGeorge and Fink (1971a)

[a] Revised by McGeorge (1971a).
[b] Quantities in parentheses are assumed in order to derive listed results.
[c] Assumed $\omega_3=0.393$, $\omega_1=0.10$, $f_{13}=0.50$.
[d] Assumed $f_{12}+f_{13}=0.73$, $\omega_3=0.32$.
[e] Assumed $\omega_2/\omega_3=1.07$ and re-evaluated the results of Byrne *et al.* (1968).
[f] Assumed $\omega_3=0.455$.

energies in atoms with an inner-shell vacancy cannot be calculated with accuracy; further work on Auger- and Coster–Kronig electron spectra can be expected to clarify this point. The approximate ranges of atomic numbers within which major Coster–Kronig transitions are energetically possible are listed in Table IV.XVI.

Theoretical f_{ij}'s are included in Table IV.XV. Of these, f_{12} and f_{13} actually pertain to the radiationless parts $f_{12}(A)$ and $f_{13}(A)$ of the L_1–L_2X and L_1–L_3X Coster–Kronig transition probabilities. However, the radiative components of these transition probabilities are very small; e.g., $f_{13}(R)=0.0003f_{13}(A)$ for Kr, and $f_{13}(R)=0.05f_{13}(A)$ for Hg; the radiative component $f_{23}(R)$ of f_{23} is even smaller, because the L_2–L_3 transition is forbidden by electric-dipole selection rules and must proceed by magnetic dipole (spin flip) (Chen *et al.*, 1971b). Only $\sim 10^{-5}$ of the total L_2-level width of elements with $70 \leq Z \leq 93$ is due to the $2p_{3/2}$–$2p_{1/2}$ radiative transition rate.

Of the calculated Coster–Kronig yields, only f_{13}

TABLE IV.XIV. Measured average L-shell yields.

Z	Element	ν_1	ν_2	ω_{KL}	$\bar{\omega}_L$	Reference
23	V				0.00235±0.00025	Konstantinov (1960)
25	Mn				0.00295±0.0004	Konstantinov (1965)
29	Cu				0.0056	Konstantinov (1961)
31	Ga				0.0064±0.0004	Konstantinov (1960)
36	Ky				0.13	Auger (1925)
					0.075	Bower (1936)
37	Rb			0.013±0.002	0.011±0.001 0.009±0.002	Hohmuth (1963)
39	Y				0.0315±0.0028	Bailey (1967)
40	Zr				0.057	Lay (1934)
				0.034±0.012		Jopson (1964b)
41	Nb			0.022±0.002		Hohmuth (1963)
				0.036±0.012		Jopson (1964b)
42	Mo				0.067	Lay (1934)
46	Pd			0.047±0.012		Jopson (1964b)
47	Ag				0.100	Lay (1934)
					0.029±0.003	Bertolini (1954)
					0.047±0.002	Bertrand (1959)
				0.045±0.003		Hohmuth (1963)
				0.044±0.003		Hohmuth (1964)
				0.054±0.014		Jopson (1964b)
					0.0659±0.0037	Bailey (1967)
48	Cd			0.055±0.014		Jopson (1964b)
49	In			0.065±0.014		Jopson (1964b)
50	Sn			0.064±0.014		Jopson (1964b)
51	Sb				0.119	Lay (1934)
				0.070±0.015		Jopson (1964b)
52	Te				0.122	Lay (1934)
				0.073±0.007		Hohmuth (1963)
54	Xe				0.25	Auger (1925)
					0.103±0.01	Fink (1955)
				0.08±0.01	0.11±0.01	Hohmuth (1964)
54	Xe			0.091±0.005		Grigor'ev (1966)
55	Cs				0.089±0.013	Nix (1972)
56	Ba			0.148		Lay (1934)
					0.093±0.012	Nix (1972)
57	La			0.158		Lay (1934)
					0.110±0.015	Nix (1972)
					0.092±0.007	Hohmuth (1963)
				0.15±0.02		Jopson (1963)
				0.123±0.022		Beste (1968)
58	Ce				0.163	Lay (1934)
				0.16±0.02		Jopson (1963)
59	Pr				0.167	Lay (1934)
				0.16±0.02		Jopson (1963)
				0.09±0.01		Hohmuth (1964)
				0.123±0.017		Nix (1972)
60	Nd				0.170	Lay (1934)
				0.16±0.02		Jopson (1963)
61	Pm			0.185±0.013		Konstantinov (1967)
62	Sm				0.188	Lay (1934)
				0.17±0.01		Jopson (1963)
63	Eu				0.17	Bisi (1956a)
				0.17±0.01		Jopson (1963)
64	Gd				0.198	Lay (1934)
				0.18±0.02		Jopson (1963)
65	Tb			0.19		Lazar (1958)
				0.19±0.01		Jopson (1963)
				0.195±0.014		Konstantinov (1967)
					0.194±0.027	Nix (1971)

TABLE IV.XIV (*Continued*)

Z	Element	ν_1	ν_2	ω_{KL}	$\bar{\omega}_L$	Reference
		0.29±0.08	0.177±0.019			McGeorge (1970)
					0.194±0.027	Nix (1972)
66	Dy				0.14±0.02	Zimmerli (1963)
				0.21±0.01		Jopson (1963)
67	Ho			0.17±0.01		Hohmuth (1963)
				0.22±0.01		Jopson (1963)
			0.22±0.04			Jopson (1964a)
68	Er			0.21±0.03		Jopson (1963)
			0.21±0.04			Jopson (1964a)
69	Tm			0.23±0.03		Jopson (1963)
70	Yb			0.20		Lazar (1958)
				0.25±0.02		Jopson (1963)
			0.34±0.05			Jopson (1964a)
				0.20±0.02		Cole (1965)
			0.218±0.013			Mohan (1970b)
71	Lu			0.26±0.03		Jopson (1963)
			0.33±0.06			Jopson (1964a)
			0.290±0.040			Price (1968)
					0.29±0.05	Gizon (1968)
72	Hf				0.260	Lay (1934)
				0.17		Bisi (1956b)
				0.24		Lazar (1958)
				0.29±0.02		Jopson (1963)
			0.37±0.06			Jopson (1964a)
			0.329±0.035			Price (1968)
73	Ta	0.284	0.326			Küstner (1935)
				0.29±0.02		Jopson (1963)
			0.37±0.06			Jopson (1964a)
			0.31±0.01			Rao (1965b)
		0.22±0.01		0.28±0.01	0.225±0.01[a]	Rao (1966)
			0.303±0.030			Price (1968)
		0.218±0.016				Mohan (1970a)
74	W				0.298	Lay (1934)
		0.305	0.311			Küstner (1935)
				0.31±0.04		Jopson (1963)
			0.330±0.045			Price (1968)
75	Re			0.30±0.04		Jopson (1963)
			0.347±0.052			Price (1968)
76	Os				0.348	Lay (1934)
				0.32±0.04		Jopson (1963)
			0.366±0.038			Price (1968)
77	Ir	0.370	0.281			Küstner (1935)
				0.31±0.04		Jopson (1963)
			0.351±0.048			Price (1968)
					0.30±0.04	Wilken (1968)
78	Pt				0.348	Lay (1934)
		0.392	0.274			Küstner (1935)
					0.32±0.02[a]	Jopson (1962)
				0.36±0.02		Jopson (1963)
			0.46±0.07			Jopson (1964a)
			0.382±0.035			Price (1968)
			0.367±0.021			Mohan (1971)
79	Au				0.365	Lay (1934)
		0.410	0.272			Küstner (1935)
					0.374±0.018	Jopson (1963)
				0.287±0.04	0.430±0.012	Lazzaro (1965)
			0.395±0.032			Price (1968)
80	Hg				0.24±0.04	Jaffe (1954)
					0.371±0.035	Haynes (1955)
					0.34±0.04	Schmid (1957)
				0.34		Lazar (1958)

TABLE IV.XIV (*Continued*)

Z	Element	ν_1	ν_2	ω_{KL}	$\bar{\omega}_L$	Reference
					0.410±0.04	Nall (1960)
				0.33±0.02		Hohmuth (1963)
				0.41±0.05		Jopson (1963)
			0.58±0.10			Jopson (1964a)
			0.42±0.02			Rao (1965b)
				0.41±0.02	0.40±0.05	Rao (1965a)
					0.39±0.06[a]	Rao (1965a)
			0.455±0.062			Price (1968)
80	Hg			0.41±0.04	0.40±0.04	Kloppenburg (1969)
81	Tl				0.50±0.02	Burde (1956)
					0.48±0.03	Risch (1958)
				0.34		Lazar (1958)
					0.32	Winkenbach (1958)
					0.41±0.04	Ramaswamy (1962)
				0.44±0.05		Jopson (1963)
			0.57±0.10			Jopson (1964a)
			0.450±0.061			Price (1968)
		0.280±0.010	0.371±0.010			Wood (1969)
			0.423±0.024			Mohan (1971)
82	Pb				0.398	Lay (1934)
		0.475	0.264			Küstner (1935)
					0.39±0.02	Patronis (1957)
				0.385		Lazar (1958)
					0.36±0.02[a]	Jopson (1962)
				0.395±0.020		Jopson (1963)
			0.410±0.039			Price (1968)
					0.297±0.030[a]	Rao (1968)
		0.295±0.010	0.417±0.015			Rao (1969)
83	Bi				0.402	Lay (1934)
					0.51±0.03	Burde (1956)
					0.38±0.02	Fink (1957)
					0.38±0.04	Lee (1958)
					0.37	Tousset (1958)
					0.40	Winkenbach (1958)
				0.414±0.021		Jopson (1963)
			0.51±0.08			Jopson (1964a)
			0.410±0.039			Price (1968)
					0.330±0.016	Freund and Fink (1969)
88	Ra				0.480±0.012	Halley (1964)
					0.40±0.03	Gil (1966)
88	Ra				0.52±0.05	Booth (1956)
90	Th				0.488±0.008	Halley (1964)
			0.540±0.043			Price (1968)
91	Pa				0.52±0.03[a]	Adamson (1962)
					0.50±0.04	Boyer (1968)
92	U				0.478±0.009	Halley (1864)
				0.409±0.04	0.603±0.04	Lazzaro (1965)
					0.570±0.019	Byrne (1968)
					0.42±0.01	Salgueiro (1968)
			0.610±0.049			Price (1968)
					0.53±0.06	Zender (1969)
93	Np				0.66±0.08	Akalaev (1964)
					0.49±0.01	Salgueiro (1961)
94	Pu				0.540±0.009	Halley (1964)
					0.73±0.10	Akalaev (1964)
					0.566±0.010	Byrne (1968)
96	Cm				0.531±0.010	Halley (1964)
			0.650±0.036			McGeorge (1971c)
		0.62±0.04				McGeorge (1971b)
		0.60±0.08				McGeorge (1971b)

[a] $\bar{\omega}_L=\omega_{LL}$: vacancies created by L-electron capture.

TABLE IV.XV. Theoretical L-subshell fluorescence yields ω_i and Coster–Kronig yields f_{ij}.[a]

Z	Element	ω_1	ω_2	ω_3	f_{12}	f_{13}	$f_{12}+f_{13}$	f_{23}	Ref.
13	Al	3.05(−6)		2.40(−3)			0.982		b
14	Si	9.77(−6)		1.08(−3)			0.975		b
15	P	2.12(−5)		4.1(−4)			0.971		b
16	S	3.63(−5)		2.9(−4)			0.968		b
17	Cl	5.60(−5)		2.3(−4)			0.964		b
18	Ar	8.58(−5)		1.9(−4)			0.965		b
19	K	1.15(−4)		2.1(−4)			0.962		b
20	Ca	1.56(−4)		2.1(−4)			0.955		b
22	Ti	2.80(−4)		1.18(−3)	0.313	0.629			b
24	Cr	2.97(−4)		3.29(−3)	0.317	0.636			b
26	Fe	3.84(−4)		5.59(−3)	0.302	0.652			b
			1.43(−3)	1.49(−3)				7.24(−2)	c
28	Ni	4.63(−4)		8.02(−3)	0.325	0.622			b
			2.69(−3)					9.97(−2)	c
29	Cu		3.57(−3)	3.83(−3)				0.109	c
30	Zn	5.23(−4)		1.08(−2)	0.322	0.624			b
32	Ge	7.70(−4)		1.44(−2)	0.266	0.671			b
			7.72(−3)					2.49(−2)	c
33	As	1.40(−3)	8.85(−3)	9.74(−3)	0.282	0.547		4.13(−2)	c, d
34	Se	1.30(−3)		1.78(−2)	0.302	0.616			b
			9.94(−3)					5.95(−2)	c
35	Br		1.09(−2)					7.64(−2)	c
36	Kr	1.85(−3)	2.20(−2)	2.36(−2)	0.230	0.686		8.97(−2)	b
		2.19(−3)	1.19(−2)	1.23(−2)	0.225	0.585		9.22(−2)	c, d
37	Rb	1.32(−2)						0.107	c
38	Sr	3.00(−3)	2.24(−2)	2.43(−2)	0.249	0.646		0.115	b
40	Zr	3.97(−3)	2.94(−2)	2.95(−2)	0.236	0.648		0.118	b
		3.96(−3)	1.89(−2)	2.01(−2)	0.271	0.522		0.123	c, d
42	Mo	5.75(−3)	3.50(−2)	3.73(−2)	0.166	0.689		0.124	b
		6.34(−3)	2.45(−2)	2.59(−2)	0.048	0.692		0.126	c, d
44	Ru	7.74(−3)	4.18(−2)	4.50(−2)	0.057	0.779		0.136	b
47	Ag	1.02(−2)	5.47(−2)	6.02(−2)	0.052	0.786		0.152	b
		1.01(−2)	4.30(−2)	4.49(−2)	0.064	0.0695		0.130	c, d
50	Sn	1.30(−2)	6.56(−2)	7.37(−2)	0.052	0.784		0.162	b
		1.30(−2)	5.67(−2)		0.072	0.693		0.136	c, d
51	Sb	3.11(−2)	6.16(−2)	6.33(−2)	0.164	0.316		0.138	c, d
54	Xe	5.84(−2)	9.12(−2)	9.70(−2)	0.179	0.274		0.173	b
56	Ba	4.46(−2)	9.07(−2)	8.99(−2)	0.168	0.336		0.151	c, d
60	Nd	7.46(−2)	0.133	0.135	0.207	0.303		0.141	b
		6.00(−2)	0.120	0.120	0.165	0.332		0.142	c, d
65	Tb		0.166	0.160				0.131	c
67	Ho	0.112	0.203	0.201	0.202	0.309		0.138	b
		0.094			0.178	0.317			d
70	Yb	0.112			0.180	0.316			d
74	W	0.115	0.287	0.268	0.195	0.332		0.123	b
		0.138	0.271	0.253	0.160	0.324		0.117	c, d
79	Au	0.105	0.357	0.327	0.083	0.644		0.132	b
80	Hg	0.098	0.352	0.321	0.101	0.618		0.108	c, d
83	Bi	0.120	0.417	0.389	0.069	0.656		0.101	b
85	At	0.129	0.422	0.380	0.082	0.612		0.100	c, d
90	Th	0.197	0.529	0.461	0.069	0.575		0.102	b
93	Np		0.460	0.472				0.209	c

[a] Figures in parentheses indicate powers of ten; e.g., 3.05(−6) means 3.05×10^{-6}.
[b] McGuire (1971a).
[c] Chen, Crasemann, and Kostroun (1971a).
[d] Crasemann, Chen, and Kostroun (1971).

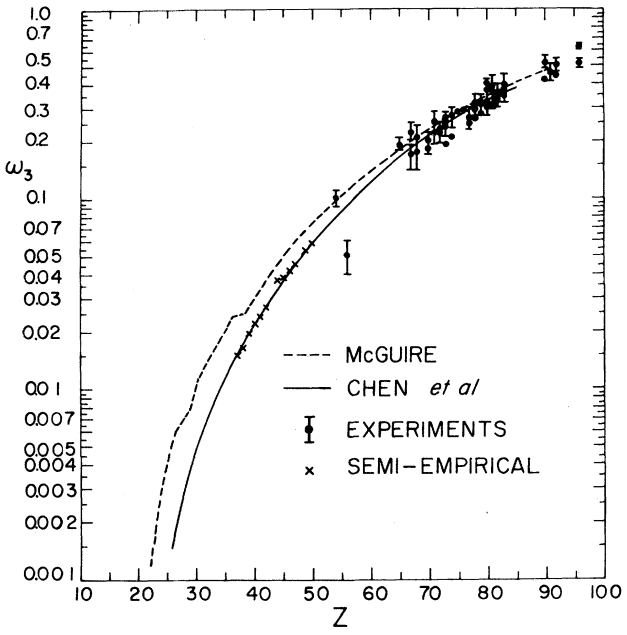

FIG. 4–27. L_3-subshell fluorescence yield ω_3 as a function of atomic number. The curves represent calculations due to Chen, Crasemann, and Kostroun (1971a) and McGuire (1971a). Dots indicate experimental data; crosses represent fluorescence yields derived from measured x-ray emission line widths and the theoretical x-ray emission rates of Scofield (1969).

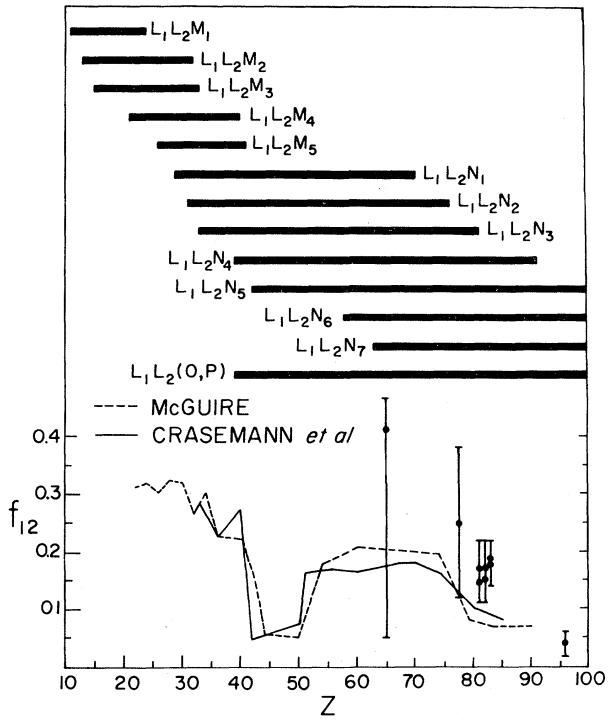

FIG. 4–28. L_1–L_2X Coster–Kronig probability f_{12} as a function of atomic number. Dots indicate experimental data, the broken curve represents theoretical results of McGuire (1971a), and the solid curve, those of Crasemann, Chen, and Kostroun (1971). Horizontal bars mark the approximate ranges of atomic numbers in which certain groups of Coster–Kronig transitions are energetically possible.

is in reasonable agreement with experiment. Most measurements of f_{12} and f_{23} generally exceed calculated values by $\sim$30%. This puzzling discrepancy has been the subject of much speculation. McGeorge, Mohan, and Fink (1971) have shown that subtraction of an unresolved $L\eta$ component in the $L\alpha$ x-ray group does not bring measured f_{23} values into agreement with theory. The possibility of a significant radiative component of f_{23} has been ruled out by the work of Chen *et al.* (1971b), and experimental results have been verified through an alternative approach by Wood, Palms, and Venugopala Rao (1972). Attempts at refinement of the theoretical approach are being made (Chen and Crasemann, private communication). A many-body approach may be required to take account of correlations (Chase, Kelly, and Kohler, 1971; Amusia, 1972).

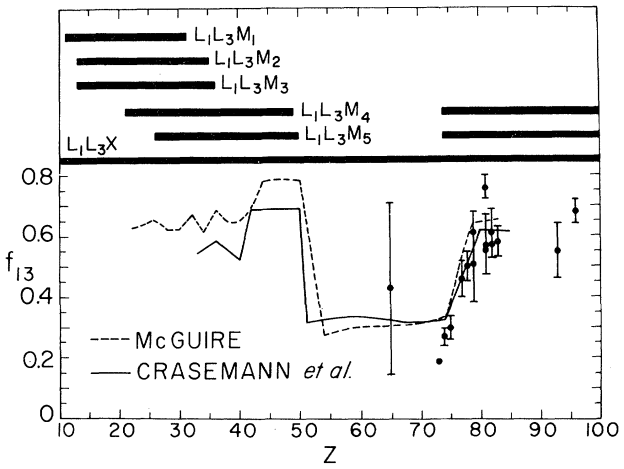

FIG. 4–29. L_1–L_3X Coster–Kronig probability f_{13} as a function of atomic number. Experimental results are indicated by dots; theoretical results of McGuire (1971a) are represented by the broken curve, and those of Crasemann, Chen, and Kostroun (1971), by the solid curve. Horizontal bars indicate ranges of atomic numbers over which certain Coster–Kronig transitions are energetically possible.

Calculated average yields ν_1, ν_2, and ω_{KL} vary smoothly with atomic number, in spite of discontinuities in the Coster–Kronig transition probabilities (Figs. 4–31, 4–32, and 4–33). Experimental average L yields (Table IV.XIV) and calculated yields are in very good agreement; this is particularly evident for ω_{KL} (Fig. 4–33) for which the largest amount of data is available.

It is interesting to note that the Coster–Kronig transfer of L vacancies to the L_3 subshell makes the average yields ν_1 and ν_2 approximately equal to ω_3. Consequently, average L-shell fluorescence yields depend very little on the initial vacancy distribution, large differences in subshell fluorescence yields notwithstanding. This somewhat surprising fact is illustrated in Fig. 4–34, where theoretical average yields $\bar{\omega}_L$ are plotted for three drastically different primary vacancy distributions; the resultant curves virtually coalesce, though the calculations of McGuire (1971a)

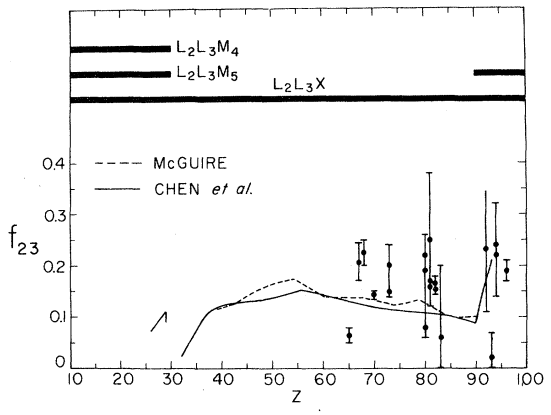

FIG. 4–30. L_2–L_3X Coster–Kronig probability f_{23} as a function of atomic number. The dots indicate experimental results; the broken curve represents the calculations of McGuire (1971a), and the solid curve, those of Chen, Crasemann, and Kostroun (1971a). Horizontal bars indicate the ranges of atomic numbers in which certain Coster–Kronig transitions are energetically possible.

yield consistently higher values than those of Chen *et al.* (1971a) and Crasemann *et al.* (1971). Measured values of $\bar{\omega}_L$ are also indicated in Fig. 4–34; while there is considerable scatter, agreement between experiment and theory is seen to be quite satisfactory.

5. *M*-SHELL FLUORESCENCE YIELDS

5.1. Special *M*-Shell Relationships

In accordance with the general relationships discussed in Sec. 1.4, the M_i-subshell fluorescence yield is

$$\omega_i{}^M = I_i{}^M / n_i{}^M, \tag{5–1}$$

where $I_i{}^M$ is the total number of M_i-subshell x rays

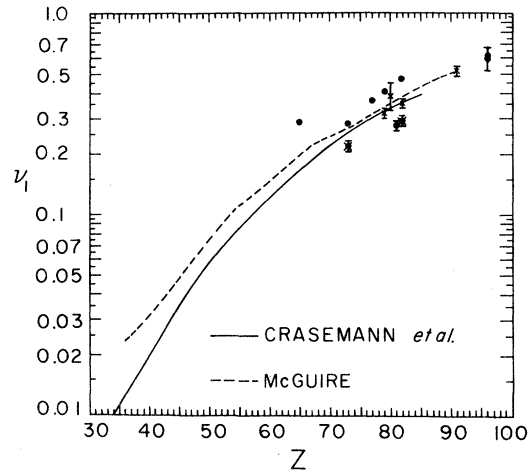

FIG. 4–31. X-ray yield $\nu_1=\omega_1+f_{12}\omega_2+(f_{13}+f_{12}f_{23})\omega_3$, as a function of atomic number. Dots indicate measured values of ν_1, crosses represent measurements of $\bar{\omega}_L$ in cases where vacancies were produced by nuclear L capture only (resulting, predominantly, in L_1 primary vacancies). Calculations of Crasemann, Chen, and Kostroun (1971) are indicated by the solid curve, and those by McGuire (1971a), by the broken curve.

TABLE IV.XVI. Approximate ranges of atomic numbers in which certain major Coster–Kronig transitions are energetically possible.

Transition	*Z* range
L_1–$L_2O(P,\cdots)$	All Z where O, $(P,\cdots)$ electrons are present
L_1–L_2N_1	$19\leq Z\leq 70$
L_1–L_2N_2	$31\leq Z\leq 76$
L_1–L_2N_3	$33\leq Z\leq 81$
L_1–L_2N_4	$39\leq Z\leq 91$
L_1–L_2N_5	$Z\geq 42$
L_1–L_2N_6	$Z\geq 58$
L_1–L_2N_7	$Z\geq 63$
L_1–L_2M_1	$11\leq Z\leq 29$
L_1–L_2M_2	$13\leq Z\leq 32$
L_1–L_2M_3	$15\leq Z\leq 33$
L_1–L_2M_4	$21\leq Z\leq 40$
L_1–L_2M_5	$26\leq Z\leq 41$
L_1–$L_3N(O,P\cdots)$	All Z where N, $(O,P,\cdots)$ electrons are present
L_1–L_3M_1	$11\leq Z\leq 31$
L_1–L_3M_2	$13\leq Z\leq 35$
L_1–L_3M_3	$15\leq Z\leq 36$
L_1–L_3M_4	$21\leq Z\leq 49$, $Z\geq 77$
L_1–L_3M_5	$26\leq Z\leq 50$, $Z\geq 74$
L_2–$L_3N(O,\cdots)$	All Z where N, $(O,\cdots)$ electrons are present
L_2–L_3M_4	$21\leq Z\leq 30$
L_2–L_3M_5	$26\leq Z\leq 30$, $Z\geq 91$

emitted by a sample with $n_i{}^M$ primary vacancies in the M_i subshell only. Since Coster–Kronig transitions shift vacancies from lower to higher subshells and vacancies are usually produced in several subshells, it is convenient to express $\omega_i{}^M$ in terms of quantities that can be measured under these practical conditions. Thus, if there are n_M primary vacancies in all M subshells,

$$n_M=\sum_i n_i{}^M, \tag{5–2}$$

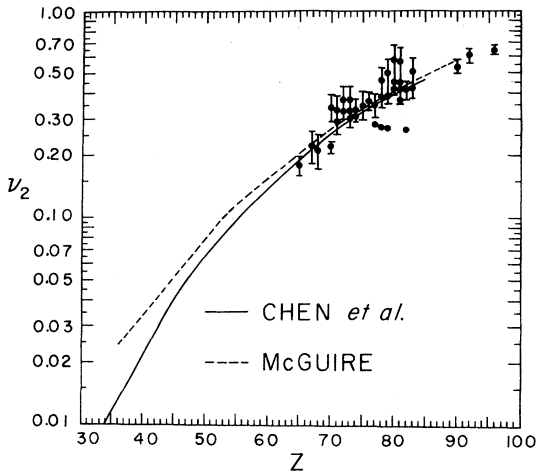

FIG. 4–32. X-ray yield $\nu_2=\omega_2+f_{23}\omega_3$, as a function of atomic number. Dots indicate experimental results. The broken curve represents theoretical results of McGuire (1971a), and the solid curve, those of Chen, Crasemann, and Kostroun (1971a).

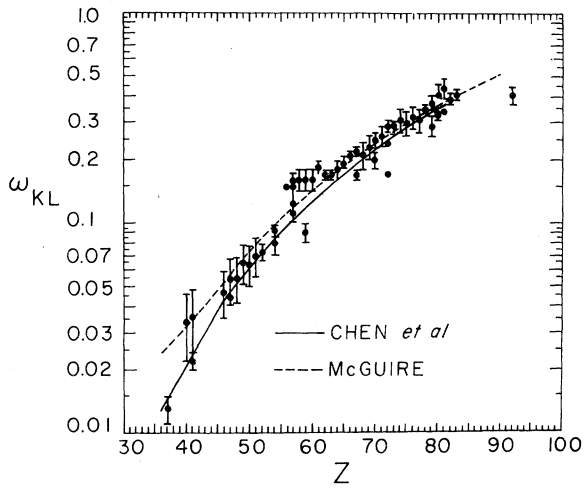

FIG. 4–33. Average L-shell fluorescence yield ω_{KL}, corresponding to the primary L-vacancy distribution produced by K x-ray emission. Experimental data are indicated by dots; theoretical results of McGuire (1971a) are indicated by the broken curve, and calculations of Chen, Crasemann, and Kostroun (1971a) are represented by the solid curve.

and I_i^M is the total number of emitted M_i-subshell x rays, then the M_i-subshell fluorescence yield is

$$\omega_i^M = I_i^M/(n_M V_i^M), \tag{5–3}$$

where V_i^M is the relative number of vacancies in the M_i subshell, including vacancies shifted to this subshell by Coster–Kronig transitions, as defined in Eq. (1–13).

The normalized primary M-subshell vacancy distribution is denoted by N_i^M:

$$n_i^M/\sum_i n_i^M = N_i^M; \tag{5–4}$$

$$\sum_i N_i^M = 1. \tag{5–5}$$

Primary vacancies in the M subshells can arise either from a *shift* of K- or L-shell vacancies or from *direct production*, e.g., from M-shell internal conversion of γ rays, M orbital electron capture (mostly affecting M_1-subshell electrons), and excitation or ionization by incident photons or charged particles. The total number n_i^M of primary vacancies produced in a subshell M_i is

$$n_i^M = n_{M_i} + n_K n_{KM_i} + \sum_j n_{L_j} n_{L_jM_i} + \sum_j n_j^L f_{jk}^L n_{L_kM_i}. \tag{5–6}$$

In this expression, n_{M_i} denotes the number of primary vacancies produced directly in the M_i subshell (not through cascading from the K or L shells); n_{KM_i} is the number of vacancies shifted from the K shell in transitions of the type K–M_i, K–LM, K–MM, K–MX; $n_{L_jM_i}$ is the number of vacancies produced by transitions to an L_j vacancy, of the type L_j–M_i, L_j–MM, L_j–MX, or L_i–L_kM, and n_K is the total number of primary K vacancies in the sample, while n_L is the total number of primary L vacancies in the sample (see Sec. 4.4). No distinction is made here between single- and multiple-vacancy states.

Explicit expressions for n_{KM_i} and n_{LM_i} are

$$n_{KM_i} = n_{KM_i}(R) + n_{KM_i}(A), \tag{5–7}$$

$$n_{L_jM_i} = n_{L_jM_i}(R) + n_{L_jM_i}(A) + n_{L_jM_i}(CK). \tag{5–8}$$

The contributions from radiative, Auger, and Coster–Kronig transitions can be separated:

$$n_{KM_i}(R) = \omega_K[I(K-M_i)/I_K(R)], \tag{5–9}$$

$$n_{KM_i}(A) = a_K\{[I(K-M_iY) + 2I(K-M_iM_i) + I(K-LM_i)]/I_K(A)\}, \tag{5–10}$$

where $I_K(R)$ and $I_K(A)$ are the total intensities of radiative and Auger transitions, respectively, to the K shell;

$$n_{L_jM_i}(R) = \omega_j^L[I(L_j-M_i)/I_{L_i}(R)], \tag{5–11}$$

$$n_{L_jM_i}(A) = a_j^L\{[I(L_j-M_iY) + 2I(L_j-M_iM_i)]/I_{L_i}(A)\} + \sum_k f_{jk}^L[I(L_j-L_kM_i)/I_{L_i}(CK)], \tag{5–12}$$

where $I_{L_i}(R)$, $I_{L_i}(A)$, and $I_{L_i}(CK)$ are the total intensities of radiative, Auger, and Coster–Kronig transitions filling L_j vacancies.

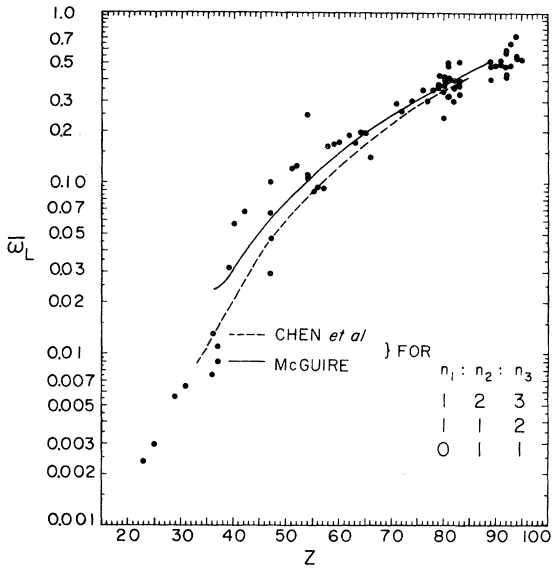

FIG. 4–34. Theoretical average L-shell fluorescence yields $\bar{\omega}_L$ according to Chen, Crasemann, and Kostroun (1971a) and Crasemann, Chen, and Kostroun (1971) (dashed curve) and according to McGuire (1971a) (solid curve), for three drastically different primary vacancy distributions, *viz.*, $n_1:n_2:n_3 = 1:2:3$, $1:1:2$, and $0:1:1$. Due to the effect of Coster–Kronig transitions, theoretical curves for the different primary distributions virtually coalesce, though McGuire's results consistently exceed those of Chen, Crasemann, and Kostroun (1971a). Also indicated are experimental points.

TABLE V.I. Probability of producing a primary M-shell vacancy through radiationless transitions $[n_{KM}(A+CK)=n_{KM}(A)+n_{KM}(CK)]$ and radiative transitions $[n_{KM}(R)]$ to a K-shell vacancy, and through radiationless transitions $[n_{L_iM}(A+CK)]$ and radiative transitions $[n_{L_iM}(R)]$ to an L_i-subshell vacancy, derived from theory. (After Venugopala Rao, Chen, and Crasemann, 1972.)

Z	$n_{KM}(A+CK)$	$n_{KM}(R)$	$n_{L_1M}(A+CK)$	$n_{L_1M}(R)$	$n_{L_2M}(A+CK)$	$n_{L_2M}(R)$	$n_{L_3M}(A+CK)$	$n_{L_3M}(R)$
16	0.201	0.0033						
20	0.221	0.0149						
22	0.212	0.0216						
24	0.197							
26	0.180	0.0371			1.863		1.937	
28	0.162				1.828			
29					1.819	0.0036	1.922	0.0039
30	0.144	0.0532						
32	0.128	0.0624			1.840			
33			1.084		1.764		1.839	
34					1.696			
35					1.612			
36	0.102	0.0806	1.167	0.0020	1.542	0.0118	1.697	0.0122
37					1.488	0.0132		
40	0.0790	0.0967	1.031	0.0034	1.415	0.0187	1.616	0.0197
42	0.0693	0.104	1.014	0.0054	1.402	0.0236	1.602	0.0250
47	0.0499	0.119	0.942	0.0084	1.349	0.0392	1.560	0.0409
50	0.0411	0.126	0.905	0.0105	1.304	0.0502		
51			0.762	0.0255	1.284	0.0545	1.497	0.0560
54	0.0318							
56	0.0281	0.137	0.673	0.0350	1.212	0.0779	1.384	0.0713
58	0.0249							
60	0.0221	0.143	0.666	0.0468	1.145	0.102	1.360	0.103
65	0.0166	0.149			1.074	0.141	1.284	0.137
67			0.614	0.0625				
70	0.0132	0.154	0.582	0.0865				
74			0.561	0.106	0.936	0.227	1.138	0.212
80			0.707	0.0730	0.819	0.288	1.024	0.265
85			0.681		0.721		0.929	
93					0.629		0.782	

It should be noted that both n_{KM_i} and $n_{L_iM_i}$ are defined in terms of transitions in which an M-subshell electron participates in the first step. If one desires to calculate the *total* number of M_i-subshell vacancies resulting from the filling of an initial K-shell or L-shell vacancy, then contributions due to two-step and three-step cascades, including Coster–Kronig transitions, must be taken into account. For example, the total number of M_i-subshell primary vacancies resulting from all the transitions initiated by the filling of a K-shell vacancy is

$$\bar{n}_{KM_i}=n_{KM_i}+\sum_j n_{KL_j}n_{L_jM_i}+n_{KL}[\sum_j V_j^L n_{L_jM_i}]. \quad (5\text{–}13)$$

Here, n_{KL_j} is the total number of primary L_j vacancies created by the filling of a K-shell vacancy, and n_{KL} is the sum of all three n_{KL_j} (see Sec. 4.4).

Similarly, the following relations hold for the total number of M_i-subshell primary vacancies that result from all transitions initiated by the filling of an L_i-subshell vacancy:

$$\bar{n}_{L_1M_i}=n_{L_1M_i}+f_{12}^L n_{L_2M_i}+(f_{13}^L+f_{12}^L f_{23}^L)n_{L_3M_i},$$

$$\bar{n}_{L_2M_i}=n_{L_2M_i}+f_{23}^L n_{L_3M_i},$$

$$\bar{n}_{L_3M_i}=n_{L_3M_i}. \quad (5\text{–}14)$$

At the present time, there are no experimental data on total M-vacancy production following the decay of K and L vacancies, but primary M-vacancy distributions have been derived from theory by Venugopala Rao, Chen, and Crasemann (1972). The results are listed in Table V.I. Average numbers $\bar{n}_{L_iM}$ of M-shell vacancies produced in the decay of an L_i vacancy have been calculated for eight elements by McGuire (1971a); these are listed in Table V.II.

Only the calculated probability of producing M vacancies through *radiative* transitions is subject to experimental test with presently available data, using

TABLE V.II. Average total number $\bar{n}_{L_iM}$ of M-shell vacancies produced in the decay of an L_i vacancy, derived from theory by McGuire (1971a).

Z	$\bar{n}_{L_1M}$	$\bar{n}_{L_2M}$	$\bar{n}_{L_3M}$
50	2.34	1.67	1.69
54	1.59	1.63	1.64
60	1.58	1.59	1.60
67	1.46	1.51	1.53
74	1.93	1.43	1.45
79	1.92	1.36	1.38
83	1.78	1.29	1.33
90	1.61	1.22	1.23

the relations

$$n_{KM}(R)=\omega_K\frac{I(K\beta_1)}{I(K\alpha_1)}\times\left\{\left[1+\frac{I(K\alpha_2)}{I(K\alpha_1)}\right]\left[1+\frac{I(K\beta)}{I(K\alpha)}\right]\right\}^{-1} \quad (5\text{–}15)$$

and

$$n_{L_iM}(R)=\omega_i/(1+s_i), \quad (5\text{–}16)$$

where the s_i are x-ray branching ratios defined by Eqs. (4–11) through (4–13). In Fig. 5–1, the theoretical probability $n_{KM}(R)$ of producing a primary M-shell vacancy through radiative transitions to an initial K-shell vacancy is compared with empirical values of $n_{KM}(R)$ calculated from Eq. (5–15) with measured K-shell fluorescence yields and x-ray intensity ratios; the experimental and theoretical curves do not deviate more than 7% from each other. Theoretical and experimental values of $n_{L_iM}(R)$ also are in satisfactory agreement. There are, as yet, almost no experimental data with which to compare the calculated probabilities of M-vacancy production due to Auger transitions. (See, however, the work on Kr and Ar by Mehlhorn, 1968, and Siegbahn, 1969).

The detectors generally used for measurements of M-subshell fluorescence yields are not capable of resolving the large number of M x rays into individual lines. Therefore, the M_i–M_j Coster–Kronig vacancy shift cannot be followed by separating x rays emitted in transitions to the M_i and M_j levels. Consequently, the M_i-subshell fluorescence yields and Coster–Kronig transition probabilities cannot be determined individually (except for the M_5 subshell, where no further Coster–Kronig transitions are possible). Thus, the measurable quantities are combinations of ν_i^M, as defined in Sec. 1.4. These average fluorescence yields are denoted by $\bar{\omega}_M$

$$\bar{\omega}_M=\sum_i N_i^M\nu_i^M. \quad (5\text{–}17)$$

However, at high Z, separation of the M x rays into groups corresponding to transitions to the $M_{3,4,5}$ and $M_{1,2}$ levels can be achieved with Si(Li) detectors that have resolution of the order of 200 eV FWHM at 6.4 keV. Then the gross Coster–Kronig transfers from the $M_{1,2}$ to the $M_{3,4,5}$ subshells as well as an average over ω_1^M and ω_2^M are observable. A list of measured M-shell quantities is contained in Table V.III.

Simplification of the basic equations can be achieved in certain experimental approaches. A particular group of M vacancies can be selected by coincidences with K or L x rays or by limiting vacancy creation to L, M, and higher shells, using radionuclides that decay without appreciable K-vacancy production (e.g., some high-Z even–even nuclei). When vacancies are created by ionization, the maximum excitation energy can be held below the K or L binding energy. Thus, the large number of quantities needed to determine M-vacancy distributions can be reduced.

Furthermore, due to energetics, contributions from Coster–Kronig transitions to $\bar{n}_{L_1M}$ are negligible for $41<Z<74$ and to $\bar{n}_{L_2M}$, for $Z\lesssim 94$.

5.2. Influence of Multiple Vacancies on M-Shell Fluorescence Yields

A nonradiative vacancy cascade from the K or an L_i shell always produces more than one L-, M-, N-, or higher-shell vacancy. The effect of such multiple vacancies on transition probabilities to the M shell has hitherto been considered negligible, but some general statements in this regard can be made.

It is convenient to distinguish three types of multiple vacancies: (1) M vacancies associated with one or two

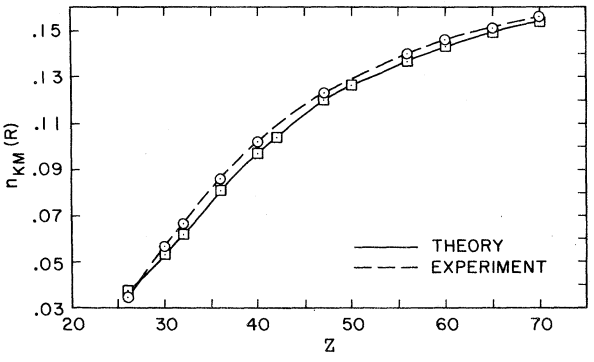

FIG. 5–1. The theoretical probability $n_{KM}(R)$ of producing a primary M-shell vacancy through radiative transitions to an initial K vacancy, according to Venugopala Rao, Chen, and Crasemann (1972) (see Table V.I), compared with values of $n_{KM}(R)$ calculated from experimental data with the aid of eq. (5–15). (Mau Hsiung Chen, private communication 1971).

TABLE V.III. Measured M-shell fluorescence yields and Coster–Kronig probabilities.

Z	Element	$\bar{\omega}_M$	ω_{LM}[a]	ω_{LM}[b]	$\omega_1+f_{12}\omega_2$	ν_i	ω_i	Reference
76	Os		0.013±0.0024	0.016±0.003				Jopson (1965)
79	Au	0.023±0.001						Konstantinov (1968)
79	Au		0.024±0.005	0.030±0.006				Jopson (1965)
82	Pb	0.029±0.002						Konstantinov (1968)
82	Pb		0.026±0.005	0.032±0.006				Jopson (1965)
83	Bi	0.037±0.007						Jaffe (1954)
83	Bi	0.035±0.002						Konstantinov (1968)
83	Bi		0.030±0.006	0.037±0.005				Jopson (1965)
92	U	0.06						Lay (1934)
93	Np				$0.002^{+0.003}_{-0.002}$	$\nu_1=0.065\pm0.014$		Karttunen (1971)
						$\nu_2=0.080\pm0.029$		
						$\nu_4=0.062\pm0.005$		
						$\nu_{4,5}=0.065\pm0.012$	$\omega_5=0.06\pm0.012$	
96	Cm				$0.0075^{+0.0089}_{-0.0075}$	$\nu_1=0.081\pm0.016$		Karttunen (1971)
						$\nu_2=0.068\pm0.023$	$\omega_2=0.0046^{+0.0051}_{-0.0046}$	
						$\nu_3=0.062\pm0.019$		
						$\nu_4=0.080\pm0.006$		
						$\nu_{4,5}=0.075\pm0.012$	$\omega_5\approx0.075\pm0.012$	

[a] Corrected for a 20% contribution from double M-shell vacancies.
[b] Uncorrected values, as reported by Jopson, Mark, Swift, and Williamson (1965).

L vacancies, (2) multiple vacancies in the M shells, and (3) a vacancy in an M shell, associated with vacancies in higher shells. In the first two cases, cascades preceding the generation of the M vacancy are primarily limited to two steps. Hence, vacancy pairs L_iM_j and M_iM_j must be considered. The less probable triple vacancies $L_iL_jM_k$, $L_iM_jM_k$, $L_iM_jN_k$, $M_iM_jM_k$, etc., can be treated as combinations of the three multiple-vacancy types identified above.

The effective nuclear charge Z^* at an M_j vacancy is enhanced if an L_i vacancy is simultaneously present; the change in screening $\Delta\sigma$ is of order unity, very roughly speaking. In the case of double M vacancies, $\Delta\sigma$ depends on the detailed configuration M_iM_j and can range, approximately, from 0.3 to 1 (Slater, 1930; Bergström and Nordling, 1965). The presence of an additional M_i vacancy also increases the effective charge at higher shells. For multiple vacancies of types (1) and (2), therefore, the radiative transition probability to the M_j vacancy is enhanced, while the Auger and Coster–Kronig transition rates are not affected as much.[8] The resulting change in the M-shell fluorescence yield is approximately the difference between the yields for Z and $Z+\Delta\sigma$. For an LM vacancy pair, the observed change is $\Delta\nu^M/\nu^M<0.1$ for $Z\approx80$. For double M vacancies, the observed fluorescence yield is the average of the yields for each of the M vacancies decaying successively. The effective change in the observed fluorescence yield is then approximately 0.15 to 0.5 times the expected change for an LM vacancy pair.

[8] An exception to this rule occurs at M–MN Coster–Kronig threshold energies.

If an M vacancy is accompanied by vacancies in higher states [type (3)], the main effect on the fluorescence yield is expected to result from the reduction in the number of electrons available for transitions to the M vacancy. A comparable reduction in radiative and radiationless transition rates is expected, resulting in a negligible effect. Moreover, the radiative filling of M vacancies occurs primarily from the $N_{5,6,7}$ subshells, which have high occupation numbers. The same is probably true for nonradiative transitions to the M shell, since transitions with high ejected-electron angular momenta are favored (Callan, 1961; Callan, Nikolai, and McDavid, 1964; Asaad, 1965a). However, little is known experimentally about M–NN Auger-electron intensities at high Z.[9] Even if the reduction in radiative and radiationless transition rates is not strictly comparable, the net effect on the M fluorescence yield is expected to be small: for L- to K-shell transitions at $Z=54$, the analogous effect on ω_K has been calculated from known K x-ray and K Auger-electron intensities (Lark, 1960) and was found to be only 1%. Some of the first calculations of radiative rates in atoms with multiple-hole configurations have been performed by Åberg (1968, 1969) and by McGuire and Mittleman (1972).

In the preceding considerations, possible correlation effects among multiple vacancies have been neglected; these may, in principle, give rise to other modes of deexcitation, such as 2-particle→2-hole transitions (of very low probability), and radiative Auger transitions. Such processes are discussed in a review by Krause (1971).

5.3. Experimental Methods for M X Rays

Current experimental methods for multichannel singles and coincidence measurements of M x rays above ~2.5 keV (i.e., for elements of $Z>80$) are based on the use of Si(Li) detectors with <150 eV FWHM resolution at 2 keV, fitted with thin beryllium windows (~0.013 mm). The application of such detectors to investigations of M x rays of ^{249}Cf and ^{241}Am is discussed in Sec. 5.5.3.

For M x rays below ~2.5 keV ($Z<80$), proportional-counter and photographic-plate methods have been used; the latter are now obsolete. Fluorescent excitation of nonradioactive targets has been employed with proportional-counter detection, as discussed in Secs. 5.4.3 and 5.5.1. Proportional counters are necessary in the region up to ~5 keV for the best measurement of absolute x-ray intensities, since their efficiency can be accurately evaluated. A detailed investigation of the efficiency of a multiwire anticoincidence proportional counter for M x rays from ^{241}Am sources has been made by Karttunen *et al.* (1971). Single-wire proportional-counter efficiencies in this energy region have been calculated from attenuation coefficients tabulated, for example, by Storm and Israel (1970).

[9] The experimental difficulties are discussed by Zender, Pou, and Albridge (1969). The only case where resolved M-subshell Auger and Coster–Kronig transitions have been investigated is that of Kr by Mehlhorn (1965).

5.4. Mean M-Shell Fluorescence Yields from Singles M X-Ray Spectra

5.4.1. Vacancies in the K, L, and M Shells

In the general case, K-, L-, and M-shell vacancies are present, and a determination of a mean M-shell fluorescence yield, $\bar{\omega}_M$, requires detailed knowledge of the various modes of K- and L-vacancy deexcitation. At present, theoretical results are just being gained that will permit the derivation of the pertinent atomic decay schemes and branching ratios (Secs. 2.3, 2.4, and 5.1).

5.4.2. Vacancies in the L and M Shells Only

When K-shell vacancies are absent, a knowledge of L Auger-electron and L x-ray transition rates to the M subshells is required in order to derive the M vacancy distribution. Only for a few radioactive nuclides has exhaustive L Auger-electron spectroscopy been performed (^{210}Pb [RaD], Haynes, Velinsky, and Velinsky, 1967; ^{233}Pa, Zender, Pou, and Albridge, 1969; and ^{113}Sn, Krisciokaitis and Haynes, 1967), so that the determination of $\bar{\omega}_M$ can be based on empirical vacancy distributions. (See also recent results in Siegbahn, 1969.)

An example of a suitable isotope for measurements of this type is ^{210}Pb [RaD]. A single well-studied γ transition is converted in the L and M shells; this is the only source of L and M vacancies. The ratio of L, M, N, O, ··· vacancies created by conversion is well known (Velinsky, Velinsky, and Haynes, 1966) and the L Auger-electron spectrum has been studied in detail (Haynes, Velinsky, and Velinsky, 1967). These results, combined with those of high-resolution x-ray spectrometry with Ge(Li) detectors, permitted Freund and Fink (1969) and Freund *et al.* (1969a) to determine the three n_{L_jM} values at $Z=83$.

5.4.3. Vacancies in the M Shell Only

When only directly produced M vacancies are present, the experimental problem is reduced to the task of absolute measurement of the total number of directly produced M vacancies and of the M x-ray intensities. A significant number of primary multiple vacancies is produced only by heavy-charged-particle bombardment. Values of mean M-shell fluorescence

yields determined by this method have been reported by Konstantinov and Sazonova (1968) for Au and Pb, using excitation of only the M shell in thin films of these elements with 5.9-keV photons from ^{55}Fe sources. A 2π proportional counter was used for absolute measurement of the incident x rays and of the fluorescent M x rays. Corrections were applied for x-ray absorption in the foils. The values obtained are listed in Table V.III. The stated errors, however, are probably underestimated, because of the large uncertainties (up to 50%) in the photoelectric cross sections for the ($\sim$2 keV) M x rays and the use of an exponential absorption law to calculate the 2π-counter efficiency.

5.5. Mean M-Shell Yields by Coincidence Methods

5.5.1. Mean M-Shell Fluorescence Yields From Unresolved (L X-Ray)–(M X-Ray) Coincidences

This method eliminates the necessity of measuring separately the M-vacancy production rate. However, the L_i-subshell quantities in the evaluation of the n_{L_iM} values have to be known, except for the Auger parts. Through this method (Figs. 5–2 and 5–3), with L_i-subshell quantities from theory and published crystal spectrometer measurements, Jopson *et al.* (1965) have measured mean M-shell fluorescence yields ω_{LM} in Os, Au, Pb, and Bi. The original values are listed in Table V.III. Corrected values are also listed, which were derived by utilizing new information on L-shell transitions (Venugopala Rao *et al.*, 1969; Freund and Fink, 1969a; Price, Mark, and Swift, 1968; Scofield, 1969) and accounting for the double M vacancy creation due to L_1–L_3M Coster–Kronig transitions. The mean fluorescence yield ω_{LM} can be deduced from the ratio of the L–M x-ray coincidence rate $C_{M(L)}$, and the L x-ray singles rate C_L according to the equation

$$\omega_{LM}=[C_{M(L)}/C_L\epsilon_M][\bar{n}_{LM}(R)+\bar{n}_{LM}(CK)]^{-1}. \quad (5\text{–}18)$$

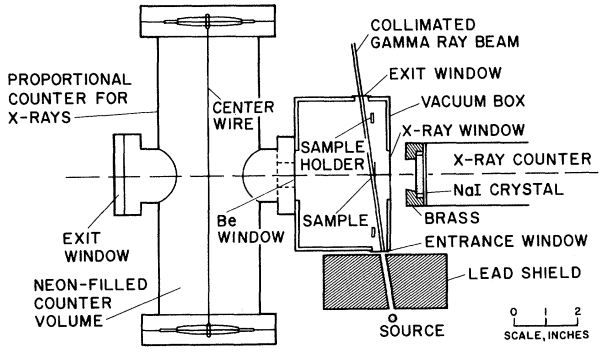

FIG. 5–2. Counter arrangement for the measurement of M x-ray fluorescence yields by foil excitation, after Jopson, Mark, Swift, and Williamson (1964b).

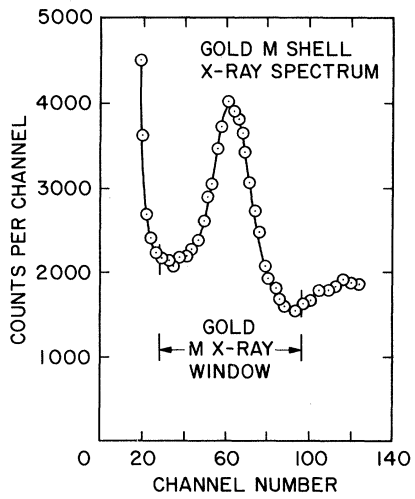

FIG. 5–3. M x-ray spectrum of gold, observed with the proportional counter shown in Fig. 5–2, after Jopson, Mark, Swift, and Williamson (1965).

Here, ϵ_M is the M x-ray detection efficiency including the effect of possible source absorption, and the quantity $\bar{n}_{LM}$ is the average number of M vacancies associated with an L x ray (Jopson *et al.*, 1965).

5.5.2. Measurement of $\bar{\omega}_{2,3}{}^M$ From ($K\beta_{1,3}$)–(M X-Ray) Coincidences

Selection of the radiative part of n_{KM_i} can be accomplished by gating with the $K\beta$ x rays, or the resolved component $K\beta_{1,3}$ that arises from the transition, in coincidence with M x rays (Karttunen, Freund, and Fink, 1971). As a result, one obtains a well-defined mean M-shell fluorescence yield $\bar{\omega}_{2,3}{}^M$, unaffected by multiple LM and MM vacancy problems, except for chance coincidences and coincident satellites:

$$\frac{C_{M(K\beta_{1,3})}}{C_{K\beta_{1,3}}\epsilon_M}=\frac{I(K-M_2)}{I(K-M_{2,3})}\nu_2{}^M + \frac{I(K-M_3)}{I(K-M_{2,3})}\nu_3{}^M=\bar{\omega}_{2,3}{}^M. \quad (5\text{–}19)$$

The quantities $\nu_i{}^M$ have been defined in Sec. 1.4.

5.5.3. Measurements of $\omega_i{}^M$ From (Resolved L X-Ray)–(M X-Ray) Coincidences

When a single L_i–M_j radiative transition or a superposition of only two single lines can be selected, it is possible to select M_j-subshell vacancies by gating on such L x rays. Thus, Ll x rays indicate the formation of M_1 vacancies, $L\alpha$ x rays signal $M_{4,5}$ vacancies, and $L\beta_1$ and $L\beta_4$ x rays signal the formation of M_4 and M_2 vacancies, respectively. Separation of these L x-ray

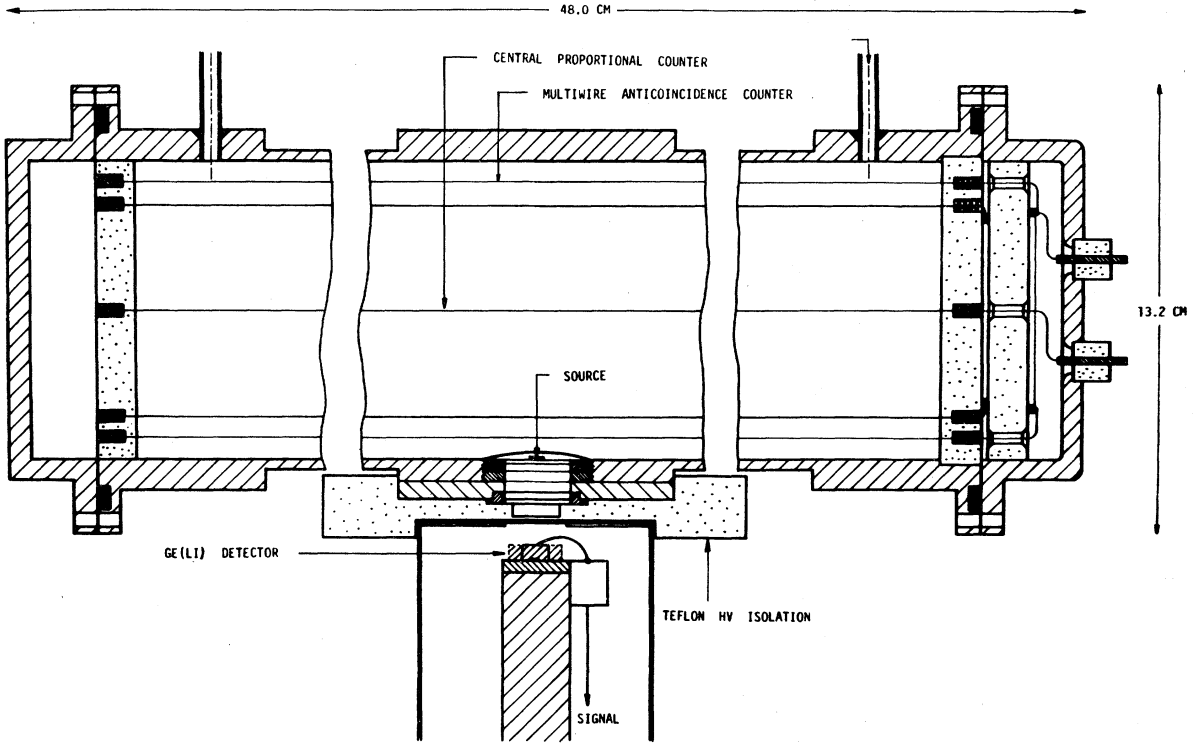

FIG. 5–4. Cross section of multiwire proportional counter operated in coincidence with Ge(Li) detector, employed by Karttunen, Freund, and Fink (1971).

transitions is possible in elements with $Z>55$. M-shell fluorescence yields can then be obtained from a comparison of the L x-ray singles and the L–M x-ray coincidence spectra, as for the following case involving $L\alpha(L_3$–$M_{4,5})$ x rays:

$$\bar{\omega}_{4,5}{}^{M}=C_{M(L\alpha)}/C_{L\alpha}\epsilon_{M}. \tag{5–20}$$

Experiments based on such considerations have been performed by Karttunen (1971) on $_{93}$Np and $_{96}$Cm, using radioactive ^{241}Am and ^{249}Cf sources (Fig. 5–4). Results are included in Table V.III. Multiple ionization creates a complication: M vacancies signaled by L_3–M x rays are often associated with an additional $M_{3,4,5}$ vacancy if there are primary L_1 or L_2 vacancies and the L_1–L_3M and L_2–L_3M Coster–Kronig transition probabilities do not vanish. For example, there are $1.7M$ vacancies associated, on the average, with each L_3–M x ray in the ^{241}Am x-ray spectrum. Consequently, $\nu_1{}^{M}$ measured by Ll gating is actually $\bar{\nu}_{1,3,4,5}{}^{M}$. In the high-$Z$ region ($Z\approx 90$), however, the observed M x-ray spectrum is resolved into separate peaks from transitions to the $M_{1,2}$ [10] and $M_{3,4,5}$ levels, and information on the quantity $\omega_1{}^{M}+f_{12}{}^{M}\omega_2{}^{M}$ can be gained from the Ll x-ray-gated M spectrum, by counting the $M_{1,2}$ x rays only (Karttunen, Freund, and Fink, 1971). Care has to be taken in this region of Z to unfold the L_1–L_3 x-ray peak from the $M_{1,2}$–N x-ray peak in the spectrum.

[10] The contribution from M_3–O x rays must be subtracted.

5.5.4. *Directional Correlation Effects*

A general discussion of directional correlation effects has been presented in Sec. 4.5.5. Since admixtures of higher multipolarities in x-ray transitions are present (Sec. 4.5.5), directional coefficients A_{22} must be calculated from theoretical mixing ratios (Scofield, 1969; Rosner and Bhalla, 1970). No experimental work on directional correlation in (K x-ray)–(M x-ray) cascades or (L x-ray)–(M x-ray) cascades has been reported.

5.6. Tables and Discussion of M-Shell Yields

Present knowledge of the details of M-shell deexcitations is incomplete. However, a general feature is apparent in the high-Z region: Coster–Kronig transitions of the type M–MN are greatly enhanced over the

TABLE V.IV. Theoretical M-subshell total level widths $\Gamma(M_i)$, Auger yields a_i (not including Coster–Kronig transitions), and fluorescence yields ω_i, according to McGuire (1972). The notation $(-n)$ stands for $\times 10^{-n}$.

Z	$\Gamma(M_1)$ (eV)	a_1	ω_1	$\Gamma(M_2)$ (eV)	a_2	ω_2	$\Gamma(M_3)$ (eV)	a_3	ω_3	$\Gamma(M_4)$ (eV)	a_4	ω_4	$\Gamma(M_5)$ (eV)	a_5	ω_5
20	0.82	0.017	8.4(−6)	3(−4)	0.938	0.062									
22	3.24	0.0040	3.2(−6)	0.21	0.0014	3.4(−5)									
23	4.18	0.0031	2.9(−6)	0.53	6.6(−4)	2.3(−5)									
24	4.92	0.0	2.6(−6)	1.32	0.0	1.6(−5)									
25	5.92	0.0019	3.1(−6)	1.52	1.7(−4)	1.6(−5)									
26	6.90	0.0016	2.8(−6)	2.15	1.4(−4)	1.6(−5)									
27	7.28	0.0013	2.8(−6)	2.85	1.2(−4)	1.7(−5)									
28	7.92	0.0011	3.5(−6)	3.80	5(−5)	1.5(−5)									
29	6.66	0.0	4.1(−6)	5.22	0.0	1.6(−5)									
30	5.90	0.0016	4.6(−6)	4.70	9(−5)	2.2(−5)									
32	4.59	0.0053	9.1(−6)	5.22	0.0017	2.6(−5)				0.048	0.997	2.7(−3)			
36	6.11	0.015	4.9(−5)	4.14	0.015	6.0(−5)	4.13	0.015	6.0(−5)	0.089	0.997	2.7(−3)			
40	6.47	0.027	7.0(−5)	2.43	0.069	1.4(−4)	2.40	0.070	1.5(−4)	0.073	0.997	2.7(−3)			
44	7.89	0.033	1.2(−4)	2.91	0.099	2.6(−4)	2.98	0.091	2.3(−4)	0.24	0.997	2.9(−3)			
47	9.62	0.036	1.7(−4)	3.74	0.098	3.9(−4)	3.88	0.089	3.2(−4)	0.44	0.997	2.7(−3)			
50	10.85	0.045	2.5(−4)	3.69	0.126	7.0(−4)	4.06	0.107	5.4(−4)	0.52	0.997	2.7(−3)			
54	10.18	0.055	4.7(−4)	4.83	0.128	9.0(−4)	5.48	0.106	6.8(−4)	0.68	0.997	2.7(−3)			
57	9.30	0.065	8.4(−4)	5.76	0.127	1.10(−3)	5.41	0.125	9.9(−4)	0.73	0.997	2.7(−3)			
60	12.87	0.053	8.1(−4)	6.69	0.127	1.32(−3)	6.81	0.113	1.05(−3)	1.39	0.722	2.6(−3)	1.00	0.997	3.2(−3)
63	14.95	0.055	8.7(−4)	8.37	0.117	1.47(−3)	7.81	0.114	1.26(−3)	1.86	0.627	4.1(−3)	1.14	0.994	5.9(−3)
67	18.3	0.056	1.08(−3)	10.4	0.106	1.85(−3)	10.2	0.103	1.45(−3)	2.41	0.585	6.7(−3)	1.38	0.989	0.0106
70	20.8	0.053	1.15(−3)	11.8	0.096	1.97(−3)	11.6	0.095	1.66(−3)	3.10	0.558	8.6(−3)	1.56	0.985	0.0149
73	19.3	0.060	1.45(−3)	12.0	0.104	2.64(−3)	10.8	0.104	2.14(−3)	3.25	0.575	0.0130	1.80	0.979	0.0205
76	20.4	0.067	1.67(−3)	13.9	0.110	3.25(−3)	9.34	0.126	3.20(−3)	4.18	0.567	0.0137	2.25	0.977	0.0232
79	20.9	0.074	2.13(−3)	14.7	0.114	4.23(−3)	9.35	0.158	4.20(−3)	2.80	0.928	0.0264	2.66	0.974	0.0256
83	21.7	0.079	2.89(−3)	14.6	0.135	6.52(−3)	10.7	0.155	5.33(−3)	2.88	0.932	0.0330	2.74	0.967	0.0325
86	20.2	0.090	3.95(−3)	13.9	0.157	9.75(−3)	11.9	0.152	6.30(−3)	3.04	0.900	0.0355	2.81	0.964	0.0362
90	22.7	0.080	4.53(−3)	15.5	0.159	1.40(−2)	12.9	0.170	8.10(−3)	3.22	0.874	0.0582	2.92	0.950	0.0497

TABLE V.V. Theoretical average numbers S_{ij} of M_j holes that arise in the *first step* of the decay of an M_i hole, and theoretical M-shell Coster-Kronig probability f_{45}. After McGuire (1972).

Z	S_{12}	S_{13}	S_{14}	S_{15}	S_{23}	S_{24}	S_{25}	S_{34}	S_{35}	f_{45}
20	0.328	0.655								
22	0.319	0.639	0.314	0.471		1.057	0.672	0.509	1.220	
23	0.315	0.631	0.335	0.503		1.089	0.820	0.558	1.280	
24	0.319	0.638	0.397	0.596		1.123	0.834	0.612	1.342	
25	0.312	0.623	0.357	0.538		1.108	0.797	0.589	1.317	
26	0.311	0.621	0.371	0.556		1.116	0.815	0.600	1.329	
27	0.308	0.616	0.376	0.564		1.120	0.817	0.602	1.335	
28	0.307	0.614	0.381	0.566		1.122	0.827	0.609	1.341	
29	0.304	0.608	0.406	0.610		1.133	0.850	0.623	1.360	
30	0.283	0.566	0.374	0.561		1.107	0.811	0.597	1.320	
32	0.249	0.522	0.273	0.409		1.085	0.786	0.580	1.292	
36	0.270	0.540	0.086	0.127		0.919	0.516	0.395	1.039	
40	0.278	0.475	0.108	0.163	0.032	0.591	0.309	0.252	0.677	
44	0.305	0.457	0.065	0.124	0.067	0.550	0.283	0.236	0.672	
47	0.343	0.461	0.065	0.097	0.073	.570	0.258	0.223	0.689	
50	0.315	0.475	0.067	0.101	0.016	0.604	0.252	0.213	0.678	
54	0.238	0.505	0.081	0.122	0.031	0.612	0.233	0.206	0.688	
57	0.195	0.506	0.094	0.140	0.034	0.557	0.282	0.198	0.678	
60	0.236	0.489	0.092	0.128	0.057	0.644	0.172	0.174	0.712	0.267
63	0.338	0.485	0.070	0.100	0.062	0.514	0.137	0.165	0.720	0.369
67	0.266	0.527	0.061	0.090	0.106	0.667	0.120	0.145	0.751	0.408
70	0.272	0.525	0.056	0.091	0.116	0.680	0.105	0.141	0.761	0.479
73	0.197	0.561	0.065	0.115	0.114	0.674	0.106	0.082	0.810	0.411
76	0.161	0.594	0.067	0.109	0.107	0.684	0.098	0.106	0.764	0.418
79	0.148	0.594	0.067	0.112	0.114	0.673	0.095	0.114	0.782	0.046
83	0.109	0.650	0.065	0.095	0.103	0.662	0.083	0.094	0.750	0.035
86	0.143	0.593	0.069	0.100	0.128	0.610	0.093	0.072	0.768	0.065
90	0.072	0.690	0.063	0.091	0.116	0.623	0.088	0.097	0.725	0.066

competing Auger transitions M–NY, M–XY, and x-ray transitions M–N, M–Y.[11] Karttunen *et al.* (1971) have found that, for $Z=93$ and 96, approximately 97% of all $M_{1,2}$ and M_3 vacancies undergo Coster–Kronig shifts to higher M subshells before they are filled from higher shells. Radiative transitions therefore lead mainly to the M_4 and M_5 subshells; $M_{4,5}$–MN Coster–Kronig transitions are energetically impossible. Hence, measured mean M-shell fluorescence yields $\bar{\omega}_M$ essentially constitute weighted averages of $\omega_4{}^M$ and $\omega_5{}^M$ and are quite insensitive to the initial M-subshell vacancy distributions.

Karttunen, Freund, and Fink (1971) have compared experimental M-shell results (Table V.III) with theoretical $M_{4,5}$ radiative widths (Rosner and Bhalla, 1970) and found the $M_{4,5}$ radiationless width to be essentially constant over the range $76<Z<96$.

As this review was being closed, McGuire (1971c) completed the first theoretical calculation of M-subshell yields. He employed the same method that he had previously applied to the calculation of K- and L-shell yields (McGuire 1971a); this is discussed in Sec. 2.2.3 Results for M-subshell widths, Auger, and fluorescence yields are listed in Table V.IV.

One aspect of M-shell Coster–Kronig transitions that deserves special attention is pointed out by McGuire: There exists the possibility, in certain regions of the Periodic Table, that a hole in the ith subshell can lead to at least two holes in higher subshells. McGuire calls such M_i–M_jM_k processes "*super Coster–Kronig transitions*" and calculates a quantity S_{ij}, defined as the average number of M_j holes that arise in the *first*

[11] A similar observation has been made by Mehlhorn (1965) at low Z: M–MN Coster–Kronig transitions are found to dominate in the de-excitation of Kr M_2 and M_3 subshells.

step in the decay of an M_i hole. Values of S_{ij}, as well as of the theoretical M_4–M_5X Coster–Kronig probabilities f_{45}, are listed in Table V.V.

Detailed comparison of theoretical M-shell results with experiment will have to await the availability of new high-resolution data as may be expected, possibly, from electron spectrometry techniques.

CONCLUDING REMARKS

An attempt has been made in this review to include references to pertinent literature published through 1 July 1971. It was possible to include a few additional items that came to our attention subsequently. Data have been quoted only if they were published in numerical form, i.e., no numbers were scaled from graphs.

Throughout this work, we deal with the deexcitation of atoms that initially are singly ionized in an inner shell. The decay of atoms with multiple inner-shell vacancies and of highly ionized atoms with single inner vacancies poses a wealth of interesting and complex questions that remain unanswered as yet; it can well be expected that experimental and theoretical work in the next several years will be directed toward this subject. Other problems that clearly call for further work relate to Auger transition-probability ratios and to refined measurements and calculations of radiative transition probabilities. Relativistic calculations of radiationless transition probabilities and fluorescence yields very much need to be extended; such calculations involve heavy demands on computer time and may have to await the advent of larger and faster computers before becoming economically feasible.

Theoretical work at this time extends from the K through the M subshells, while experimental information still is confined mostly to the K and L shells. Further development of experimental techniques, including a wider application of electron spectrometry, and refinement of theoretical approaches (including more detailed consideration of many-body effects) can be expected to lead to work on outer atomic shells, where chemical effects become important and the subject of this article begins to merge with molecular physics.

Many aspects of the current status of the field, and of its perspectives, have been discussed at the first International Conference on Inner-Shell Ionization Phenomena, held in Atlanta in 1972; the Proceedings of the Conference will be published by North-Holland.

We wish to thank the many colleagues who assisted in the preparation of this review by providing us with preprints and informal reports on work in progress. Furthermore, we are indebted to G. Bambynek of Leverkusen, Germany, and D. Reher of the Bureau Central de Mesures Nucléaires, Geel, Belgium, for computations related to the fit of ω_K. Finally, our very special thanks go to Mrs. Carol Tinling of the NASA—Ames Research Center for her expert editorial assistance.

GLOSSARY

Symbol	Definition	Dimensions	Section where first used
Primary vacancies	Primary vacancies in a subshell X_i are vacancies which, when they first appear in the X shell, are in the X_i subshell; Coster–Kronig transitions may then alter this primary distribution		1.4.1
A_{22}	Directional correlation coefficient		4.5.5
a_i^X	Auger yield of the X_i subshell; the probability that a vacancy in subshell X_i is filled in a *radiationless* electron transition from another principal shell		1.4.3
a_K	The (unique) Auger yield of the K level		3.1
$\bar{a}_X$	The average Auger yield of excited atoms having some definite distribution of vacancies in the X shell		1.4.3
b_i	The probability that a K–LL transition produces an L_i-subshell vacancy as a primary vacancy		4.4
C	Counting rate; the number of photons (or particles) detected per unit time	time^{-1}	1.4.4 iv
C_x	Counting rate of events x; the number of photons (or particles) x detected per unit time	time^{-1}	1.4.4 iv
$C_{x(y)}$	x coincidence counting rate gated by y. The number of photons or particles x detected in coincidence with detected events y, per unit time	time^{-1}	1.4.4 iv
D	Disintegration rate; the number of disintegration events per unit time	time^{-1}	1.4.4 iv

Symbol	Definition	Dimensions	Section where first used
f	Attenuation factor for material between (but excluding) source and detector		1.4.4 iv
f_{ij}^X	Coster–Kronig transition probability. The probability that a vacancy in subshell X_i is filled by an electron from subshell j of the same shell X		1.4.2
$f_{ij}^X(A)$	The radiationless component of the Coster–Kronig transition probability. The probability that a vacancy in the subshell X_i is shifted in a *radiationless* transition to the subshell j of the same shell X [cf. $f_{ij}^X(R)$].		1.4.4
$f_{ij}^X(R)$	The radiative component of the Coster–Kronig transition probability. The probability that a vacancy in the subshell X_i is shifted in a *radiative* transition to the subshell j of the same shell X [cf. $f_{ij}^X(A)$]		1.4.4
f_Ω	Finite-solid-angle correction to directional-correlation correction term		4.5.5
g	Subscript designating a particular radiation used for gating in a coincidence experiment		4.5
$\hbar^2/me^2$	Atomic unit of length; 0.52918×10^{-8} cm; radius of the first Bohr orbit of hydrogen (Bohr radius)	length	2.3.1
$\hbar^3/me^4$	Atomic unit of time; 2.4189×10^{-17} sec; reciprocal of the circular frequency of the electron in the first Bohr orbit of hydrogen	time	2.3.1
I	Intensity; the number of photons (or particles) emitted in a source or incident on a sample per unit time	time^{-1}	1.4.4 iv
I_A	The number of nonradiative de-excitation events per unit time	time^{-1}	3.1.1
I_e	The number of conversion electrons emitted per unit time	time^{-1}	3.1.2
I, I_i, I_f	Total angular momenta of the intermediate, initial, and final states in a pair of transitions	mass length^2 time^{-1}	4.5.5
I_i^X	The number of characteristic x rays emitted in transitions to the X_i subshell from outside the X shell per unit time	time^{-1}	1.4.1
I_R	The number of radiative events per unit time	time^{-1}	3.1.1
I_{RA}	The number of radiative or nonradiative events per unit time	time^{-1}	3.1.2
I_X	The number of characteristic X-shell photons emitted per unit time	time^{-1}	1.4.1
$I(x)$	Intensity of radiation x per unit time	time^{-1}	4.4
i, j	Integers denoting an individual subshell; numbered generally from most to least tightly bound		1.4.1
i, j, k	Integers		
k	The number of subshells of a shell		1.4.1
$me^4/\hbar^2$	Atomic unit of energy 27.212 eV; potential energy of the electron in the first Bohr orbit of hydrogen	mass length^2 time^{-2}	2.3.1
N_i^X	The number of *primary* vacancies in the X_i subshell relative to the total number of primary vacancies in the X shell (cf. n_X)		1.4.1
n_i^X	The number of primary vacancies in the X_i subshell		1.4.1
n_X	The total number of *primary* vacancies in the X shell		1.4.1
n_{X_i}	The number of vacancies created by direct ionization of the X_i subshell		5.1
$n_{X_iY_j}$	The number of *primary* Y_j-subshell vacancies directly created in the filling of an X_i-subshell vacancy, averaged over the possible modes of filling the X_i vacancy, per X_i vacancy		4.4
$\bar{n}_{X_iY_j}$	The number of *primary* Y_j-subshell vacancies created directly or via cascades, in the filling of an X_i-subshell vacancy, averaged over the possible modes of filling the X_i vacancy, per X_i vacancy		4.4
$n_{X_iY_j}(R)$ $n_{X_iY_j}(A)$ $n_{X_iY_j}(\mathrm{CK})$	The number of vacancies due to radiative (R), Auger (A), or Coster–Kronig (CK) transitions which are included in $n_{X_iY_j}$		4.4

Symbol	Definition	Dimensions	Section where first used
P_X	The fraction of nuclear disintegrations which proceed by capture of X-shell electrons		3.1.2
p, p_X	Probability of producing a vacancy in the X shell in some specified decay process. In this paper, p_X refers to the L shell and the subscript is omitted		4.5
$R_{A\beta}$	Ratio of Auger-electron to β-particle intensities		3.1.2
$R_{R\beta}$	Ratio of K x-ray to β-particle intensities		3.1.2
s_1	The intensity ratio $I_{L\gamma}$: $I_{L\beta}$ for x rays emitted in filling L_1 vacancies		4.5
s_2	The intensity ratio $I_{L\gamma}$: $(I_{L\eta}+I_{L\beta})$ for x rays emitted in filling L_2 vacancies		4.5
s_3	The intensity ratio $I_{L\beta}$: $(I_{Ll}+I_{L\alpha})$ for x rays emitted in filling L_3 vacancies		4.5
V_i^X	The relative number of vacancies in the X_i subshell, after the primary vacancy numbers N_i^X have been altered by the Coster–Kronig transitions.		1.4.2
$W(\theta)$	Directional correlation function		4.5.5
w	Transition probability	time^{-1}	2.1.1
X	Represents K, L, M, N, $\cdots$ to denote one of the principal atomic shells		1.4.1
XYZ	The notation XYZ or X–YZ (where X, Y, and Z can be K, L, M, N, $\cdots$, referring to the principal atomic shells) denotes the nonradiative transition of a vacancy from shell X to shell Y, with production of another vacancy in shell Z. The notation K–LX, for example, excludes K–LL. (Any of the shell designations may be subscripted.)		3.1.2
Z	Atomic number		2.2.1
Z^*	Z^*e is the effective nuclear charge		2.2.1
α_t	Total internal conversion coefficient; the ratio of internal conversion events to γ-decay events		4.3.2
α_{X_i}	Internal conversion coefficient; the ratio of internal conversion events in the X_i subshell to γ-ray decay events		4.3.2
Γ	Width of an energy level (state)	mass length^2 time^{-2}	1.4
Γ_A, Γ_A^X	Radiationless partial width of a level	mass length^2 time^{-2}	1.4
Γ_R, Γ_R^X	Radiative partial width of a level	mass length^2 time^{-2}	1.4
$\Delta\Omega$	Fractional solid angle: $1/4\pi\times$(solid angle in steradians)		1.4.4 iv
ϵ_0	Intrinsic detector efficiency		1.4.4 iv
ϵ_X	Over-all efficiency for detecting radiation X		3.1.2
ν_i^X	Probability that any filling of a *primary* X_i-subshell vacancy leads to emission of any X-shell characteristic x ray		1.4.2
τ	Mean life of a level (state)	time	1.4
ω	Fluorescence yield. The probability that a vacancy in an atomic shell or subshell is filled in a *radiative* electron transition from another principal shell. Unless otherwise stated, only a single vacancy is present		1.4
ω	Circular frequency of radiation (in Sec. 2)	time^{-1}	2.1.2
ω_i^X	Fluorescence yield of X_i sublevel; fluorescence yield of state having an X_i vacancy		1.4.1
ω_K	The (unique) fluorescence yield of the K level		1.4
$\bar{\omega}_X$	Average fluorescence yield of excited atoms having some definite distribution of vacancies in the X shell		1.4.1
ω_{XY}	The average fluorescence yield of the Y shell when the subshell vacancy numbers are those produced by $X\rightarrow Y$ transitions		1.4.4

IDENTIFICATION OF CHARACTERISTIC X RAYS AFTER BEARDEN (1967a)

K Series		*L* Series		*M* Series	
α_2	KL_2	β_4	L_1M_2	γ	M_3N_5
α_1	KL_3	β_3	L_1M_3		
		β_{10}	L_1M_4	ζ_2	M_4N_2
		β_9	L_1M_5	β	M_4N_6
		γ_2	L_1N_2		
		γ_3	L_1N_3		
		γ_4	$L_1O_{2,3}$		
β_3	KM_2			ζ_1	M_5N_3
β_1	KM_3	η	L_2M_1	α_2	M_5N_6
β_5	$KM_{4,5}$	β_1	L_2M_4	α_1	M_5N_7
β_2	$KN_{2,3}$	γ_5	L_2N_1		
β_4	$KN_{4,5}$	γ_1	L_2N_4		
		ν	L_2N_6		
		γ_8	L_2O_1		
		γ_6	L_2O_4		
		l	L_3M_1		
		t	L_3M_2		
		s	L_3M_3		
		α_2	L_3M_4		
		α_1	L_3M_5		
		β_6	L_3N_1		
		β_{15}	L_3N_4		
		β_2	L_3N_5		
		u	$L_3N_{6,7}$		
		β_7	L_3O_1		
		β_5	$L_3O_{4,5}$		

REFERENCES

Åberg, T., 1968, Phys. Letters **26A,** 515.
——, 1969, Ann. Acad. Sci. Tenn. **AV1,** 308, 1.
Abramowitz, M., and I. E. Stegun, eds., 1964, *Handbook of Mathematical Functions.* Applied Mathematics Series 55 (National Bureau of Standards, Washington, D.C.)
Adamson, A. M., M. Duquesne, and R. Foucher, 1962, J. Phys. Radium **23,** 580.
Akalaev, G. G., N. A. Vatanov, and P. S. Samoilov, 1964, Izv. Akad. Nauk SSSR, Ser. Fiz. **28,** 1259 [Bull. Acad. Sci. USSR, Phys. Ser. **28,** 1158 (1964)].
Albridge, R. G., and J. M. Hollander, 1961, Nucl. Phys. **27,** 554.
Allison, S. K., 1933, Phys. Rev. **44,** 63.
Amusia, M. Ya., M. P. Kazachkov, N. A. Cherepkov, and L. V. Chernysheva, 1972, Phys. Letters **39A,** 93; M. Ya. Amusia, N.A. Cherepkov, and L. V. Chernysheva, JETP Zh. Eksp. i teor. Fiz. **60,** 160 (1971).
Arends, E., 1935, Ann. Phys. **22,** 281.
Arnous, E., and W. Heitler, 1953, Proc. Roy. Soc. (London) **A220,** 290.
Asaad, W. N., 1959, Proc. Roy. Soc. (London) **A249,** 555.
——, 1960, Proc. Phys. Soc (London) **76,** 641.
——, 1963a, Nucl. Phys. **44,** 399.
——, 1963b, Nucl. Phys. **44,** 415.
——, 1965a, Nucl. Phys. **63,** 337.
——, 1965b, Nucl. Phys. **66,** 494.
——, 1967, Z. Phys. **203,** 362.
Asaad, W. N., and E. H. S. Burhop, 1958, Proc. Phys. Soc. (London) **71,** 369.
——, and W. Mehlhorn, 1968, Z. Phys. **217,** 304.
Auger, P., 1925, J. Phys. Radium **6,** 205.
——, 1926, Ann. Phys. (Paris) **6,** 183.
Azuma, T., 1954, J. Phys. Soc. (Japan) **9,** 443.
Babushkin, F. A., 1964, Acta Phys. Polon. **25,** 749.
——, 1965a, Opt. Spectrosk. **19,** 3 [Opt. Spectrosc. **19,** 1 (1965)].
——, 1965b, Opt. Spectrosk. **19,** 978 [Opt. Spectrosc. **19,** 545 (1965).]
——, 1967, Acta Phys. Polon. **31,** 459.
Backhurst, I., 1936, Phil. Mag. **22,** 737.
Bahcall, J. N., 1962, Phys. Rev. Letters **9,** 500.
——, 1963a, Phys. Rev. **129,** 2683.
——, 1963b, Phys. Rev. **131,** 1756.
——, 1963c, Phys. Rev. **132,** 362.
——, 1965, Nucl. Phys. **71,** 267.
Bailey, L. E., and J. B. Swedlund, 1967, Phys. Rev. **158,** 6.
Balderston, M., 1926, Phys. Rev. **27,** 696.
Bambynek, W., 1965, Europäische Atomgemeinschaft EURATOM Report EUR 2632.d.
——, 1967a, Z. Phys. **206,** 66.
——, 1967b, Standardization of Radionuclides (International Atomic Energy Agency, Vienna), p. 373.
——, E. de Roost, and E. Funck, 1968, in *Proceedings of the Conference on Electron Capture and Higher-Order Processes in Nuclear Decay,* edited by D. Berényi (Eötvös Lóránd Physical Society, Budapest), p. 253.
——, O. Lerch, and A. Spernol, 1966, Nucl. Inst. Methods **39,** 104.
——, and D. Reher, 1967, Int. J. Appl. Rad. Isotopes **18,** 19.
——, and D. Reher, 1968, Z. Phys. **214,** 374.
——, and D. Reher, 1970, Z. Phys. **238,** 49.
——, and D. Reher, 1972, Z. Phys. (in press).
Band, I. M., L. N. Zyrianova, and T. Chen-Zhui, 1956, Izv. Akad. Nauk SSSR, Ser. Fiz. **20,** 1387 [Bull. Acad. Sci. USSR. Phys. **20,** 1269 (1956)].
——, L. N. Zyrianova, and Y. P. Suslov, 1958, Izv. Akad. Nauk SSSR, Ser. Fiz. **22,** 952, [Bull. Acad. Sci. USSR, Phys. **22,** 943 (1958)].
Bang, J., and J. M. Hansteen, 1959, Kgl. Dan. Vidensk. Selsk., Mat.-Fys. Medd. **31,** 13.
Barkla, C. C., 1918, Phil. Trans. Roy. Soc. (London), Ser. **A217,** 315.
Barkla, C. C., and A. J. Philpot, 1913, Phil. Mag. **25,** 832.
Barton, G. W., Jr., 1950, Univ Calif. Lawrence Radiation Laboratory Report UCRL–670 (unpublished).
——, H. P. Robinson, and I. Perlman, 1951, Phys. Rev. **81,** 208.
Bashilov, A. A., and L. C. Chervinskaya, 1964, Vestn. Leningrad Univ. Ser. Fiz. KHIM. **4,** 71.
Bearden, J. A., 1966, J. Appl. Phys. **37,** 1681.
——, 1967, Rev. Mod. Phys. **39,** 78.
——, and A. F. Burr, 1967, Rev. Mod. Phys. **39,** 125.
——, and T. M. Synder, 1941, Phys. Rev. **59,** 162.
Beatty, R. T., 1911, Proc. Roy. Soc. (London) **A85,** 230.
Beeman, W. W., and H. Friedman, 1939, Phys. Rev. **56,** 392.
Behrens, H., and W. Bühring, 1968, in Berényi, p. 61.
——, and J. Jänecke, 1969, Landolt-Börnstein, *Numerical Data and Functional Relationships in Science and Technology,* New Series, Group I, Vol. 4: *Numerical Tables for β-Decay and Electron Capture* (Springer–Verlag, Berlin).
Bellicard, J. B., A. Moussa, and S. K. Haynes, 1956, Nucl. Phys. **3,** 307.
——, A. Moussa, and S. K. Haynes, 1957, J. Phys. Radium **18,** 115.
Benoist, P., 1954, C. R. Acad. Sci. **238,** 1498.
Berényi, D., ed., 1968, *Proceedings of the Conference on Electron Capture and Higher-Order Processes in Nuclear Decay* (Eötvös Lóránd Physical Society, Budapest).
Bergström, I., and C. Nordling, 1965, in Siegbahn, p. 1523.
——, and S. Thulin, 1950, Phys. Rev. **79,** 538.
Berkey, D. K., 1934, Phys. Rev. **45,** 437.
Bertolini, G., A. Bisi, E. Lazarrini, and L. Zappa, 1954, Nuovo Cimento **11,** 539.
——, A. Bisi, and L. Zappa, 1953, Nuovo Cimento **10,** 1424.

Bertrand, F., G. Charpak, and F. Suzor, 1959, J. Phys. Radium **20,** 462; **20,** 956.
Beste, H. W., 1968, Z. Phys. **213,** 333.
Bethe, H. A., and E. E. Salpeter, 1957, *Quantum Mechanics of One- and Two-Electron Atoms* (Springer-Verlag, Berlin).
Bhalla, C. P., 1967, Phys. Rev. **157,** 1136.
——, 1970a, J. Phys. **B3,** L9.
——, 1970b, Phys. Rev. **A2,** 722.
——, 1970c, J. Phys. **B3,** 916.
——, 1970d, Phys. Rev. **A2,** 2575.
——, and D. J. Ramsdale, 1970a, J. Phys. **B3,** L14.
——, and D. J. Ramsdale, 1970b, Z. Phys. **239,** 95.
——, D. J. Ramsdale, and H. R. Rosner, 1970a, Phys. Letters **31A,** 122.
——, H. R. Rosner, and D. J. Ramsdale, 1970b, J. Phys. **B3,** 1232.
——, A. R. Rosner, and D. J. Ramsdale, 1970c, J. Phys. **B3,** 1232.
Biedenharn, L. C., and N. V. V. J. Swamy, 1964, Phys. Rev. **133,** B1353.
Bisi, A., E. Germagnoli, and L. Zappa, 1956a. Nucl. Phys. **1,** 593.
——, L. Zappa, and L. Zimma, 1956b, Nuovo Cimento **4,** 307.
Bissinger, G. A., J. M. Joyce, E. J. Ludwig, N. S. McEver, and S. M. Shafroth, 1970, Phys. Rev. A**1,** 841.
Blauth, E., 1957, Z. Phys. **147,** 228.
Blokhin, M. A., 1957, *The Physics of X Rays* (State Publishing House of Technical-Theoretical Literature, Moscow), 2nd ed. [English transl.: U.S.A.E.C. Report AEC-TR-4502. German transl.: *Physik der Röntgenstrahlen* (VEB Verlag Technik, Berlin, 1957)].
Boehm, F., 1970, Phys. Letters **33A,** 417.
Booth, E., L. Madansky, and F. Rasetti, 1956, Phys. Rev. **102** 800.
Bothe, W., 1925, Phys. Z. **26,** 410.
Bower, J. C., 1936, Proc. Roy. Soc. (London) **A157,** 662.
Boyer, P., and J. L. Barat, 1968, Nucl. Phys. **A115,** 521.
Brabets, V., K. Gromov, B. Dzhelepov, A. Dmitriev, and V. Morozov, 1959, Izv. Akad. Nauk. SSSR, Ser. Fiz. **23,** 812 [Bull. Acad. Sci. USSR, Phys. Ser., **23,** 805 (1959)].
Brandt, W., 1972, in *Proceedings of the International Conference on Inner-Shell Ionization Phenomena.* (North-Holland Publ. Co., Amsterdam, in press).
——, and R. Laubert, 1969, Phys. Rev. **178,** 225.
Breit, G., and F. L. Yost, 1935a, Phys. Rev. **47,** 508.
——, and F. L. Yost, 1935b, Phys. Rev. **48,** 203.
Brogren, G., 1954, Ark. Fys. **8,** 391.
Brown, G. M., C. H. Emeleus, J. G. Holland, and R. Phillips, 1970, Science **167,** 601.
Browne, C. I., 1952, Univ. Calif. Lawrence Radiation Laboratory Report 1766 (unpublished).
——, J. O. Rasmussen, J. P. Surls, and D. F. Martin, 1952, Phys. Rev. **85,** 146.
Broyles, C. D., D. A. Thomas, and S. K. Haynes, 1953, Phys. Rev. **89,** 715.
Brysk, H., and M. E. Rose, 1958, Rev. Mod. Phys. **30,** 1169.
Burde, J., and S. G. Cohen, 1956, Phys. Rev. **104,** 1085.
Burford, A. O., and S. K. Haynes, 1958, Bull. Amer. Phys. Soc. **3,** 208.
Burhop, E. H. S., 1935, Proc. Roy. Soc. (London) **A148,** 272.
——, 1952, *The Auger Effect and Other Radiationless Transitions* (Cambridge U. P., Cambridge).
——, 1955, J. Phys. Radium **16,** 625.
——, and W. N. Asaad, 1962, "The Auger Effect" in *Advances in Atomic and Molecular Physics,* edited D. R. Bates (Academic, New York, in press), Vol. 8.
Byrne, J., W. Gelletly, M. A. S. Ross, and F. Shaikh, 1968, Phys. Rev. **170,** 80.
——, and N. Howarth, 1970, J. Phys. **B3,** 280.
Callan, E. J., 1961, Phys. Rev. **124,** 793.
——, 1963a, in *Role of Atomic Electrons in Nuclear Transformations, Proceedings of International Conference* (Nuclear Energy Information Center, Warsaw), Vol. 3, p. 398.
——, 1963b, in *Role of Atomic Electrons in Nuclear Transformations, Proceedings of International Conference* (Nuclear Energy Information Center, Warsaw), Vol. 3, p. 419.
——, 1963c, Rev. Mod. Phys. **35,** 524.
——, P. Nikolai, and W. L. McDavid, 1964, in *Atomic Collision Processes,* edited by M. R. C. McDowell (North-Holland Publ. Co., Amsterdam).
——, 1969, private communication.
Campbell, J. L., R. J. Goble, and H. J. Smith, 1970, Nucl. Inst. Methods **82,** 183.
Campion, P. J., 1959, Int. J. Appl. Rad. Isotopes **4,** 232.
Carlson, T. A., C. W. Nestor, Jr., F. B. Malik, and T. C. Tucker, 1969, Nucl. Phys. **A135,** 57.
Casey, W. R., and R. C. Albridge, 1969, Z. Phys. **219,** 216.
Catz, A. L., and C. D. Coryell, 1969, Bull. Amer. Phys. Soc. **14,** 85.
Catz, A. L., 1970, Phys. Rev. Letters, **24,** 127; Phys. Rev. **A2,** 634.
——, and E. S. Macias, 1971a, Phys. Rev. **A3,** 849.
——, and E. S. Macias, 1971b, Bull. Amer. Phys. Soc. **16,** 126.
Cauchois, Y., 1932, J. Phys. Radium **3,** 320.
Chase, R. L., H. P. Kelly, and H. S. Kohler, 1971, Phys. Rev. **A3,** 1550.
Chattarji, D., and B. Talukdar, 1968, Phys. Rev. **174,** 44.
Chen, M. H., B. Crasemann, and V. O. Kostroun, 1971a, Phys. Rev. **A4,** 1.
——, B. Crasemann, P. Venugopala Rao, J. M. Palms, and R. E. Wood, 1971b, Phys. Rev. **A4,** 846.
Chew, W., 1972, Thesis, Georgia Institute of Technology (unpublished).
Chu, Y. Y., M. L. Perlman, P. F. Dittner, and C. E. Bemis, Jr., 1972, Phys. Rev. **A5,** 67.
Cole, G. D., and A. Mukerji, 1965, Bull. Amer. Phys. Soc. **10,** 262.
Compton, A. H., 1929, Phil. Mag. **8,** 961.
——, and S. K. Allison, 1935, *X Rays in Theory and Experiment* (Van Nostrand, Princeton).
Condon, E. U., and G. H. Shortley, 1953, *The Theory of Atomic Spectra* (Cambridge U. P., Cambridge).
Coster, D., and R. de L. Kronig, 1935, Physica **2,** 13.
Coulson, C. A., and F. A. Gianturco, 1968, J. Phys. **B1,** 605.
Cowan, R. D., A. C. Larson, D. Liberman, J. B. Mann, and J. Waber, 1966, Phys. Rev. **144,** 5.
Crasemann, B., M. H. Chen, and V. O. Kostroun, 1971, Phys. Rev. **A4,** 2161.
Crone, W., 1936, Ann. Phys. **5,** 27, 405.
Crow, E. L., F. A. Davis, and M. W. Maxfield, 1960, *Statistical Manual* (Dover, New York).
Curran, C. S., J. Angus, and A. L. Cockroft, 1949, Phil. Mag. **40,** 36.
Davidson, F. D., and R. W. G. Wyckoff, 1962, J. Appl. Phys. **33,** 3528.
Day, P. P., 1957, Phys. Rev **97,** 689.
Deodhar, G. B., and P. P. Varma, 1969, J. Phys. **B2,** 410.
de Pinho, A. G., 1971, Phys. Rev. **A3,** 905.
de-Shalit, A., and I. Talmi, 1963, *Nuclear Shell Theory* (Academic, New York).
Deslattes, R. D., 1959, Thesis, Johns Hopkins University (unpublished).
Dick, C. E , and A. C. Lucas, 1970, Phys. Rev. **A2,** 580.
Dingus, R. S., and N. Rud, 1968, Nucl. Phys. **A117,** 73.
Dionisio, J. S., 1964, Ann. Phys. (Paris) **9,** 29.
Dobrilović, L. J., V. Voljen, Dj. Bek-Uzarov, K. Buraei, and A. Milojević, 1970, in *Proceedings of the Fifth Congress of Mathematicians, Physicists and Astronomers of Yugoslavia, Ohrid.*
——, 1972, in *Proceedings of the International Conference on Inner-Shell Ionization Phenomena,* 1972 (North-Holland Publ. Co., Amsterdam, in press).
Dragoun, O., H. C. Pauli, and F. Schmutzler, 1969, Nuclear Data **A6,** 235.
Drever, R. W. P., and A. Moljk, 1957, Phil. Mag. **2,** 427.
D'Yakov, B. B., and I. M. Rogachev, 1962, Izv. Akad. Nauk SSSR, Ser. Fiz. **26,** 191 [Bull. Acad. Sci. USSR, Phys. Ser., **26,** 191 (1962)].
Ebert, P. J., and V. W. Slivinsky, 1969, Phys. Rev. **188,** 1.
Ellis, C. D., 1933, Proc. Roy. Soc. (London) **A139,** 336.
Erman, P., J. Rossi. E. C. O. Bonacalza, and J. Miskel, 1964, Ark. Fys. **26,** 135.
——, and Z. Sujkowski, 1961, Ark Fys. **20,** 209.
Ewan, G. T., 1952, Thesis, University of Edinburgh (unpublished).
Faessler, A., E. Huster, O. Kraft, and F. Krahn, 1970, Z. Phys. **238,** 352.
Fairbrother, J. A. V., D. G. Parkyn, B. M. O'Connor, 1957, Proc. Phys. Soc. (London) **70,** 262.
Falk-Vairant, P., J. Teillac, G. Vallados, and P. Benoist, 1954, C. R. Acad. Sci. **238,** 1409.

Fano, U., and J. W. Cooper, 1968, Rev. Mod. Phys. **40,** 441.
Ferentz, M., and N. Rosenzweig, 1955, Argonne National Laboratory Report ANL-5324 (unpublished).
Ferreira, J. G., 1955, C. R. Acad. Sci. **241,** 1929.
——, M. O. Costa, M. I. Gonçalves, L. Salgueiro, 1965, J. Phys. (Paris) **26,** 5.
Fink, R. W., 1957, Phys. Rev. **106,** 266.
——, 1968, Nucl. Phys. **A110,** 379.
——, and H.-U. Freund, 1971, Phys. Rev. **C3,** 1701.
——, R. C. Jopson, Hans Mark, and C. D. Swift, 1966, Rev. Mod. Phys. **38,** 513.
——, and B. L. Robinson, 1955, Phys. Rev. **98,** 1293.
Fitzgerald, R., and P. Gantzel, 1970, in *Energy Dispersion X-Ray Analysis*, edited by J. B. Wheeler (Amer. Soc. Testing Matls. Pub. STP-485, Philadelphia).
Flammersfeld, A., 1939, Z. Phys. **114,** 227.
Foin, C., A. Gizon, and J. Oms, 1968, Nucl. Phys. **A113,** 241.
Forrest, R. N., and H. T. Easterday, 1958, Phys. Rev. **112,** 950.
Frauenfelder, H., and R. M. Steffen, 1965, in Siegbahn, p. 997.
Frey, W. F., R. E. Johnston, and J. I. Hopkins, 1959, Phys. Rev. **113,** 1057.
Freund, H.-U., and R. W. Fink, 1969, Phys. Rev. **178,** 1952.
——, H. Genz, J. B. Siberts, and R. W. Fink, 1969a, Nucl. Phys. **A138,** 200.
——, J. S. Hansen, E. Karttunen, and R. W. Fink, 1969b, in *Proceedings of the International Conference on Radioactivity in Nuclear Spectroscopy*, edited by J. H. Hamilton (unpublished).
Frilley, M., G. B. Gokhale, and M. Valaderas, 1951, C. R. Acad. Sci. **23,** 157.
Froese, C., 1966, *Hartree-Fock Parameters for the Atoms from Helium to Radon*. Univ. of British Columbia (unpublished).
Garcia, J. D., 1970a, Phys. Rev. **A1,** 280.
——, 1970b, Phys. Rev. **A1,** 1402.
Garfinkel, S. B., and G. R. Newbery, 1968, International Commission on Radiation Units and Measurements, Technical Report 12 (unpublished).
Garstang, R. H., 1962, in *Atomic and Molecular Processes*, edited by D. R. Bates (Academic, New York), p. 1.
Gaunt, J. A., 1930, Phil. Trans. **A229,** 163.
Gaspar, R., 1954, Acta Phys. Acad. Sci. Hung, **3,** 263.
Gautier, A. A., 1969, Thesis, Cornell University (unpublished).
Geoffrion, G., F. Bonenfant, and G. Nadeau, 1959, U.S. Air Force Office of Scientific Research, Research Report TR-59-145 (unpublished).
Gehrling, V., J. W. Hammer, and K.-W. Hoffmann, 1971, Z. Phys. **246,** 376.
Geiger, J. S., R. L. Graham, and J. S. Merritt, 1963, Nucl. Phys. **48,** 97.
Germain, L. S., 1950, Phys. Rev. **80** 937.
Gil, F. B., C. F. Miranda, J. S. Lobo, and J. G. Ferreira, 1965, Port. Phys. **4,** 17.
Gizon, J., A. Gizon, and J. Valentin, 1968, Nucl. Phys. **A120,** 321.
Glupe, G., 1971, Ph.D. Thesis, University of Münster (unpublished).
——, and W. Mehlhorn, Phys. Letters **25A,** 247 (1967).
Godeau, C., 1961, U.S. National Bureau af Standards Technical Note 91 (unpublished).
Gokhale, B. G., 1952, Ann. Phys. (Paris) **7,** 852.
——, and S. N. Shukla, 1970, J. Phys. **B3,** 438.
Gold, R., and E. F. Bennett, 1965, Phys. Rev. **147,** 201.
Goldberg, M., 1962, Ann. Phys. (Paris) **7,** 329.
Gordon, W., 1928, Z. Phys. **48,** 180.
Goulding, F. S., and Y. Stone, 1970, Science **170,** 280.
Graham, R. L., I. Bergström, and F. Brown, 1962, Nucl. Phys. **39,** 107.
——, F. Brown, G. T. Ewan, and J. Uhler, 1961, Can. J. Phys. **39,** 1086 (and private communication).
——, and J. S. Merritt, 1961, Can. J. Phys. **39** 1058 (and private communication).
Gray, P. R., 1956, Phys. Rev. **101,** 1306.
Grigor'ev, O. I., and N. S. Shimanskaya, 1966, Izv. Akad. Nauk SSSR, Ser. Fiz. **30,** 459 [Bull. Acad. Sci. USSR, Phys. Ser., **30,** 466 (1966)].
Grotheer, H. H., J. W. Hammer, and K. W. Hoffmann, 1969, Z. Phys. **225,** 293.
Gryzinski, M., 1965, Phys. Rev. **138,** A336.
Guttman, A. J., and W. Wagenfeld, 1967, Acta Crystallogr. **22,** (3), 334.
Haas, M., 1932, Ann. Phys. **5,** 16, 473.
Hagedoorn, H. L., 1958, Thesis, University of Delft (unpublished).
——, and J. Konijn, 1957, Physica **23,** 1069.
——, and A. H. Wapstra, 1960, Nucl. Phys. **15,** 146.
Hager, R. S., and E. C. Seltzer, 1968, Nucl. Data **A4,** 1 and **A4,** 2.
Halley, J. W., and D. Engelkemeir, 1964, Phys. Rev. **134,** A24.
Hamilton, J. H., A. V. Ramayya, B. van Nooijen, R. G. Albridge, E. F. Zganjar, S. C. Pancholi, J. M. Hollander, V. S. Shirley, and C. M. Lederer, 1966, Nucl. Data. **A1,** 521.
Hammer, W., 1968, Z. Phys. **216,** 355.
Hansen, J. S., 1971, Thesis, Georgia Institute of Technology (unpublished).
——, H.-U. Freund, and R. W. Fink, 1970a, Nucl. Phys. **A142,** 604.
——, H.-U. Freund, and R. W. Fink, 1970b, Nucl. Phys. **A153,** 465.
——, J. C. McGeorge, R. W. Fink, P. V. Rao, R. E. Wood, and J. M. Palms, 1971, Bull. Amer. Phys. Soc. **16,** 578; Z. Phys. **249,** 373 (1972).
Harms, M. I., 1927, Ann. Phys. **82,** 87.
Harris, L. A., 1968, J. Appl. Phys. **39,** 1419.
Harrison, G. R., C. R. Crawford, and J. I. Hopkins, 1955, Phys. Rev. **99,** 1629A; Phys. Rev. **100,** 841.
Hartree, D., 1957, *The Calculation of Atomic Structures* (Wiley, New York).
Haynes, S. K., M. Velinsky, and L. J. Velinsky, 1967, Nucl. Phys. **A90,** 573.
Heintze, J., 1955, Z. Phys. **143,** 153.
Heitler, W., 1954, *The Quantum Theory of Radiation* (Clarendon Press, Oxford), 3rd ed.
Henke, B. L., R. L. Elgin, R. E. Lent, and R. B. Ledingham, 1967, Norelco Rep. **14,** 112.
Herman, F., and S. Skillman, 1963, *Atomic Structure Calculations* (Prentice-Hall, Englewood Cliffs, New Jersey).
Hink, W., and H. Päschke, 1971, Phys. Rev. A **4,** 507.
——, A. N. Scheit, and A. Ziegler, 1970a, Nucl. Instr. Meth. **84,** 244.
——, A. N. Scheit, and A. Ziegler, 1970b, Nucl. Instr. Meth. **87,** 137.
Hoffman, D., and B. Dropesky, 1958, Phys. Rev. **109,** 1282.
Hohmuth, K., G. Müller, and J. Schintlmeister, 1963, Nucl. Phys. **48,** 209.
——, and G. Winter, 1964, Phys. Letters **10,** 58.
Hollander, J. M., 1966, Nucl. Inst. Methods **43,** 65.
Hollstein, M., 1970, Nucl. Inst. Methods **82,** 249.
Holmes, C. P., and V. O. Kostroun, 1970, Bull. Amer. Phys. Soc. **15,** 561.
Hornfeldt, O., 1962, Ark. Fys. **23,** 235.
Hull, M. H., and G. Breit, 1957, in *Handbuch der Physik*, edited by S. Flügge (Springer-Verlag, Berlin), Vol. 35, p. 408.
Huber, O., F. Humbel, H. Schneider, and A. de-Shalit, 1952, Helv. Phys. Acta **24,** 627 (1951); **25,** 3.
Ingelstam, E., 1936, Acta Regia. Soc. Sci. Uppsala **10,** 5.
Jaffe, H., 1954, Univ. Calif. Lawrence Radiation Laboratory Rept UCRL-2537 (unpublished).
——, T. O. Passell, C. I. Browne, and I. Perlman, 1955, Phys. Rev. **97,** 142.
Jauch, J. M., and F. Rohrlich, 1955, *The Theory of Photons and Electrons* (Addison-Wesley, Reading, Massachusetts).
Johansson, T. B., R. Akselsson, and S. A. E. Johannson, 1970, Nucl. Inst. Meth. **84,** 141.
Jopson, R. C., Hans Mark, and C. D. Swift, 1962, Phys. Rev. **128,** 2671.
——, J. M. Khan, Hans Mark, C. D. Swift, and M. A. Williamson, 1964a, Phys. Rev. **133,** A381.
——, Hans Mark, C. D. Swift, and M. A. Williamson, 1963, Phys. Rev. **131,** 1165.
——, Hans Mark, C. D. Swift, and M. A. Williamson, 1964*b*, Phys. Rev. **136,** A69.
——, Hans Mark, C. D. Swift, and M. A. Williamson, 1965, Phys. Rev. **137,** A1353.
Karttunen, E., H.-U. Freund, and R. W. Fink, 1969, Nucl. Phys. **A131,** 343.
——, H.-U. Freund, and R. W. Fink, 1971, Phys. Rev. **A4,** 1695.

Ketelle, B. H., H. Thomas, and A. R. Brosi, 1956, Phys. Rev. **103,** 190.
Khan, J. M., D. L. Potter, and R. D. Worley, 1965, Phys. Rev. **139,** A1735.
——, D. L. Potter, and R. D. Worley, 1966, Phys. Rev. **145,** 23.
Kieffer, L. J., and G. H. Dunn, 1966, Rev. Mod. Phys. **38,** 78.
Kinsey, B. B., 1948, Can. J. Res. **A26,** 421.
Kohn, W., and J. L. Sham, 1965, Phys. Rev. **140,** A1133.
Knudson, A. R., *et al.*, 1971, Phys. Rev. Letters **26,** 1149.
Kondaiah, E., 1951, Phys. Rev. **83,** 471.
Konijn, J., H. L. Hagedoorn, and B. van Nooijen, 1958, Physica **24,** 129.
——, B. van Nooijen, and H. L. Hagedoorn, 1958, Physica **24,** 377.
Konstantinov, A. A., V. V. Perepelkin, and T. E. Sazonova, 1964, Izv. Akad. Nauk. SSSR, Ser. Fiz. **28,** 107 [Bull. Acad. Sci. USSR, Phys. Ser., **28,** 103 (1964)].
——, T. E. Sazonova, and V. V. Perepelkin, 1960, Izv. Akad. Nauk SSSR, Ser. Fiz. **24,** 1480 [Bull. Acad. Sci. USSR, Phys. Ser., **24,** 1472 (1960)].
——, and T. E. Sazonova, 1965, Izv. Akad. Nauk SSSR, Ser. Fiz. **29,** 302 (1965) [Bull. Acad. Sci. USSR, Phys. Ser., **29,** 305].
——, and T. E. Sazonova, 1967, in *Standardization of Radionuclides* (International Atomic Energy Agency, Vienna, in Russian), p. 357.
——, and T. E. Sazonova, 1968, Izv. Akad. Nauk SSSR, Ser. Fiz. **32,** 631 [Bull. Acad. Sci. USSR, Phys. Ser., **32,** 581 (1968)].
——, I. A. Sokolova, and T. E. Sazonova, 1961, Izv. Akad. Nauk SSSR, Ser. Fiz. **25,** 228 [Bull. Acad. Sci. USSR, Phys. Ser., **25,** 219 (1961)].
Kossel, W., 1923, Z. Phys. **19,** 333.
Kostroun, V. O., 1968, Thesis, University of Oregon (unpublished).
——, M. H. Chen, and B. Crasemann, 1971, Phys. Rev. **A3,** 533.
Kramer, P., A. De Beer, E. C. Bos, and J. Blok, 1962, Physica **28,** 582; 1961 Thesis, University of Amsterdam, unpublished.
Krause, M. O., 1971, J. Physique **32,** C4-67.
Krisciokaitis, R. J., and S. K. Haynes, 1967, Nucl. Phys. **A104,** 466.
Küstner, H., and E. Arends, 1935, Ann. Phys. **22,** 443.
Kyles, J., J. C. McGeorge, F. Shakh, and J. Byrne, 1970, Nucl. Phys. **A150,** 143.
Laberrigue-Frolow, J., P. Radvanyi, and M. Langevin, 1956, J. Phys. Radium **17,** 530, 944.
Lark, N. L., 1960, Thesis, Cornell University (unpublished).
Larkins, F. P., 1971, J. Phys. **B4,** 1 and **B4,** 14.
Laskar, W., 1955, J. Phys. Radium **16,** 644.
——, 1958, Ann. Phys. (Paris) **3,** 258.
——, and Y. Raffray, 1967, C. R. Acad. Sci. **B265,** 1307.
Lay, H., 1934, Z. Phys. **91,** 533.
Lazar, N. H., and W. S. Lyon, 1958, Bull. Amer. Phys. Soc. **3,** 29.
di Lazzaro, M. A., 1965, Instituto Superiore di Sanita Report ISS 65/11 (unpublished).
Lee, N. K., 1958, Thesis, Vanderbilt University, U.S. Atomic Energy Commission Rep. TID-14963 (unpublished).
Legrand, J., 1965, Commissariat á L'Energie Atomique, Rapport CEA-R 2813 (unpublished).
Leisi, H. J., J. H. Brunner, C. F. Perdrisat, and P. Scherrer, 1961, Helv. Phys. Acta **34,** 161.
Leistner, M. and K. Friedrich, 1962, Atomkernenergie **10,** 311.
Lieberman, D., J. T. Waber, and D. T. Cromer, 1965, Phys. Rev. **137,** A27.
Listengarten, M. A., 1960, Izv. Akad. Nauk SSSR, Ser. Fiz. **24,** 1041 [Bull. Acad. Sci. USSR, Phys. Ser., 24, 1050 (1960)].
——, 1961, Izv. Akad. Nauk SSSR, Ser. Fiz. **25,** 803 [Bull. Acad. Sci. USSR, Phys. Ser., **25,** 803 (1961)].
——, 1962, Izv. Akad. Nauk SSSR, Ser. Fiz. **26,** 182 [Bull. Acad. Sci. USSR, Phys. Ser., **26,** 182 (1962)].
Locher, G. L., 1932, Phys. Rev. **40,** 484.
Lotz, W., 1970, J. Opt. Soc. Am. **60,** 206.
Löwdin, P.-O., and K. Appel. 1956, Phys. Rev. **103,** 1746.
Mann, J. B., 1968, Los Alamos Scientific Laboratory Report LA-369 (unpublished).
Martin, L. H., 1927, Proc. Roy. Soc. (London) **A115,** 420.
——, J. C. Bower, and T. H. Laby, 1935, Proc. Roy. Soc. (London) **A148,** 40.
——, and F. H. Eggleston, 1937, Proc. Roy. Soc. (London) **A158,** 46.
Martin, M. J., and P. H. Blichert-Toft, 1970, Nucl. Data Tables **A8,** 1.
Massey, H. S. W., and E. H. S. Burhop, 1936, Proc. Roy. Soc. (London) **A153,** 661.
Mayer, J. W., 1966, Nucl. Instr. Methods **43,** 55.
McGeorge, J. C., H.-U. Freund, and R. W. Fink, 1970, Nucl. Phys. **A154,** 526.
——, and R. W. Fink, 1971a, Bull. Amer. Phys. Soc. **16,** 847; Z. Phys. **250,** 293 (1972).
——, and R. W. Fink, 1971b, Z. Phys. **248,** 208.
——, S. Mohan, and R. W. Fink, 1971, Phys. Rev. **A4,** 1317.
McGilvary, C., and K. Lansdale, 1965, *International Tables for X-Ray Crystallography* (Kynoch Press, Birmingham), 2nd ed.
McGuire, E. J., 1969, Phys. Rev. **185,** 1.
——, 1969, Sandia Laboratories Research Report SC-RR-69-137 (unpublished).
——, 1970a, Phys. Rev. A **2,** 273.
——, 1970b, Sandia Laboratories Research Report SC-RR-70-429 (unpublished).
——, 1970c, Sandia Laboratories Report SE-DC-70-5066 (unpublished).
——, 1970d, Sandia Laboratories Report SC-RR-70-721 (unpublished).
——, 1971a, Phys. Rev. **A3,** 587.
——, 1971b, Phys. Rev. **A3,** 1801.
——, 1971c, Sandia Laboratories Report SC-DC-71-4303 (unpublished).
——, 1972, Phys. Rev. **A5,** 1043.
McGuire, J. H., and M. H. Mittleman, 1972, Phys. Rev. **A5,** 1971.
McMaster, W. H., N. Kerr Del Grande, J. H. Mallett, and J. H. Hubbell, 1969, Univ. Calif. Lawrence Radiation Laboratory Report UCRL-50174 (unpublished).
Mehlhorn, W., 1960, Z. Phys. **160,** 247.
——, 1965, Phys. Letters **15,** 46; Z. Phys. **187,** 21 (1965).
——, 1968, Z. Phys. **208,** 1.
——, and W. N. Asaad, 1966, Z. Phys. **191,** 231.
Meitner, L., 1922, Z. Phys. **9,** 131.
Merrill, J. J., and J. W. M. DuMond, 1960, in *Proceedings of the International Conference on Nuclear Structure* (Toronto U. P.), p. 637.
——, and J. W. M. DuMond, 1961, Ann. Phys. (New York) **14,** 166.
Middleman, L. M., R. L. Ford, and R. Hofstadter, 1970, Phys. Rev. **A2,** 1429.
Mistry, V. D., and C. A. Quarles, 1971, Nucl. Phys. **A164,** 219.
Mladjenović, M., Ark. Fys. **8,** 27 (1965).
——, and H. Slätis, 1955, J. Phys. Radium **16,** 638.
Moellering, W., and J. H. D. Jensen, 1956, Z. Phys. **144,** 252.
Mohan, S., 1971, Thesis, Georgia Institute of Technology (unpublished).
——, R. W. Fink, R. E. Wood, J. M. Palmes, and P. Venugopala Rao, 1970a, Z. Phys. **239,** 423.
——, H.-U. Freund, R. W. Fink, and P. Venugopala Rao, 1970b, Phys. Rev. **C1,** 254.
Moisewitch, B. L., and S. J. Smith, 1968, Rev. Mod. Phys. **40,** 238.
Møller, C., 1931, Z. Phys. **70,** 786.
Monnand, E., and A. Moussa, 1961, Nucl. Phys. **25,** 292.
Moszkowski, S. A., 1965, "Theory of Multipole Radiation", in *Alpha- Beta- and Gamma-Ray Spectroscopy*, edited by K. Seigbahn (North-Holland, Publ. Co., Amsterdam) 2nd ed., Vol. II, p. 863.
Mukerji, A., and J. B. McGouch, Jr., 1967, Nucl. Phys. **A94,** 95.
——, J. B. McGouch, Jr., and G. D. Cole, 1967, Nucl. Phys. **A100,** 81.
Nall, J. C., Q. L. Baird, and S. K. Haynes, 1960, Phys. Rev. **118,** 1278.
Nelson, G. C., W. John, and B. G. Saunders, 1969, Phys. Rev. **187,** 1.
——, W. John, and B. G. Saunders, 1970, Phys. Rev. **A2,** 542.
——, and B. G. Saunders Phys. Rev. **188,** 108.
——, B. G. Saunders, and S. I. Salem, 1970, Atomic Data **1,** 377.
Nichols, H. H., 1956, United States Atomic Energy Commission Report TID-15703 (unpublished).

Nicholls, R. W., and A. L. Steward, 1962, in *Atomic and Molecular Processes*, edited by D. R. Bates (Academic, New York), p. 47.
Nigam, A. N., K. B. Garg, and Q. S. Kapoor, 1968, J. Phys. **B1,** 492.
Nix, D., 1972, Thesis, Georgia Institute of Technology (unpublished).
O'Connell, R. F., and C. O. Carroll, 1963, in *Internal Conversion Processes*, edited by J. H. Hamilton (Academic, New York), p. 333.
Oms, J., C. Foin, and A. Baudry, 1968, C. R. Acad, Sci. **B266,** 1292.
Oppenheimer, J. R., 1929, Z. Phys. **55,** 725.
Pahor, J., 1971, private communication.
——, A. Kodre, M. Hribar, and A. Moljk, 1969, Z. Phys. **221,** 490.
——, A. Kodre, and A. Moljk, 1968, Nucl. Phys. **A109,** 62.
——, A. Kodre, and A. Moljk, 1970, Z. Phys. **230,** 287.
——, A. Kodre, and A. Moljk, 1971b, Z. Phys. (in press).
——, and A. Moljk, 1967, Compt. Rend. **B264,** 550.
——, A. Moljk, A. Kodre, and M. Hribar, 1971c (to be published).
Palmberg, P. N., and T. N. Rhodin, 1968, J. Appl. Phys. **39,** 2425.
Palms, J. M., P. Venugopala Rao, and R. E. Wood, 1969, Nucl. Inst. Meth. **76,** 59.
——, R. E. Wood, P. Venugopala Rao, and V. O. Kostroun, 1970, Phys. Rev. **C2,** 592.
Parilis, E. S., 1969, *The Auger Effect*, edited by Anifov. (U.A.) (Academy of Sciences, USSR, Tashkent) (in Russian).
Park, J. J. H., and P. Christmas, 1967, Can. J. Phys. **45,** 2621.
Parratt, L. G., 1936, Phys. Rev. **50,** 1.
——, 1938, Phys. Rev. **54,** 99.
——, 1959, Rev. Mod. Phys. **31,** 616.
Päschke, R., 1963, Z. Phys. **176,** 143.
Patronis, Jr., E. T., C. H. Braden, and L. D. Wyly, 1957, Phys. Rev. **105,** 681.
Pauli, H. C., 1967, *Tables of Internal Conversion Coefficients and Particle Parameters*, Purdue Univ. Rep. COO–1420–137 (unpublished).
Payne, W. B., and J. S. Levinger, 1956, Phys. Rev. **101,** 1020.
Peed, W. F., L. E. Burkhart, R. A. Staniforth, and L. G. Fauble, 1957, Phys. Rev. **105,** 588.
Persson, L., and Z. Sujkowski, 1961, Ark. Fys. **19,** 309.
Petel, M., and H. Houtermans, 1967, *Standardization of Radionuclides* (International Atomic Energy Agency, Vienna), p. 301, and private communication.
Pincherle, L., 1935, Nuovo Cimento **12,** 81.
Powell, J. L., and B. Crasemann, 1961, *Quantum Mechanics* (Addison-Wesley, Reading Mass.).
Price, R. E., Hans Mark, and C. D. Swift, 1968, Phys. Rev. **176,** 3.
Pruett, C. H., and R. G. Wilkinson, 1954, Phys. Rev. **96,** 1340.
Rakavy, G., and A. Ron, 1967, Phys. Rev. **159,** 50.
Ramaswamy, M. K., 1962, Nucl. Phys. **33,** 320.
Ramberg, E. G., and F. K. Richtmyer, 1937, Phys. Rev. **51,** 913.
Ramsdale, D. J., 1969, Thesis, Kansas State University (unpublished).
Rao, P. Venugopala, 1968, in Berényi, p. 222.
——, M. H. Chen, and B. Crasemann, 1972, Phys. Rev. **A5,** 997.
——, and B. Crasemann, 1965a, Phys. Rev. **137,** B64.
——, and B. Crasemann, 1965b, Phys. Rev. **139,** A1926.
——, and B. Crasemann, 1966, Phys. Rev. **142,** 768.
——, J. M. Palms, and R. E. Wood, 1971, Phys. Rev. **A3,** 1568.
——, R. E. Wood, J. M. Palms, and R. W. Fink, 1969, Phys. Rev. **178,** 1997.
Ravier, J., P. Marguin, and A. Moussa, 1961, J. Phys. Radium **22,** 249.
Renier, J. P., H. Genz, K. W. Ledingham, and R. W. Fink, 1968, Rev. **166,** 935.
Richard, P., T. I. Bonner, T. Furuta, and I. L. Morgan, 1970, Phys. Rev. **A1,** 1044.
Richtmyer, F. K., and S. W. Barnes, 1934, Phys. Rev. **46,** 352.
——, S. W. Barnes, and E. Ramberg, 1934, Phys. Rev. **46,** 843.
Rightmire, R. A., F. R. Simanton, and T. R. Kohman, 1959, Phys. Rev. **113,** 1069.
Risch, K., 1958, Z. Phys. **150,** 87.
Robinson, B. L., 1965, Nucl. Phys. **64,** 197.
——, and R. W. Fink, 1955, Rev. Mod. Phys. **27,** 424.
——, and R. W. Fink, 1960, Rev. Mod. Phys. **32,** 117.
Robinson, H., 1923, Proc. Roy. Soc, (London) **A104,** 455.
Roos, C. E., 1954, Phys. Rev. **93,** 401.
——, 1955, Phys. Rev. **100,** 1267A.
——, 1957, Phys. Rev. **105,** 931.
Rose, M. E., 1955, *Multipole Fields* (Wiley, New York).
——, 1958, *Internal Conversion Coefficients* (North-Holland Publ. Co., Amsterdam).
——, 1961, *Relativistic Electron Theory* (Wiley, New York).
Rose, H. J., and D. M. Brink, 1967, Rev. Mod. Phys. **39,** 306.
——, F. Cuttitta, E. J. Dwornik, M. K. Carrou, R. P. Christian, J. R. Lindsay, D. T. Lignon, and R. R. Larson, 1970, Science **167,** 520.
Rosner, H. R., and C. P. Bhalla, 1970, Z. Phys. **231,** 347.
Ross, M. A. S., A. J. Cochran, J. Hughes, and N. Feather, 1955, Proc. Soc. (London) **A68,** 612.
Rubenstein, R. A., and J. N. Snyder, 1955a, Thesis, University of Illinois; Phys. Rev. **97,** 1653.
——, and J. N. Snyder, 1955b, Phys. Rev. **99,** 189.
Rubinson, W., and K. P. Gopinathan, 1968, Phys. Rev. **170,** 969.
Rumsh, M. A., and V. N. Shchemelev, 1962, Zh. Eksp. Teor. Fiz. **42,** 727 [Soviet Phys. JETP **15,** 727 (1962)].
Russ, J. C., and E. McNatt, 1969, *Proceedings of the Annual Meeting of the Electron Microscopy Society of America*, edited by C. J. Arceneaux (Claitor's Publishing Div., Baton Rouge, Louisiana), p. 38.
Sachenko, V. P., 1967, and E. V. Burtsev, Izv. Akad. Nauk SSSR, Ser. Fiz. **31,** 980 [Bull. Acad. Sci. USSR, Phys. Ser., **31,** 980 (1967)].
——, and V. F. Demekin, 1967, Izv. Akad. Nauk SSSR, Ser. Fiz. **31,** 1942 [Bull. Acad. Sci. USSR, Phys. Ser., **31,** 957 (1967)].
Salem, S. I., B. G. Saunders, and G. C. Nelson, 1970, Phys. Rev. **A1,** 1563.
——, R. T. Tsutsui, and B. A. Rabbani, 1971, Bull. Amer. Phys. Soc. **16,** 848; Phys. Rev. **A4,** 1728.
——, and R. J. Wimmer, 1970, Phys. Rev. A **2,** 1121.
Salgueiro, L., J. G. Ferreira, J. J. H. Park, and M. A. S. Ross, 1961, Proc. Phys. Soc. (London) **77,** 657.
——, J. G. Ferreira, M. T. Ramos, M. J. Bettencourt, and F. B. Gil, 1968, C. R. Acad. Sci. **267B,** 1293.
——, M. A. Campos, and J. G. Ferreira, 1965, Portugal Phys. **4,** 131.
Saris, F. W., and D. Onderdelinden, 1970, Physica **49,** 441.
Schmied, H., and R. W. Fink, 1957, Phys. Rev. **107,** 1062.
Schippert, M. A., S. H. Moll, and R. E. Ogilvie, 1967, Anal. Chem. **39,** 867.
Schmolz, A., and K. W. Hoffmann, 1968, Z. Phys. **214,** 1.
Schult, O. W. B., 1971, Z. Naturforsch. **26a,** 368.
Schofield, J. H., 1969, Phys. Rev. **179,** 9.
Sen, S. K., and I. O. Durosinmi-Etti, 1966, Nukleonik **8,** 127.
Sevier, K. D., 1972, *Low-Energy Electron Spectrometry* (Wiley-Interscience, New York).
Shacklett, R. L., and J. W. M. DuMond, 1957, Phys. Rev. **106,** 501.
Shore, B. W., and D. H. Menzel, 1968, *Principles of Atomic Spectra* (Wiley, New York).
Siegbahn, K., ed., 1965, *α-, β-, and γ-Spectroscopy* (North Holland Publ. Co., Amsterdam).
——, C. Nordling, A. Fahlman, R. Nordberg, K. Hamrin, J. Hedman, G. Johansson, T. Bergmark, S.-E. Karlsson, I. Lindgren, and B. Lindberg, 1967, *ESCA: Atomic, Molecular, and Solid State Structure Studied by Means of Electron Spectroscopy* (Nova Acta Regiae Societatis Upsaliensis, Uppsala).
——, et. al., 1969, *ESCA Applied to Free Molecules* (North-Holland, Amsterdam).
Slater, J. C., 1930, Phys. Rev. **36,** 57.
Sliv, L. A., and I. M. Band, 1956, 1958, *Coefficients of Internal Conversion of γ-Radiation* (USSR Academy of Sciences, Moscow-Leningrad) [reprinted as University of Illinois Reports 57ICCK1 and 58ICCL1].
Slivinsky, V. W., and P. J. Ebert, 1969, Phys. Letters **29A,** 463.
Smither, R. K., M. S. Freedman, and F. T. Porter, 1970, Phys. Letters **32A,** 405.
Spernol, A., 1967, *Standardization of Radionuclides* (International Atomic Energy Agency, Vienna), p. 277.
Steffen, R. M., O. Huber, and F. Humbel, 1949, Helv. Phys. Acta **22,** 167.
Stephas, P., and B. Crasemann, 1971, Phys. Rev. C **3,** 2495.
Stephenson, R. J., 1937, Phys. Rev. **51,** 637.

Stockmeyer, W., 1932, Ann. Phys. **12,** 71.
Storm, E., and H. I. Israel, 1970, Nucl. Data **A7,** 565.
Sujkowski, Z., and O. Melin, 1961, Ark. Fys. **20,** 193.
Suter, T., and P. Reyes-Suter, 1961, Ark. Fys. **20,** 393.
Suzor, F., and G. Charpak, 1959, J. Phys. Radium **20,** 462.
Talukdar, B., and D. Chattarji, 1970, Phys. Rev. **A1,** 33.
Tawara, H., K. G. Harrison, and F. J. de Heer, 1972, Physica (in press).
Taylor, G. R., and W. B. Payne, 1960, Phys. Rev. **118,** 1549.
Taylor, J. G. V., and J. S. Merritt, 1963, in *Role of Atomic Electrons in Nuclear Transformations* (Nuclear Energy Information Center, Warsaw, Poland), p. 465.
Taylor, B. N., N. H. Parker, and D. N. Langenberg, 1969, Rev. Mod. Phys. **41,** 375.
Toburen, L. H., and R. G. Albridge, 1967, Nucl. Phys. **A90,** 529.
Tombuolian, D. H., 1948, Phys. Rev. **74,** 1887.
Topping, J., 1969, *Errors of Observation and Their Treatment* (Chapman and Hall, London).
Tousset, J., and A. Moussa, 1958, J. Phys. Radium **19,** 39.
Troughton, M. E., 1967, *Standardization of Radionuclides* (International Atomic Energy Agency, Vienna), p. 323.
Vaninbroukx, R., and G. Grosse, 1966, Int. J. Appl. Rad. Isotopes **17,** 41.
Vatai, E., 1970, Nucl. Phys. **A156,** 541.
Velinsky, L. J., M. A. Velinsky, and S. K. Haynes, 1966, in *Internal Conversion Processes,* edited by J. H. Hamilton (Academic, New York), p. 393.
Victor, C., 1961, Ann. Phys. (Paris) **6,** 183.
Walter, F. J., 1970, IEEE Trans. Nucl. Sci. **17,** 196.
Walters, D. L., and C. P. Bhalla, 1971, Phys. Rev. **A3,** 519.
Wapstra, A. H., 1953, thesis, University of Amsterdam (unpublished).
——, G. J. Nijgh, and R. van Lieshout, 1959, *Nuclear Spectroscopy Tables* (North-Holland Publ. Co., Amsterdam).
Watanabe, T., H. W. Schnopper, and F. N. Cirillo, 1962, Phys. Rev. **127,** 2055.
Weber, R. E., and W. T. Peria, 1967, J. Appl. Phys. **38,** 4355.
Wehring, B. W., and M. E. Wyman, 1968, Nucl. Inst. Meth. **61,** 189.
Weimer, P. K., J. D. Kurbatov, and M. L. Pool, 1944, Phys. Rev. **66,** 209.
Weisskopf, V., and E. Wigner, 1930, Z. Phys. **63,** 54 and **65,** 18.
Welker, J. P., and M. L. Perlman, 1955, Phys. Rev. **100,** 74.
Wentzel, G., 1927, Z. Phys. **43,** 524.
West, D., and P. Rothwell, 1950, Phil. Mag **41,** 873.
Wilken, B., 1968, Z. Phys. **213,** 56.
Winkenbach, H., 1958, Z. Phys. **152,** 387.
Winter, G., 1968, Nucl. Phys. **A113,** 617.
Wood, R. E., J. M. Palms, and P. Venugopala Rao, 1969, Phys. Rev. **187,** 1497.
——, J. M. Palms, and P. Venugopala Rao, 1972, Phys. Rev. **A5,** 11.
Wyckoff, R. W. G., and F. D. Davidson, 1965, J. Appl. Phys. **36,** 1883.
Yost, F. L., J. A. Wheeler, and G. Breit, 1936, Phys. Rev. **49,** 174.
Zender, M. J., W. Pou, and R. G. Albridge, 1969, Z. Phys. **218,** 245.
Zimmerli, T., and A. Flammersfeld, 1963, Z. Phys. **176,** 323.
Zyryanova, L. N., 1968, in Berényi (1968), p. 5.
——, and Yu. P. Suslov, 1968, in Berényi (1968), p. 45.